



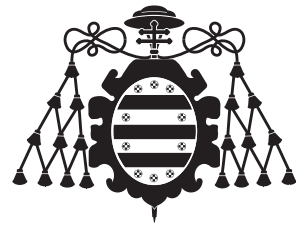
Universidad de Oviedo
Departamento de Biología de Organismos y Sistemas

Programa de Doctorado: “Biología aplicada a la sostenibilidad de recursos naturales
(Mención de calidad)”

Aplicación de Satélites Oceanográficos al Estudio del Impacto del
Cambio Global sobre los Ecosistemas Pelágicos del Atlántico Norte

TESIS DOCTORAL

Fernando González Taboada
Oviedo 2014



Universidad de Oviedo
Department Biology of Organisms and Systems

PhD Program: “Biology Applied to the Sustainability of Natural Resources
(Quality Certified)”

Application of Satellite Oceanography to the Study of
Global Change Impacts on North Atlantic Pelagic Ecosystems

PHD THESIS

Fernando González Taboada
Oviedo 2014



RESUMEN DEL CONTENIDO DE TESIS DOCTORAL

1.- Título de la Tesis

Español: Aplicación de Satélites Oceanográficos al Estudio del Impacto del Cambio Global sobre los Ecosistemas Pelágicos del Atlántico Norte	Inglés: Application of Satellite Oceanography to the Study of Global Change Impacts on North Atlantic Pelagic Ecosystems
----------------------------------------------------------------------------------------------------------------------------------------------	--------------------------------------------------------------------------------------------------------------------------

2.- Autor

Nombre: Fernando González Taboada DNI: 71660667G

Programa de Doctorado: Biología aplicada a la sostenibilidad de recursos naturales

Órgano responsable: Departamento Biología de Organismos y Sistemas

RESUMEN (en español)

Los satélites de observación terrestre recogen información de gran interés para el estudio del impacto global sobre los ecosistemas pelágicos marinos. Este tipo de sistemas de observación proporcionan medidas de distintas propiedades de la superficie del océano con una resolución espacial y temporal muy alta. Esta particularidad permite analizar la dinámica de los ecosistemas pelágicos desde el punto de vista de su componente biológico. En esta memoria se utiliza esta aproximación para analizar los cambios en la temperatura de la superficie del mar y en la fenología del fitoplancton en el Atlántico Norte durante las últimas décadas, así como para evaluar la importancia de la variación ambiental frente a la sobreexplotación en el colapso de la pesquería de anchoa del Cantábrico. En primer lugar, se propone una aproximación complementaria para el análisis de los cambios en la temperatura de la superficie del mar que da mayor énfasis a posibles cambios en la estacionalidad, así como a la distribución espacial de los cambios. Entre 1982 y 2010, los cambios en la temperatura de la superficie del mar registrados al analizar la serie producida a partir de las observaciones de los satélites NOAA-AVHRR fueron coherentes con el proceso de cambio climático global. La respuesta fue diferente en intensidad y en su distribución espacial entre estadísticos representando cambios en la temperatura media, el ciclo estacional y el período de estratificación, o la estructura espacial del campo de temperaturas. A continuación, se introduce un nuevo método para el análisis de los cambios en la estacionalidad del fitoplancton marino, tratando de incorporar la incertidumbre en las medidas satelitales de concentración de clorofila a la estimación de los cambios en la fenología. Este método permitió detectar un aumento de la prevalencia de ciclos estacionales propios de latitudes subtropicales en la zona templada entre 1998 y 2013, así como cambios en el momento del año en que producen las floraciones y en su intensidad congruentes con los impactos del cambio climático. Estas tendencias parecen responder principalmente a cambios en los patrones de circulación atmosférica, y en menor medida a cambios en la radiación incidente o la temperatura. Este método ha demostrado también la mayor robustez de los algoritmos semi-analíticos de clorofila sobre los tradicionales al combinar datos procedentes de distintos sensores (SeaWiFS y MODIS). En último lugar, se analizó el colapso de la pesquería de anchoa del Cantábrico combinando técnicas de modelado de poblaciones con una cuidadosa caracterización de los cambios en ambientales en el golfo de Vizcaya basado principalmente en el análisis de datos satelitales. Se encontró que el éxito del reclutamiento de la anchoa se puede predecir con bastante precisión a partir de los cambios en la fenología y la estabilidad durante primavera en las áreas de desove o a partir del efecto del afloramiento estival sobre la deriva de larvas y huevos de anchoa fuera de la plataforma Armónica. Pese a que la regulación ambiental de la dinámica poblacional es muy importante, la sobrepesca parece haber jugado un papel fundamental en el colapso de la pesquería en 2005. En conjunto, el trabajo presentado en esta memoria indica la necesidad de una aproximación local y regional en los estudios de impacto del cambio global. Desde un punto de vista metodológico, también ilustra algunas de las ventajas que ofrecen las técnicas de análisis Bayesiano para mejorar la gestión y conservación de los recursos naturales, así como para mejorar los sistemas de detección y caracterización de impactos. Finalmente, este trabajo demuestra el valor de los datos satelitales en Oceanografía y la importancia de apoyar los programas públicos de observación a largo plazo del medio ambiente.



RESUMEN (en Inglés)

Earth Observing Satellites gather information of great interest to the study of global change impacts on marine pelagic ecosystems. These observing systems measure different properties of the surface of the ocean at high spatial and temporal resolutions, allowing the study of the dynamics of pelagic ecosystems. In this memoir, we use this general approach to analyze changes in sea surface temperature (SST) and in the phenology of phytoplankton in the North Atlantic during the last decades, as well as to assess the importance of environmental forcing and of overfishing on the recent collapse of Bay of Biscay anchovy. First, we propose a complementary approach to the analysis of changes in SST that emphasizes potential changes in the seasonal cycle and in the spatial distribution of temperature anomalies. We analyzed the NOAA-AVHRR SST series (1982-2010) using our approach to reveal changes in SST that were coherent with those expected under climate change. The statistics analyzed presented a varied response both in intensity and in their spatial distribution depending on whether they represented changes in the mean, the seasonal cycle and the period of stratification, or the spatial structure of the SST field. Then, we introduce a novel method to analyze changes in the seasonality of marine phytoplankton based on ocean color data. The method accounts for uncertainties in the detection and characterization of seasonal peaks based on remote sensing chlorophyll a concentration estimates, that was further propagated to estimates of recent trends in phenology. By combining long term series retrieved by SeaWiFS and Aqua MODIS sensors (1998--2013), we detected an increase in the prevalence of seasonal cycles characteristic of subtropical regions at temperate latitudes, as well as changes in the timing and magnitude of seasonal blooms matching climate change predictions. These trends were mainly associated to changes in atmospheric circulation and, to a lesser extent, to changes in irradiance and sea surface temperature. Our approach demonstrated also the greater robustness of semi-analytical chlorophyll algorithms over empirical ones when combining data from different sensors. Last, we analyzed the collapse of Bay of Biscay anchovy combining population modeling with a careful characterization of recent changes in the recruitment environment of this species. Recruitment strength was predicted with relative success after taking into account either changes in plankton phenology and stability in spawning areas during spring, or changes in the drift of anchovy eggs and larvae out of Armorican shelf during summer. Although external environmental forcing on recruitment was a key driver of population fluctuations, overfishing seems to be behind the collapse of the fishery in 2005. Altogether, our work highlights the need to develop local and regional approaches to analyze global change impacts. From a methodological point of view, it also stresses the advantages of Bayesian analysis techniques to improve natural resource management and conservation, as well as to improve impact detection and monitoring systems. Finally, our work demonstrates the high value of remote sensing data in Oceanography and the importance of a continued support of long term observation programs.

SR. DIRECTOR DE DEPARTAMENTO DE BIOLOGÍA DE ORGANISMOS Y SISTEMAS

A mis padres

Contents

Contents	ix
List of tables	xi
List of figures	xiii
Acknowledgements	xv
Abstract	xvii
1 Introduction	3
1.1 Objectives	6
2 Sea surface temperature	9
2.1 Introduction	9
2.2 Materials and Methods	11
2.2.1 Sea surface temperature data	11
2.2.2 Derived indexes and estimation of trends	11
2.2.3 Decorrelation scales	12
2.2.4 Proxy for the duration of the period of stratification	13
2.3 Results	16
2.3.1 Mean SST	16
2.3.2 Seasonal SST extremes and seasonal range	17
2.3.3 Changes in decorrelation scales	19
2.3.4 Timing of SST extremes and duration of the period of stratification	20
2.4 Discussion	23
3 Ocean color and plankton phenology	29
3.1 Introduction	30
3.2 Materials and Methods	30
3.2.1 Data sources and data preparation	31
3.2.2 Characterization of seasonal changes in chl <i>a</i> concentration . . .	32
3.2.3 Analyses of changes in the seasonality of chl <i>a</i> concentration . .	35

3.3	Results	39
3.3.1	Incidence of different types of seasonality	39
3.3.2	Timing and magnitude of seasonal peaks	41
3.3.3	Impact of environmental factors on the timing and magnitude of blooms	43
3.4	Discussion	44
3.4.1	Limitations and advantages of the methods employed to characterize seasonal changes in phytoplankton biomass	45
3.4.2	Changes in phytoplankton seasonality	46
	Appendices	49
3.A	Supporting text	49
3.A.1	Detection and characterization of blooms: SeaWiFS vs. Aqua MODIS	49
3.A.2	Effect of chl <i>a</i> algorithm on incidences and derived estimates .	50
3.A.3	Retrieval of chl <i>a</i> data and estimation of bloom metrics (extra discussion)	51
3.B	Supporting tables and figures	52
3.B.1	Supporting Material and Methods	52
3.B.2	Supporting Results: Incidence of different types of seasonality .	60
3.B.3	Supporting Results: Timing and magnitude of seasonal peaks .	63
3.B.4	Supporting Results: Impact of environmental factors on blooms metrics	71
	4 Anchovy recruitment	77
4.1	Introduction	77
4.2	Material and Methods	78
4.2.1	European anchovy fisheries in the Bay of Biscay	78
4.2.2	Data sources and preparation	79
4.2.3	Population model	81
4.2.4	Model fitting and inference	83
4.3	Results	90
4.3.1	Model diagnostics and environmental effects on anchovy recruitment	90
4.3.2	Fishing, environmental variability and anchovy collapse	93
4.4	Discussion	94
	Appendices	97
4.A	Primary data	97
4.A.1	Ancillary data	98
4.B	Model fitting algorithms	112

4.C	Surrogate analysis of anchovy collapse	115
4.D	Supplementary results	115
5	Discussion and conclusions	133
5.1	Conclusions	137
6	Summary and conclusions (<i>in Spanish</i>)	141
6.1	Resumen	141
6.2	Conclusiones generales	142

List of tables

3.1	Environmental variables related to interannual changes in phytoplankton seasonality	38
3.B.1	Agreement between bloom statistics derived from different sensors	52
3.B.2	Parameter estimates for the Dirichlet model on the prevalence of different types of seasonal cycle	60
4.1	Hypotheses proposed to explain fluctuations in fish recruitment	80
4.2	Environmental variables and indexes employed to assess environmental forcing on the strength of anchovy recruitment	83
4.3	Model diagnostics for the age structured population models	89
4.1	Summary of the posterior distribution of process model parameters	92
4.A.1	Spawning stock biomass at age of European anchovy in the Bay of Biscay.	97
4.B.1	Outline of the model fitting process.	113
4.B.2	Model parameters and prior distributions	114
4.D.1	Summary of the posterior distribution of model parameters	116

List of figures

1.1	Map of the North Atlantic Ocean	5
2.1	Mapped changes in SST mean and in seasonal extremes	14
2.2	Zonal and meriodional averages of changes in SST levels	15
2.3	Isotherm migration for SST mean and annual extremes	17
2.4	Eastward and northward migration rates for SST isotherms	20
2.5	Mapped changes in SST seasonality	22
2.6	Mapped changes in SST spatial structure	25
2.7	Zonal and meriodional averages for changes in the timing of SST events .	27

3.1	Different types of seasonal cycles of surface chlorophyll <i>a</i> concentration in the North Atlantic	32
3.2	Prevalence of different types of seasonal cycle in the main biogeochemical regions of the North Atlantic	36
3.3	Timing and magnitude of spring and autumn/winter blooms	40
3.4	Association between the sign of trends in bloom metrics for spring and autumn/winter blooms	43
3.5	Environmental variables explaining more deviance in interannual changes in the timing and magnitude of spring and autumn/winter blooms in the North Atlantic	45
3.B.1	Probability maps for different types of seasonal cycles derived from SeaWiFS and MODIS	53
3.B.2	Zonal differences in the probability of different types of seasonal cycles for SeaWiFS and MODIS	54
3.B.3	Differences in the probability of detection for different seasonal cycles between SeaWiFS and MODIS	55
3.B.4	Differences in the timing of spring and autumn/winter blooms between SeaWiFS and MODIS	56
3.B.5	Differences in the magnitude of spring and autumn/winter blooms between SeaWiFS and MODIS	57
3.B.6	Schematic of the algorithm employed to detect and characterize phytoplankton seasonality	58
3.B.7	Map of Longhurst provinces in the North Atlantic	59
3.B.8	Probability maps for regions where no peak was detected (lack of data or no peak detected)	61
3.B.9	Changes in the prevalence of different types of seasonal cycle in the North Atlantic for OC4v6 data (same as figure 3.2 in the main text)	62
3.B.10	Maps with time trends in bloom metrics averaged over 5° boxes	63
3.B.11	Association between bloom metrics for spring and autumn/winter blooms	64
3.B.12	Relationship between trend estimates based on different chlorophyll algorithms	64
3.B.13	Maps of the standard error of parameter estimates presented in figure 3.3 in the main text	65
3.B.14	Maps of climatological means, bias terms and trends for spring and autumn/winter blooms based on OC4v6 data (same as figure 3.3 in the main text)	66
3.B.14	Mosaic plots for trends in bloom metrics for spring and autumn/winter blooms based on GSM data	68
3.B.15	Same as figure 3.B.14, but based on OC4v6 data	69

3.B.16 Time trends in mean chl α concentration in the North Atlantic (1998–2012)	70
3.B.17 Association between the sign of trends in mean chl α concentration during the entire year and the sign of trends bloom metrics	70
3.B.18 Importance of environmental variables in explaining changes in bloom metrics	71
3.B.19 Association between spring and autumn bloom metrics and environmental variables	72
3.B.19 Time trends in seasonal averages of environmental variables	74
4.1 Distribution and life cycle of European anchovy in the Bay of Biscay	87
4.2 Anchovy catches in the Bay of Biscay	90
4.1 Summary of best performing models fits on spawning stock biomass	93
4.1 Summary of surrogate analysis of anchovy collapse	95
4.A.1 Spatial domains used to integrate environmental indexes	98
4.A.2 Larval survival index for anchovy recruitment in the Bay of Biscay	99
4.A.3 Map of the attracting finite size Lyapunov exponents	107
4.A.4 Relationship between selected environmental indexes and anchovy larval survival	109
4.A.5 Correlation matrix between selected environmental indexes and anchovy larval survival	111
4.D.1 Posterior estimates of the recruitment function	117
4.D.2 Posterior estimates for models with varying environmental forcing and renewal function	118

Acknowledgements

This work has been possible thanks to the dedicated effort of many people and organizations. I would like to thank first those organizations responsible of the public availability of the databases used in this study and especially their personnel;

- NOAA National Climatic Data Center (NCDC) for the availability, production and maintenance of NOAA-Optimum Interpolation 1/4 Degree Daily Sea Surface Temperature Analysis (OISST version 2), especially Chunying Liu and Richard W. Reynolds.
- NASA Ocean Biology Processing Group, for the availability, production and maintenance of SeaWiFS and MODIS data.
- Physical Oceanography Distributed Active Archive Center (PO.DAAC), especially the people involved in the CCMP MEaSUREs project [see Atlas et al. 2011].
- Centre National d'Etudes Spatiales (CNES); the altimeter products were produced by Ssalto/Duacs and distributed by Aviso with support from CNES.

I would also like to thank the International Commission for the Exploration of the Sea (ICES), especially the Working Group on Southern Horse Mackerel, Anchovy and Sardine (WGHANSA), and the International Commission for the Conservation of Atlantic Tunas (ICCAT), for the production and availability of fish biomass data used in this study. We also acknowledge the use of river discharge data produced by the Directions Régionales de l'Environnement, de l'Aménagement et du Logement (DREAL) and Banque HYDRO, Ministère de L'Écologie, du Développement Durable et de L'Énergie, France.

This work was also possible thanks to a FICYT "Severo Ochoa" grant (PCTI 2006-2009, Gobierno del Principado de Asturias), and has been supported by projects CARPOS, COSTAS and DOS MARES (REN2003-09532-C03-03, CTM2006-05588/MAR and CTM2010-21810-C03-02, Ministerio de Economía y Competitividad, Gobierno de España), and by the project ECOANCHOA (Dirección General de Pesca, Principado de Asturias). I would also like to acknowledge project RADIALES (IEO and Universidad de Oviedo) and the crew of RV José Rioja, that provided a continued opportunity to learn by going to the sea. It is also a good opportunity to acknowledge the professionalism and good times at sea with members of UTM and the crews of RV Hespérides, García del Cid and Sarmiento de Gamboa. In more

academic grounds, I have also benefited from the uninterested help of several anonymous and non anonymous referees; please receive a great thank you. The same can be said with respect to many uninterested people who solved doubts of many people in mailing lists associated to *R* (especially *ggplot2*), *MatLab*, *LATEX* and, of course, Stack Overflow.

At a more personal level, several key events brought me here. I had excellent teachers during my entire academic life from school to university, so this is a good opportunity to apologize for not being myself a diligent and disciplined student in all occasions. After completing the degree in Biology, I spent four months at the Centro Oceanográfico de Gijón (Spanish Institute of Oceanography, IEO) under the supervision of Luis Valdés. I would also like to thank all the personnel there, especially Quique Nogueira, Ángel López-Urrutia, Xelu Morán and Luis Ángel Suárez. Before beginning the PhD, I spent two years at Instituto de Recursos Naturales y Ordenación del Territorio (INDUROT), leaded by Miguel Ángel Álvarez (García). I had there my very first contact with Geographical Information Systems and Remote Sensing technologies. I had really good times with all the people there and would like to thank especially Raúl Martínez and Edyta Wozniak.

At the Department of Biology of Organisms of Systems (BOS) I have spent a long time since 2006, both as a doctoral student and as a graduate teaching assistant. I would like to thank all the people at BOS, especially the current and past members of the Marine Ecology group. I would like to thank professors teaching the subjects I have been involved over these years, especially Ricardo Anadón, Florentina Álvarez-Marqués, Chely Fernández, Alfredo González-Nicieza, and particularly Miguel Ángel Álvarez for his continuous mentorship during the years. José Luis Acuña and the rest of people involved in the Master in Marine Biodiversity and Conservation also deserve a great thank you. I would also like to thank all the office mates –Leticia Viesca, José Herrera, José Rico and Rebeca Fernández– and hope they enjoyed that time at least the same as me. Jorge Sostres also deserved a warm thank you for keeping everything working properly and for his continuous good humor. Finally, a big thank you to my oceanographic friends and colleagues at Oviedo, Juan Höfer, Carlos Cáceres, Ricardo González-Gil and Axa Molina; foray colleagues Leo Blanco, Doug Bruggeman, Francesco Conzo, Mareike Volkenandt and Thorsten Wiegand; and land-based friends Nacho Norniella, Fonso Fernández-Ceballos, Eduardo Sariego and Tania Iglesias.

I have reserved this penultimate paragraph to thank Ricardo Anadón for supervising this work and for his mentorship and help over the years. Ricardo is a great scientist and teacher who piqued my interest in ecology; I wish I have acquired at least part of his qualities.

Finally, I would like to thank my partner Isa and the rest of my family, especially my sister María and my brothers Alfonso and Santiago, as well as my parents, María del Carmen and Alfonso.

Abstract

Earth Observing Satellites gather information of great interest to the study of global change impacts on marine pelagic ecosystems. These observing systems measure different properties of the surface of the ocean at high spatial and temporal resolutions, allowing the study of the dynamics of pelagic ecosystems. In this memoir, we use this general approach to analyze changes in sea surface temperature (SST) and in the phenology of phytoplankton in the North Atlantic during the last decades, as well as to assess the importance of environmental forcing and of overfishing on the recent collapse of Bay of Biscay anchovy. First, we propose a complementary approach to the analysis of changes in SST that emphasizes potential changes in the seasonal cycle and in the spatial distribution of temperature anomalies. We analyzed the NOAA–AVHRR SST series (1982–2010) using our approach to reveal changes in SST that were coherent with those expected under climate change. The statistics analyzed presented a varied response both in intensity and in their spatial distribution depending on whether they represented changes in the mean, the seasonal cycle and the period of stratification, or the spatial structure of the SST field. Then, we introduce a novel method to analyze changes in the seasonality of marine phytoplankton based on ocean color data. The method accounts for uncertainties in the detection and characterization of seasonal peaks based on remote sensing chlorophyll *a* concentration estimates, that was further propagated to estimates of recent trends in phenology. By combining long term series retrieved by SeaWiFS and Aqua MODIS sensors (1998–2013), we detected an increase in the prevalence of seasonal cycles characteristic of subtropical regions at temperate latitudes, as well as changes in the timing and magnitude of seasonal blooms matching climate change predictions. These trends were mainly associated to changes in atmospheric circulation and, to a lesser extent, to changes in irradiance and sea surface temperature. Our approach demonstrated also the greater robustness of semi-analytical chlorophyll algorithms over empirical ones when combining data from different sensors. Last, we analyzed the collapse of Bay of Biscay anchovy combining population modeling with a careful characterization of recent changes in the recruitment environment of this species. Recruitment strength was predicted with relative success after taking into account either changes in plankton phenology and stability in spawning areas during spring, or changes in the drift of anchovy eggs and larvae out of Armorican shelf during summer. Although external environmental forcing on recruitment was a key driver of population fluctuations, overfishing

seems to be behind the collapse of the fishery in 2005. Altogether, our work highlights the need to develop local and regional approaches to analyze global change impacts. From a methodological point of view, it also stresses the advantages of Bayesian analysis techniques to improve natural resource management and conservation, as well as to improve impact detection and monitoring systems. Finally, our work demonstrates the high value of remote sensing data in Oceanography and the importance of a continued support of long term observation programs.

Chapter 1

Introduction

Global change is the major environmental problem that humankind should face during this century [Steffen et al., 2004]. The triad composed by human population growth, increasing resource use and demand, and technological development have lead to a global scale perturbation of the Earth system. This perturbation is associated to a variety of interdependent global impacts like climate change, increased pollution and the so called biodiversity crisis.

Ocean ecosystems are a major component of the Earth system, covering 72% of its surface. They provide several key services that are necessary for our survival and well-being [UNEP, 2006], including among others climate regulation, nutrient cycling and food provision, as well as a variety of cultural services and recreational uses. As a consequence of the excess of atmospheric CO₂ derived from our emissions [Le Quéré et al., 2012], oceans are currently warming at unprecedented rates [Levitus et al., 2009; Hansen et al., 2010]; sea level is rising [Nicholls and Cazenave, 2010]; pH of seawater is decreasing [Feely et al., 2004]; and oxygen minimum and dead zones are expanding [Diaz and Rosenberg, 2008; Stramma et al., 2008]. All these trends are expected to continue in a near future and even to accelerate unless there is a rapid curtail in CO₂ emissions [Sto]. These changes interact with other human driven processes altering ocean ecosystems [Halpern et al., 2008]. Oceans receive human wastes and pollutants [UNEP-GPA, 2006], and have been overexploited for centuries, even leading to the depletion and extinction of some species [Jackson et al., 2001; Jackson, 2008].

Taken together, global change impacts threaten marine ecosystems and affect the services they provide, compromising human well-being [Worm et al., 2006]. This poses the huge challenge to our society of coping with these impacts and, at the same time, being able to preserve and restore marine ecosystems. A first constraint to achieve this goal is our limited knowledge of marine ecosystems and their functioning [Jackson and Jacquet, 2011]. Monitoring and characterizing global change impacts is a first step towards this end. This requires sampling at the small scales where most marine organisms interact

with the environment, as well as those relevant for the development of our activities. At the same time, the ample extension covered by marine pelagic ecosystems and the global scale of some agents of change limit the value of traditional approaches. Until just a few decades ago, it was not possible to sample the oceans at the appropriate spatial and temporal scales. The development of Earth Observing Satellites (EOS) brought a new era to Earth sciences and especially to oceanography [OSB–NRC, 2000; CSAEOS–NRC, 2008], revealing new phenomena and portraying a globally integrated view of ocean ecosystems [Robinson, 2004, 2010; Yoder et al., 2010].

Satellite oceanography brings the possibility of sampling the ocean surface covering wide extents but maintaining a reasonable spatial resolution and short revisit times. Borne on satellite sensors measure five primary properties of the surface ocean [Robinson, 2004]; namely their color, temperature, salinity, roughness and slope. Except in the case of salinity, satellite records of more than a decade long are available for each of these properties. Ocean color actually refers to the retrieval of water leaving radiances to characterize the reflection spectra of surface waters in the visible range [Gordon, 2010]. These spectra can be inverted to derive many variables like the concentration of chlorophyll *a* and dissolved and particulate materials and, more recently, other variables like fluorescence, particle size structure, or the abundance of different phytoplankton groups [McClain, 2009]. Combined with other measurements, ocean color has revealed the complex spatial patterns of distribution of phytoplankton [*e.g.* d’Ovidio et al. 2010], from the influence of mesoscale structures to basin scale processes like seasonal blooms [Yoder et al., 1998; McClain et al., 1990; Yoder et al., 1993]. Also, ocean color is at the basis of most modern estimates of marine primary production [Perry, 1986; Platt and Sathyendranath, 1988], a key component of the global carbon cycle [Falkowski et al., 1998].

Sea surface temperature can be retrieved based on measurements at infrared or microwave wavelengths [Wentz et al., 2000; Casey et al., 2010; Gentemann et al., 2010], and has proved to be of great value to analyze the impact of the ocean on atmospheric climate as well as to monitor global climate change [CSAEOS–NRC, 2008; Stocker et al., 2013]. The microwave emission spectra can be used to retrieve salinity measurements, although EOS missions were launched recently [Lagerloef and Font, 2010]. Microwave instruments measure also surface roughness, a property that can be used to retrieve ocean winds and wave height. These variables are important for an improved characterization of ocean-atmosphere fluxes and to monitor climate change impacts [Liu and Katsaros, 2001; Chelton et al., 2004; Wentz et al., 2007; Young et al., 2011]. Radar altimeters also provide sea height data that allow reconstructing ocean surface topography field. These measurements allow the assessment of long term changes in sea level and, especially, they have provided unique insights on mesoscale variability, ocean circulation and planetary waves [Chelton and Schlax, 1996; Fu, 2010; Le Traon, 2013]. Other sensors like imaging spectrometers and radars are also useful in ocean remote sensing, especially in coastal environments [Hol-

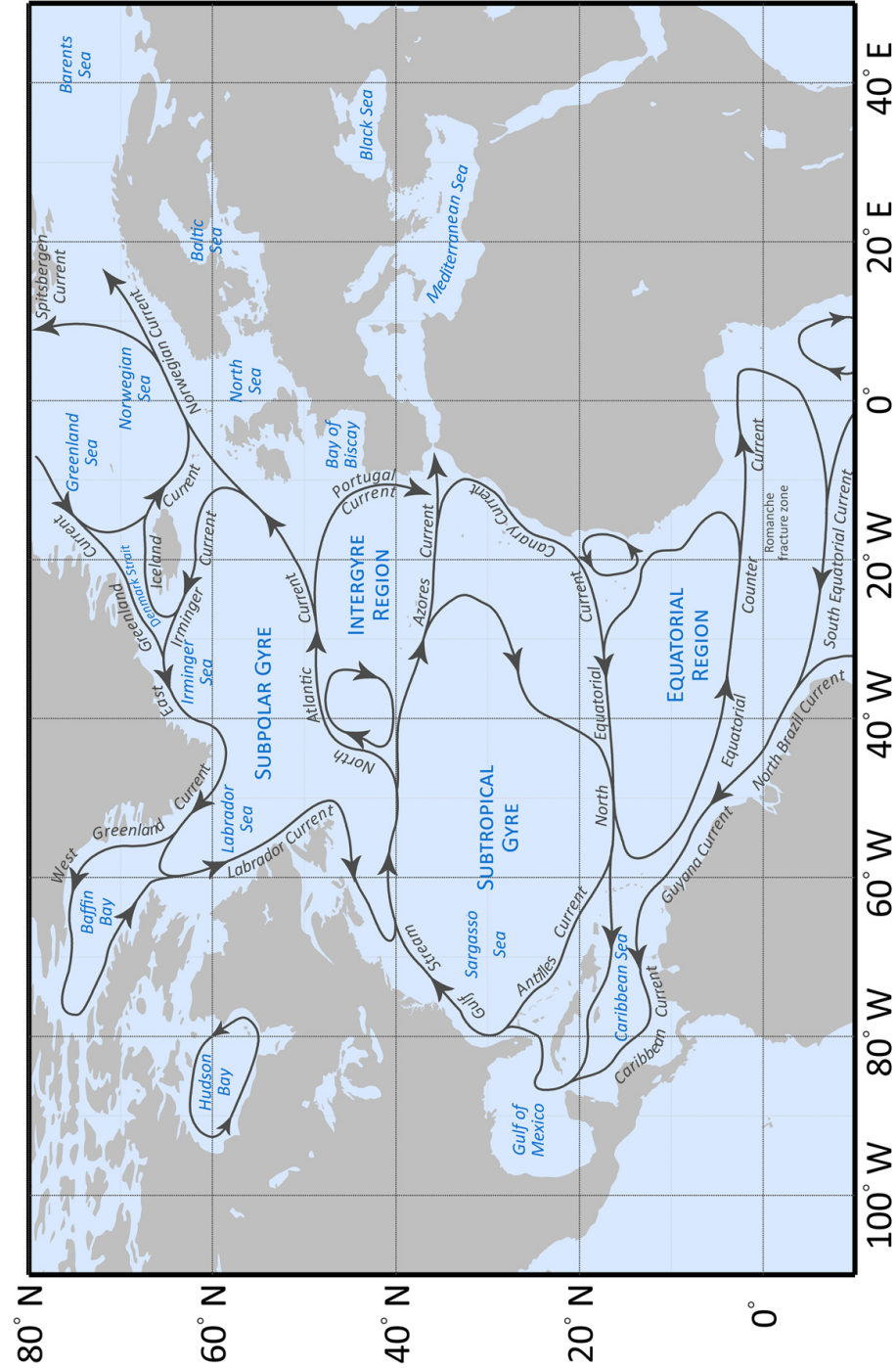


Figure 1.1: Main regions and surface currents of the North Atlantic. Based on Schmitz Jr. and McCartney [1993] and Tomczak and Godfrey [2003].

man and Haller, 2013]. We also omitted deliberately remote sensing measurements of sea ice that rely on a variety of techniques and have great interest in polar regions [Serreze et al., 2007]. This short overview provides just a glimpse of the many advances that satellite oceanography have brought to marine science (see for instance Robinson 2004, 2010 for a complete overview). Also, it is important to note that remote sensing techniques have also proved of great value for the implementation of better management and conservation practices in marine ecosystems [IOCCG, 2008; Morales et al., 2010].

We present here some contributions to satellite oceanography that focus on the application of remote sensing techniques to the study of global change impacts on pelagic ecosystems. We focused on changes in the North Atlantic Ocean and its marginal seas (figure 1.1), that provide a unique setting for oceanographic studies, beyond their long tradition in this region. The major features of the North Atlantic Ocean include (*i*) the well developed subpolar and subtropical gyres, (*ii*) the presence of deep ocean convection regions, and (*iii*) the development each year of a strong spring phytoplankton bloom that, despite the relatively narrow width of the basin, results in nutrient depletion in the mixed layer due to the export of organic materials to deep waters [Schmitz Jr. and McCartney, 1993; Tomczak and Godfrey, 2003; Longhurst, 2007]. Taking advantage of this setting, we studied recent changes in North Atlantic pelagic ecosystems making extensive use of remote sensing data. In contrast to most ocean remote sensing applications, especially those related to climate change studies, we prioritized the small spatial and temporal scales that are relevant to the biological component of these ecosystems. We begin proposing a complementary approach to study changes in sea surface temperature focusing on the seasonal and spatial aspects that might be associated to climate change (chapter 2). Then, we present a novel approach to characterize the seasonality of marine phytoplankton. The method accounts for the particularities of ocean color data, and it was used to highlight recent changes in the phenology of North Atlantic ecosystems (chapter 3). In the last major chapter, we combined previous approaches with state of the art fisheries modeling to analyze the recent collapse of the anchovy fishery in the Bay of Biscay (chapter 4). Each chapter can be read independently and provides a detailed introduction and discussion of each specific topic. The last chapter provides an overall discussion of the main findings and results, and highlight the main conclusions reached (chapter 5).

1.1 Objectives

- Provide an analysis of recent changes in sea surface temperature in the North Atlantic Ocean and adjacent seas, with a focus on spatial and temporal scales appropriate to understand the response of ocean ecosystems to global change.
- Develop an approach based on ocean color remote sensing data to study plankton phe-

nology that accounts for uncertainty in these products as well as for sampling biases. Based on this approach, analyze recent changes in the phenology of North Atlantic phytoplankton.

- Assess the importance of different mechanisms on the recent collapse of European anchovy (*Engraulis encrasicolus*) in the Bay of Biscay, taking advantage of remote sensing data to characterize changes in its environment.

Chapter 2

Sea surface temperature in pelagic ecosystems

Abstract Sea surface temperature (SST) is an important indicator of changes in the climate system and a key driver of marine ecosystems. Here we studied the strength and spatial patterns of changes in North Atlantic SST during the last three decades (1982–2010). Regional and local patterns of change were studied using data derived from the Advanced Very High Resolution Radiometer (AVHRR) sensors. Apart from changes in mean SST, we studied changes in the seasonal cycle, in the spatial patterning of temperature anomalies and in the location of selected isotherms. We quantified the degree of nonlinearity in mean SST as an indicator of the rate at which SST trends changed during the study period. Changes in the timing and intensity of seasonal extremes were explored, and a heuristic method was used to derive the length of the period of stratification and to estimate its variation. Our results were in general coherent with the main impacts predicted by climate change projections, with greatest changes located at northern latitudes and near land. Marked variation in the spatial patterns was also found for different variables, strengthening the view that physical changes could be promoting the arrangement of novel marine biological communities. The observed changes in ocean SST highlighted the need of a more local and regional focus in future climate change studies.

Keywords Advanced Very High Resolution Radiometer, Climate change impacts, North Atlantic Ocean, Sea Surface

2.1 Introduction

The oceans have been warming at rates of an unprecedented magnitude during the last decades. This signal is now detectable at greater depths and in pelagic, remote zones far from the coastline [Barnett et al., 2005; Levitus et al., 2005, 2009; Hansen et al., 2006; Good et al., 2007; Gouretsky and Koltermann, 2007]. These trends reflect changes in energy and mass fluxes which are disrupting ocean circulation patterns [Hakkinen and Rhines, 2004, 2009; Toggweiler and Russell, 2008]. Increases in ocean temperature are related to other impacts of human-induced global change. It has been shown that the steric component is

an important driver of recent sea level rise [Cabanes et al., 2001; Milly et al., 2003; Milne et al., 2009; Nicholls and Cazenave, 2010], and that increasing temperatures might enhance the effects of increased ocean alkalinity [Feely et al., 2004; Doney et al., 2009; Omta et al., 2011].

Ocean warming is more than a homogeneous increase in temperature. It is expected to alter seasonal extremes and patterns of stratification, and to promote that oceans become more homogeneous in space [Sarmiento et al., 1998; IPCC, 2007]. These aspects are of great concern, especially for the maintenance of ecosystem function and biological diversity [Parmesan, 2006; Philippart et al., 2007, 2011]. Species extinctions and range shifts have been identified as one of the components of dangerous anthropogenic interference with climate, given its practical irreversibility and potential impacts (*sensu* Hansen et al., 2006; see also Smith et al., 2009). For those species in which distributional limits are constrained by thermal tolerance, local temperature extremes and short time scale oceanic variations will be more important than long term trends extracted from regional averages [Easterling et al., 2000].

More subtle effects on species performance induced by increased temperature might promote reduced biological CO₂ influx [Sarmiento et al., 1998; Behrenfeld et al., 2006] and enhanced N₂ fixation [Hood et al., 2004; Deutsch et al., 2007]. The regulation of food webs is also modulated by ocean temperature through bottom-up effects [Frank et al., 2007; Longhurst, 2007], as well as through mismatches associated with the spatiotemporal decoupling of species interactions [Platt et al., 2003; Durant et al., 2007]. Long-term sampling programs have found that these impacts are currently occurring in the ocean [Easterling et al., 2000; Beaugrand et al., 2002, 2008; Hiddink and Ter Hofstede, 2008; Thackeray et al., 2010], while projections of modeling studies suggest even worse impacts for the near future [Boyd and Doney, 2002; Sarmiento et al., 2004; Schmittner, 2005; Litchman et al., 2006]. In nearly all cases, future projections have ignored changes in species composition and in their relative abundances, despite the potential highly nonlinear effects associated [Verity and Smetacek, 1996; Drake et al., 2005; Duffy and Stachowicz, 2006; Brander, 2007].

The comparison of changes in ecologically meaningful climate variables is a first step to assess whether changes in the physical environment could be promoting the assemblage of novel marine communities [Williams and Jackson, 2007; Williams et al., 2007]. Finer resolution in time and space is necessary to properly study changes in the timing of the seasonal cycle or in spatial patterns [Selig et al., 2010]. The development and maintenance of long term observational programs based on satellite sensors allows such inferences (Kilpatrick et al., 2001; Casey et al., 2010; McClain et al., 2004a). Satellites bring together information on several variables [Robinson, 2004, 2010; Barale et al., 2010], which can be used to derive different indexes to study impacts [Halpern et al., 2008], and to explore to what extent current changes in the ocean are coherent.

In this study, we use data retrieved with AVHRR sensors to examine recent changes

on sea surface temperature (SST) in the North Atlantic Ocean and adjacent seas. Previous analyses of AVHRR data have focused mainly on trends in mean SST, and devoted most of their attention to the wide scale and regional patterns appropriate for climate studies [Good et al., 2007; Casey and Cornillon, 2001; Lawrence et al., 2004]. On the other hand, few studies have focused on the analysis of indexes derived from spatial and temporal scales appropriate to understand the effects of climate on ecosystem functioning and management [Halpern et al., 2008; Selig et al., 2010]. Here, we focus on statistical measures, apart from the mean, which could play an important role in the response of ocean ecosystems to global change. We studied changes in the seasonal cycle, in the spatial patterning of temperature anomalies and in the location of isotherms. With this approach, we expect to infer whether changes in SST are altering species distributions and/or their temporal overlap in an idiosyncratic way. We also expect to identify regions where changes have been more acute and thus, where greater impacts can be expected.

2.2 Materials and Methods

2.2.1 Sea surface temperature data

We employed sea surface temperature (SST) time series derived from the NOAA-Optimum Interpolation 1/4 Degree Daily Sea Surface Temperature Analysis (OISST version 2). The methods employed to derive SST are described in Reynolds et al. [2007]. The database of SST images is produced and maintained by C. Liu and R. W. Reynolds at National Climatic Data Center (NCDC, www.ncdc.noaa.gov/sst). The SST analysis is computed daily in a quadrangular grid of 0.25° resolution (*i.e.* ~27.5 km at the Equator). The analysis is based on combining satellite SST data with *in situ* measurements from ships and buoys collected in the International Comprehensive Ocean-Atmosphere Data Set (ICOADS, icoads.noaa.gov). In ice covered zones, SSTs are derived as a function of sea ice concentration. Two different SST products are produced depending on the origin of satellite SST observations. The first one is based only on Advanced Very High Resolution Radiometer (AVHRR) data from the Pathfinder Version 5 dataset [Casey et al., 2010], which is available from November 1981. The second product blends AVHRR data with SST retrievals from the Advanced Microwave Scanning Radiometer (AMSR). Despite the fact that the inclusion of AMSR data improves the quality of OISST in cloudy regions, it is only available from June 2002. Thus, we used the product based only on AVHRR data to ensure temporal homogeneity [Reynolds and Chelton, 2010]. A box covering 110°W 10°S to 50°E 80°N was selected to study SST variation in the North Atlantic (Fig. 1.1; Schmitz Jr. and McCartney 1993; Tomczak and Godfrey 2003). Data were reordered to obtain individual daily time series at each pixel location between January 1982 and December 2010, which were later analyzed as described below. Changes in both cell area and intercell distances with latitude were accounted for in all the

calculations presented using a spherical approximation to the shape of the Earth [Banerjee, 2005].

2.2.2 Derived indexes and estimation of trends

We estimated changes in the following variables and indexes for the SST time series at each pixel location: (*i*) mean SST; (*ii*) rate of change of the trend in mean SST; (*iii*) seasonal SST maxima, (*iv*) seasonal SST minima, (*v* and *vi*) Julian day of SST maxima and minima; (*vii–ix*) location of isotherms for selected levels of annual mean SST and of seasonal extremes; (*x*) extent of the seasonal SST range; and (*xi*) duration of the period of stratification. We further analyzed variables *i*, *iii* and *iv* to estimate spatial scales of decorrelation for each season (*xii–xiv*), to later study its time evolution. We estimated a linear trend at each pixel location using simple, robust linear regression of each variable on time using Tukey's bi-weight function to weight the influence of residuals in the estimation of model parameters [Street et al., 1988]. Daily anomalies were derived using a daily climatology to estimate changes in mean SST. In the case of the rate of change of the trend in mean SST, we included a quadratic term in the trend (*i.e.* $SST_t = a + bt + ct^2$) to later derive a constant rate of change of the trend in mean SST. Although not shown, both models resulted in a similar goodness of fit.

The timing of the seasonal maxima was determined using yearly subsets, while the seasonal minima were later located within inter-maxima periods. We recorded the timing (calendar day) and intensity (temperature in Celsius degrees). In regions and years with continuous coverage of sea ice (*i.e.* a prolonged period with $SST = -1.8^\circ\text{C}$), the timing of SST minima was taken as the first day with 100% sea ice coverage. Prior to trend estimation, the timing of extremes was standardized as deviations from the middle (maxima) and beginning (minima) of each year. Finally, we constructed maps of the mean and seasonal maximum and minimum SST for each year from which we estimated a climatological map for each variable. For both the annual and the climatological maps, we extracted the position of isotherms covering the range $-1.5\text{--}30^\circ\text{C}$ in 0.5°C steps. The location of isotherms was estimated for each longitude of the original 0.25° grid. Deviations from the climatological location of each isotherm were then collected to estimate zonal and meridional components of isotherm migration during the study period. The estimated rates of migration were then integrated over each reference temperature level to estimate mean migration rates for each isotherm. In addition, the rates of migration were mapped by assigning each value to the mean position of the corresponding isotherm. These values were later linearly interpolated to estimate changes in the rate of migration with latitude and longitude.

The length of the time series analyzed in this study facilitated in some way the justification of the trends obtained by deriving significant p -values, given the great number of data points available in some cases. Nevertheless, we opted to not comment on the statistical

significance of our results and instead stress the need to interpret our results with caution, given the short time window analyzed (29 years) and the transient nature and long memory of any climatic signal (*e.g.* Wunsch, 2001).

2.2.3 Decorrelation scales

Seasonal maps of mean, minimum and maximum SST were further analyzed to estimate spatial decorrelation scales using variograms, *i.e.* a function that describes spatial dependence. If it is assumed that the variable under study is intrinsically stationary (there is no spatially structured variation in the mean) and isotropic (values do not vary preferentially in a particular orientation), spatial correlation, and the variogram, can be modeled as a function that only depends on geographical distance. We used a second order polynomial on a 5 x 5 degree moving window to remove spatial trends in the data before estimating the robust empirical variogram following Cressie and Hawkins [1980],

$$2\gamma(d) = \left(\frac{1}{|N_d|} \sum_{(s_i, s_j) \in N_d} |s_i - s_j|^{0.5} \right)^4 / \left(0.457 + \frac{0.494}{|N_d|} \right) \quad (2.1)$$

where $\gamma(d)$ is the estimated semivariogram value for the distance class d ; N_d is the set of $|N_d|$ pairs of distinct points s_i and s_j which pertain to the same distance class. The denominator is a Gaussian bias adjustment. These empirical values were fitted using nonlinear least squares to a Gaussian semivariogram model,

$$2\gamma(d) = \begin{cases} \tau^2 + \sigma^2(1 - e^{-\phi^2 d^2}) & \text{if } d > 0 \\ 0 & \text{otherwise} \end{cases} \quad (2.2)$$

where τ^2 is the nugget, which represents covariance at scales less than those resolved by the data at hand; $\tau^2 + \sigma^2$ is the sill, the asymptotic semivariogram value (σ^2 is the partial sill); and ϕ is the decay parameter, which can be used to define the range or decorrelation scale as $R = \sqrt{3}/\phi$, *i.e.* the distance at which the correlation has dropped to 0.05 [Banerjee et al., 2004]. This last quantity was retained because spatial variation in its value reflects differences in spatial structure. Estimated ranges for each pixel were then rearranged to analyze its temporal variation using the methods described above (Section 2.2.2).

2.2.4 Proxy for the duration of the period of stratification

The analysis of the SST time series was completed by studying the variation in the duration of the period of stratification. The seasonal stratification of surface waters is tightly

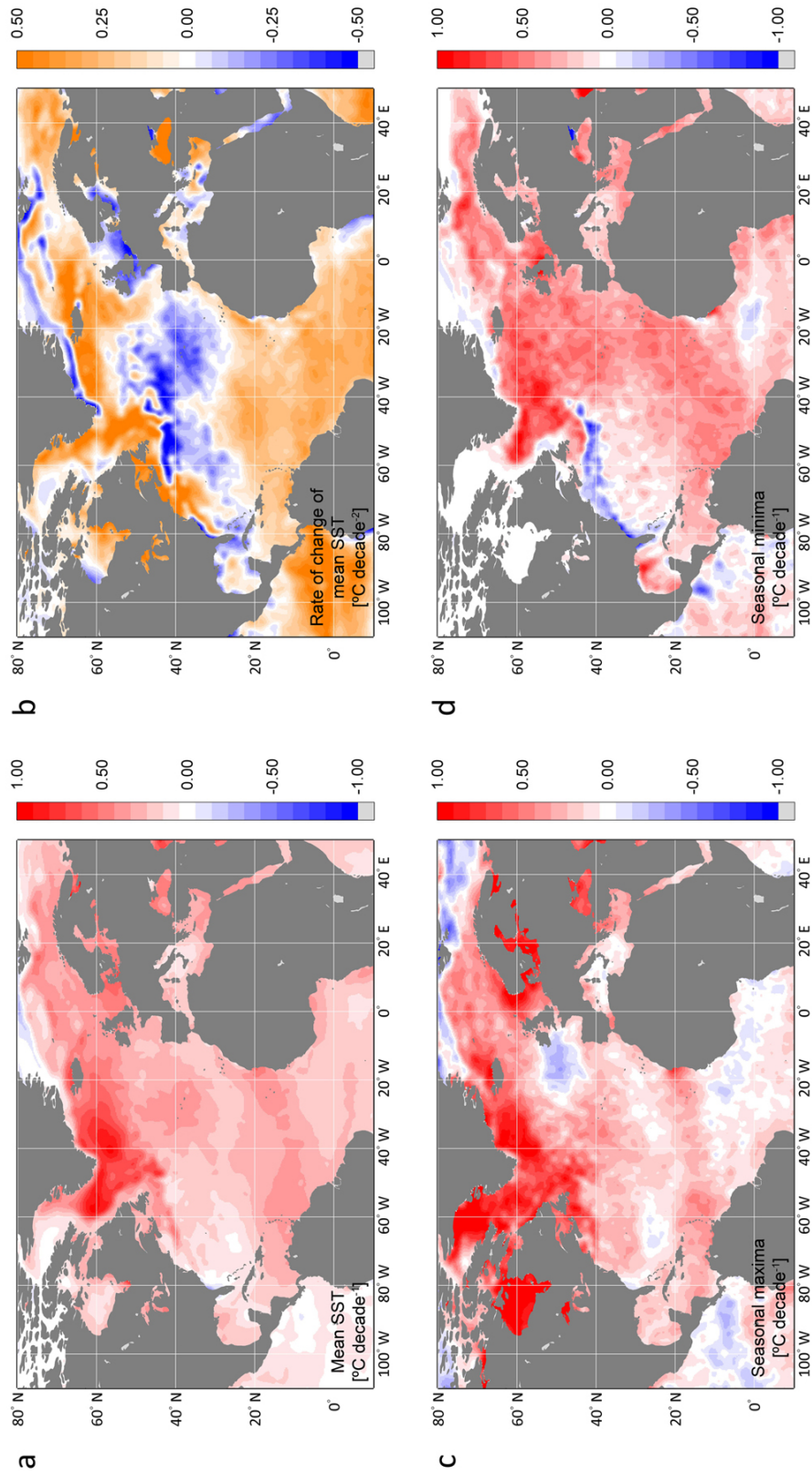


Figure 2.1: Maps of estimated linear trends for (a) changes in mean sea surface temperature (SST) [$^{\circ}\text{C decade}^{-1}$]; (b) for the rate of change of mean SST, estimated using a potential model to fit the trend [$^{\circ}\text{C decade}^{-2}$]; and for linear trends in seasonal (c) maxima and (d) minima [$^{\circ}\text{C decade}^{-1}$]. Zones without enough data for estimation were colored in light gray.

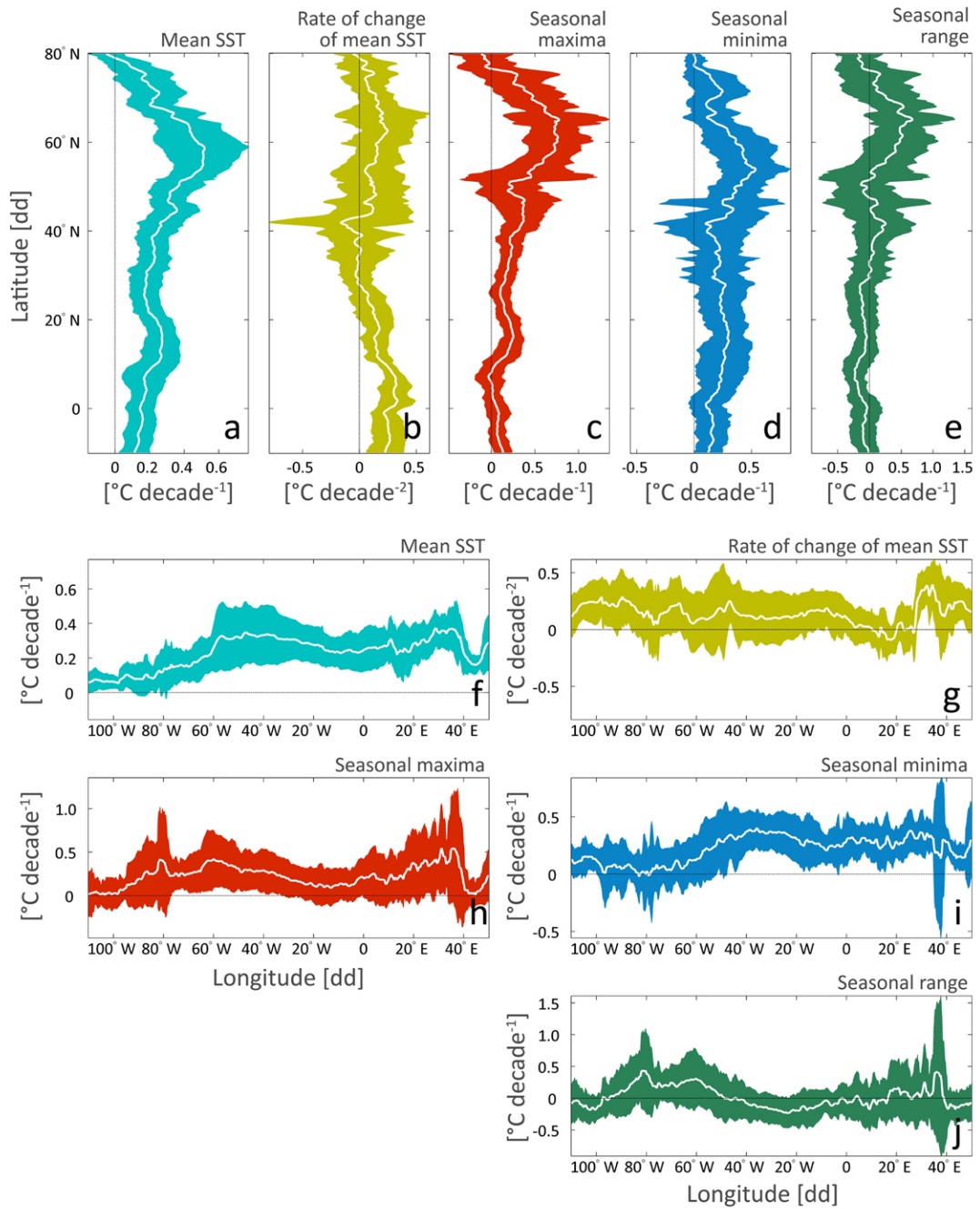


Figure 2.2: Zonal (a-e) and meridional (f-j), area corrected averages (\pm SD) of trends for indexes related to changes in sea surface temperature (SST) magnitude. Note that axis scales differ among indexes.

linked to biological activity, with prolonged stratification usually associated with nutrient depletion and lower production [Longhurst, 2007]. The period of stratification is defined by the formation of a shallow, seasonal mixed layer delimited by the depth at which wind stress mixing occurs. Temperature dominates density variation for most of the region under study, except for northern latitudes influenced by ice melting, and other localized areas affected by upwelling or by the discharge of large rivers. Common methods to determine mixed layer depth (MLD) are based on the analysis of profiles of temperature, salinity or density [Thomson and Fine, 2003]. The most simple method consists in the application of a threshold temperature increase (ΔT) with respect to surface temperature, usually taken as the temperature at 10 m depth. Satellite data only provide near surface temperature values [Kilpatrick et al., 2001; Rayner et al., 2003], thus complicating the characterization of the vertical structure (see Chu et al., 2000).

This limited our approach to a crude proxy of the duration of the period of stratification, which is based on the following rationale. During winter, and especially at the timing of winter minima, a deep convective homogeneous layer is developed that, in some places, reaches the permanent thermocline. As winter progresses towards spring, solar warming and reduced storminess promote the sudden development of a seasonal mixed layer that survives until autumn, when stronger winds destabilize and break up the seasonal thermocline. These events define the onset and ending of the period of stratification. Thus, we can assume that at the time of the winter minimum SST, the column is well mixed and there is no upper stratification (or at least, not above the photic layer). If we further assume that this value is representative of the temperature conditions under the seasonal pycnocline, we could apply the same ΔT used to define MLD from profile data to SST time series. In this way, the onset stratification would coincide with SST rising ΔT degrees above the seasonal minimum. Note that we are ignoring a variety of factors which could alter seawater temperature below the seasonal thermocline, like the advection of waters with different properties, mesoscale features and short term variability. We also assumed that satellite based SST values were not affected by diurnal stratification events and, in this way, they can be considered nearly equal to temperature at 10 m. This last assumption is weaker in summer months, although OISST is bias adjusted to avoid any diurnal signal in SST [Reynolds et al., 2007].

Among the various ΔT estimates available, we chose $\Delta T = 0.5^\circ\text{C}$, as proposed by Levitus [1982]. This value is intermediate between other proposals, although the value chosen did not alter our main conclusions (e.g. $\Delta T = 0.2$ or 0.8°C , as proposed by Kara et al. [2000] and de Boyer Montégut et al. [2004], respectively). To determine the end of the period of stratification we could not rely on the same reasoning advocated to determine its onset, and thus employed a much cruder, practical approach. Specifically, we assumed that the seasonal thermocline erodes as SST decreases from the seasonal maximum towards the minimum, and that when this descending curve has attained the middle of this SST range, surface

stratification is no longer present. The idea was based on the sudden reduction in SST rate of change expected when mixing extends in depth, although estimates based directly on empirical SST time derivatives resulted in misleading results. Because we used next year minima to determine the end of the period of stratification, the length of this yearly time series was reduced in two points. For all the caveats exposed, and also stressing that advection has been completely ignored, this estimate should be considered only as a proxy, although we prefer it to the time between seasonal SST extremes, given that it incorporates the sudden transitions in SST at the onset and end of the period of stratification.

2.3 Results

2.3.1 Mean SST

Linear trends in mean SST revealed a widespread process of warming in the North Atlantic Ocean during the last three decades (Figs. 2.1a and 2.2a,f). The Gulf Stream front, the subpolar gyre and Labrador Sea on the western margin, and the European continental shelf above 50°N in the east, presented the highest warming rates, with values well above 0.50°C decade⁻¹ (Fig. 2.1a; see Fig. 1.1 for the location of the main regions and surface currents referred). The estimated nonlinear trends suggested a decrease in the rate at which SST has been increasing at some of the regions presenting a rapid change in mean SST (Fig. 2.1b). This response was observed in most of the European shelves (North Sea, Baltic Sea, and central Mediterranean) and in the temperate North Atlantic, with the exception of an eastern fringe coincident with the returning track of the Portuguese Current (Fig. 2.1b). Nevertheless, the rate of change in mean SST has increased in most of the North Atlantic. The rate of change in mean SST was slightly positive in the tropical and equatorial North Atlantic and in the eastern Mediterranean, with values around 0.25°C decade⁻². Changes in the trend were also positive and higher in the Black Sea, in the Gulf Stream region and in the subpolar gyre, with values above 0.50°C decade⁻². On the other hand, Eastern Greenland and Florida margins were recognized as areas with a decreasing trend in mean SST. The rate of northward migration of annual mean SST isotherms was in general positive and greater than 50 km decade⁻¹, with two peaks around 20° and 50°N (Figs. 2.3a and 2.7d,h). These regions corresponded to the migration towards the northwest of isotherms corresponding to temperatures near 25°C and to the migration towards the northeast of isotherms near 10°C (Figs. 2.3a and 2.4a,d).

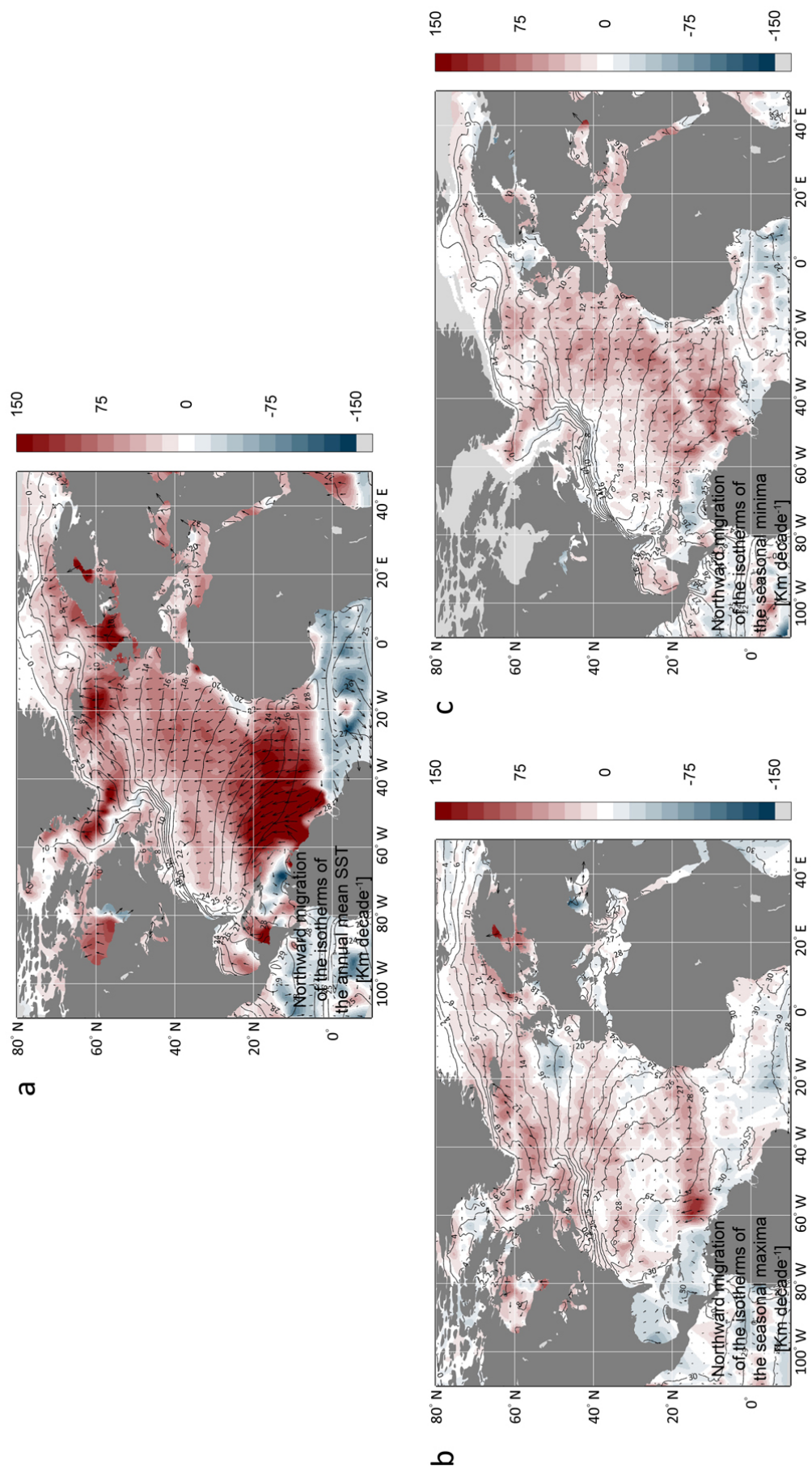
2.3.2 Seasonal SST extremes and seasonal range

The changes observed in seasonal maxima and minima paralleled trends in mean SST to some extent (Fig. 2.1c-d, Pearson product-moment correlation, $r = 0.49$ and 0.64 , respec-

tively), although there were important differences in the magnitude of these changes. Also, changes in maxima and minima were nearly unrelated between them ($r = 0.06$). The highest rates of change in seasonal maxima were located in the subpolar gyre, northern Iceland, and in semi enclosed seas such as the North Sea and the Baltic Sea, and Hudson Bay and Baffin Bay (Figs. 2.1c and 2.2c,h). Within these areas, seasonal maxima trends were even greater than $1.00^{\circ}\text{C decade}^{-1}$, and the rate of northward displacement of isotherms of SST maxima was in general greater than $50 \text{ Km decade}^{-1}$ (Figs. 2.3b and 2.7e,j). The magnitude of the seasonal maxima increased almost everywhere in the rest of the North Atlantic, although rates were much weaker. Seasonal maxima decreased in some northern regions of the Greenland Sea and of the Barents Sea, in the intergyre region in the Northeast Atlantic, in the Mediterranean Sea, in the southern subtropical gyre and in the eastern equatorial region. The changes observed in the seasonal minima were much more homogeneous in space, with increases in the entire North Atlantic basin except in the Gulf Stream region and in the equatorial Atlantic, near the Romanche fracture zone. As expected, changes were weaker near the ice margin and on ice-covered regions at northern latitudes. Linear trends in the seasonal minima were positive and high in the rest of the North Atlantic (Figs. 2.1d and 2.2d,i). In the Labrador Sea, the seasonal minimum increased more than $0.50^{\circ}\text{C decade}^{-1}$. Northward migration of seasonal minima isotherms was especially intense in the tropical, eastern and northern North Atlantic (Figs. 2.3c and 2.7f,l). No clear pattern emerged for individual isotherms (Fig. 2.4c,f).

Patterns in the seasonal range of SST summarized the observed changes in maxima and minima (Figs. 2.2e,j and 2.5a). The map clearly shows a general pattern of increased seasonal variability near continental shelves on both sides of the North Atlantic. The rates of change in this variable were mainly related to changes in the seasonal maxima ($r = 0.79$ vs. $r = -0.51$ for seasonal minima), and they were nearly unrelated to changes in mean SST ($r = 0.05$). The seasonal range increased more in northern semi enclosed seas like Baffin Bay and the Baltic Sea, and in the Gulf Stream front, with values which in some cases were above $1.00^{\circ}\text{C decade}^{-1}$. Other areas with high rates of increase of the seasonal SST range included the Greenland Sea and the Grand Banks, where rates were above $0.5^{\circ}\text{C decade}^{-1}$. Changes were weaker in other areas with positive rates. Reduced variability in the seasonal

Figure 2.3 (following page): Isotherm migration for (a) mean, (b) maximum and (c) minimum sea surface temperature (SST) during the period 1982-2010. Migration rates were estimated for isotherms covering the range $-1.5\text{--}30.0^{\circ}\text{C}$ in 0.5°C steps, based on a time series of deviates from the climatological location of each isotherm. The background surface presents the northward component of migration rates, while the arrows integrate the zonal and meridional components. Both the surface and the arrows were linearly interpolated from rates estimated for the mean location of each isotherm; some reference contours were included as a guide. Zones without enough data for estimation were colored in light gray. Rates are expressed in [Km decade^{-1}]; an arrow length of three decimal degrees roughly corresponds to a migration rate with a magnitude of at least $150 \text{ Km decade}^{-1}$. Figure 2.4 shows integrated trends for each isotherm, while Fig. 2.7 presents zonal and meridional averages of the northward components integrated for different isotherms.



cycle was found in most of the tropical North Atlantic and in most of the eastern margin, including the Mediterranean Sea and the southern North Sea. These areas corresponded in general to zones where seasonal minima increased at rates higher than the seasonal maxima (Figs. 2.1c,d). Except for Barents Sea and Norwegian Sea (where rates were as high as $-0.75^{\circ}\text{C decade}^{-1}$), rates were relatively greater than $-0.5^{\circ}\text{C decade}^{-1}$.

2.3.3 Changes in decorrelation scales

The spatial range of mean SST and seasonal extremes provide estimates of the distance at which values at two different locations can be regarded as independent. Positive trends in these indexes reflect thus a local homogenization of SST conditions, while negative trends correspond to areas which have become spatially more heterogeneous. Figure 2.6 presents maps showing the different patterns for the response of mean SST and the seasonal extremes. Detected changes were nevertheless important, representing deviations between a 2.5 and a 5.0% change from mean conditions. In the case of annual mean SST, changes in the spatial range indicated a trend towards greater spatial variability, especially in the subtropical and temperate North Atlantic. Nevertheless, spatial homogenization was found in most of the tropical North Atlantic and in the eastern subpolar gyre. Positive trends predominated when analyzing changes in the spatial patterning of seasonal extremes, especially in the case of the seasonal minima. Increases in the spatial range of seasonal minima were especially important on both sides of the subtropical North Atlantic. Nevertheless, greater heterogeneity was found for some regions like the Gulf Stream front or the North Sea. In the case of the seasonal maxima, spatial homogenization increased mainly in the subpolar gyre, the eastern subtropics and Barents Sea.

2.3.4 Timing of SST extremes and duration of the period of stratification

Timing statistics revealed still more heterogeneity in changes in seasonal SST cycles in the North Atlantic (Figs. 2.5 and 2.7). Seasonal maxima tended to occur earlier (negative values in Fig. 2.5c) in the subpolar gyre, Greenland Sea, tropical and equatorial Atlantic, the western subtropical gyre and the western Mediterranean Sea. Trends toward delayed seasonal maxima were found in most of eastern subtropical gyre, the Iberian margin, Norwegian Sea and in northern semi enclosed seas. Estimated rates of delay for the seasonal maxima were up to $5 \text{ days decade}^{-1}$ in these zones. The rates of delays and advancements were much larger in the case of seasonal minima (Fig. 2.5d), with magnitudes in excess of $\pm 10 \text{ days decade}^{-1}$. High, positive rates indicating later occurrence of the minima were observed in the western subtropical gyre and for most regions north of 40°N , in the western Mediterranean, and along the eastward returning flow of the subtropical gyre. On the other hand, advanced minima were found in some northern regions like Baffin Bay, Hudson Bay and

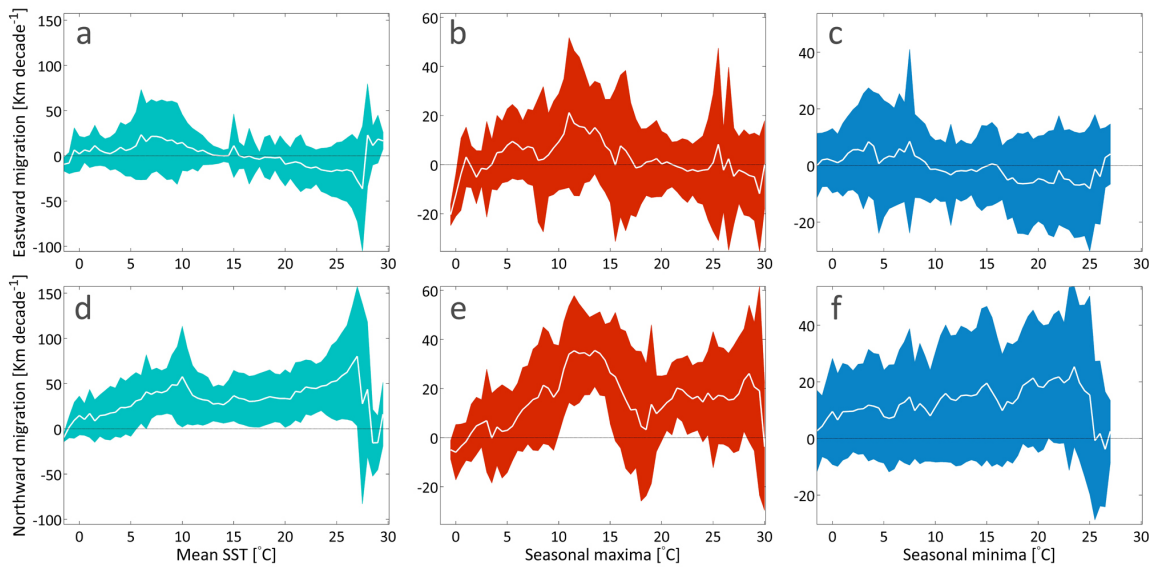


Figure 2.4: Eastward (a-c) and northward (d-f) migration rates ($\text{mean} \pm \text{SD}$, [Km decade^{-1}]) averaged for isotherms corresponding to different temperature levels of (a,d) annual mean sea surface temperature (SST), and of seasonal (b,e) maxima and (c,f) minima. Only data from isotherms located north of 10°N were considered for the integration. Note that the y-axis scale differ among indexes. Maps representing the spatial variation in isotherm migration are presented in Fig. 2.3.

in some parts of Greenland Sea and Barents Sea. Earlier minima were also found in most of the subtropical North Atlantic, the Bay of Biscay and the intergyre region, and in the eastern tropical and equatorial Atlantic. It should be noted that in regions fully covered by sea ice in winter, the date of the minimum was taken as the day when maximum ice coverage was attained. Thus, the observed trends for northern regions indicate mainly a delay or an advancement in the formation of the ice cap.

Changes in the proxy of the duration of the seasonal period of stratification were also highly heterogeneous in space, with a trend towards longer periods of stratification in most of the regions north of 40°N , in the equatorial region and in almost all the semi enclosed waters. Shortened periods predominated in the border of the subtropical gyre, especially in the Azores front and in the eastward returning flow around 20°N , as well as in the western Mediterranean Sea. In both cases, the estimated rates were as high as ± 20 days decade^{-1} . When the relation between these rates and those estimated for the other variables was analyzed, no clear relationship emerged, especially in the case of the timing of the seasonal extremes. Only the rates of change in the duration of the period of stratification showed a slight relationship with changes in the intensity of seasonal minima ($r = -0.24$).

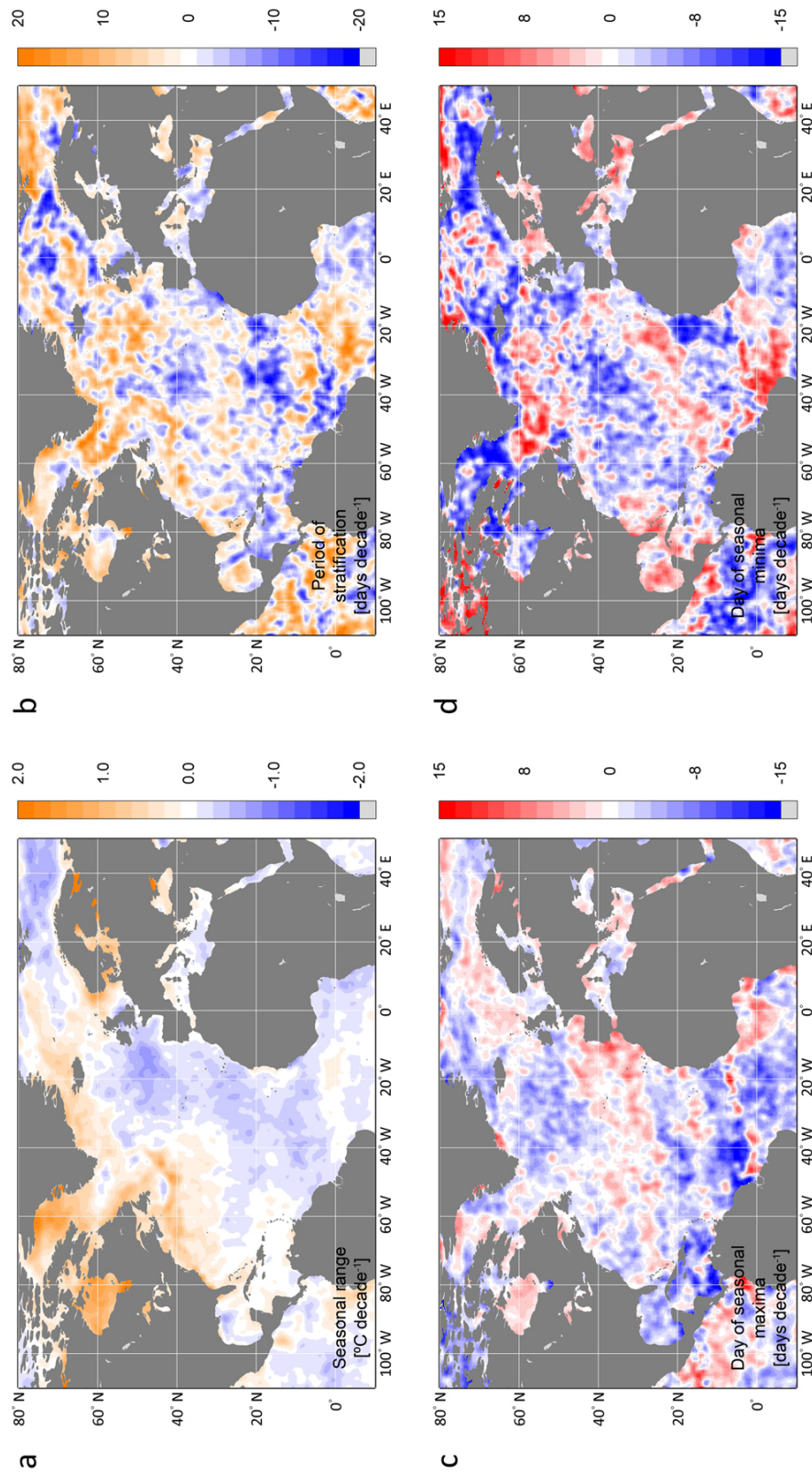


Figure 2.5: Maps of estimated linear trends for (a) the change on the seasonal range in sea surface temperature [$^{\circ}\text{C decade}^{-1}$]; (b) a proxy for the duration of the period of stratification [days decade^{-1}]; and for the changes in the timing of seasonal (c) maxima and (d) minima [days decade^{-1}]. Positive and negative rates in (c) and (d) correspond to a later or earlier occurrence of seasonal extremes. Zones without enough data for estimation were colored in light gray.

2.4 Discussion

The use of satellite data allowed us to perform a synoptic study of SST variation in the North Atlantic basin using nearly three decades of infrared satellite data. Despite the short time window considered (1982-2010), our results confirmed previous studies as well as model based climate change predictions [IPCC, 2007]. In this way, warming of surface waters in the North Atlantic is a widespread process, especially at higher latitudes and in coastal areas [Barnett et al., 2005; Levitus et al., 2005; Hansen et al., 2006; Good et al., 2007; Gouretsky and Koltermann, 2007; Toggweiler and Russell, 2008]. The rates of increase have been accelerating for most of the North Atlantic (72.4% of the surface), except at mid latitudes in the open ocean and in the Atlantic European shelf. This process might be explained in terms of an increased heat content derived from anthropogenic disturbance and an enhanced transport of the excess energy absorbed in the subtropics towards northern latitudes [Hansen et al., 2006; Toggweiler and Russell, 2008], overlapped with fluctuations in long term climate modes like the North Atlantic Oscillation (NAO) [Hurrell and Dickson, 2005; Visbeck et al., 2006; Hurrell and Deser, 2009b].

The patterns obtained when other aspects of SST were considered resulted in more complex responses. For instance, changes in mean SST and seasonal SST extremes were not coherent in space. The same occurred for timing statistics, which changes were indeed nearly independent of mean SST. Changes in other indexes were more subtle, like the trend towards a greater spatial homogenization. Nevertheless, our analyses of spatial decorrelation scales revealed that North Atlantic SST is becoming more homogeneous in space, especially in the case of seasonal extremes. To our knowledge, the long term behavior of these kind of events has received little attention, although our results suggest they are an important factor in assessing climate change impacts. Despite the great resolution of satellite data, it has the inconvenience of providing only a surface view. Some of the patterns found, especially those showing a contrasted pattern between the response of subpolar and subtropical gyres, can be explained in terms of recent trends in the NAO [Visbeck et al., 2006; Hurrell and Deser, 2009b]. Nevertheless, the nature of our approach limits any mechanistic inference and, given the results obtained, highlights the importance of modeling approaches focused on regional scales [Christensen et al., 2007].

Studies of atmospheric dynamics have shown that warming has been more important in winter temperatures [Michaels et al., 1998; Stine et al., 2009]. Our analyses of recent SST variation resulted in rates of change for seasonal maxima and minima which to some extent presented a similar spatial pattern to those found when analyzing mean SST. Nevertheless, the absolute value of these rates of change was quite different, and changes in maxima and minima did not match spatially among them. As a consequence, changes in the seasonal SST range were not related to changes in mean SST. The magnitude of the seasonal minima changed at a rate greater than the rate estimated for the seasonal maxima in

a great portion of the North Atlantic (61.5% of the area analyzed), although this percentage changed radically when considering only data from northern latitudes (*e.g.* the rate for the seasonal maxima were greater in a 71.7% of the area for regions north of 60°N). At the same time, isotherm migration was greater for both mean SST levels and seasonal extremes in the tropical and subpolar North Atlantic. This result confirms and expands previous evidence based on satellite ocean color data, which have revealed an expansion of subtropical gyres during the last decade [McClain et al., 2004b; Polovina et al., 2008]. Thus, our results suggest that during the last three decades, changes in the ocean have been more important during winter in tropical and subtropical regions, and during summer in the subpolar and polar ocean.

Potential changes in the timing of the different events characterizing the seasonal cycle have received much less attention than trends in mean levels [Stine et al., 2009]. The timing of seasonal extremes showed marked contrasts in both the spatial patterning and the magnitude of the rates of change. Indeed, both advancements and delays were in general greater in the case of the timing of the seasonal minima, indicating that changes were more important in winter. As a consequence of the variation in timing, it can be expected that the duration of the seasonal period of stratification was also altered. The duration of this period is a key variable for the functioning of pelagic ecosystems, given that prolonged periods of stratification are associated with a decrease in primary productivity and thus a reduction of the ocean CO₂ sink [Sarmiento et al., 1998]. This expected impact of climate change is based on the assumption that increased heat content should be associated with longer periods of stratification. With our heuristic approach, using the pattern of SST increase and decrease following seasonal minima and maxima, we found marked changes in the duration of the period of stratification, which in most cases indicated a trend towards longer periods. Contrary to our expectations, we found shortened periods of stratification at some places, especially in the subtropical Atlantic and in some northern regions. Nevertheless, most of the North Atlantic presented a trend towards longer periods of stratification, especially in northern regions. At the same time, northern regions are experiencing high rates of change in mean SST, and in the magnitude and timing of seasonal extremes, causing increased variability. Thus, it seems that the increasing and decreasing phases of the seasonal cycle are changing towards more sudden increments in these regions to result in longer periods of stratification. Because of the rather heuristic approach adopted here, it would be desirable to examine these results using other sources of data, as well as to incorporate this measurement (as well as other employed in this study) to the common set of statistics reported in modeling studies.

Physical processes are one of the main drivers of marine community structure and dynamics [Longhurst, 2007]. This fact should not be confounded with a deterministic view of ocean ecosystems as static entities that respond to physical forcing within a set of defined properties and constant behavior. We tried to assess the extent to which this approach is

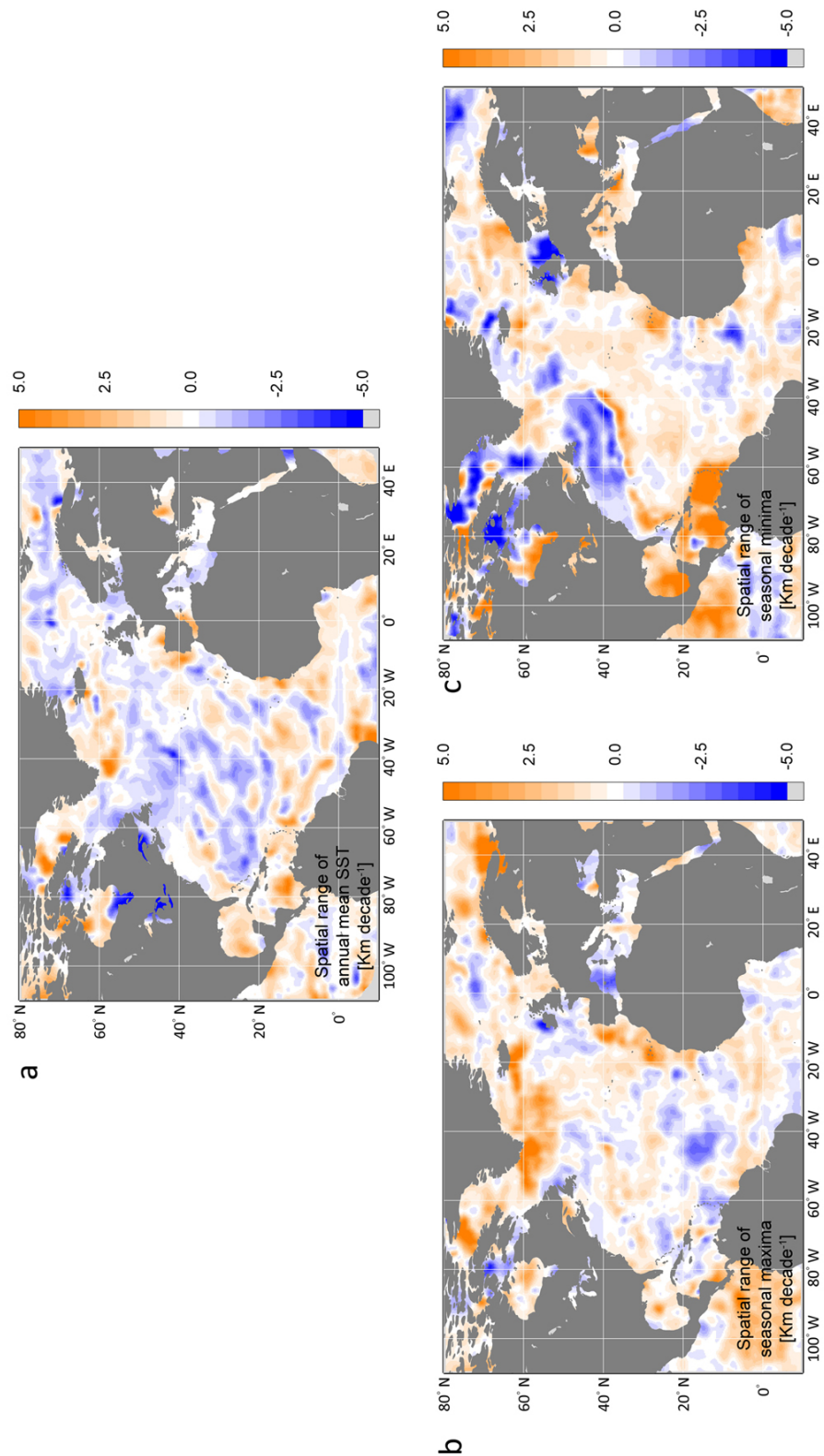


Figure 2.6: Maps of estimated linear trends for changes in decorrelation scales for (a) annual mean sea surface temperature, and for the seasonal (b) maxima and (c) minima [Km decade^{-1}]. Zones without enough data for estimation were colored in light gray.

justified in the context of predicting climate change impacts by studying a set of variables which, despite their biological significance, have been commonly ignored in most studies. Our main findings did not support this static view. Indeed, the process of warming in the surface waters of the North Atlantic Ocean were found to be much more complex than a simple homogeneous increase in SST, or a consequence of the contraction and expansion of current climate regimes. This result suggests that variation in SST during the last decades has been promoting a reorganization of biological communities and it further suggest that this process will continue and strength in the near future. Timing statistics further stressed that climate change is not only promoting changes in the patterns of spatial overlap between species, but it will also promote temporal mismatches. The occurrence of such spatiotemporal readjustments on the short time scales analyzed here thus establishes a major challenge for both scientist and managers.

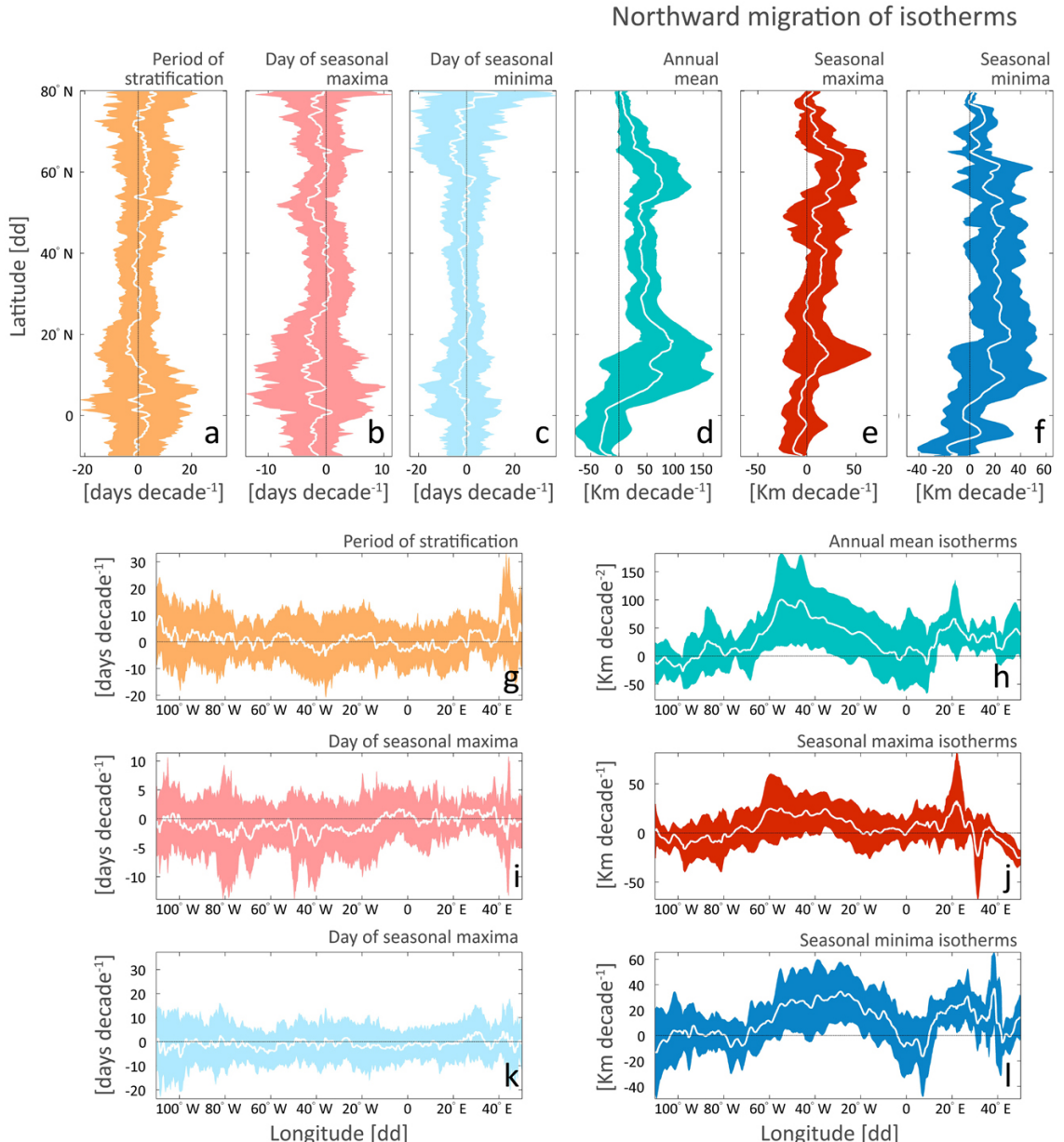


Figure 2.7: Zonal (a-f) and meridional (g-l), area corrected averages (\pm SD) of trends for indexes related to changes in the timing of sea surface temperature events and for the northward migration of isotherms. In contrast to Fig. 2.4d-f, only northward migration rates are presented. Rates for different isotherms located at the same longitude or latitude were integrated together. Note that axis scales differ among indexes.

Chapter 3

Ocean color and plankton phenology

Abstract Seasonal pulses of phytoplankton drive seasonal cycles of carbon fixation and particle sedimentation, and might condition recruitment success in many exploited species. Taking advantage of long term series of remotely sensed chlorophyll *a* (1998–2012), we analyzed changes in phytoplankton seasonality in the North Atlantic Ocean. Phytoplankton phenology was analyzed based on a probabilistic characterization of bloom incidence. This approach allowed us to detect changes in the prevalence of different seasonal cycles and, at the same time, to estimate bloom timing and magnitude taking into account uncertainty in bloom detection. Deviations between different sensors stressed the importance of a prolonged overlap between successive missions to ensure a correct assessment of phenological changes, as well as the advantage of semi-analytical chlorophyll algorithms over empirical ones to reduce biases. Earlier and more intense blooms were detected in the subpolar Atlantic, while advanced blooms of less magnitude were common in the Subtropical gyre. In the temperate North Atlantic, spring blooms advanced their timing and decreased in magnitude, whereas fall blooms delayed and increased their intensity. At the same time, the prevalence of locations with a single autumn/winter bloom or with a bimodal seasonal cycle increased, in consonance with a poleward expansion of subtropical conditions. Changes in bloom timing and magnitude presented a clear signature of environmental factors, especially wind forcing, although changes on incident photosynthetically active radiation and sea surface temperature were also important depending on latitude. Trends in bloom magnitude matched changes in mean chlorophyll *a* during the study period, suggesting that seasonal peaks drive long term trends in chlorophyll *a* concentration. Our results link changes in North Atlantic climate with recent trends in the phenology of phytoplankton, suggesting an intensification of these impacts in a near future.

Keywords MODIS, North Atlantic Ocean, Ocean Color, Phytoplankton phenology, Remote sensing, SeaWiFS

3.1 Introduction

Seasonal pulses of phytoplankton growth set the rhythm of marine ecosystems [Barnes and Hughes, 1999], and represent an important influx of atmospheric CO₂ into the oceans [Falkowski et al., 1998]. These events drive seasonal cycles of particle sedimentation [Deuser and Ross, 1980; Honjo, 1982; Billett et al., 1983] and are tightly linked to the ecology of zooplankton [Longhurst, 2007], including the early stages of many exploited species [Hjort, 1914; Cushing, 1990; Townsend et al., 1994; Durant et al., 2007]. The timing and characteristics of seasonal peaks are a major indicator of the functioning of marine pelagic ecosystems [Platt and Sathyendranath, 2008; Racault et al., 2012]. In land, both the phenology of vegetation and migratory species have been altered by recent climate change [Peñuelas and Filella, 2001; Parmesan, 2007; Sletzer and Post, 2009], while in the sea analyses based on long term field sampling programs have shown consistent changes both in the phenology and biomass of marine plankton [Reid et al., 1998; Edwards et al., 2001; Edwards and Richardson, 2004].

The ephemeral nature of phytoplankton and their spatial extent make their characterization difficult by classical sampling techniques. This has been remediated to some extent by the availability of decade long, high quality remotely sensed monitoring of chlorophyll *a* concentration (hereafter, chl *a*) [McClain et al., 2004a; McClain, 2009]. Analyses incorporating satellite data have revealed a tight link between climate variability and recent decreases in phytoplankton biomass and primary productivity at the global scale [Gregg and Conkright, 2002; Antoine et al., 2005; Gregg et al., 2005; Behrenfeld et al., 2006; Martinez et al., 2009; Vantrepotte and Mélin, 2009], the expansion of low chl *a* concentration areas in the subtropics [McClain et al., 2004b; Polovina et al., 2008; Irwin and Oliver, 2009] and a decline in mean phytoplankton cell size [Polovina and Woodworth, 2012]. Studies on marine phenology have focused on the main peak of phytoplankton growth in temperate and polar regions, *i.e.* the spring phytoplankton bloom, and have highlighted the great variability of this event and a trend towards an early occurrence of these blooms in northern latitudes in recent years [Siegel et al., 2002; Platt and Sathyendranath, 2008; Henson et al., 2009; Kahru et al., 2011; Zhai et al., 2011], as well as the importance of trophic mismatches [Platt et al., 2003; Beaugrand et al., 2003; Koeller et al., 2009; Kristiansen et al., 2011]. Secondary pulses during the fall in temperate latitudes and autumn/winter blooms in subtropical and tropical regions have received in general less attention (but see Ueyama and Monger 2005; Martinez et al. 2011; Cole et al. 2012; Sapiano et al. 2012).

Here, we combine SeaWiFS and MODIS data to study recent changes in the seasonality of phytoplankton in the North Atlantic Ocean. We develop a methodology which accommodates the different nature of spring and autumn/winter blooms, allowing us to study both events simultaneously. At the same time, the method allows propagating uncertainty in bloom detection to estimates of the change in the extent of areas presenting different

types of seasonal cycles, as well as to estimates of the timing and magnitude of seasonal peaks. Based on this approach, we examine whether recent ocean color observations reveal (*i*) a geographical shift in the incidence of different kind of seasonal cycles; (*ii*) changes in the timing and magnitude of spring and autumn/winter blooms, and their relationship to decadal trends in chl *a*; and (*iii*) the potential ability of different environmental factors to explain recent changes in the phytoplankton seasonality in the North Atlantic.

3.2 Materials and Methods

3.2.1 Data sources and data preparation

A box between 110°W 10°S and 50°E 80°N was selected to study changes in the seasonality of phytoplankton the North Atlantic Ocean and its marginal seas. Chlorophyll *a* is commonly used as an index of phytoplankton biomass and thus of changes in phytoplankton abundance or size. The main advantage of chl *a* is that its concentration in the near surface can be readily measured from space [McClain, 2009], but at the cost of ignoring deep chlorophyll maxima. The use of chl *a* as an index of phytoplankton biomass is further confounded in general by changes in nutrient availability and in the light regime that modulate pigment cell levels [Laws and Bannister, 1980], problems that might be especially important in subtropical latitudes (see below). Moreover, changes in phytoplankton species composition might alter as well the relationship between chl *a* concentration and biomass.

Daily time series of remotely sensed chl *a* concentration [mg m^{-3}] between September 1997 and April 2013 were retrieved from Level 3 (L3, geolocated, corrected and averaged over a regular grid) SeaWiFS (Sept. 1997–Dec. 2007, reprocessing R2010.0) and Aqua MODIS (Jul. 2002–Apr. 2013, reprocessing R2013.0) standard mapped images (SMI) available at the Ocean Color Web (Feldman and McClain 2012; Goddard Space Flight Center, NASA; oceancolor.gsfc.nasa.gov). Note that long data gaps due to instrument failures beginning in January 2008 prevented the use of SeaWiFS data available up to December 2010. Original data at a nominal scale of 0.08° were averaged over a 0.25° grid (cell side ~25 km). We used chl *a* concentration maps estimated using the Garver-Siegel-Maritorena semi-analytical model (GSM, Garver and Siegel 1997; Maritorena et al. 2002). The GSM presents some advantages over other algorithms when data from different missions are combined, given that it is based on a common parameterization independent of the sensor employed to measure ocean color (Maritorena et al. 2010; note that problems reported in this paper related to the drift of the 412 and 443 nm bands of Aqua MODIS were corrected in the last reprocessing [R2013.0]; see Meister et al. 2012 and oceancolor.gsfc.nasa.gov/WIKI/OCReproc2013%282e%290MA.html). Despite this advantage, deviations between different sensors are still expected as a consequence of differences in their radiometry [Maritorena et al., 2010]). To assess the impact of our choice of the GSM algo-

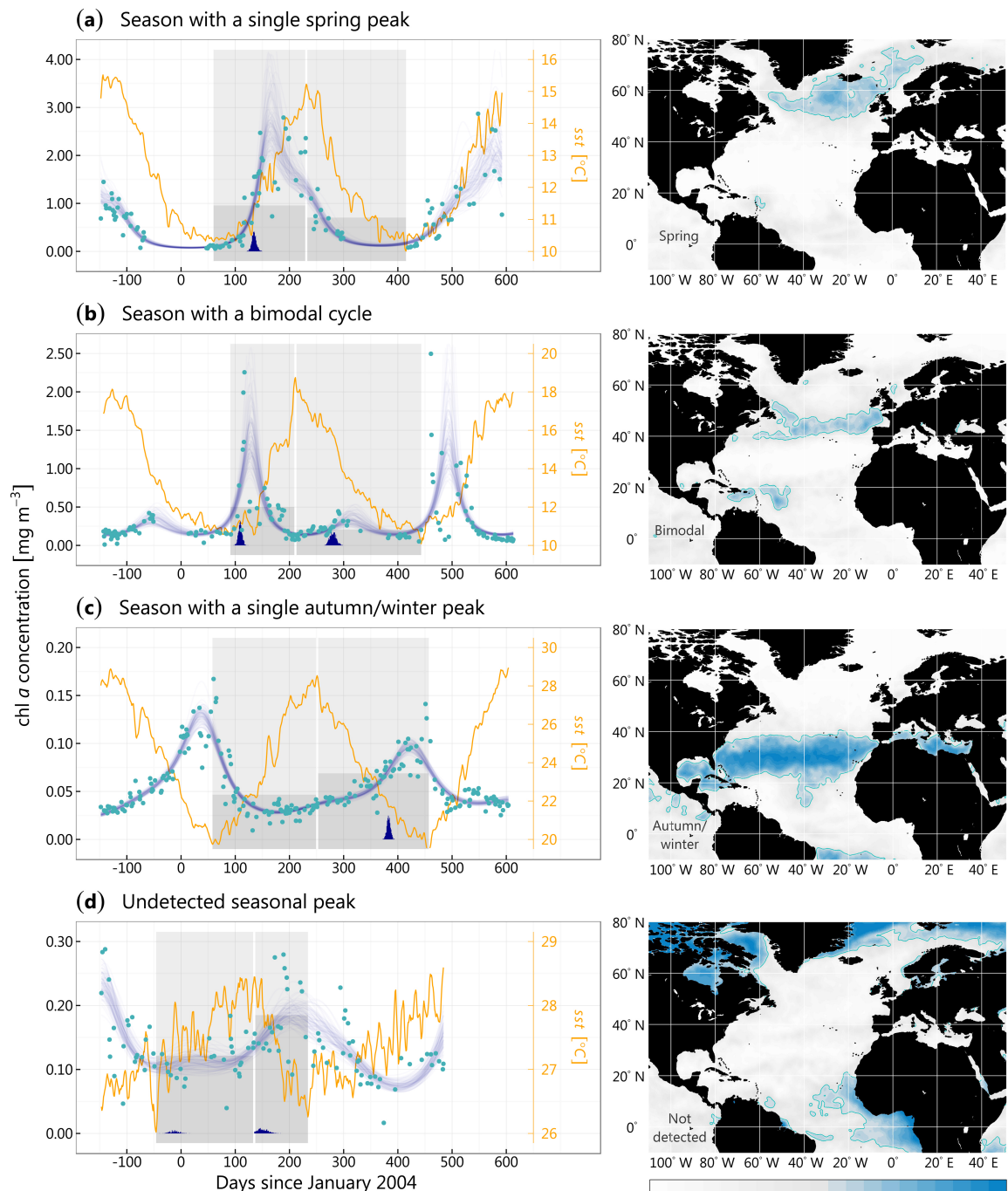
rithm, we repeated all the analyses using chl a estimates retrieved using the sixth version (OCv6, oceancolor.gsfc.nasa.gov/REPROCESSING/R2009/ocv6) of the OC4 (SeaWiFS) and OC3M (Aqua MODIS) empirical band-ratio algorithms [O'Reilly et al., 2000], in order to check the robustness of our approach to the algorithm employed to estimate chl a concentration (see the Appendix).

Sea surface temperature (SST) data was used to delimit different seasons and thus to help in the detection and characterization of increases in chl a concentration (a five day filter was previously applied to time series to avoid spikes). Data for other environmental variables and indexes were retrieved to study the physical forcing on the timing and magnitude of seasonal peaks during the study period. Climate variables gridded to the same spatial and temporal scale of the chl a observations included SST, incident photosynthetically available radiation (PAR), wind speed and eddy kinetic energy (table 3.1).

3.2.2 Characterization of seasonal changes in chl a concentration

Seasonal cycles of chl a concentration present a wide variation in the North Atlantic, reflecting changes in physical, chemical and biological conditions from the equator to the poles [e.g. Longhurst, 2007]. This includes seasonal regimes characterized by either one or two peaks in chl a , which have been typically associated with seasonal changes in stratification (*i.e.* the spring phytoplankton bloom) or mixing (autumn/winter blooms) [Dutkiewicz et al., 2001]. Seasonal increases in chl a concentration near the surface reflect both changes in phytoplankton abundance and in the amount of chl a per cell. Cell concentration might change due to population growth, horizontal advection and dispersion, or as a consequence of changes in vertical distribution [Behrenfeld, 2010]. Pigment cell levels vary depending on nutrient availability and on the light field [Laws and Bannister, 1980]. The photoacclimation response is especially important following autumn mixing in subtropical latitudes,

Figure 3.1 (following page): Different types of seasonal cycles of surface chlorophyll a concentration in the North Atlantic. Rows *a-d* correspond to the four different types of seasonal cycles distinguished. The plots on the left side of each row illustrate the approach employed to characterize seasonal peaks (see also Fig. S6), while the maps on the right present the corresponding probability of occurrence of each type of seasonal cycle in the entire North Atlantic. In the left panels, posterior simulations (*blue lines*) from a model fitted to remotely sensed observations of chlorophyll a concentration (*chl a , green dots*) were used to assess the probability of detecting different peaks in phytoplankton biomass and their timing (*histograms*). A peak qualified as a bloom after surpassing a threshold chl a concentration (dark gray shading). Identified peaks were classified either as spring or autumn/winter blooms based on the timing of sea surface temperature extremes (*SST, orange line*), which determined spring or fall candidate periods (gray shaded areas). The series were extracted from the following pixel locations: (*a*) 12.6°W55.1°N, (*b*) 9.6°W47.6°N, (*c*) 55.1°W30.1°N, and (*d*) 32.6°W0.6°S. Probability maps were derived from 15 consecutive seasonal cycles (1998-1999 to 2012-2013; data for Aqua MODIS and SeaWiFS was averaged for overlapping seasons), and were based on one thousand posterior simulations of model equation 3.2 fitted to data available during each season. The contour line encloses areas with a probability of detection greater than 0.5. figure 3.B.8 in the Supporting Information presents maps distinguishing regions with no data and regions where, despite data was available, no peak was detected (*e.g.* the case illustrated in *d*).



when the recirculation of phytoplankters in a deeper mixed layer decreases light exposure and results in an increase of chl a concentration in the water column [Letelier et al., 1993; DuRand et al., 2001; Behrenfeld et al., 2005; Siegel et al., 2005; Westberry et al., 2008; Vantrepotte et al., 2011].

Episodic changes in surface chl a concentration due to other processes alter these seasonal cycles, reflecting for instance the influence of mesoscale features, coastal upwelling and land inputs, to name a few of them. Satellite data allow the identification of all these events, with the main constraint arising from limited data availability during cloudy conditions. Here we adopted a rather practical approach for the identification and characterization of seasonal peaks, trying to avoid the influence of high frequency events. Seasonal extremes in SST were used to delimit each season and to identify candidate periods for seasonal peaks of increase in chl a concentration. We considered a period centered on each calendar year but covering the time period between previous and next year SST maxima [see Jönsson and Eklundh, 2002]. The chl a time series for this period was then smoothed by fitting a generalized linear model assuming Gamma distributed errors using the canonical, inverse link function:

$$\begin{aligned} p(chl_t | \widehat{chl}_t) &\sim \text{Gamma}(u, v) \\ (\widehat{chl}_t)^{-1} &\sim \text{Normal}(\beta X, \sigma_\varepsilon) \end{aligned} \quad (3.1)$$

The estimation of the shape and rate parameters of the *Gamma* distribution (u and v) is surpassed in this way by linking the expected chl a values to the linear predictor ($\eta_t = \beta X$). The linear predictor included an intercept, a linear trend on time, and sine and cosine waves to represent the seasonal cycle by annual and semi-annual harmonics ($\omega = 1/365$; see Vargas et al. 2009; Sapiano et al. 2012), yielding:

$$\begin{aligned} \eta_t = \beta_0 + \beta_1 t + \beta_2 \sin(2\pi\omega t) + \beta_3 \cos(2\pi\omega t) + \\ + \beta_4 \sin(4\pi\omega t) + \beta_5 \cos(4\pi\omega t) + \\ + \beta_6 t \sin(2\pi\omega t) + \beta_7 t \cos(2\pi\omega t) \end{aligned} \quad (3.2)$$

Note that the model allowed also a linear trend in the amplitude of the annual harmonics. This model specification was redundant for some of the series, so we determined an optimal structure based on model ranks determined using the Akaike Information Criterion (AIC, Burnham and Anderson 2003), a relative measurement of goodness of fit that includes a penalty term to weight down model complexity and avoid over fitting. The model was fitted under a Bayesian framework, employing the modified Expectation-Maximization (EM) algorithm developed by Gelman et al. [2008] and implemented in the *R* package *arm* (Gelman et al.

man et al. 2009; see also Gelman and Hill 2007). We assumed standard, weakly informative priors for each j parameter in equation 3.2, *i.e.*:

$$\beta_j \sim \text{Cauchy}(\mu, v),$$

$$\mu = 0 \text{ and } \begin{cases} v = 10, & j = 0 \\ v = 2.5/(2sd(x_j)), & j > 0 \end{cases} \quad (3.3)$$

where the location parameter μ centers our prior belief about the mean of posterior parameter values in zero and the scale parameter was tuned depending on the standard deviation of each covariate x_j (a larger the variation in x_j puts more a priori weight in small values of β_j).

Posterior parameter distributions were then used to generate an envelope of model realizations (1000) that was employed to propagate model uncertainty to a set of bloom metrics (timing and magnitude) used to characterize the seasonal cycle. Local extremes in chl a delineated periods of accumulation that were considered as candidate blooms if they reached a level above the 60th percentile of a *Gamma* distribution fitted to chl a observations between consecutive *SST* extremes (*i.e.* a minimum and a maximum or *viceversa*). The choice of this threshold was arbitrary but helped us to reject small amplitude waves. Candidate blooms were then classified either as spring or autumn/winter blooms based on the relative timing of bloom metrics with respect to *SST* extremes. We considered that a candidate bloom corresponded to a spring bloom if its timing and peak occurred after the seasonal *SST* minimum but before the *SST* maximum. Similarly, the timing of autumn/winter blooms must occur between the seasonal *SST* maximum and the next minimum (avoiding thus possible confusions with next year's spring blooms), even if the timing of the peak occurred after the *SST* minimum. For a given model realization, only the first candidate bloom meeting the criteria above was retained, although in some cases all the candidates were rejected.

Determining the occurrence of a bloom in this way does not presuppose the development of a bloom every year and compensates to some extent the lack of data during cloudy periods [Gregg and Casey, 2007; Cole et al., 2012]. It is important to note that we defined the timing of the bloom as the day when the net rate of increase of chl a concentration attained a maximum. The definition is similar to other approaches based on a predefined threshold level, although our intention was not to determine the date of bloom initiation. Our definition also differs from the timing of bloom onset, defined by Sverdrup [1953] as the date when the net rate of phytoplankton increase becomes positive. With our definition, we tried to prevent potential measurement errors in the net rate of increase associated to the small changes in chl a concentration at the onset of the bloom, and due to the lack of data during cloudy periods in northern latitudes. On the other hand, bloom magnitude was defined as the peak chl a concentration attained during the bloom. We also estimated

mean chl *a* concentration during the entire bloom (*i.e.* between consecutive chl *a* minima), but only to complement analyses of changes in bloom timing and magnitude. A set of examples have been included in figure 3.1, and a diagram summarizing bloom determination was included in the Appendix.

3.2.3 Analyses of changes in the seasonality of chl *a* concentration

The characterization of seasonal chl *a* time series resulted in four different possibilities attending to the presence or absence of different peaks. We distinguished mean seasonal cycles presenting (*i*) a single spring or (*ii*) a single autumn/winter bloom, (*iii*) a spring bloom followed by an autumn/winter one (*i.e.* a bimodal seasonal cycle), and (*iv*) mean seasonal cycles in which neither of the blooms were detected. Each of the 1000 posterior model realizations was assigned to any of these categories, resulting in a raw estimate of the probability of each kind of seasonal cycle occurring at each pixel location. These probabilities were then integrated over regions defined by grouping biogeochemical provinces delimited by Longhurst [2007] to obtain a weighted estimate of the total areal extent corresponding to each kind of seasonal cycle. Longhurst [2007] regions were further subset to avoid marginal seas and to account for differences in the detectability of different seasonal cycles (see figure 3.B.7). Trends in the prevalence of each type of seasonal cycle were analyzed based on a Dirichlet regression model that included a second order trend in time (see table 3.B.2 in the Appendix). This kind of model has an error structure ideally suited to analyze compositional data (proportions adding up to unity) in the presence of covariates [Campbell and Mosimann, 1987; Hijazi and Jernigan, 2009], and was fitted using an adaptive Metropolis algorithm [Roberts and Rosenthal, 2009].

Simulations of the model fitted to chl *a* time series were also employed to obtain an augmented sample of the timing (defined as the day of maximum net increase in chl *a*) and magnitude (defined as the peak chl *a* concentration during a bloom) of blooms occurring at each pixel location. Median timings and magnitudes were estimated at the pixel level, but detection probabilities were retained and employed to weight the reliability of different observations, propagating in this way uncertainty in bloom detection to estimates based on bloom statistics. Interannual changes in bloom metrics were analyzed using a model including a fixed effects factor to account for biases between different sensors and a linear trend in time. We assumed normally distributed errors for the residuals of this model, which we considered a reasonable assumption for both bloom timing and bloom magnitude, although in the latter case only after log transformation. Temporal trends in bloom metrics were later compared to trends in mean chl *a* during the entire year, estimated after fitting equation 3.2 to the complete daily chl *a* series using a log link function to ease interpretation. This model included thus a linear trend, a term to account for sensor bias, and terms to account for a seasonal cycle potentially changing its amplitude between years.

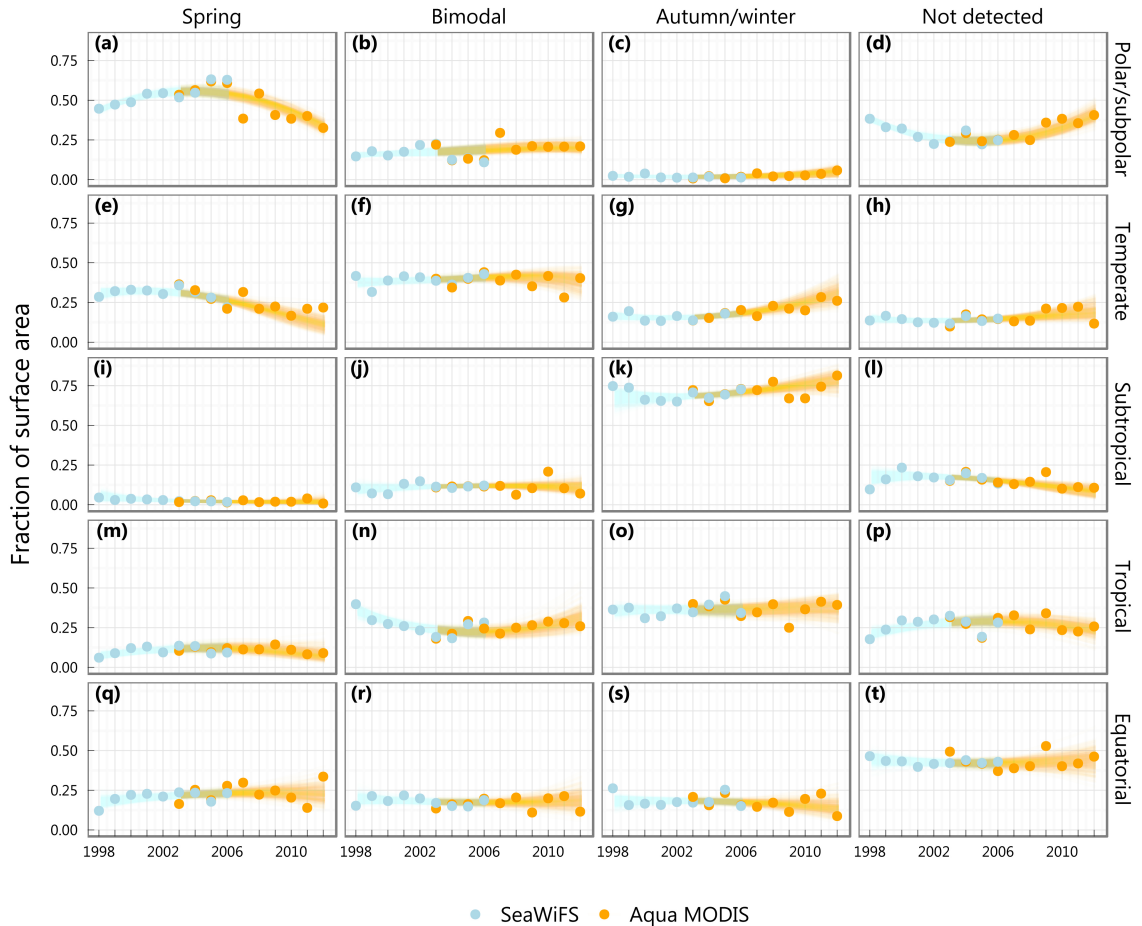


Figure 3.2: Prevalence of different types of seasonal cycle in the main biogeochemical regions of the North Atlantic. Each panel presents the incidence of each type of seasonal cycle after correcting for differences in detectability between sensors. Estimates were derived from a weighted integral considering the probabilities for each kind of seasonal cycle (e.g. figure 3.1). Lines correspond to posterior simulations ($n = 400$) from a Dirichlet regression model accounting for differences between sensors and including a second degree polynomial trend to account for nonlinear time trends (table 3.B.2). Alpha blending was employed to represent model uncertainty, with $\alpha = 1/80$ (i.e. the overlap of 80 lines correspond to full opacity). The regions group biogeochemical provinces defined by [Longhurst, 2007] (see figure 3.B.7 in the Appendix). See figure 3.B.9 in the Appendix for the same figure based on chl a estimates retrieved using the OCv6 band-ratio algorithm.

Estimates of bloom timing and magnitude were also compared to a set of environmental factors to assess the potential importance of climate forcing to explain interannual changes in phytoplankton seasonality. The models included again a linear trend and a term to account for sensor bias and we assumed normally distributed errors. Time series of linearly detrended anomalies of (i) sea surface temperature, (ii) incident photosynthetically active radiation, (iii) wind stress and (iv) eddy kinetic energy, were standardized to mean zero and standard deviation one. All these variables modulate phytoplankton dynamics and might alter bloom timing and magnitude (table 3.1). Detrended anomalies were preferred to represent short term effects on bloom metrics and to prevent problems of collinearity in models including more than one covariate. Detrending did not affect the patterns of association found with original data in models with a single covariate. The models fitted to time series of bloom metrics assumed normally distributed errors (after log transformation in the case of bloom magnitude) and included again a linear trend and a term to account for sensor bias. Models included all the covariates, although only wind stress or one of its components was included to avoid problems of collinearity (best model structure based on AIC). The fraction of deviance explained by each environmental factor was determined by fitting models excluding sequentially each covariate. A 0.5° spatial moving window was employed to augment areal coverage and to reduce spatial noise in all the estimates. The overlap between SeaWiFS and Aqua MODIS during four entire seasons (2003-04 thru 2006-07) allowed us to assess potential biases derived from using data coming from different sensors and satellites, as further detailed in the Appendix. All calculations involving different pixel locations accounted for changes in cell area with latitude using the reference ellipsoid WGS84.

Table 3.1: Environmental variables employed to assess the potential importance of climate forcing to explain interannual changes in phytoplankton seasonality.

Variable name (abbreviation [units])	Data source and processing details	Comments
Sea Surface Temperature (SST [K])	NOAA Optimum interpolation 0.25° daily sea surface temperature analysis (OISST version 2, Reynolds et al. 2007). Database produced and maintained by C. Liu and R. W. Reynolds at NCDC (www.ncdc.noaa.gov/sst).	SST accelerates the rate of physiological and ecological processes (of phytoplankton and of grazers, Townsend et al. 1994), but it is also a tracer of vertical mixing and of the advection of waters with different properties. Warmer (cooler) waters might be related to increased (decreased) stratification and light exposure and reduced (increased) nutrient availability.
Integrated Photosynthetically Available Radiation (PAR [Einstein mm ⁻² day ⁻¹])	Daily time series of Level 3 PAR from 400 to 700 nm, available at the Ocean Color Web (Feldman and McClain 2012; Goddard Space Flight Center, NASA; oceancolor.gsfc.nasa.gov).	Together with vertical attenuation and mixing depth, incident PAR determines the subsurface light field (e.g. Platt et al. 1991). In this way, a lower PAR might alter chl <i>a</i> concentration by limiting phytoplankton growth rates or by increasing pigment cell levels, and <i>viceversa</i> .
Wind stress (τ [N m ⁻²])	Derived from daily wind speed [m s ⁻¹] maps integrated from the six-hourly, Level 3 Cross-Calibrated Multi-Platform Ocean Surface Wind Velocity product (CCMP, Atlas et al. 2011, available at PO.DAAC, podaac.jpl.nasa.gov). The drag coefficient was estimated based on Yelland and Taylor 1996; Yelland et al. 1998.	Wind stress is a proxy of wind surface mixing and turbulence, so increased wind stress is related to an increased mixed layer ventilation and nutrient renewal, as well as deeper phytoplankton entrainment, and, in principle, higher dilution and lower encounter rates with grazers [Irigoin et al., 2005; Behrenfeld, 2010]. Nevertheless, air-sea heat fluxes and vertical convection are also important drivers of mixed layer depth at high latitudes.
Eddy kinetic energy (EKE [m ² s ⁻²])	Derived from the reference series of daily geostrophic velocity anomalies produced by Ssalto/Duacs and distributed by Aviso (www.aviso.altimetry.fr), with support from CNES (Centre National d'Etudes Spatiales). The reference series is obtained by merging data from various missions (Topex/Poseidon, Jason-1, European Remote Sensing satellites [ERS 1 and 2], and Envisat) using the methods developed by Le Traon et al. 1998.	Eddy kinetic energy is a proxy of variability in ocean currents and mesoscale features which might promote an early stratification and enhance bloom development [Karrasch et al., 1996].

3.3 Results

3.3.1 Incidence of different types of seasonality

The cumulated probability of different types of seasonal cycle presented a clear latitudinal pattern with a single spring bloom in the subpolar Atlantic, a single autumn/winter bloom in subtropical latitudes, and a bimodal cycle in temperate latitudes (figure 3.1). There was a clear transition among each pair of regions, with a relatively sharp gradient in detection probabilities (decaying shade intensity outside green contours in figure 3.1). No single type of seasonal cycle dominated in transitional regions, although recurrent blooms were detected when seasons with single and double peaks were pooled together to estimate the probability of occurrence of spring and autumn/winter blooms (indeed they qualified for the estimation of trends in blooms statistics, figure 3.3). This explains for instance the failure to highlight spring blooms in the northwestern Mediterranean [Bosc et al., 2004], that were obscured due to the detection of bimodal cycles in some years. Our approach failed to detect a marked seasonal cycle in pixel locations north of $\sim 70^{\circ}\text{N}$ due to data scarcity (see Figs. 3.B.2 and 3.B.8 in the Appendix), and in most of the tropical and equatorial Atlantic, due to multimodal and highly irregular small amplitude seasonal oscillations [Longhurst, 2007]. The western tropical Atlantic, near the Antilles, presented an exception to this general pattern. Bimodal and even spring seasonal cycles were common in this region where seasonal peaks are driven by enhanced biological N₂-fixation [Coles et al., 2004; Subramaniam et al., 2008].

The prevalence of different types of seasonal cycles changed between seasons (figure 3.2; see also table 3.B.2). The Dirichlet regression results in nonlinear trends in prevalence, so model based estimates for the first and last years will be used to illustrate changes during the study period (1998–2012). In the polar and subpolar North Atlantic (Fig. 2a-d), the prevalence of seasons with a single spring bloom was coupled to changes in the frequency of pixel locations where no bloom was detected (Kendall's $\tau = -0.75$ [-0.59,-0.90]; model based estimates of the median and 90% posterior density interval). The prevalence of spring peaks presented also a decrease (e.g. from an estimated fraction of 0.44 [0.43,0.45] in 1998–1999 to 0.33 [0.30,0.37] in 2012–2013, equivalent to a change in extent of $5.14 [3.28,6.91] \times 10^5 \text{ km}^2$), that was compensated in part by a weak increase of bimodal cycles ($2.14 [0.85,3.85] \times 10^5 \text{ km}^2$).

In temperate regions (Fig. 2e-h), there was a clear decline in the prevalence of locations with a single spring bloom (fraction of area reduced from 0.31 [0.28,0.34] to 0.11 [0.06,0.16], equivalent to a reduction in extent of $13.2 [9.8,16.0] \times 10^5 \text{ km}^2$). Although this trend was again negatively related to changes in detectability (e.g. $2.5 [-0.0,6.1] \times 10^5 \text{ km}^2$; $\tau = -0.81$ [-0.36,-1.00]), it was compensated mainly by an increase in the extent of locations with a single autumn/winter bloom ($7.68 [3.89,12.28] \times 10^5 \text{ km}^2$, $\tau = -0.98$ [-0.79,-1.00]) and, to

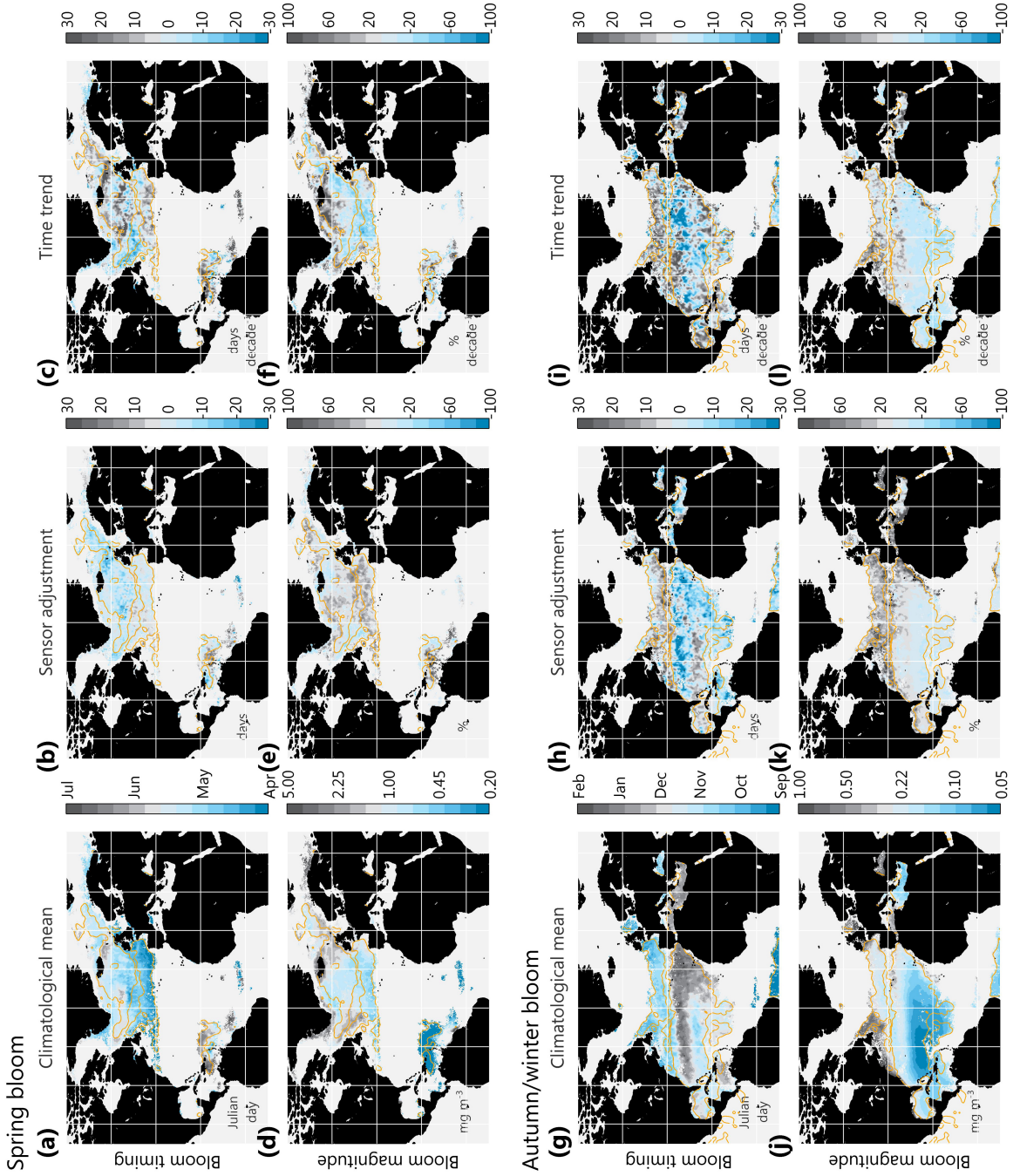


Figure 3.3: Timing and magnitude of spring (*upper panels*) and autumn/winter blooms (*lower panels*). Maps in each column correspond to the posterior mean date (Julian date) and chl a concentration (mg m^{-3}), the differences between sensors (in days and as a percentage, respectively) and the time trends (days or percentage per decade) during 1998–2012 (units are also indicated in the bottom left corner of each map). A model including a linear trend in time was fitted to estimates of bloom statistics. The model included also a fixed effect factor to account for biases in mean bloom metrics between different sensors. Bloom statistics estimated from SeaWiFS data were taken as baseline. The timing (defined as the day when the net rate of increase of chl a concentration attained a maximum during each wave of increase) and the magnitude (defined as the peak chl a concentration attained during a bloom) of spring and autumn/winter blooms was determined for each season and pixel location from posterior simulations of the smoothing model fitted to chl a observations (equation 3.2). Only locations where the cumulated probability of detecting either type of bloom was greater than 0.5 were considered. Estimates corresponding to single-peaked and bimodal seasonalities were pooled together. **Orange contours** delimit regions where the probability of each type of seasonal cycle is greater than 0.5 (see figure 3.1). figure 3.B.13 and figure 3.B.14 in the Appendix present the uncertainty associated to all these estimates and results based on chl a estimates retrieved using the OCv6 band-ratio algorithm, respectively.

a lesser extent, by an increase in bimodal cycles ($1.25 [-3.07,4.78] \times 10^5 \text{ km}^2$, $\tau = -0.50 [0.41,-0.93]$). In the subtropics (Fig. 2i-l), posterior estimates indicated a slight increase in the dominance of seasonal cycles with a single autumn/winter cycle (from a fraction of 0.68 [0.61,0.73] to 0.78 [0.71,0.84]), mainly at the expense of a reduced incidence of areas where no peak was detected ($\tau = -0.93 [-0.66,-1.00]$). No clear temporal trends were detected in tropical and equatorial regions (Fig. 2m-t), where the prevalence of different seasonal cycles remained almost constant except for some high frequency excursions away from mean prevalence levels coinciding with El Niño events (*i.e.* 2005–06).

3.3.2 Timing and magnitude of seasonal peaks

Mean levels and time trends in the timing (defined as the day when the net rate of increase of chl a concentration was maximized during the phase of accumulation in modeled chl a series) and in the magnitude of seasonal peaks (*i.e.* the peak chl a concentration attained) presented a marked spatial structure during the study period (Fig. 3a,d,g,j, see also figure 3.B.10, and especially figure 3.B.13 in the Appendix for the uncertainty associated to these estimates). The comparison of bloom statistics based on data retrieved by different sensors resulted in differences structured in space that were especially important in the case of bloom magnitude (Fig. 3e,k). Spring peaks were detected early in April in the temperate North Atlantic and up to June in the Subpolar gyre (Fig. 3a), although there were some noticeable exceptions, especially in coastal regions. The mean magnitude of spring peaks covered almost two orders of magnitude ($0.2\text{--}14.4 \text{ mg m}^{-3}$, Fig. 3d) and increased with latitude, although it was mainly influenced by the proximity to land. In the western subtropical Atlantic ($10^\circ\text{--}23.5^\circ\text{N}$), low magnitude spring peaks ($0.13 [0.06,0.65] \text{ mg m}^{-3}$) occurred in late June, except in the region influenced by the Amazon river outflow (mean peaks of up to 9.4 mg m^{-3} , but note that chl a concentration retrievals are less reliable in case 2 waters). The timing of autumn/winter peaks presented a more complicated pattern (Fig. 3g). Small amplitude seasonal peaks ($0.13 [0.06,0.31] \text{ mg m}^{-3}$, Fig. 3j) were detected in late November and December in the southwestern side of the Subtropical gyre, and occurred up to early February towards the north and in the eastern side. The autumn/winter bloom of bimodal seasonal cycles of temperate regions was more intense ($0.26 [0.19,0.90] \text{ mg m}^{-3}$). The timing of bimodal autumn/winter blooms occurred later towards the south; as early as September in regions like the North Sea and up to early November near the Subtropical gyre.

The timing and the magnitude of either spring or autumn/winter blooms presented in general a positive temporal association at the pixel level, except in the case of spring blooms in some locations in the western Subpolar gyre and in polar latitudes (figure 3.4; see also figure 3.B.11). At large scale, this relationship resulted in a slight predominance of regions with either delayed and more intense blooms or advancing blooms declining in

magnitude (29.0 and 30.1%, respectively, *i.e.* 59.0% of the area presented trends of the same sign, figure 3.4). Nevertheless, trends in timing were more heterogeneous in space than trends in bloom magnitude. Trends towards delayed blooms predominated at the basin scale (58.7%; similar figures for either kind of bloom). Declining bloom magnitudes were more frequent in the case of autumn/winter blooms (62.3%), and to lesser extent, in the case of spring blooms (54.1%). The magnitude of spring blooms increased in coastal regions and in the northern North Atlantic, while the magnitude of autumn/winter blooms increased mainly in regions presenting a bimodal cycle.

In general, delays and advances in the timing of spring and autumn/winter blooms were of the same magnitude, although changes in the mean magnitude of blooms of either sign were more important in the case of spring blooms (figure 3.3, see also Figs. 3.B.10 and 3.B.14). Advanced and less intense spring blooms were common in polar regions (north of 65°N) and in both sides of the Atlantic between 45°N and 60°N. In contrast, trends towards delayed and more intense blooms were common in the Faroe-Iceland ridge, in the Irminger Sea and, in general, in areas north of 55°N in the central North Atlantic (*e.g.* 65.7% of the locations within the box 40°W 55°N and 20°W 65°N). Delayed spring and autumn/winter blooms predominated also along the southern limit of regions presenting bimodal cycles in temperate latitudes. Interestingly, trends towards a longer interval between the timing of both blooms predominated in temperate regions presenting bimodal cycles (71.4%). At the same time, the magnitude of spring blooms declined whereas autumn/winter blooms were more pronounced. This last result contrasted with the conspicuous predominance of trends towards less intense blooms in regions with a single autumn/winter bloom (67.1%). Advanced autumn/winter blooms predominated in the interior of the Subtropical gyre, although delayed blooms were common along its southern boundary and in marginal seas like the Mediterranean Sea and the Caribbean Sea.

Mean chl *a* concentration decreased in most of the North Atlantic during the study period (60.5%). This pattern was determined mainly by the higher prevalence of negative trends in the tropical and subtropical North Atlantic (figure 3.B.16). Changes in mean chl *a* concentration varied between regions depending on the type of mean seasonal cycle. Areas with a single autumn/winter bloom presented in general a decrease in mean chl *a* (78.0%), while increasing and decreasing trends were equally important in areas with bimodal seasonal cycles (46.5%). In the case of areas with a single spring bloom, trends towards increased chl *a* predominated (81.2%). This contrasting response is indicative of the tight link between changes in seasonal peaks and decadal changes in mean chl *a* concentration. We further examined the correspondence between changes in bloom timing and magnitude and changes in mean chl *a* concentration at the pixel level (figure 3.B.17). Changes in the magnitude of seasonal peaks were of the same signs as changes in mean chl *a* (*i.e.* coherent changes in 59.2 and 77.4% of the areas presenting spring and autumn/winter blooms, respectively), something relevant considering the lower coherence with trends in mean chl

a during the entire bloom (53.4 and 64.0%, *i.e.* between consecutive chl a minima). On the other hand, no clear association was detected between the sign of trends in bloom timing and in mean chl a concentration (*i.e.* coherent sign of trends in just 49.3 and 53.4% for spring and autumn/winter blooms, respectively).

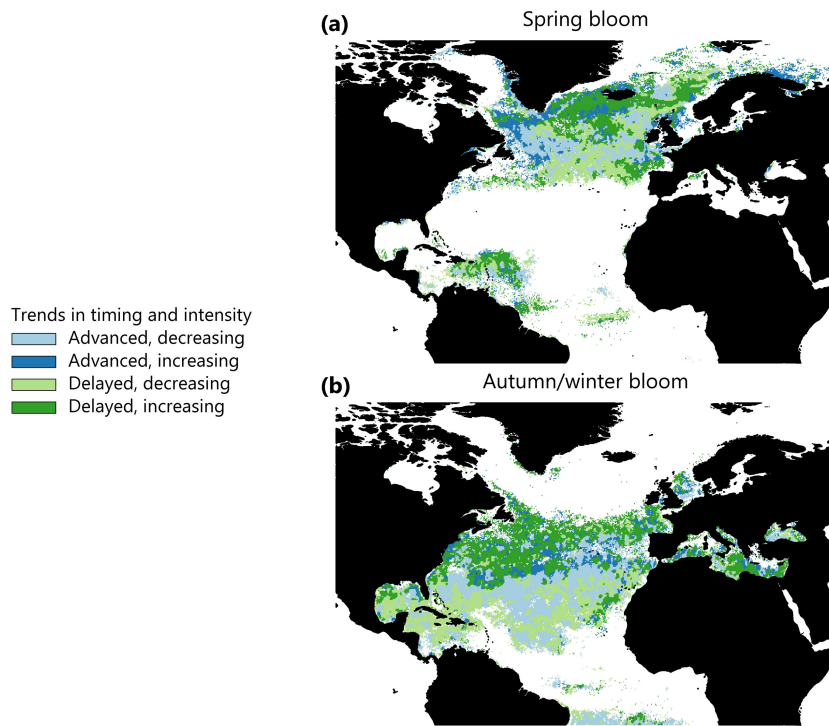


Figure 3.4: Categorical maps showing the association between the sign of time trends in the timing and in the magnitude of spring and autumn/winter blooms in the North Atlantic during 1998–2012. Each color depicts the four combinations between blooms with an advancing or delaying timing and an increasing or decreasing magnitude.

3.3.3 Impact of environmental factors on the timing and magnitude of blooms

The influence of environmental factors on spring and autumn/winter blooms presented a similar spatial pattern for bloom timing and magnitude (figure 3.5 and Figs. 3.B.18 and 3.B.19 in the Appendix). Each environmental variable presented marked and spatially coherent trends that in some cases varied between the cold and the warm seasons (figure 3.B.19). These trends also varied spatially, although they were indicative of a basin scale trend towards warmer surface waters and increased cloudiness (*i.e.* reduced PAR). Changes in wind stress were more complex, with a decline in most of the basin associated with the negative trend in the North Atlantic Oscillation index during the study period [Henson et al., 2009; Hurrell and Deser, 2009a], but with increased wind stress in some locations, especially along the western North Atlantic. After removing these trends, models containing all the

environmental factors considered at the same time –but including only total wind stress or one of its components to avoid collinearity problems– explained an amount of variation in bloom timing and magnitude of 0.24 [0.08,0.62] (fraction of deviance explained, median and 90% interval, figure 3.B.18). The importance of different variables varied depending on latitude and on the type of bloom (figure 3.B.19). The variable contributing to explain more deviance in bloom metrics presented a patchy distribution, although changes in wind forcing played a critical role in determining bloom characteristics in most of the basin (figure 3.5).

Sea surface temperature (*SST*) during the cold season was positively associated with delayed and more intense blooms in the polar North Atlantic and in the Irminger Sea. This result contrasted with the prevailing negative association found in the rest of the North Atlantic, either when considering spring or autumn/winter blooms. Zonal wind stress (τ_u) and, to a lesser extent incident *PAR*, appeared as the most important factors in the rest of the northern North Atlantic. Seasons with stronger westerlies corresponded to delayed and more intense spring blooms, while seasons with *PAR* above the average presented delayed and, to less extent, enhanced spring blooms. The positive association between a delay in the timing of the bloom and its magnitude might seem counterintuitive, although it is partially a consequence of the way we defined the timing of the bloom. If we assume that chl *a* dynamics obey a logistic function, an increase in the carrying capacity of the environment might cause a delay in the peak rate of increase (Reynolds 1997 proposed this reasoning to explain delays in the timing of the spring bloom associated with eutrophication). Positive anomalies in the meridional wind stress component (τ_v) were associated with delayed and stronger spring blooms along the European shelf. Changes in both spring and autumn/winter blooms in the transition zone were mainly associated with changes in *SST* and *PAR*, with a less important association with easterly winds and an important contribution of eddy kinetic energy along the Azores front. In contrast, wind stress (τ) was the main factor related to changes in the timing and intensity of autumn/winter blooms in the region presenting seasonal cycles with a single peak, especially in the Subtropical gyre.

3.4 Discussion

We developed a novel approach to study changes in the seasonality of remotely sensed phytoplankton biomass based on a probabilistic characterization of bloom incidence. This allowed us to detect changes in the prevalence of different seasonal cycles and to propagate uncertainty in bloom detection to estimates derived from bloom statistics. We found a greater incidence of seasonal cycles typical of subtropical latitudes in the temperate North Atlantic, as well as changes in the timing and magnitude of blooms in the whole basin. Phytoplankton seasonality responded to environmental factors related to climate change,

especially changes in wind patterns in lower and mid-latitudes, and sea surface temperature and light available for photosynthesis in the northern North Atlantic. Before discussing detected changes in the context of previous work, we proceed to review the advantages and pitfalls of the approach employed, and the results of our comparison between different satellite sensors and between remote sensing chl *a* algorithms.

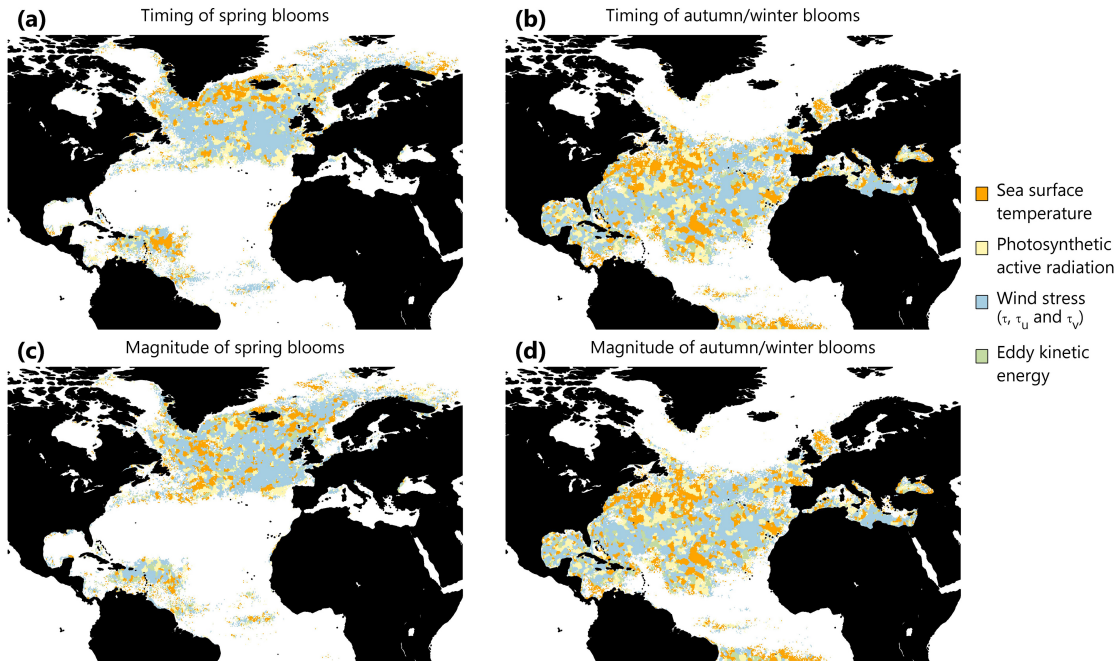


Figure 3.5: Environmental variables explaining more deviance in interannual changes in the timing (*upper maps*) and magnitude (*lower maps*) of spring and autumn/winter blooms in the North Atlantic during 1998–2012. A model including all the covariates considered in the study (table 3.1) was fitted to bloom statistics, although combinations resulting in problems of collinearity were excluded (e.g. those including wind stress and its components). The covariate explaining more deviance was determined by comparing the decline in deviance explained after deleting each covariate one at a time. The amount of deviance explained is presented in figure 3.B.18 in the Appendix.

3.4.1 Limitations and advantages of the methods employed to characterize seasonal changes in phytoplankton biomass

A variety of approaches have been proposed to characterize phytoplankton seasonality using remote sensing data [Ueyama and Monger, 2005; Rolinski et al., 2007; Platt and Sathyendranath, 2008; Thomalla et al., 2011; Zhai et al., 2011; Racault et al., 2012; Sapiano et al., 2012]. Daily observations are usually aggregated and smoothed spatially and/or in time before analysis in an attempt to surpass the limitations imposed by data scarcity during cloudy periods [Gregg and Casey, 2007], which might otherwise result in huge biases in bloom statistics (Cole et al. [2012] report typical errors of 30 and 15 days for the timing of onset and peak date in subpolar regions). Here we have preserved the daily time scale of chl *a* time series to minimize errors in bloom timing statistics, and instead tried to avoid

problems derived from data gaps by increasing spatial coverage and, especially, by fitting a model to smooth available observations. We have not conducted a proper assessment of the effect of data gaps (*e.g.* Gregg and Casey [2007]; Cole et al. [2012]), but the relatively good agreement between estimates based on SeaWiFS and MODIS data indicates that this effect might remain low (the same cannot be ensured with respect to different chl a algorithms, see Appendix), especially considering the larger number of valid chl a retrievals provided by MODIS sensor each season. The detection of trends with different signs at the same latitudes also point in this direction (*e.g.* systematic biases usually consist in later bloom detections at high latitudes, see Cole et al. [2012]).

Analyses of phytoplankton phenology usually proceed by determining the occurrence or not of a bloom to later retrieve the date of onset, bloom magnitude and other statistics like bloom duration or mean chl a [*e.g.* Racault et al., 2012]. Frequently, the timing of the bloom is determined as the date when either modeled or observed chl a concentration reach the annual maximum or a threshold level which, in many cases, is determined based on a small fraction above median chl a concentration (*e.g.* 0.05). Both approaches assume that a bloom has occurred and thus, that chl a data contain enough information to characterize it. Here, we fitted a model with enough flexibility to characterize different types of seasonal cycles of chl a concentration [see Vargas et al., 2009; Sapiano et al., 2012]. Seasonal chl a data were previously subset based on sea surface temperature time series. This allowed us to accommodate interannual changes in the shape of the seasonal cycle [Jönsson and Eklundh, 2002], and to determine directly the nature of blooms (*i.e.* spring vs. autumn/winter). An alternative approach consist in requiring chl a series to be above the threshold during two consecutive observations, a criterion which might be combined with setting a minimum variation in chl a to consider that a bloom might have occurred in a given location (*e.g.* Cole et al. [2012]).

The main difference with previous approaches consisted in avoiding the assumption that a bloom must have occurred and that it should be detected every year, *i.e.* ignoring changes in data availability or in the type of seasonal cycle. Our approach was similar in this aspect to Sapiano et al. [2012], although it does not require a nearly constant seasonal cycle year after year at the same location to determine the lack or not of a seasonal cycle (see Vantrepotte and Mélin [2009] for an alternative approach to the analyses of changes in chl a). Instead, we explored each oscillation in posterior simulations of models fitting available seasonal data. Observations retrieved during the target season –either spring or autumn/winter– were employed to estimate a threshold chl a concentration. The number of posterior simulations exceeding this selected chl a level was then used as an estimator of the probability of a bloom occurring or not. It should be noted that this procedure allowed us to detect changes in the prevalence of different seasonal cycles, to characterize uncertainty in bloom detection and, at the same time, to propagate this uncertainty to estimates derived from bloom statistics.

3.4.2 Changes in phytoplankton seasonality

We analyzed changes in phytoplankton seasonality considering changes in the prevalence of different types of seasonal cycle, before examining changes in bloom timing and magnitude. In both cases, the length of the series poses a great limitation to ascribe observed trends to climate change [Henson et al., 2010], although it revealed a clear signature of climate forcing on interannual changes in bloom statistics. Other problems include the difficulties to interpret changes in remotely sensed chl *a* concentration (see Materials and Methods), the direct treatment of mixed layer dynamics and the lack of some important drivers of phytoplankton and bloom dynamics, like advection and sub-mesoscale features [Lehahn et al., 2007; Mahadevan et al., 2012]. Another interesting aspect revealed by this study was the importance of taking into account potential differences between satellite missions and between chl *a* algorithms (see the Supporting text in the Appendix).

In agreement with previous studies highlighting an increased prevalence of oligotrophic conditions [McClain et al., 2004b; Polovina et al., 2008; Irwin and Oliver, 2009]; we found an increased prevalence of mean seasonal cycles with two peaks or even with a single autumn/winter bloom in the transition zone between regions presenting seasonal cycles with a single bloom, characteristic of subpolar and subtropical conditions. In the temperate North Atlantic, trends towards less apparent spring blooms contrasted with trends towards autumn/winter blooms of increased magnitude. At the same time, diverging trends in the timing of different peaks suggested an increase in seasonal stratification, the main consequence of increased surface warming [Sarmiento et al., 1998]. Changes in bloom timing and magnitude might have also impacted several fisheries around the Atlantic [Platt et al., 2003; Koeller et al., 2009].

In the temperate North Atlantic, the association between changes in bloom metrics and environmental variables suggests that trends in bloom timing and magnitude reflect reduced light availability during winter and especially, an increased stratification due to surface warming and reduced wind stress [Henson et al., 2009]. Indeed, opposite trends in mean chl *a* at both sides of the basin in middle latitudes might be explained by different trends in wind stress. Weaker westerlies during winter might result in a decrease in mixed layer ventilation and nutrient renewal in the Northeast Atlantic, resulting in spring blooms of a reduced magnitude and a decrease in annual mean chl *a* concentration. These changes in seasonal wind patterns are probably related to the widening of tropical wind circulation systems [Seidel et al., 2007], and thus its effects on phytoplankton seasonality might continue and even strengthen in the next decades.

Delayed and more intense blooms were found in most of the Subpolar gyre, although advanced and less intense blooms were more common in polar latitudes [Kahru et al., 2011; Racault et al., 2012]. These changes were mainly associated with surface warming and light availability. In the Subtropical gyre, the different response in both sides of the North At-

lantic can be explained again by changes in wind stress, although in this case the mechanism involved might be related to an increase in pigment cell levels in response to deeper mixing [Siegel et al., 2005]. Advanced and less intense blooms in the eastern side contrasted with delayed blooms of increased magnitude in the western subtropics, coinciding with trends of the same sign in mean chl *a*. All these changes in the seasonality of North Atlantic phytoplankton highlight the tight link between climate forcing and the dynamics of ocean ecosystems, stressing the value of remote sensing data for the monitoring, assessment, and projection of future climate change impacts on ocean ecosystems.

Appendix

3.A Supporting text

3.A.1 Detection and characterization of blooms: SeaWiFS vs. Aqua MODIS

Data corresponding to the seasons between 2003-2004 and 2006-2007 were used to explore the agreement between estimates of the probability of different types of seasonal cycles retrieved from SeaWiFS and MODIS measurements (table 3.B.1 and Figs. 3.B.1 and 3.B.2). Except for two remarkable exceptions associated mainly with spatial variations in sampling efficiency, the main patterns depicted in figure 3.2 in the main text remained almost unaltered. First, the amount of sampling dates at northern latitudes was higher for Aqua MODIS, resulting in an extension of the northern limit of the single bloom region in the Arctic region. The probability of detecting bimodal cycles was also slightly higher in data retrieved by Aqua MODIS. Second, the probability of detecting any kind of seasonal cycle in the equatorial and eastern tropical Atlantic was in general higher when chl *a* time series derived from the SeaWiFS sensor were employed. The same results were found when using chl *a* estimates retrieved using the OCv6 band-ratio algorithm. With respect to the GSM algorithm, there was a greater similarity between sensors in the probability of detecting single spring bloom seasonal cycles in northern latitudes, but a larger disagreement in the detection of autumn/winter blooms in the tropics (figure 3.B.2).

Despite the better match between probabilities derived from different sensors in northern latitudes when using the OCv6 algorithm, the disagreement in the tropics was much more important, even without attending to differences in total area. For instance, the difference (SeaWiFS – Aqua MODIS) in the probability of detection of spring blooms were -0.127 (GSM) vs. -0.048 (OCv6) at 75°N, but -0.056 (GSM) vs -0.206 (OCv6) for autumn/winter blooms at 20°N. These figures further support our choice of GSM based chl *a* retrievals. At the same time, these differences motivated the exclusion of locations north of 70°N in the analyses concerning changes in incidence at the basin scale (see Incidence of different types of seasonality at the beginning of the Results section in the main text). At the level of each pixel location, the distribution of the differences in estimated probabilities had zero mode for all years and for all the types of seasons distinguished (figure 3.B.3). Similar results were found with OCv6 data (not shown).

The timing (defined as the day of maximum increase in accumulated chl *a*) and the magnitude of seasonal peaks (defined as the peak chl *a* concentration during a bloom) were estimated for each season and pixel location from posterior simulations of the smoothing model fitted to chl *a* observations. We considered only locations where the cumulated probability of detecting either type of bloom was greater than 0.5 during the entire period (figure 3.2). Estimates corresponding to single-peaked and bimodal seasonalities were pooled together. The agreement between estimates retrieved from SeaWiFS and Aqua MODIS measurements was in general good (table 3.B.1 and Figs. 3.B.4 and 3.B.5, respectively). The distribution of differences in estimates at the pixel level were symmetric and centered around zero, except for a slight bias in estimates of the timing of autumn/winter peaks and a trend towards higher peak chl *a* values in estimates retrieved using Aqua MODIS data. Curiously, this last pattern reversed (but did not disappear) when using chl *a* data based on the OCv6 algorithm. Distributions revealed nevertheless for either sensor the noisy nature of both statistics, so we analyzed changes between years by fitting a linear model to estimates derived from posterior simulations for each season including a fixed effects factor to account for the sensor employed to retrieve chl *a* values. This allowed us to characterize mean patterns and to estimate potential trends and, at the same time, to take into account uncertainty in timing and magnitude estimates based on data gathered by different sensors.

3.A.2 Effect of chl *a* algorithm on incidences and derived estimates

The results presented in the main text contrasted to some extent with those found when chl *a* estimates were retrieved using the OCv6 band-ratio algorithm. In the case of changes in the incidence of different types of seasonal cycles (table 3.B.2 and figure 3.B.9), posterior estimates indicated a trend towards an increased incidence of spring seasonal cycles in polar and subpolar regions. This increase was compensated by reduced bimodal cycles, with even a slight decrease in the prevalence of locations where no peak was detected. The positive trend in autumn/winter cycles in temperate latitudes and changes in other regions of the North Atlantic remained almost unaltered, although trends in tropical and equatorial regions were noisier. There were some biases between estimates derived with different algorithms for both the climatological mean and the rate of change of the timing and magnitude of seasonal peaks (figure 3.B.12). Biases included even reversals in the sign of time trends in some localized regions (figure 3.B.14). The disagreement was more important for trends in the timing of autumn/winter blooms, with a greater prevalence of trends towards advanced blooms in the Subtropical gyre. The same difference was detected in the region with bimodal cycles, with an increase in rates towards earlier blooms in the temperate Northeast Atlantic. On the other hand, the slight predominance of areas presenting delayed spring blooms in the northern North Atlantic was displaced in favor of earlier blooms (e.g. a decline from 56.0 to 51.2%), whereas the proportion of areas pre-

senting increasing or decreasing peaks became almost the same. The agreement between changes in magnitude was in general better than between estimates of changes in timing (figure 3.B.12), so the relationship with changes in total biomass remained almost unaltered. Finally, the relationship between bloom statistics and the environmental factors considered remained almost identical (e.g. the correlation between maps was always greater than 0.75).

3.A.3 Retrieval of chl *a* data and estimation of bloom metrics (extra discussion)

One of the main strengths advocated for the use of remotely sensed phytoplankton phenology in the monitoring of ocean ecosystems is the independence of bloom statistics to the sensor employed to retrieve chl *a* data [Platt and Sathyendranath, 2008]. However, our study highlighted on the one hand the importance of considering potential biases derived from employing data retrieved by different sensors and, on the other, the importance of the remote sensing algorithm used to convert water leaving radiances into chl *a* concentration estimates. The overlap between SeaWiFS and MODIS allowed us to examine differences between bloom metrics and between derived statistics. We found in general a good agreement between both sensors, although differences in data coverage impacted estimates of the prevalence of different types of seasonal cycle [Gregg and Casey, 2007]. There were also small differences between estimates of the timing and magnitude of the bloom. We tried to prevent these biases by restricting the areas considered in our analyses and, especially, by including a term identifying the sensor that retrieved chl *a* data in all analyses. Otherwise, serial deviations in bloom statistics might seriously alter estimates of climatological patterns and time trends.

Differences between sensors depended upon the type of algorithm employed to retrieve chl *a*. We chose in advance the Garver-Siegel-Maritorena semi-analytical algorithm (GSM, Siegel et al. 2005; Maritorena et al. 2002), but we repeated all our analyses using chl *a* data retrieved using the empirical Ocean Color algorithm, which is more commonly used. Bloom statistics, especially the incidence of different types of seasonal cycle, were better replicated when chl *a* observations retrieved by different sensors were estimated using the GSM algorithm. These differences resulted in important changes in all the patterns examined in this study, especially in the tropics and in the subtropics. An improvement in bloom detection and characterization in these regions might be expected from recent advances in empirical algorithms [Hu et al., 2012]. Nevertheless, taken together our results highlight the need to consider carefully potential biases in phenological studies that involve merging data from different satellite sensors (something unavoidable for long term studies), as well as the need to take into consideration the advantages of using chl *a* data estimated using semi-analytical algorithms. Ensuring a prolonged overlap between consecutive ocean color missions might improve the monitoring of marine phytoplankton phenology.

3.B Supporting tables and figures

3.B.1 Supporting Material and Methods

Table 3.B.1: Agreement between bloom statistics estimated from different platforms and sensors (SeaWiFS and MODIS). Differences in the probabilities of detecting different seasonal peaks, and in the timing and magnitude of spring and autumn/winter blooms, were extracted from 1000 posterior simulations of models fitted to chl a retrievals from each sensor (see Materials and Methods). The magnitude of blooms was defined as the peak chl a concentration attained during the bloom, and in this case differences were calculated in a log₁₀ scale. In all cases, statistics derived from MODIS data were subtracted from SeaWiFS estimates and, for timing and magnitude statistics, only locations where $p_{detection} > 0.5$ were considered. The mean, and the median and 90% highest probability density regions (square brackets) were estimated to summarize the agreement between both sets of estimates. The statistics cover the effective period of overlap between both sensors (e.g. four seasons between 2003-2004 and 2006-2007). figure 3.B.1 presents probability maps for SeaWiFS and MODIS separately, while figure 3.B.2 shows zonal averages. Figs. 3.B.3, 3.B.9 and 3.B.4 present density plots for the different statistics.

	Season			
	2003-2004	2004-2005	2005-2006	2006-2007
Δ Probability of detection _{SeaWiFS-MODIS}				
Spring	0.03 [-0.44, 0.00, 0.57]	0.01 [-0.49, 0.00, 0.55]	0.02 [-0.43, 0.00, 0.52]	0.02 [-0.47, 0.00, 0.56]
Autumn/winter	-0.02 [-0.51, 0.00, 0.36]	-0.00 [-0.42, 0.00, 0.43]	-0.00 [-0.43, 0.00, 0.43]	-0.01 [-0.46, 0.00, 0.42]
Bimodal	0.00 [-0.54, 0.00, 0.56]	-0.01 [-0.52, 0.00, 0.50]	-0.01 [-0.53, 0.00, 0.52]	-0.01 [-0.57, 0.00, 0.55]
No peak detected	0.00 [-0.74, 0.00, 0.63]	0.00 [-0.75, 0.00, 0.64]	-0.00 [-0.70, 0.00, 0.60]	-0.00 [-0.73, 0.00, 0.63]
Not enough data	-0.01 [-0.25, 0.00, 0.17]	-0.00 [-0.19, 0.00, 0.17]	0.00 [-0.15, 0.00, 0.16]	0.00 [-0.20, 0.00, 0.23]
Δ Timing of the bloom _{SeaWiFS-MODIS}				
Spring	1.19 [-24.00, 1.00, 27.00]	0.14 [-29.00, 0.00, 28.00]	0.50 [-27.00, 1.00, 28.00]	0.68 [-26.00, 0.00, 29.00]
Autumn/winter	2.82 [-33.00, -3.00, 86.00]	-0.53 [-36.00, -3.00, 44.00]	1.63 [-34.00, -1.00, 50.00]	2.62 [-34.00, 0.00, 48.00]
Δ Log ₁₀ Magnitude of the bloom _{SeaWiFS-MODIS}				
Spring	-0.05 [-0.34, -0.04, 0.25]	-0.08 [-0.39, -0.07, 0.19]	-0.05 [-0.30, -0.04, 0.19]	-0.04 [-0.36, -0.03, 0.25]
Autumn/winter	-0.07 [-0.30, -0.04, 0.08]	-0.06 [-0.27, -0.02, 0.08]	-0.06 [-0.26, -0.02, 0.08]	-0.07 [-0.55, -0.03, 0.11]

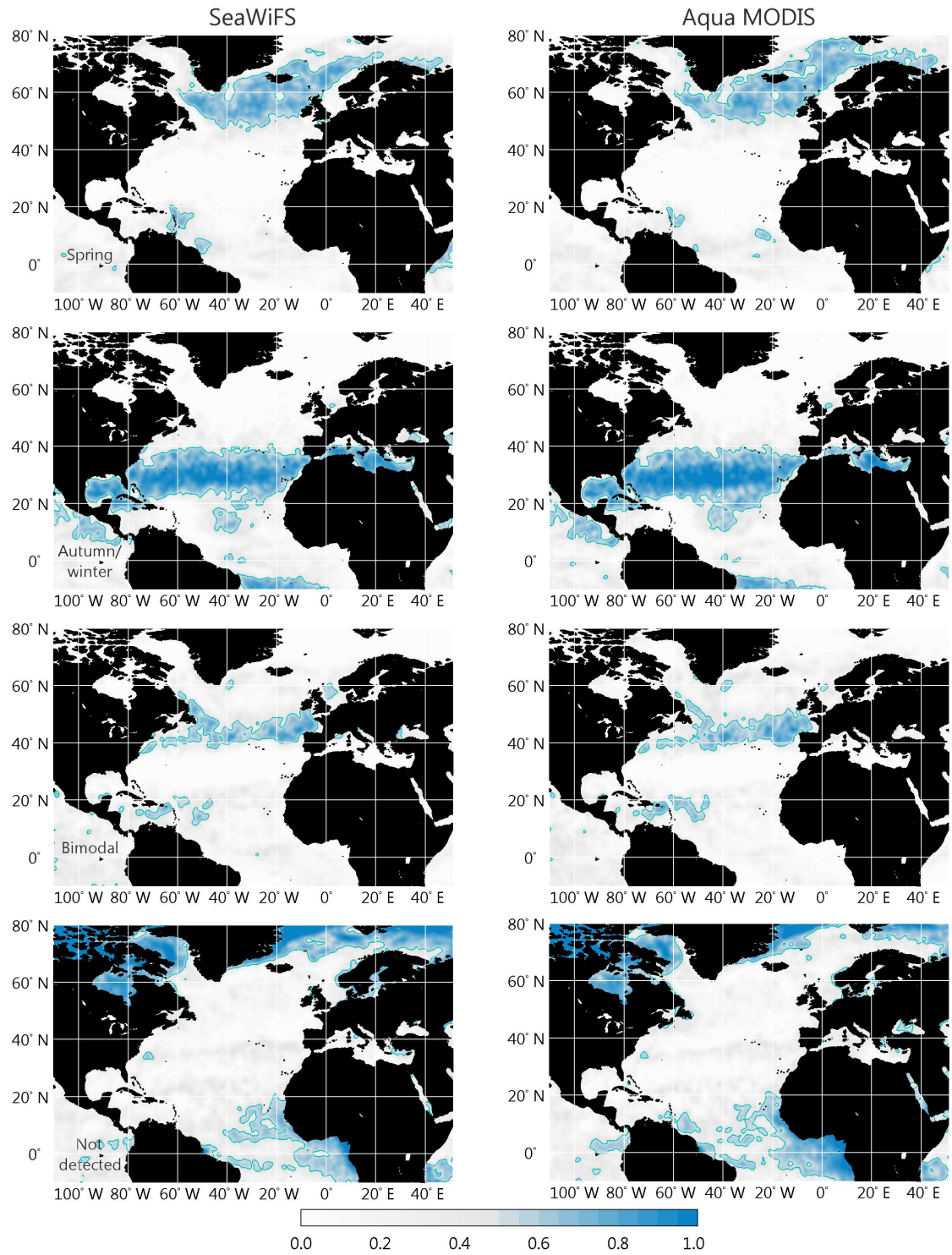


Figure 3.B.1: Comparison between the probability of detecting different types of seasonal cycles derived from either SeaWiFS (left) or Aqua MODIS (right) chl *a* time series for the four overlapping seasons available (2003-04 thru 2006-07). Two different possibilities lead to the failure of the proposed methodology to detect a bloom in some regions; there were not enough data (*left panel*) or, even if data were available, posterior simulations of the model fitted each season did not contain a peak meeting the conditions assumed to define a seasonal peak (see Materials and Methods for further details).

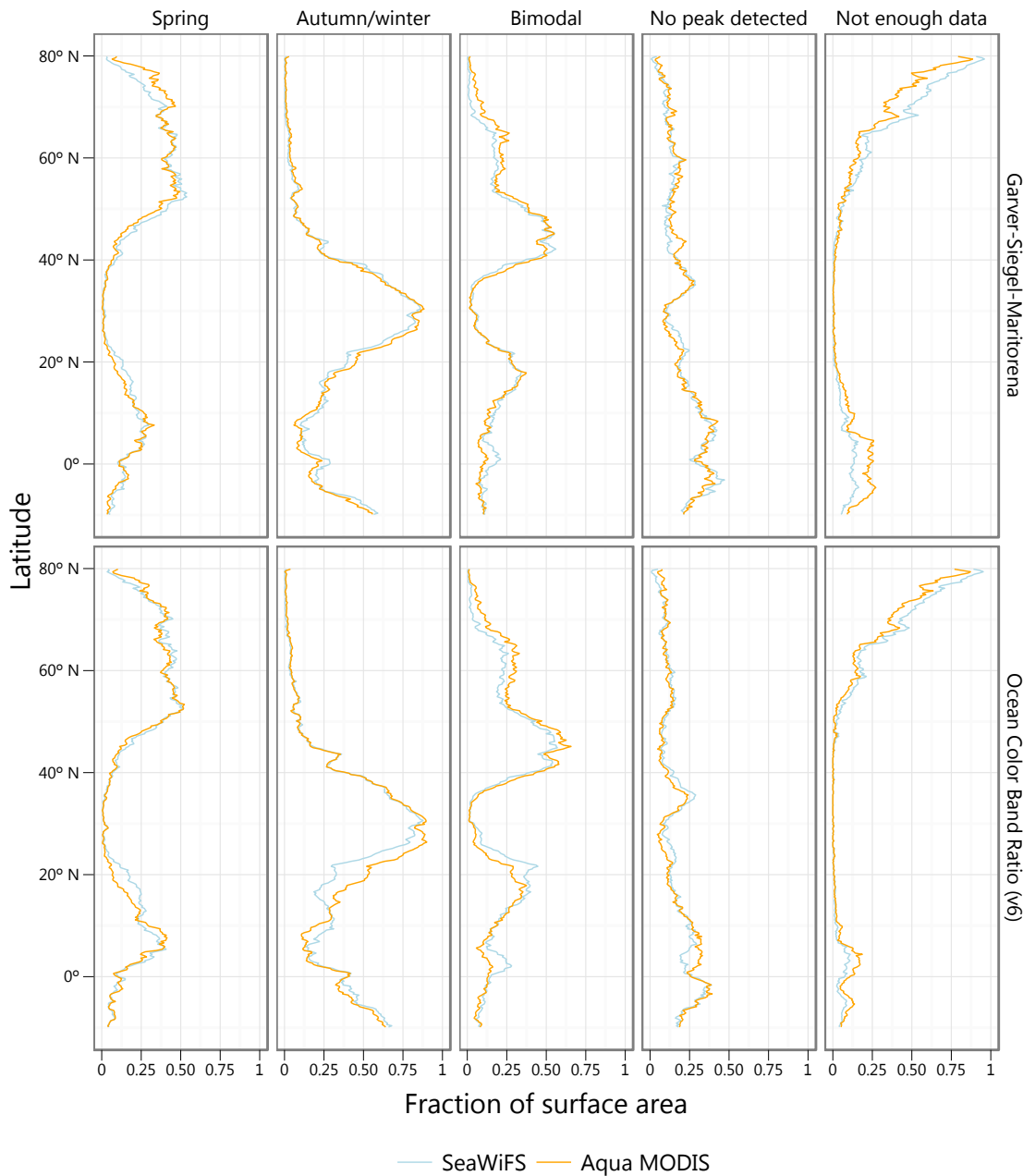


Figure 3.B.2: Zonal averages of the probability of detecting different types of seasonal cycles derived from either SeaWiFS or Aqua MODIS Chla *a* time series for the four overlapping seasons available (2003-04 thru 2006-07). Graphs in the first row are based on chl *a* concentration estimates retrieved using the Garver-Siegel-Maritorena (GSM) algorithm, while graphs in the second row are based on data retrieved using the Ocean Color band ratio (OCv6) algorithms (see Materials and Methods for further details).

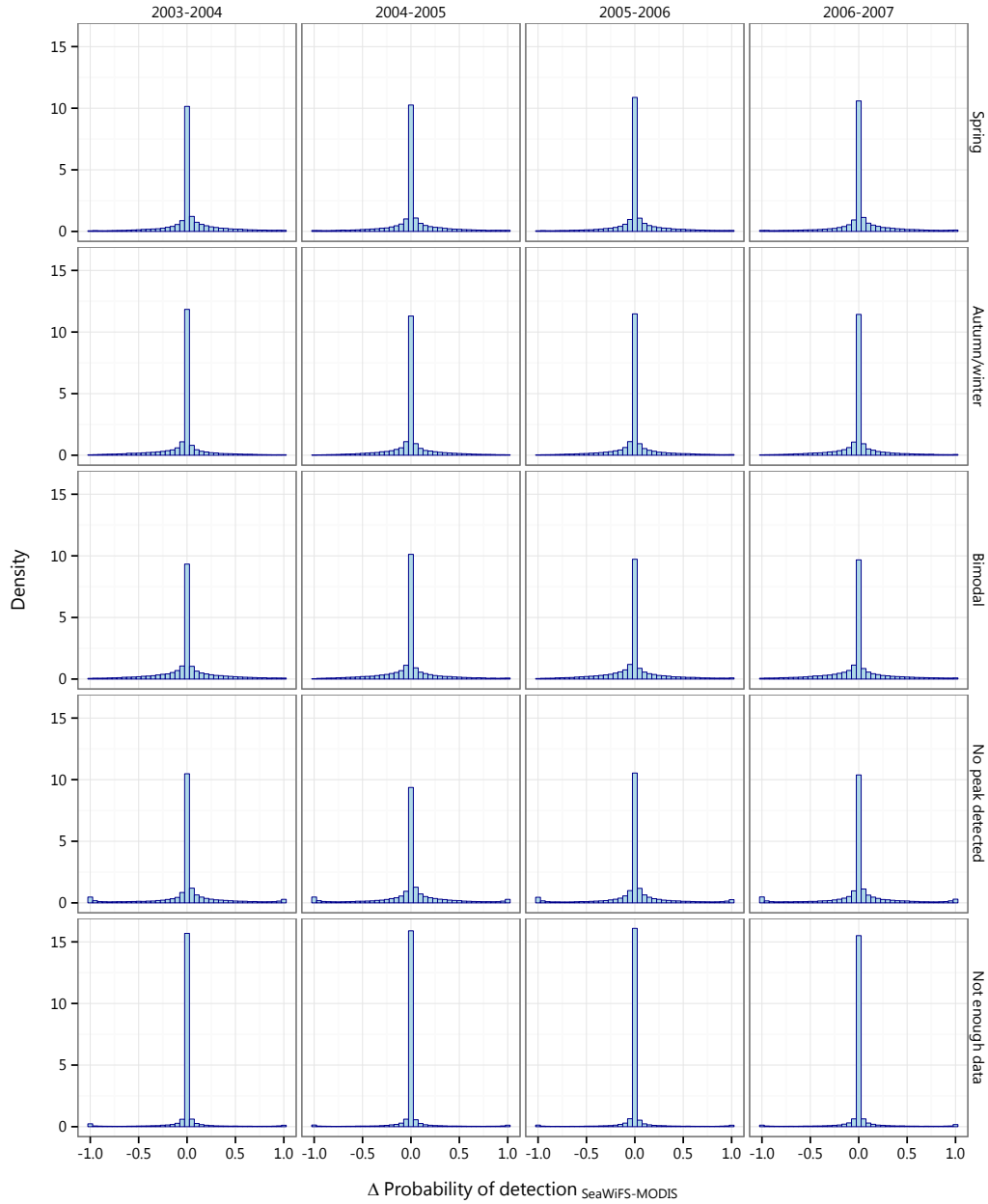


Figure 3.B.3: Density plots showing the distribution of the differences between SeaWiFS and MODIS based estimates of the probability of detection for different seasonal cycles. Differences were calculated from 1000 posterior simulations of models fitted to chl *a* retrievals for each sensor (see Materials and Methods). In all the cases, statistics derived from MODIS data were subtracted from SeaWiFS estimates. The statistics cover the effective period of overlap between both sensors (e.g. four seasons between 2003-2004 to 2006-2007).

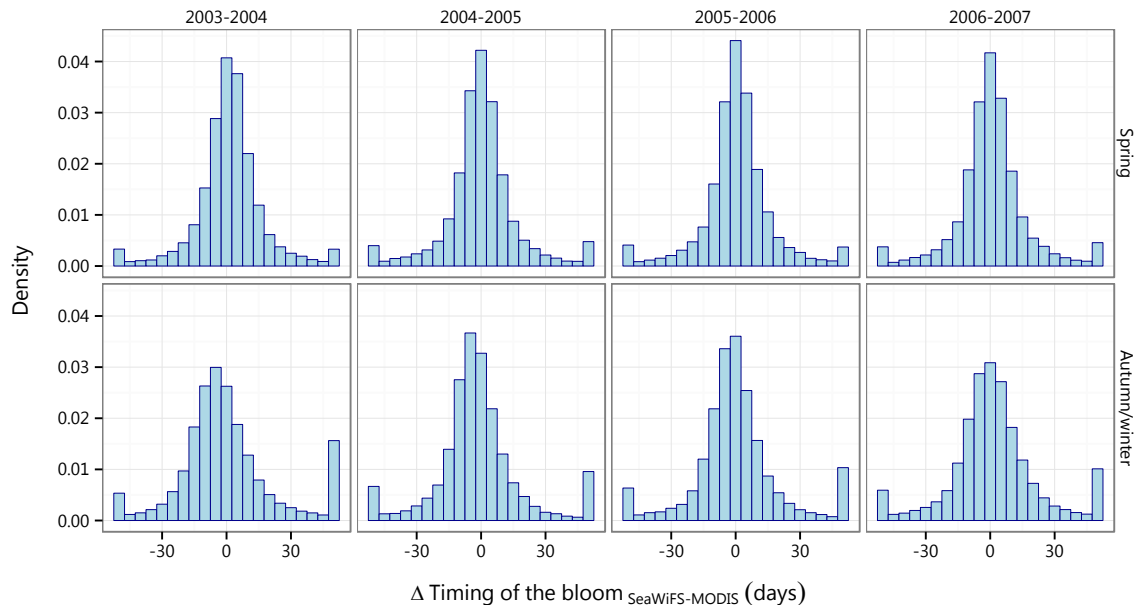


Figure 3.B.4: Density plots showing the distribution of the differences between SeaWiFS and MODIS based estimates of the median timing of spring and autumn/winter peaks in chl *a*. Medians were extracted from 1000 posterior simulations of models fitted to chl *a* retrievals for each sensor (see Materials and Methods). In all the cases, statistics derived from MODIS data were subtracted from SeaWiFS estimates, and only locations where $P_{\text{detection}} > 0.5$ were considered. The statistics cover the effective period of overlap between both sensors (e.g. four seasons between 2003-2004 to 2006-2007). A binwidth of 5 days was employed to build the histograms, although differences greater than 50 days were pooled together in the last bin (they represent the 4.0% and 8.5% of the cases for spring and autumn/winter blooms, respectively). These larger deviations correspond to sporadic huge differences arising in the transition zone, in pixels that were classified in a different category by different sensors (this effect was more important in the case of bimodal and autumn/winter blooms).

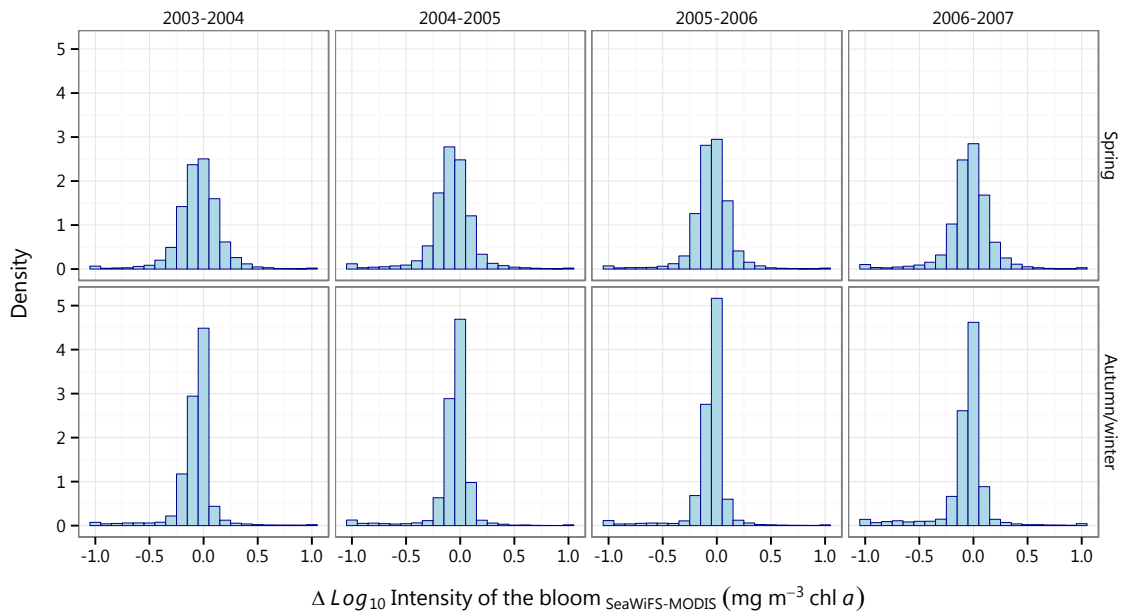


Figure 3.B.5: Density plots showing the distribution of the differences between SeaWiFS and MODIS based estimates of the magnitude of spring and autumn/winter blooms in chl a . The magnitude of blooms was defined as the peak chl a concentration attained during the bloom. Medians were extracted from 1000 posterior simulations of models fitted to chl a retrievals for each sensor (see Materials and Methods), and differences were calculated in a \log_{10} scale. In all the cases, statistics derived from MODIS data were subtracted from SeaWiFS estimates, and only locations where $p_{\text{detection}} > 0.5$ were considered. The statistics cover the effective period of overlap between both sensors (e.g. four seasons between 2003-2004 to 2006-2007). A binwidth of $\log(0.05) \text{ mg m}^{-3}$ was employed to build the histograms, although differences greater than a factor of 10 were pooled together in the last bin (they represented less than 1.0% of the cases).

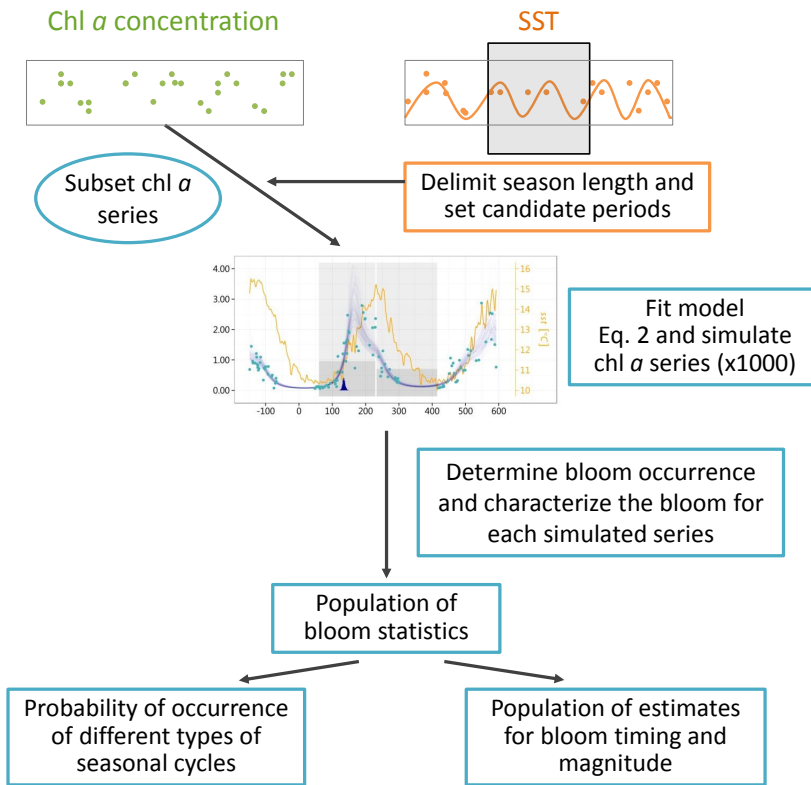


Figure 3.B.6: Schematic representation of the algorithm employed to detect and characterize phytoplankton seasonality using time series of remotely sensed chl α . Seasonal extremes in SST were used to delimit each season and to identify candidate periods for seasonal peaks of increase in chl α concentration. We considered a period centered on each calendar year but covering the time period between previous and next year SST maxima (see Jönsson and Eklundh 2002). Local extremes in chl α delimited periods of accumulation that were considered as candidate blooms if they reached a level above the 60th percentile of a Gamma distribution fitted to chl α observations between consecutive SST extremes (*i.e.* a minimum and a maximum or viceversa). The choice of this threshold was arbitrary but helped us to reject small amplitude waves. Candidate blooms were then classified either as spring or autumn/winter blooms based on the relative timing of bloom metrics with respect to SST extremes. We considered that a candidate bloom corresponded to a spring bloom if its timing and peak occurred after the seasonal SST minimum but before the SST maximum. Similarly, the timing of autumn/winter blooms must occur between the seasonal SST maximum and the next minimum (avoiding thus possible confusions with next year's spring blooms), even if the timing of the peak occurred after the SST minimum. For a given model realization, only the first candidate bloom meeting the criteria above was retained, although in some cases all the candidates were rejected. Each bloom was later characterized by its timing and by its magnitude, which were estimated for each model realization and retained for further analysis. The timing of the bloom was defined as the day when the net rate of increase of chl α concentration attained a maximum during each wave of increase, while bloom magnitude was defined as the peak chl α concentration attained during the bloom.

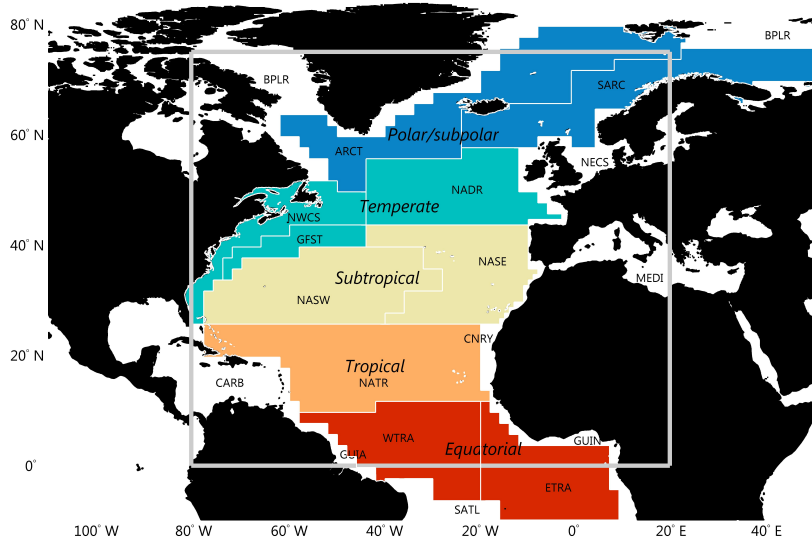


Figure 3.B.7: Map of the North Atlantic presenting the regions employed to estimate different statistics by grouping biogeochemical provinces delimited by Longhurst [2007]. These regions were further constrained to the area delimited by the grey rectangle in order to minimize the mismatch between estimates based on different sensors.

Abbreviations [Province (biome)]: ARCT, Atlantic Arctic (Polar); BPLR, Bolear Polar (Polar); CARB, Caribbean (Trades); CNRY, Canary Coastal (Coastal); ETTRA, Eastern Tropical Atlantic (Trades); GFST, Gulf Stream (Westerlies); GUILA, Guianas Coastal (Coastal); GUIN, Guinea Current Coastal (Coastal); MEDI, Mediterranean Sea and Balck Sea (Westerlies); NADR, North Atlantic Drift (Westerlies); NASE, North Atlantic Subtropical Gyral East (Westerlies); NASW, North Atlantic Subtropical Gyral West (Westerlies); NATR, North Atlantic Tropical Gyral (Trades); NECS, North East Atlantic Shelves (Coastal); NWCS, Northwest Atlantic Shelves (Coastal); WTRA, Western Tropical Atlantic (Trades); SARC, Atlantic Subarctic (Polar); SATL, South Atlantic Gyral (Trades).

3.B.2 Supporting Results: Incidence of different types of seasonality

Table 3.B.2: Changes in the prevalence of different types of seasonal cycle in the North Atlantic for regions defined by grouping biogeochemical provinces delimited by Longhurst [2007] (see figure 3.B.7). A Dirichlet regression model was fitted to areal corrected estimates of the proportion $\pi_{i,j,t}$ of each kind of seasonal cycle (i) and region (j) for each year (t) integrated over the amount of surface where enough data were available. The parameter of the Dirichlet distribution was modeled as a linear combination in the log scale of terms accounting for differences in the mean level ($\mu_{i,j}$), and a second degree polynomial to account for temporal trends. Potential differences in the mean associated with the sensor employed to retrieve chl a concentration were also taken into account by including the kind of Sensor (SeaWiFS or Aqua MODIS) as a fixed effects factor nested within the kind of seasonal cycle ($\delta_{i,j}$). Diffuse, vague uninformative priors were assumed for all model parameters. Note also that orthogonal polynomials were used to represent temporal trends. The mean, the median and 90% highest probability density regions (square brackets) for each coefficient of the model were estimated from 400 posterior samples taken after a five step thinning of chains with a length of 2000 iterations following a 18000 iterations burn in period, which was judged long enough to allow convergence. The model was fitted using an adaptive Metropolis algorithm [Roberts and Rosenthal, 2009].

$\pi_{i,j,t} \sim Dir(\alpha_{i,j,t})$, $\log(\alpha_{i,j,t}) = \mu_{i,j} + \delta_{i,j} \times Sensor + \gamma_1 \times t + \gamma_2 \times t^2$					
i	j	$\mu_{i,j}$	$\delta_{i,j}$	$\gamma_1 [yr^{-1}]$	$\gamma_2 [yr^{-2}]$
<i>Polar/subpolar</i>					
Spring	Spring	4.58 [4.20, 4.64, 4.91]	0.27 [-0.14, 0.16, 0.78]	-1.85 [-3.22,-1.57,-1.22]	3.63 [2.10, 3.47, 5.04]
Autumn/winter	Spring	1.50 [0.88, 1.50, 2.04]	0.55 [-0.20, 0.52, 1.41]	-0.63 [-2.19,-0.41, 0.45]	5.00 [3.24, 4.89, 6.53]
Bimodal	Spring	3.58 [3.26, 3.55, 3.97]	0.55 [0.11, 0.48, 1.04]	-1.17 [-2.34,-0.92,-0.58]	4.11 [2.58, 4.01, 5.56]
Notdetected	Spring	4.03 [3.71, 4.14, 4.31]	0.11 [-0.24, 0.05, 0.54]	-1.38 [-2.74,-1.15,-0.71]	4.86 [3.29, 4.54, 6.24]
<i>Temperate</i>					
Spring	Spring	4.57 [4.34, 4.57, 4.83]	-1.64 [-2.06,-1.64,-1.23]	-1.75 [-3.21,-2.03, 0.21]	-1.21 [-2.91,-1.25, 0.46]
Autumn/winter	Spring	4.28 [4.03, 4.28, 4.56]	-1.58 [-2.01,-1.56,-1.19]	0.30 [-0.98, 0.10, 1.93]	-0.18 [-1.70,-0.20, 1.32]
Bimodal	Spring	5.04 [4.82, 5.03, 5.30]	-1.57 [-2.03,-1.55,-1.15]	-0.47 [-1.72,-0.65, 1.31]	-0.67 [-2.31,-0.72, 0.97]
Notdetected	Spring	4.07 [3.80, 4.07, 4.35]	-1.43 [-1.87,-1.43,-0.96]	-0.13 [-1.35,-0.32, 1.55]	-0.32 [-1.90,-0.28, 1.12]
<i>Subtropical</i>					
Spring	Spring	2.45 [2.15, 2.45, 2.70]	-1.90 [-2.56,-1.86,-1.29]	1.21 [-0.69, 1.13, 3.46]	-2.74 [-5.24,-2.70,-0.52]
Autumn/winter	Spring	5.84 [5.66, 5.83, 6.02]	-1.95 [-2.60,-1.92,-1.46]	2.63 [0.90, 2.42, 4.77]	-3.26 [-5.62,-3.23,-0.89]
Bimodal	Spring	4.01 [3.85, 4.00, 4.22]	-1.85 [-2.50,-1.81,-1.32]	2.57 [0.73, 2.37, 4.77]	-3.53 [-5.85,-3.30,-1.39]
Notdetected	Spring	4.27 [4.12, 4.26, 4.48]	-2.07 [-2.71,-2.03,-1.57]	1.53 [-0.28, 1.33, 3.82]	-3.76 [-6.27,-3.67,-1.54]
<i>Tropical</i>					
Spring	Spring	2.56 [2.06, 2.58, 2.98]	-0.47 [-0.97,-0.49, 0.05]	-0.47 [-3.39,-0.08, 1.16]	0.51 [-0.95, 0.57, 2.17]
Autumn/winter	Spring	3.81 [3.43, 3.77, 4.25]	-0.01 [-0.40,-0.04, 0.55]	-0.40 [-3.16, 0.09, 1.18]	1.22 [-0.29, 1.38, 3.07]
Bimodal	Spring	3.44 [3.05, 3.44, 3.90]	-0.22 [-0.64,-0.25, 0.29]	-0.61 [-3.20,-0.25, 1.01]	1.80 [0.38, 1.93, 3.53]
Notdetected	Spring	3.50 [3.13, 3.49, 3.93]	-0.21 [-0.61,-0.23, 0.28]	-0.34 [-3.36, 0.13, 1.27]	0.83 [-0.68, 0.96, 2.61]
<i>Equatorial</i>					
Spring	Spring	3.50 [2.96, 3.52, 3.91]	-0.72 [-1.37,-0.85, 0.09]	-0.33 [-2.03,-0.39, 1.27]	-2.17 [-3.96,-2.10,-0.81]
Autumn/winter	Spring	3.26 [2.73, 3.26, 3.69]	-1.12 [-1.75,-1.28,-0.25]	-0.93 [-2.71,-0.83, 0.65]	-2.17 [-4.26,-2.04,-0.65]
Bimodal	Spring	3.30 [2.76, 3.29, 3.73]	-1.28 [-1.87,-1.42,-0.45]	-0.69 [-2.37,-0.75, 1.05]	-1.83 [-3.71,-1.73,-0.54]
Notdetected	Spring	4.17 [3.64, 4.16, 4.63]	-0.67 [-1.32,-0.82, 0.18]	-0.62 [-2.57,-0.65, 1.10]	-1.91 [-3.78,-1.76,-0.49]

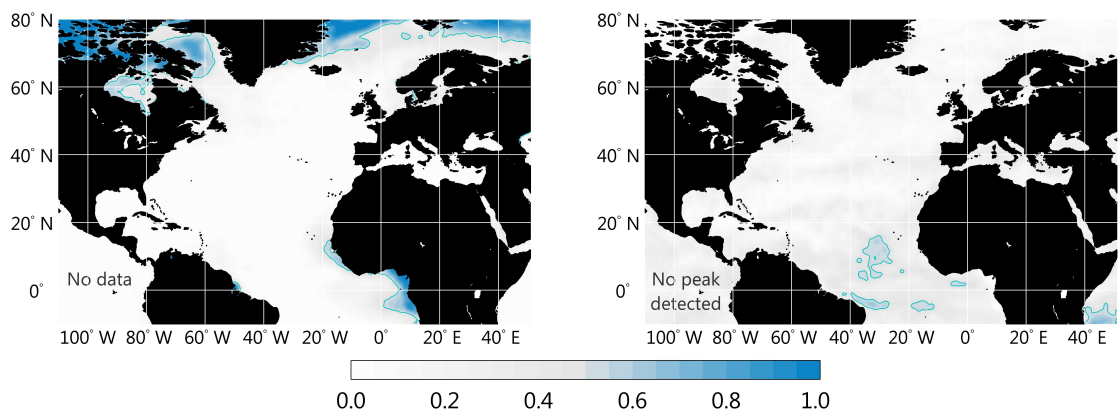


Figure 3.B.8: Probability of not observing any of the characteristic types of seasonal cycle of phytoplankton during 15 seasonal cycles (1998-99 thru 2012-13; data for Aqua MODIS and SeaWiFS was averaged for overlapping seasons). Two different possibilities lead to the failure of the proposed methodology to detect a bloom in some regions; there were not enough data (*left panel*) or, even if data were available, posterior simulations of the model fitted each season did not contain a peak meeting the conditions assumed to define a seasonal peak (see Materials and Methods for further details).

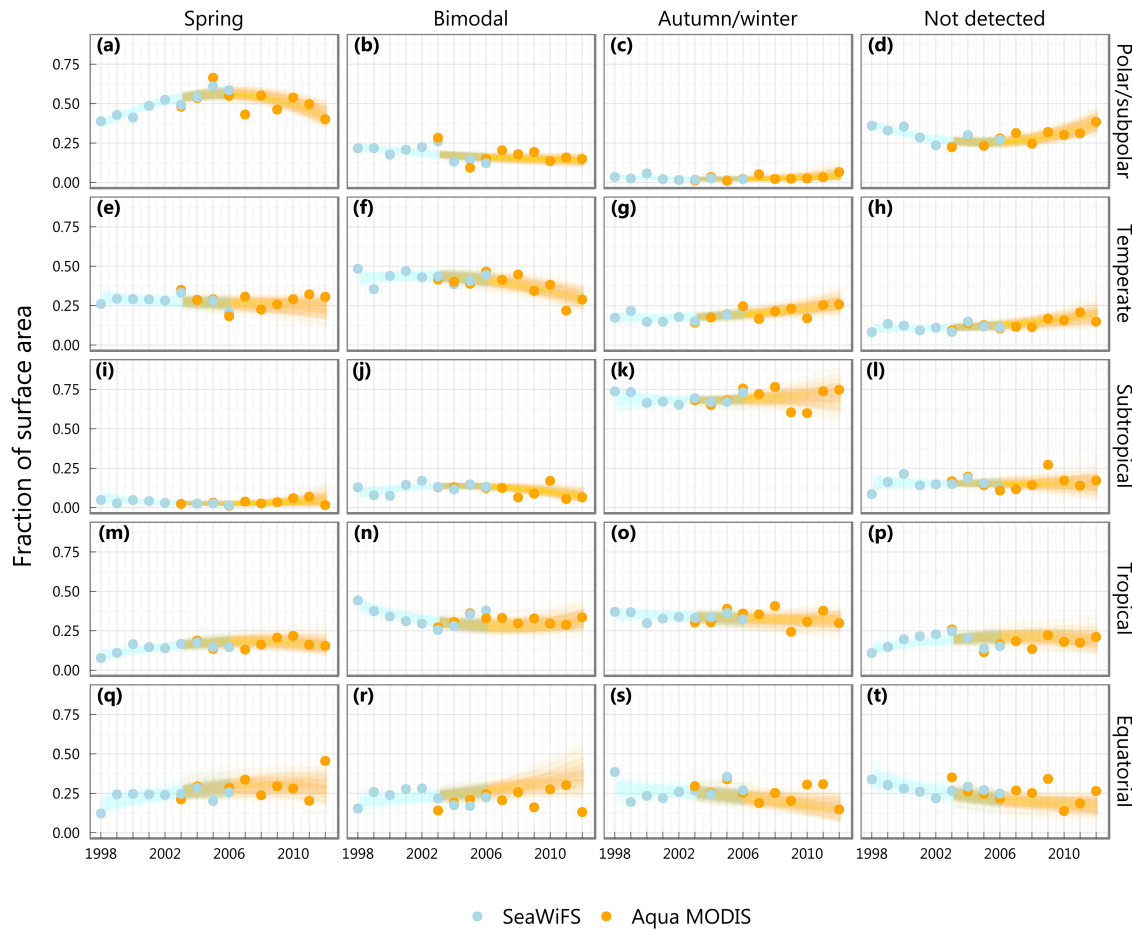


Figure 3.B.9: Prevalence of different types of seasonal cycle in the main biogeochemical regions of the North Atlantic. In contrast to Fig. 2 in the main text, the statistics presented are based on chl *a* estimates retrieved using the OCv6 band-ratio algorithm. Each panel presents the incidence of each type of seasonal cycle after correcting for differences in detectability between sensors (see Detection and characterization of blooms: SeaWiFS vs. Aqua MODIS). Estimates were derived from a weighted integral considering the probabilities for each kind of seasonal cycle (e.g. Fig. 1 in the main text). Lines correspond to posterior simulations ($n = 400$) from a Dirichlet regression model accounting for differences between sensor and including a second degree polynomial to account for temporal trends (table 3.B.2). Alpha blending was employed to represent model uncertainty, with $\alpha = 1/80$ (i.e. the overlap of 80 lines correspond to full opacity). Regions were based on the biogeochemical provinces defined by Longhurst [2007] (see figure 3.B.7).

3.B.3 Supporting Results: Timing and magnitude of seasonal peaks

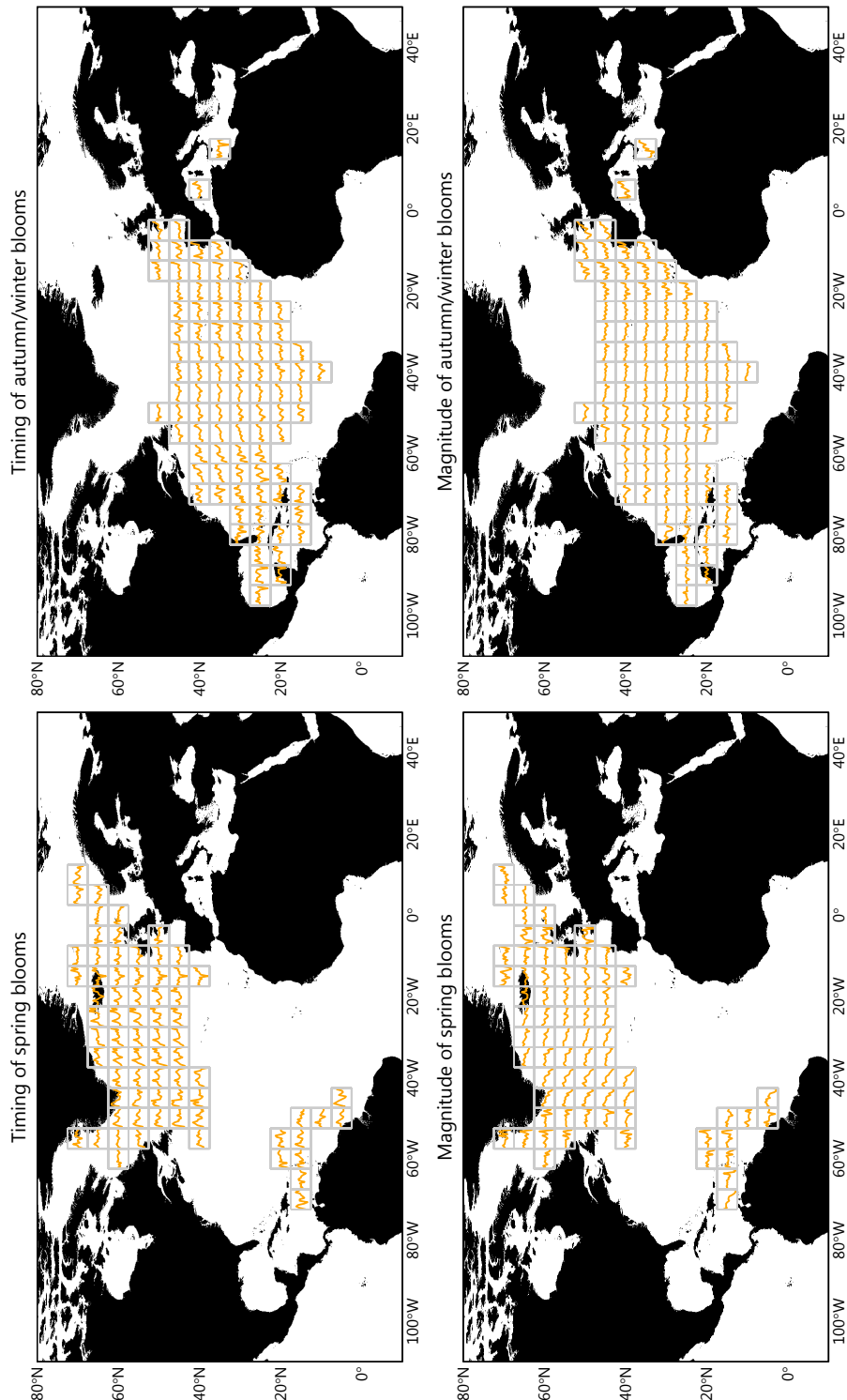


Figure 3.B.10: Time trends in the timing and magnitude of spring and autumn/winter blooms in the North Atlantic during 1998–2012, averaged over five degree boxes. Lines levelling up (down) correspond to boxes where bloom date is delaying (advancing) or where bloom magnitude is increasing (decreasing). See figure 3.3 in the main text for higher scale estimates of mean levels and time trends for each statistic.

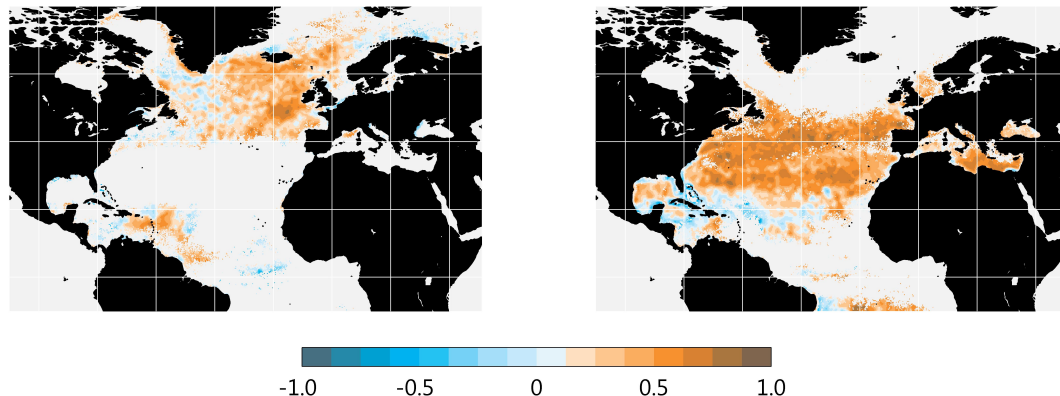


Figure 3.B.11: Temporal association between the magnitude and the timing of spring (*left panel*) and autumn/winter (*right*) blooms in the North Atlantic during 1998–2012. A positive association between these indexes might promote in principle a predominance of trends towards earlier (later) blooms of decreased (increased) magnitude.

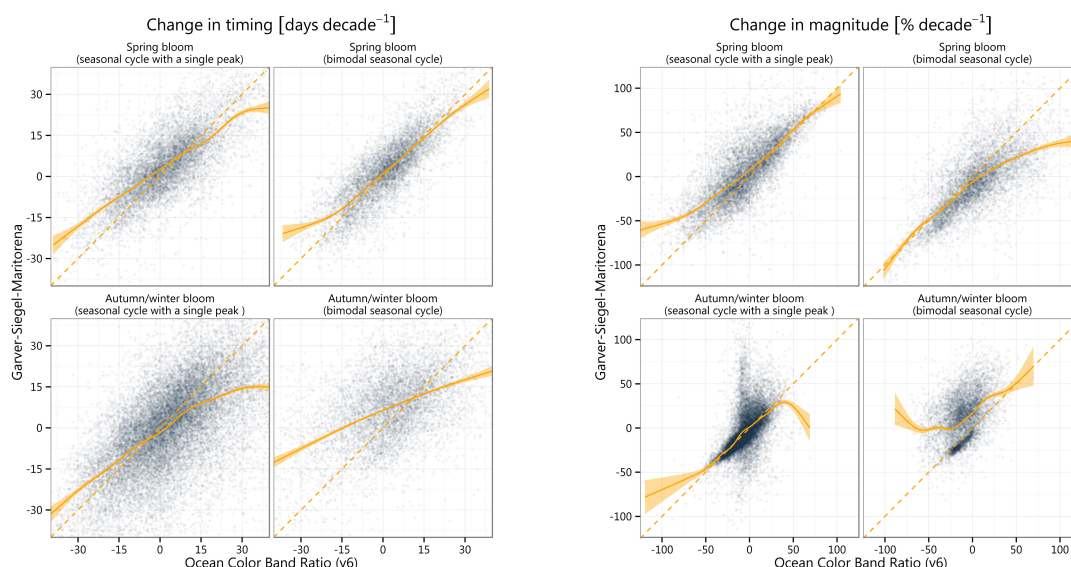


Figure 3.B.12: Relationship between temporal trends in the timing (days decade⁻¹) and in the magnitude (% decade⁻¹) of spring and autumn/winter blooms in the North Atlantic between 1998–2012 derived from chl *a* concentrations estimated using the Garver-Siegel-Maritorena (GSM) algorithm and the Ocean Color band ratio (OCv6) algorithm (see Materials and Methods for further details). Blue dots represent trend estimates for each algorithm which, in case of a perfect match, would be distributed around the dashed orange line. The orange continuous line is a nonlinear estimator included as a guide. Alpha blending was applied to the points to provide an impression of their relative density, with $\alpha = 1/10$ (i.e. the overlap of 10 points correspond to full opacity).

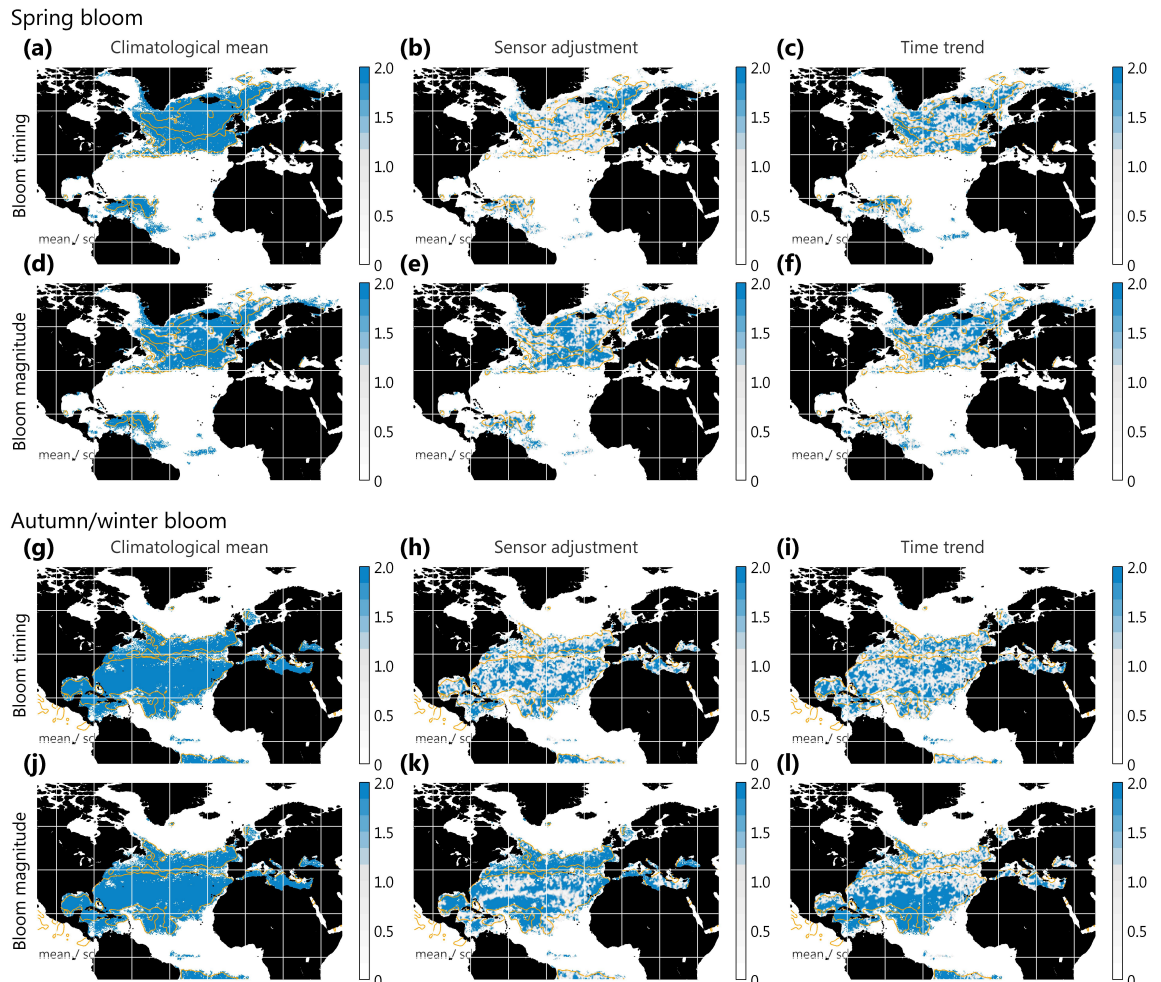


Figure 3.B.13: Uncertainty maps for parameter estimates presented in figure 3.3 in the main text. Each map presents the ratio between the mean and standard deviation of each coefficient estimate. The panels correspond to the posterior mean date and chl *a* concentration, differences between sensors and time trends in the timing and magnitude of spring (*upper panels*) and autumn/winter blooms (*lower panels*). Note also the change in scale between panels. Only locations where the cumulated probability of detecting either type of bloom was greater than 0.5 were considered. Estimates corresponding to single-peaked and bimodal seasonalities were pooled together. **Orange contours** delimit regions where the probability of each type of seasonal cycle is greater than 0.5 (see figure 3.1 in the main text).

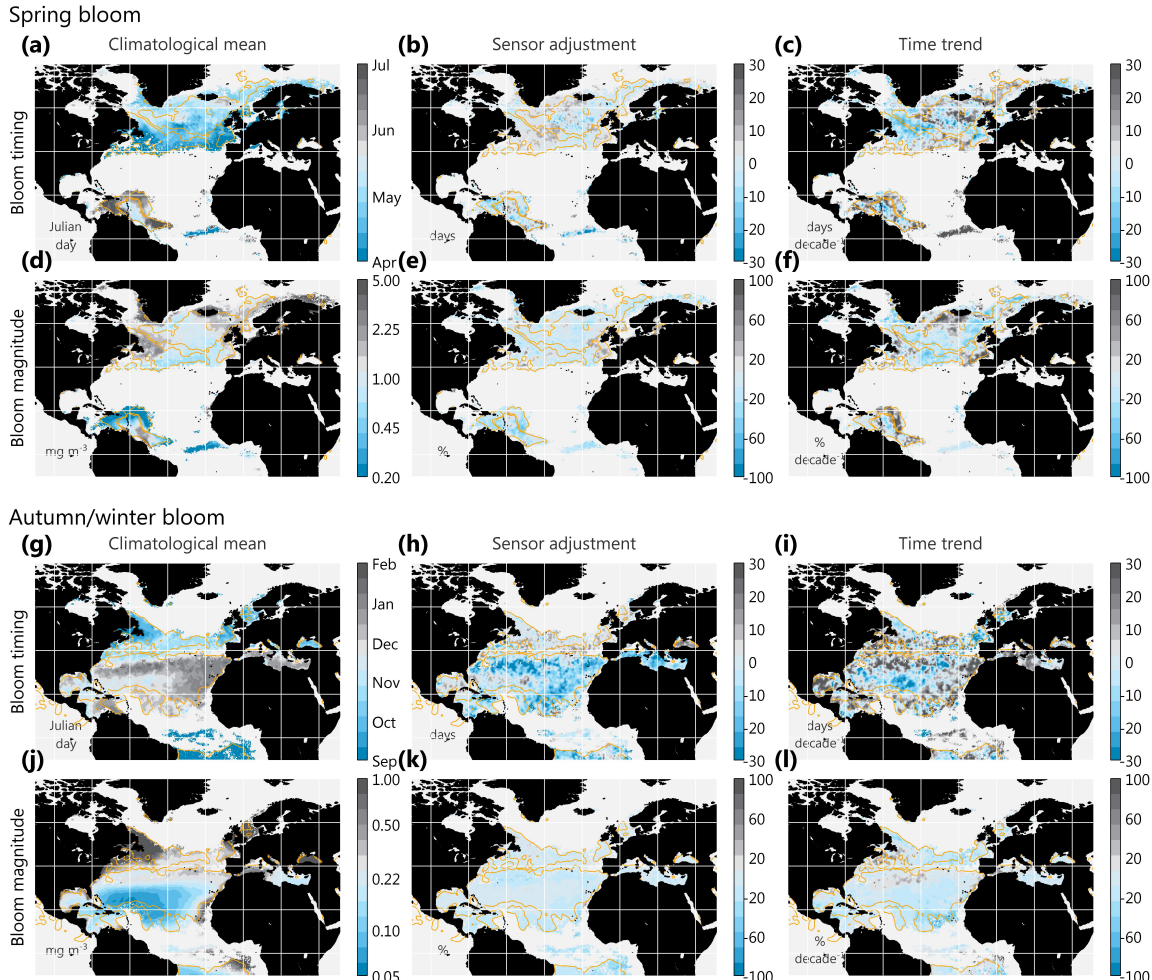


Figure 3.B.14: Timing and magnitude of spring (*upper panels*) and autumn/winter blooms (*lower panels*) derived from OC4v6 data (same as figure 3.3 in the main text). Maps in each column correspond to the posterior mean date (Julian date) and chl a concentration (mg m^{-3}), the differences between sensors (in days and as a percentage, respectively) and the time trends (days or percentage per decade) during 1998–2012 (units are also indicated in the bottom left corner of each map). Uncertainty maps for each estimate are presented in the next page (*i.e.* the ratio between the mean and standard deviation of each coefficient estimate). A model including a linear trend in time was fitted to estimates of bloom statistics. The model included also a fixed effect factor to account for biases in mean bloom metrics between different sensors. Bloom statistics estimated from SeaWiFS data were taken as baseline. The timing (defined as the day when the net rate of increase of chl a concentration attained a maximum during each wave of increase) and the magnitude (defined as the peak chl a concentration attained during a bloom) of spring and autumn/winter blooms was determined for each season and pixel location from posterior simulations of the smoothing model fitted to chl a observations (equation 3.2). Only locations where the cumulated probability of detecting either type of bloom was greater than 0.5 were considered. Estimates corresponding to single-peaked and bimodal seasonalities were pooled together. Orange contours delimit regions where the probability of each type of seasonal cycle is greater than 0.5 (see figure 3.1 in the main text).

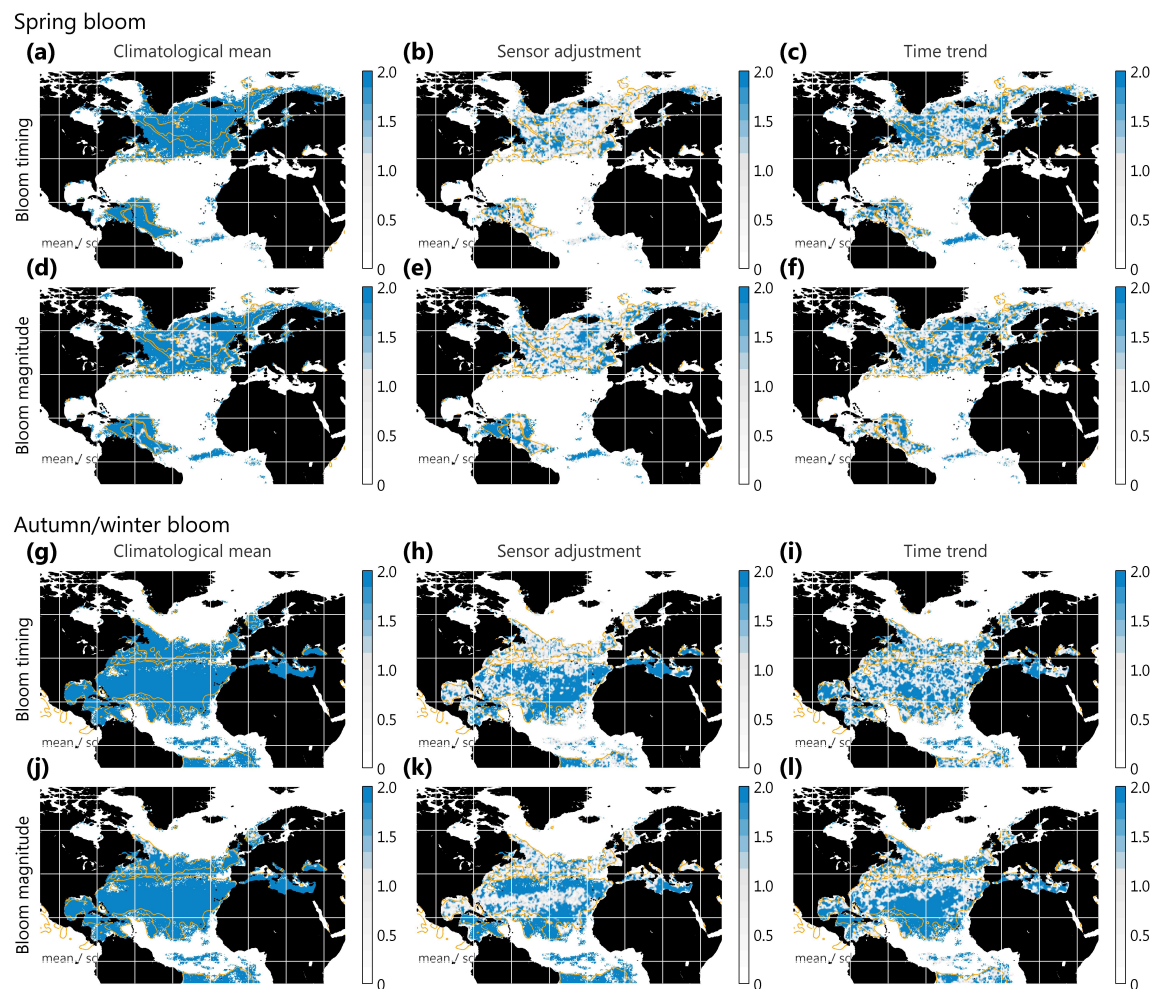


Figure 3.B.13: (continued).

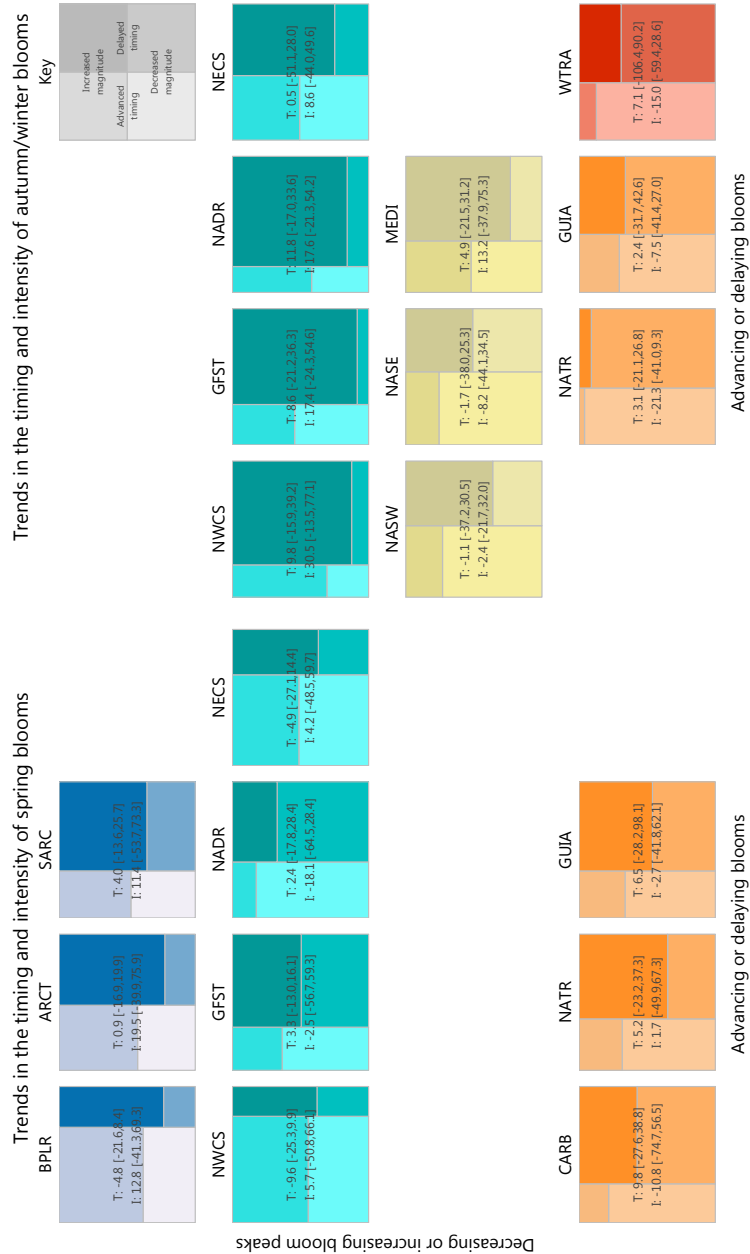


Figure 3.B.14: Prevalence of temporal trends in the timing and magnitude of spring and autumn/winter blooms in the North Atlantic during 1998–2012. A mosaic plot was prepared for each of the Longhurst 2007 provinces, given that only trends estimated in locations where one kind of seasonal cycle predominated were considered (*i.e.* $p > 0.5$, see figure 3.1 in the main text). Rows and colors correspond to the classification presented in figure 3.B.7. Within each panel, the area of each rectangle is proportional to the relative frequency of the four possible combinations of the sign of trends in the timing and in the magnitude of spring and autumn/winter blooms. Beginning in the top left and moving clockwise, each rectangle corresponds to (*i*) blooms occurring earlier and increasing in magnitude, (*ii*) blooms occurring earlier and decreasing in magnitude, (*iii*) blooms occurring later and decreasing in magnitude, and (*iv*) blooms occurring earlier and decreasing in magnitude. A summary of the distribution of absolute values was included in the center of each panel, consisting in the median and 90% posterior density interval for estimated trends in the timing (T , days decade $^{-1}$) and in the magnitude of blooms (I , %decade $^{-1}$). Note that the Longhurst 2007 provinces represented are not the same for each kind of bloom. See figure 3.B.7 for a map presenting Longhurst provinces.

Abbreviations [Province (biome):] ARCT, Atlantic Arctic (Polar); BPLR, Boreal Polar (Polar); CARB, Caribbean (Trades); GFST, Gulf Stream (Westerlies); GUIA, Guianas Coastal Province (Coastal); MEDI, Mediterranean Sea and Black Sea (Westerlies); NADR, North Atlantic Drift (Westerlies); NASE, North Atlantic Subtropical Gyral East (Westerlies); NASW, North Atlantic Subtropical Gyral West (Westerlies); NATR, North Atlantic Tropical Gyral (Trades); NECS, North East Atlantic Shelves (Coastal); NWCS, Northwest Atlantic Shelves (Coastal); SARC, Atlantic Subarctic (Polar); WTRA, Western Tropical Atlantic (Trades); ETRA, Eastern Tropical Atlantic (Trades).

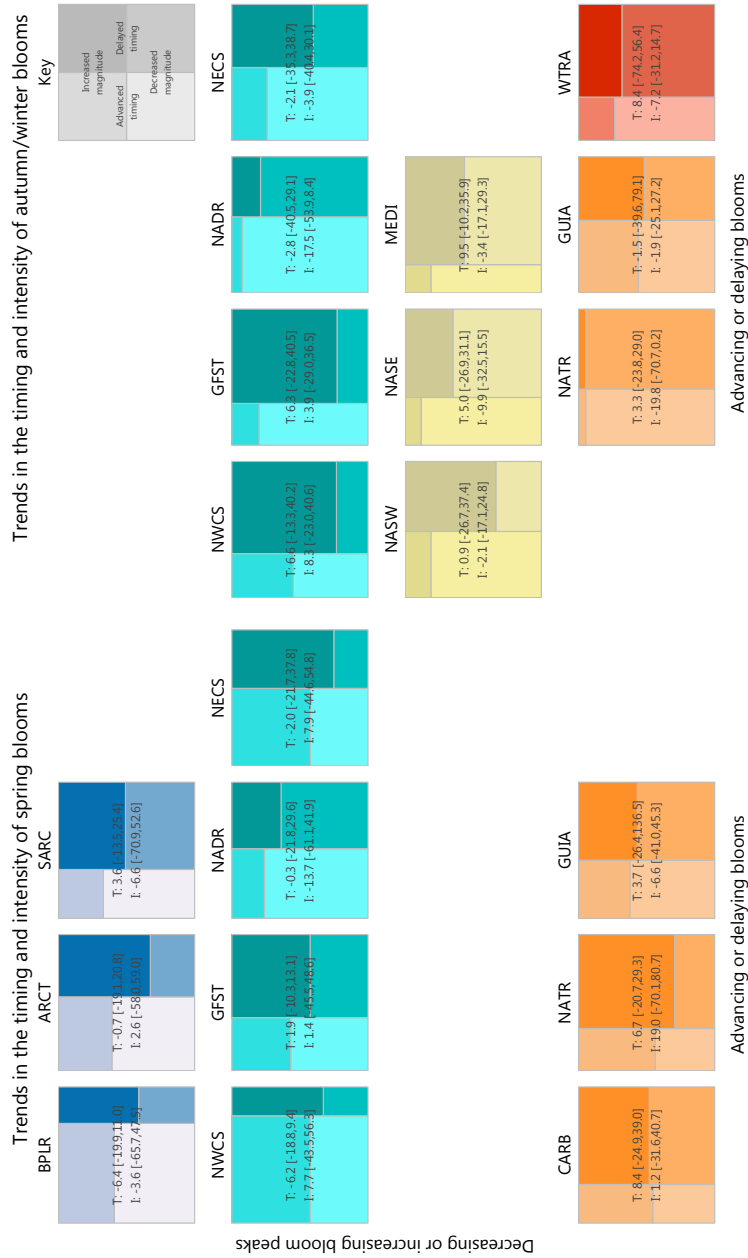


Figure 3.B.15: Same as figure 3.B.14 but based on data retrieved using the Ocean Color band ratio (OCv6) algorithms (see figure 3.B.15 for figure conventions and Materials and Methods for further details).

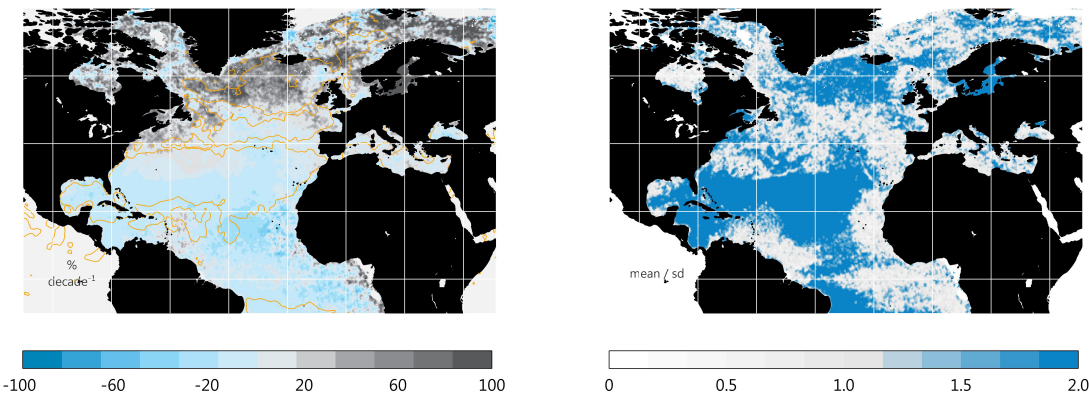


Figure 3.B.16: Time trends ($\% \text{ decade}^{-1}$) in mean chl a concentration in the North Atlantic during 1998–2012 (*left panel*) along with a map of the ratio between the mean and standard deviation of the trend coefficient estimate, *i.e.* a measure of uncertainty (*right panel*). A flexible model (equation 3.1) including a linear trend in time was fitted to all the daily chl a observations available at each pixel location. In contrast to analyses at the seasonal level, the logarithmic link function was employed to ease the interpretation of linear trends. The model also included a fixed effects factor to account for potential biases between sensors. Orange contours delimit regions where the probability of each type of seasonal cycle is greater than 0.5 (see figure 3.1 in the main text).

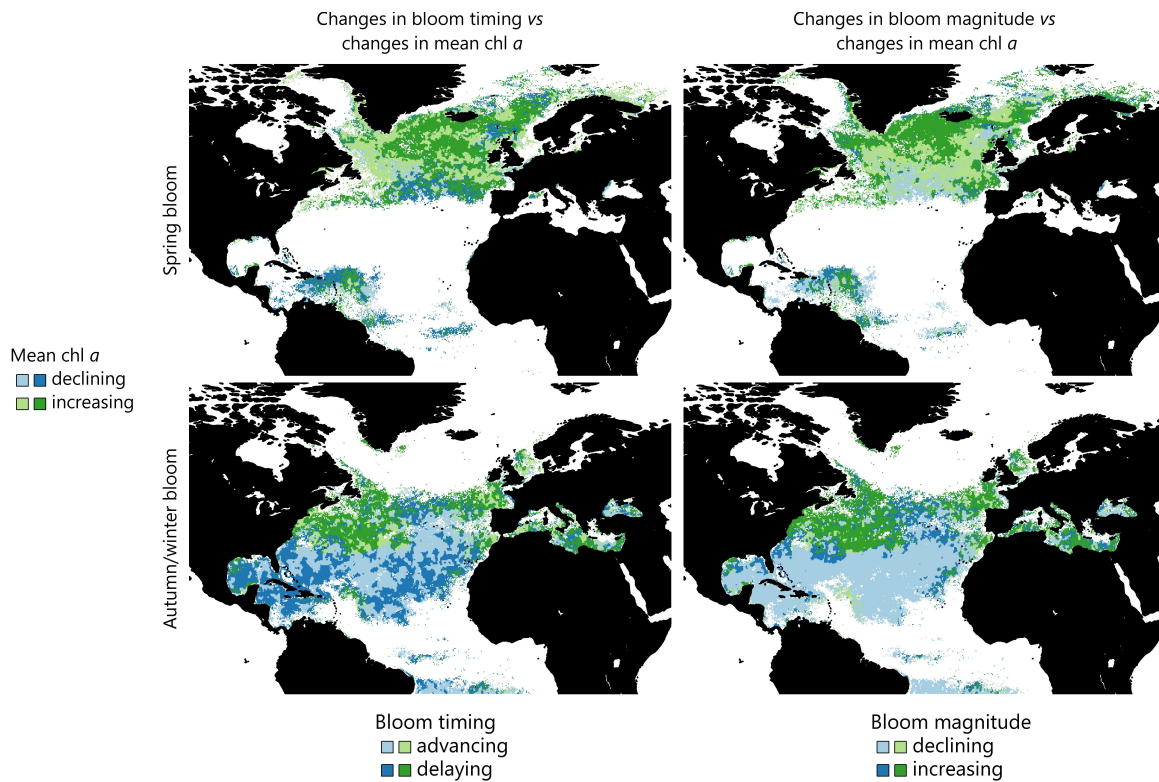


Figure 3.B.17: Association between the sign of trends in mean chl a concentration during the entire year and the sign of trends in either the timing (*left panels*) or the magnitude (*right*) of spring and autumn/winter blooms in the North Atlantic during 1998–2012. Different colors correspond to pixel locations where chl a concentration is declining and green indicates increases), whereas different shades of either color indicate changes in bloom statistics.

3.B.4 Supporting Results: Impact of environmental factors on blooms metrics

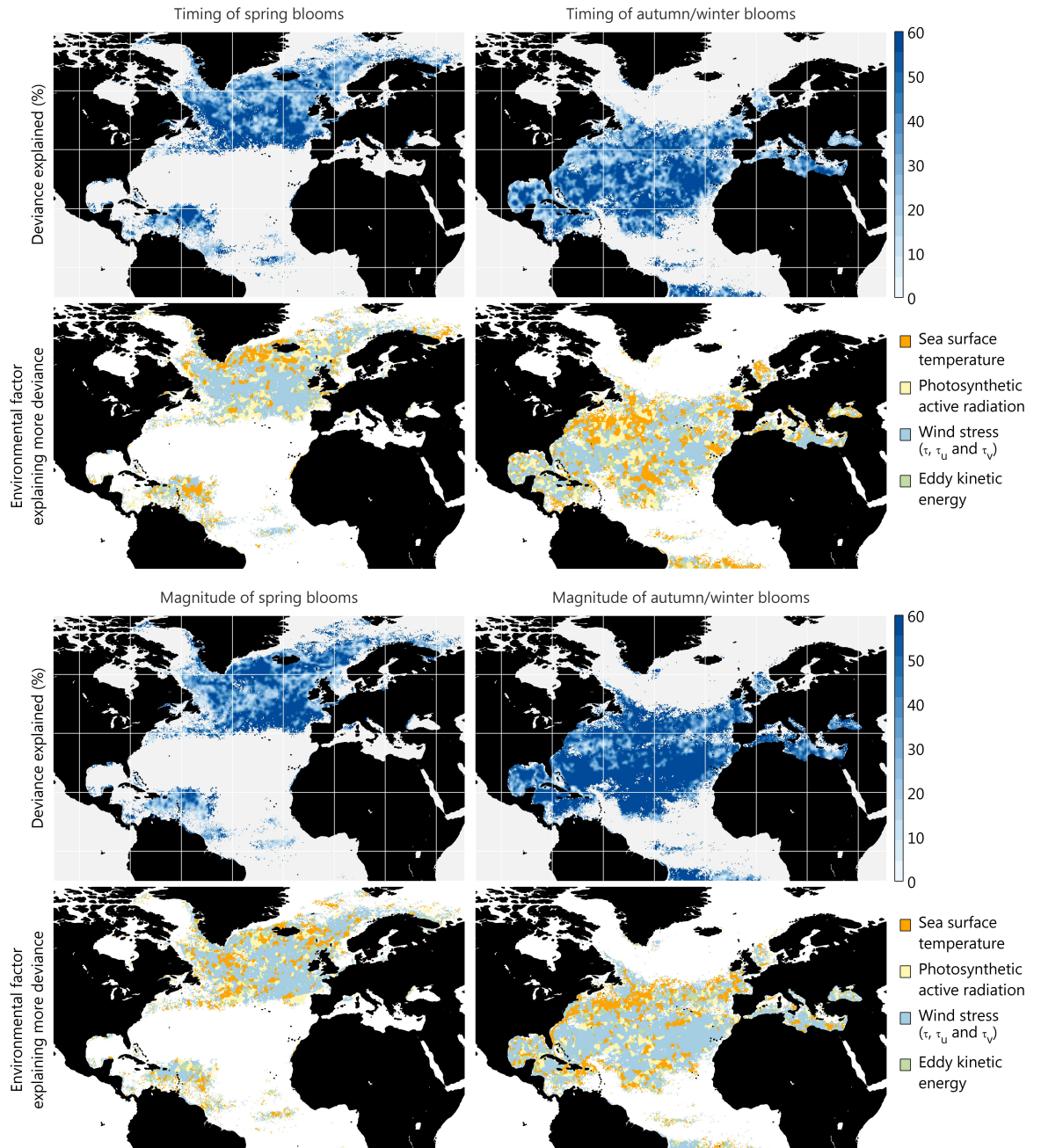


Figure 3.B.18: Importance of environmental variables to explain interannual changes in the timing (*upper panel*) and magnitude (*lower panel*) of spring and autumn/winter blooms in the North Atlantic during 1998–2012. The amount of deviance explained (*upper maps*) was estimated by fitting a model including all the covariates considered in the study (see Materials and Methods), although excluding combinations resulting in problems of collinearity (e.g. wind stress and its components). The covariate explaining more deviance (*lower maps*) was determined by comparing the decline in deviance explained after deleting each covariate one at a time.

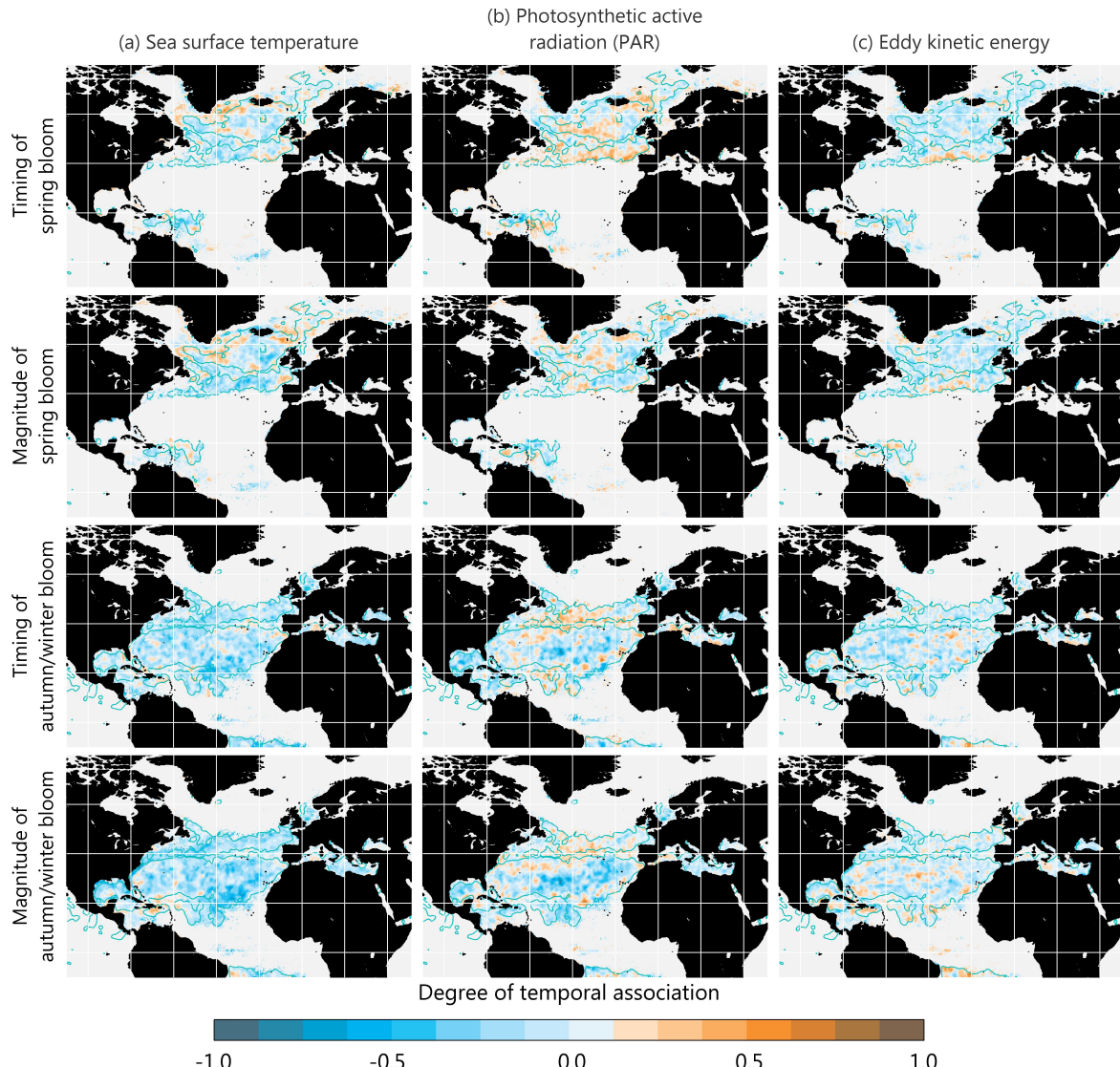


Figure 3.B.19: Temporal association between the timing and the magnitude of spring and autumn/winter blooms and seasonal averages of different environmental variables in the North Atlantic during 1998–2012. A positive (negative) association between either bloom statistic and an environmental variable might indicate that seasons with levels of that covariate above (below) its mean promote blooms occurring later (earlier) or with an increased (decreased) magnitude. The degree of temporal association was estimated by fitting a linear model to bloom metrics including an intercept, a term to account for differences between sensors and a linear trends in time. Bloom estimates were standardized before analyses to ease interpretation.

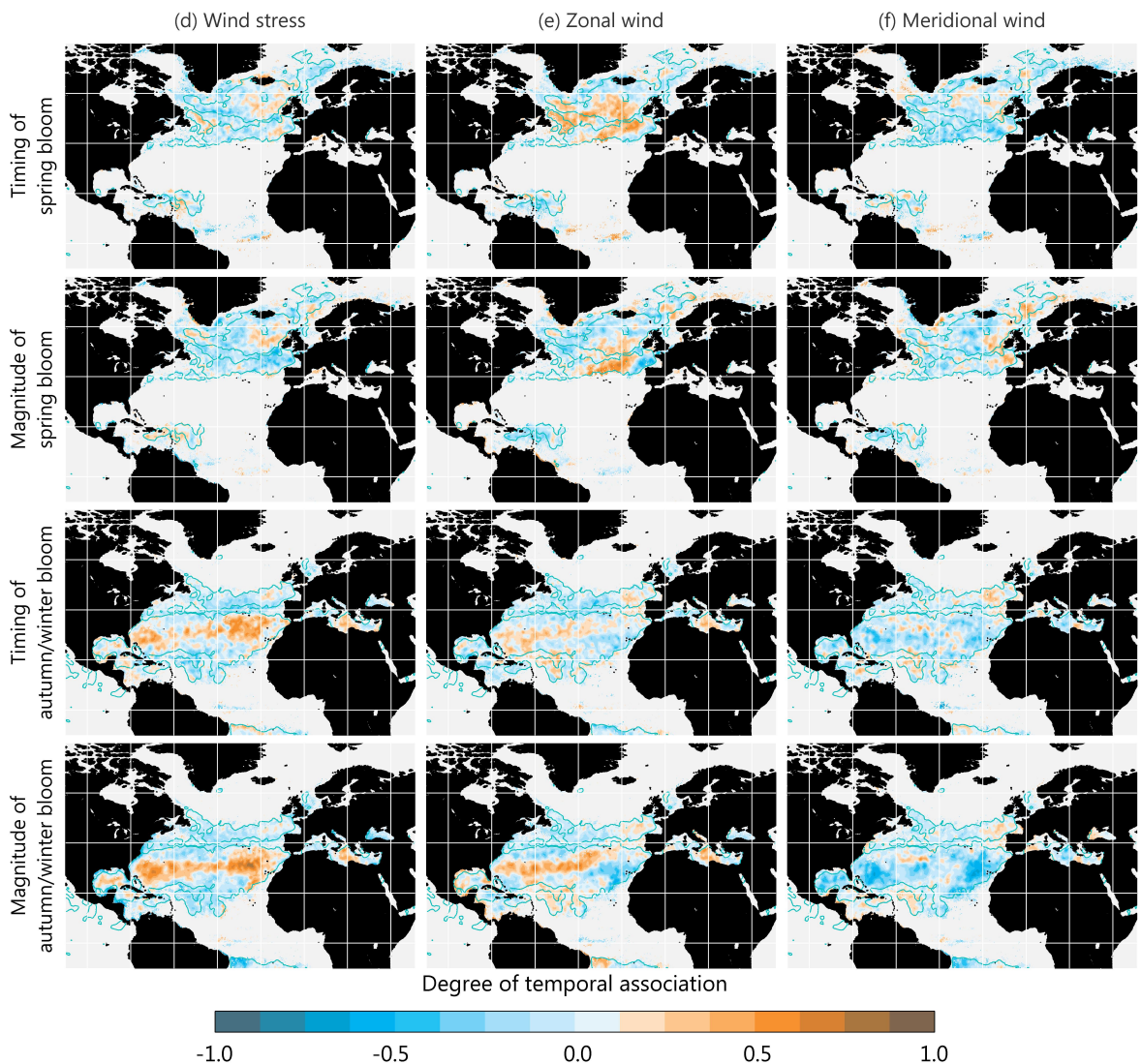


Figure 3.B.18: (continued).

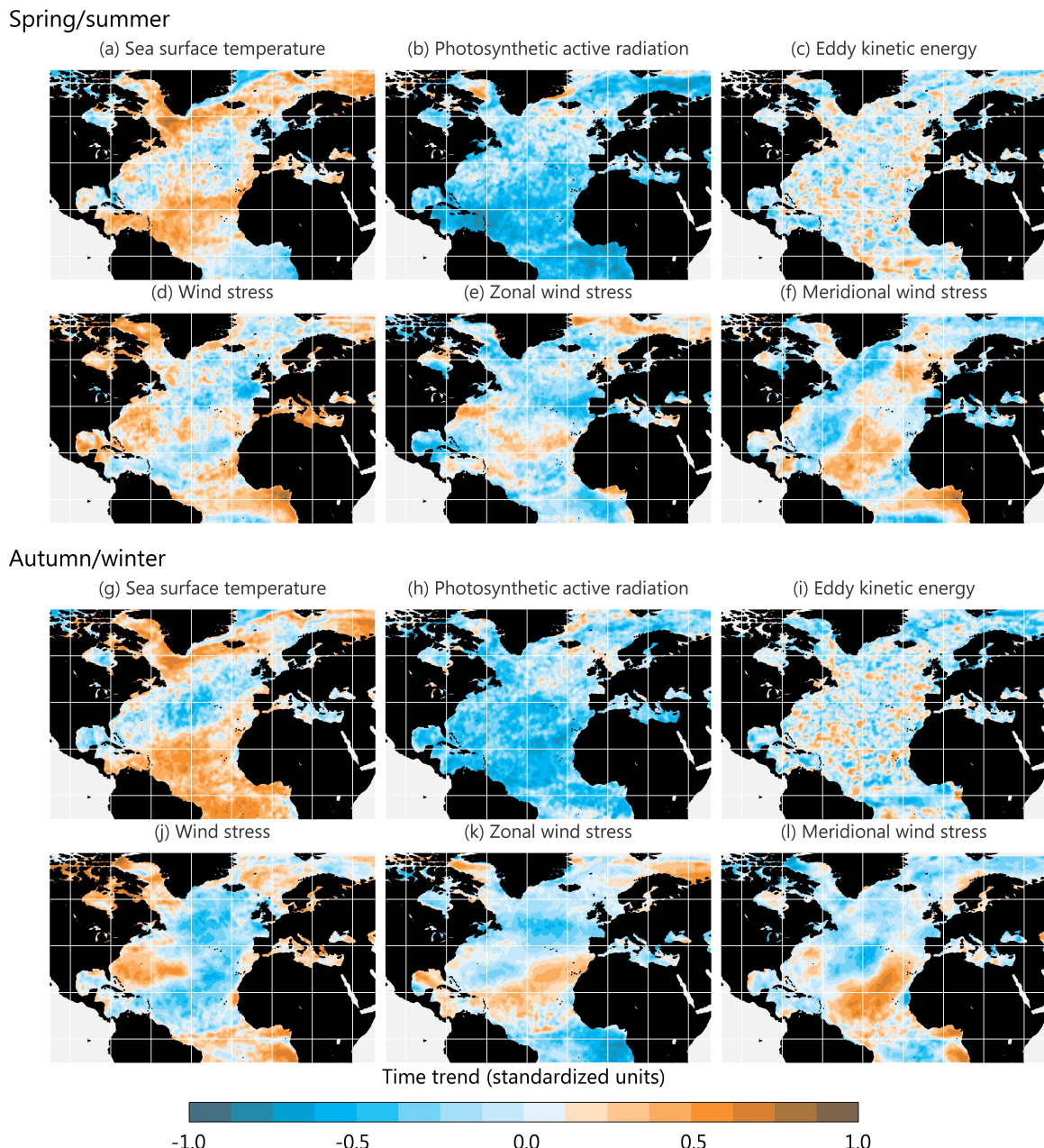


Figure 3.B.19: Time trends in seasonal averages of the different environmental variables used to explain interannual changes in bloom statistics during 1998–2012 (see figure 3.B.19). Seasonal data was scaled to mean zero and standard deviation one at each pixel location before estimating time trends, making estimates comparable between regions and panels.

Chapter 4

Recruitment of Bay of Biscay anchovy

Abstract Small pelagic fish species present irregular dynamics that challenge fishery scientist and complicate fisheries management. These complex dynamics are due to huge fluctuations in recruitment that have been traditionally related to changes in external environmental forcing, although no clear mechanism seems to be generally applicable. On the other hand, theory predicts that other mechanisms like density dependent population regulation and overfishing can increase the likelihood of oscillations. Here, we assessed the importance of different mechanisms on the recent collapse of European anchovy (*Engraulis encrasicolus*) in the Bay of Biscay. We analyzed anchovy dynamics using a nonlinear, age structured population model incorporating external environmental forcing on recruitment. Despite model fits revealed some evidence of compensatory dynamics, density dependence was weak and unable to generate huge oscillations in abundance. Instead, models including an effect of phytoplankton phenology or larval drift on recruitment resulted in a greatest prediction skill, pointing the importance of external forcing mechanisms. In any case, extensive model simulations showed that environmental fluctuations alone barely explain the collapse of the anchovy fishery in the Bay of Biscay without considering the impact of fishing.

Keywords Bayesian statistics, *Engraulis encrasicolus*, European anchovy, Larval drift, Match–mismatch, Nonlinear population dynamics, Recruitment, Remote sensing, Sequential Monte Carlo

4.1 Introduction

Small pelagic fish species support the largest fisheries around the world [FAO, 2013]. These fisheries are characterized by huge fluctuations in catches and yield that compromise their long term sustainability [Fréon et al., 2005]. The early maturation and short life span of small pelagic fish species make their populations especially sensitive to fluctuations in environmental factors, including those related to human induced climate change and overfishing [Checkley et al., 2009]. Despite external forcing is usually invoked to explain the irregular dynamics observed in these species, their potential to attain high population growth

rates make them also good candidates to develop complex dynamics [Tuljapurkar et al., 1994]. Put together, these ecological traits result in the practical inability to anticipate a failure in recruitment and to assess fishing impacts in advance.

Population regulation in fish species usually operates at early stages and results from the combined effect of both density dependent and density independent mechanisms [Wootton 1999; see also Lorenzen 2008]. Several non exclusive and complementary hypotheses have been proposed to explain fluctuations in recruitment (see Bakun 2010 for a recent review and table 4.1), although most of them are centered around three main themes [Cowan and Shaw, 2002; Houde, 2008]; (i) the existence of a critical period where either food quantity or quality determines recruitment through its effect on larval growth and survival (e.g. Hjort [1914]–Cushing’s [1990] Match-mismatch, Lasker’s [1978] Stable Ocean or Rothschild and Osborn’s [1988] Plankton Contact Hypotheses), (ii) the dependence of recruitment success on hydrographic conditions that modulate the dispersal or retention of planktonic eggs and larvae in nursery grounds (Iles and Sinclair’s [1982] Member/Vagrant hypotheses), and (iii) the importance of negative interactions with predators (Houde’s [2008] Stage Duration Hypothesis, Bakun’s [1996] Loopholes) and competitors (Bakun and Cury’s [1999] School trap). The combination of these mechanisms leads to other hypothesis like Cury and Roy’s [1989] Optimal Environmental Windows or Bakun’s [1996] «triads».

Determining whether any candidate explanation can shed light on the recruitment process is complicated by the difficulties associated with the study of early fish stages (*i.e.* widely but discontinuously distributed massive amounts of tiny eggs and larvae, Fuiman and Werner 2002). Nevertheless, an attempt can be made to infer indirectly the relative importance of different mechanisms by studying how changes in the environment impact population dynamics (e.g. Hilborn and Mangel 1997; Turchin 2003). Here, we apply this approach to study the recent collapse of European anchovy (*Engraulis encrasicolus* L. 1758) fishery in the Bay of Biscay. We derived a set of indexes to represent the main candidate hypotheses postulated to explain fluctuations in the recruitment of small pelagic species. Then, we assessed the importance of both density dependent and density independent mechanisms of population regulation by fitting a nonlinear, age structured population model to detailed scientific survey data available for the stock [ICES, 2012]. Model structures considering different mechanisms were compared based on their ability to anticipate recruitment fluctuations. Indexes related to plankton phenology and upwelling presented the greatest prediction skill, pointing the importance of match-mismatch mechanisms and larval drift, respectively. Nevertheless, extensive model simulations showed that environmental fluctuations alone barely explain the collapse of the anchovy fishery in the Bay of Biscay without considering the impact of fishing.

4.2 Material and Methods

4.2.1 European anchovy fisheries in the Bay of Biscay

European anchovy, *Engraulis encrasicolus* L., is a small pelagic fish species (up to 20 cm length) widely distributed along the Mediterranean and eastern Atlantic coasts (Whitehead et al. 1988; see also www.fao.org/fishery/species/2106). It is a short lived (usually does not exceed three years of age) and fast growing species that reaches maturity during its first year of life. As other Cupleoids, it is a planktivorous fish that forms large migrating schools preyed upon a wide variety of predators, including other fish species, seabirds and marine mammals. It is also extensively exploited for food consumption and as live bait throughout its range.

Anchovy supports one of the most important fisheries in the Bay of Biscay (figure 4.1, Uriarte et al. 1996; ICES 2012), where a small scale fleet of purse-seiner and pelagic trawlers operates seasonally (figure 4.2). The fishery targets spawning aggregations of adult anchovies in spring and early summer, as well as feeding shoals migrating along the coasts of the Bay of Biscay. Juveniles are also fished to a less extent in late autumn (less than 2.5% of total catches). Shoals disaggregate in late autumn when anchovies move to deeper waters for overwintering, and captures remain low until the next spring. The fishery peaked in the early 60's with catches above 80×10^3 tonnes that have decreased steadily since then (figure 4.2). A long-term monitoring program was established in the late 80's following a period of extraordinarily low catches. Catches recovered but anchovy declined again and collapsed in recent years, with the establishment of a fishery closure in July 2005. The fishery was reopened in 2010 but a low fishing quota was established, setting a constant harvest rate of 30% of the spawning stock biomass bounded to the interval $7 - 33 \times 10^3$ tonnes [ICES, 2012].

4.2.2 Data sources and preparation

Detailed statistics on the anchovy population in the Bay of Biscay are available thanks to long term scientific monitoring of the fishery (ICES 2012). We took advantage of catch at age data and scientific surveys during 1987–2011 to study anchovy dynamics (table 4.A.1 in the Appendix). Each spring, spawning stock biomass at age is estimated using two different methods. Daily egg production method (*depm*) estimates are available since 1987 [Motos, 1994; Somarakis et al., 2004], and are derived from the relationship between field estimates of egg abundance and of adult fecundity and age structure [Parker, 1980]. Acoustic surveys (*acst*) have been conducted regularly since 1989 [Massé, 1996], and estimate total biomass based on the combination of cross-shelf acoustic transects with midwater trawl hauls to determine species composition and age structure, as well as a variety of ancillary data needed to calibrate the sensors [ICES, 2009, 2012]. Both surveys are conducted over the southeast-

Table 4.1: Summary of the main hypotheses proposed to explain fluctuations in fish recruitment as a consequence of changes in the external environment. We grouped the hypotheses around three main themes following Cowan and Shaw [2002]. These groupings have their roots in Hjort's [1914] critical period and aberrant drift hypotheses, and in Houde's [2008] recognition in the late 1980s of the potential importance of predation. Although not mentioned, none of these mechanisms excludes the potential operation of density dependent regulation. Indeed, an interaction between both types of mechanisms can be expected to modulate recruitment. Note that the abbreviations in the left column match those used in table 4.2.

(i) *Existence of a critical period*

MATMIS	Hjort [1914]–Cushing's [1990] Match-mismatch hypothesis. Plankton phenology determines recruitment strength in seasonal environments. Larval survival depends critically on resource availability, which depends on the degree of overlap in time between spawning and seasonal pulses of production (<i>e.g.</i> the spring phytoplankton bloom). Direct effects of total resource availability or species composition on early survival are also possible [Lasker, 1975; Durant et al., 2007].
STBOCN	Lasker's [1978] Stable Ocean hypothesis. Periods of relatively calm winds promote that food and larvae became vertically concentrated together (“Lasker events”), enhancing larval survival and recruitment [Lasker, 1975]. Storms and wind induced mixing or upwelling might prevent the formation of aggregations and might produce a failure in recruitment [Lasker, 1978].
PLNCNT	Rothschild and Osborn's [1988] Plankton Contact hypothesis. Intermediate levels of wind-driven turbulence increase feeding rates by increasing contact rates between fish larvae and their prey; lower or excessive turbulence levels lead to reduced feeding and survival rates [MacKenzie et al., 1994; MacKenzie, 2000].

(ii) *Aberrant drift*

MMBVGR	Iles and Sinclair's [1982] Member/Vagrant hypothesis. Wind and current conditions determine larval survival through its effect on larval retention or dispersion away from or towards nursery areas.
--------	------------------------------------------------------------------------------------------------------------------------------------------------------------------------------------------------------

(iii) *Predation and competition*

STGDUR	Houde's [2008] Stage Duration hypothesis. Predation is the major source of egg and larval mortality so minimizing predation risk through fast individual growth ultimately determines recruitment success.
LOOPH	Bakun's [1996] Loopholes. Escape from predation determines recruitment success, even if this escape implies a disadvantage in terms of resource acquisition or habitat stability.
SCHTRP	Bakun and Cury's [1999] School trap. Depending on the abundance of other species, the advantages of schooling behavior might be reversed in mixed schools by guiding individuals of the target species to inappropriate habitats or by forcing them to perform suboptimal behavior. The overall performance within the schools determines individual survival and at the end, recruitment strength.
UPWRAT	Rykaczewski and Checkley's [2008] Upwelling rate hypothesis. Upwelling rate determines feeding success by altering the size spectra of planktonic prey. With respect to other species, anchovy is favored by quick coastal upwelling, that promotes an increase in the relative abundance of large plankters.

(iv) *Combination of several mechanisms*

OPTENV	Cury and Roy's [1989] Optimal Environmental Window hypothesis. In upwelling ecosystems, intermediate wind levels result in a perfect balance between enhanced production and dispersal, with levels above or below this optimal window resulting in recruitment failure. Turbulence can contribute as well to create such a relationship [MacKenzie, 2000].
OCTNTRD	Bakun's [1996] Ocean «triads». Recruitment success depends on the coincidence of three processes conforming a «fundamental triad» of habitat suitability: a relative enrichment of resources, a concentration mechanism yielding increased feeding opportunities, and a retention or dispersal mechanisms preventing larvae from leaving suitable habitat.

ern portion of the Bay of Biscay and cover the main spring spawning aggregations (see ICES 2012 for further details and references).

Fluctuations in anchovy recruitment are behind changes in fishery yield, given that age 1 recruits account for more than half of the catches (56.6% [13.0 – 86.9%] mean and range during the period 1987–2011, ICES 2012). Weak upwelling intensity and water column stability seem to favor larval dispersal and survival over the shelf, and have been related to recruitment success [Borja et al., 1996, 1998, 2008; Allain et al., 2001, 2007a,b]. River discharge during spawning also seems to enhance larval survival by increasing water column stability and productivity [Bergeron, 2004; Bergeron et al., 2010], although the negative association found when analyzing the recruitment series points towards alternative mechanisms [Planque and Buffaz, 2008; Borja et al., 2008]. On the other hand, it has been also suggested that larval growth and survival can be maximized instead in open waters off the shelf, where the negative impacts of competition for resources and predation might be less intense [Irigoién et al., 2007; Bachiller et al., 2013]. In order to account for environmental effects on recruitment, we assembled ancillary data to represent these and other candidate hypotheses using a variety of data sources (table 4.2, see also the section *Ancillary data in the Appendix*). We selected *a priori* only a small subset of candidate indexes based on their ability to explain changes in a larval survival index derived from stock assessment estimates (Platt et al. 2003; ICES 2012; see *Appendix*). The larval survival index presumes constant productivity and might be confounded by density dependent effects, so we further examined selected environmental indexes in a nonlinear context.

4.2.3 Population model

We modeled the dynamics of European anchovy using an age-structured biomass model including a nonlinear recruitment function [Deriso, 1980; Schnute, 1985; Quinn and Deriso, 1999]. Our approach was a slight modification of models developed by Ibaibarriaga et al. [2008, 2011] to assess the status of the fishery and to establish total allowable catch. In this way, our aim was to model spawning stock biomass considering density dependent and density independent mechanisms of population regulation simultaneously.

The biomass of spawners at age a in year t , $x_{t,a}$, was modeled at the time of biomass surveys ($\Delta t_s = 0.375$, i.e. 15 May; see Ibaibarriaga et al. 2008, 2011). The stock was modeled as a closed population in which changes in $x_{t,a}$ were only due to recruitment, the balance between growth and natural mortality (collapsed in a constant rate of biomass decrease or physiological mortality rate, m), and monthly fishing ($f_{t,a}(s)$, the catch rate at age a at fractional time s within the year; see Mertz and Myers 1996):

$$x_{t,a} = \left(x_{t,a}^i - \int_0^{\Delta t_s} e^{ms} f_{t,a}(s) ds \right) e^{-m\Delta t_s + u_{t,a}} \quad (4.1)$$

where both population renewal and survival to the beginning of the year ($x_{t,a}^i$) were subjected to demographic noise, represented by an unstructured, mean zero normally distributed process, $u_t \sim N(0, \sigma_a^2)$. Process noise variance differed and was considered *a priori* independent between age classes.

The model considered two age groups; age 1 individuals are new recruits entering the fishery at the beginning of each year ($x_{t,1}^i$), while the age 2+ class includes recruits and older adults surviving from previous years ($x_{t,2+}^i$). In the latter case, the dynamics were modeled by a constant rate decrease in biomass:

$$x_{t,2+}^i = \sum_{a=1,2+} \left(x_{t-1,a} - \int_{\Delta t_s}^1 e^{ms} f_{t-1,a}(s) ds \right) e^{-m(1-\Delta t_s)} \quad (4.2)$$

Recruitment was considered a more complex process subjected to strong population regulation. Indeed, this phase embraces planktonic development and growth and it is usually associated with very high mortality rates [Houde, 2002]. Despite the prolonged reproductive season of European anchovy in the Bay of Biscay [Motos et al., 1996], population renewal was reduced to a single pulse of age 1 adults recruiting into the fishery at the beginning of each natural year ($x_{t,1}^i$). Individuals from both age classes were sexually mature and contributed to next year recruitment with the same fecundity, an assumption justified to a great extent by available observations [Motos, 1996].

The potential biomass of new recruits entering the fishery was related to spawning biomass in the previous year at the time of the surveys using a Deriso-Schnute stock-recruitment relationship [Deriso, 1980; Schnute, 1985],

$$g(x_{t-1,\cdot})_{[0,\infty)} = \alpha x_{t-1,\cdot} (1 - \beta \gamma x_{t-1,\cdot})^{1/\gamma}, \quad x_{t-1,\cdot} = \sum_{a=1,2+} x_{t-1,a} \quad (4.3)$$

where the strength of recruitment depends on the productivity parameter α [kg of recruit per kg of adult]; the optimality parameter β [1/kg of adult]; and the dimensionless recruitment limitation parameter γ [Schnute, 1985]. Note that both α and β should be positive. This relation allows a great flexibility in the shape of the renewal function [Schnute, 1985], including as special cases common stock-recruitment relationships like (i) the non-regulatory, constant productivity model (if $\gamma = -\infty$), (ii) the compensatory but saturating Beverton and Holt [1957] function ($\gamma = -1$), (iii) the over compensatory Ricker [1954] recruitment function ($\gamma = 0$), and (iv) the also over compensatory but symmetric Schaefer [1954] function ($\gamma = 1$). Note that the recruitment function does not allow for depensation.

Although this model specification might consider only density dependent mechanisms of population regulation and is fully deterministic, it gives rise to a rich variety of dynamics, including complex cycles and chaos [Tuljapurkar et al., 1994]. Nevertheless, we assessed

the potential importance of density independent mechanisms by allowing interannual variation in the strength of recruitment. Potential population renewal from equation 4.3 was modulated in this way by the effect of unstructured demographic noise (*i.e.* equation 4.1), but also by structured perturbations due to environmental forcing on potential recruitment:

$$x_{t,1}^i = g(x_{t-1,.})e^{\eta(z_{t-1}-z_{ref})} - \int_{\Delta t_s}^1 f_{t-1,0}(s) ds \quad (4.4)$$

where the first term on the right hand side represents potential recruitment and the second accounts for catches of age 0 juveniles during the fall of the year preceding recruitment [Uriarte et al., 1996]. Environmental forcing had a multiplicative effect on expected recruitment that we assumed to occur before fishing. We assessed the potential effect of a set of environmental variables and indexes summarized in table 4.2, that were selected to represent to some extent different hypotheses about recruitment variation [table 4.1, Cowan and Shaw 2002; Houde 2008]. Each index z_t was standardized to mean zero and variance one before the analysis to ease comparisons among different covariates. The strength of the effect of each environmental factor on next year recruitment was determined by the parameter η . The effect was proportional in a logarithmic scale to deviations from z_{ref} , a reference level corresponding to an inflection point in the sign of the effect of a given covariate. This parameter is unidentifiable, so we redefined the productivity parameter in equation 4.3 as $\alpha' = \alpha e^{-\eta z_{ref}}$, that can be interpreted as fish productivity at average environmental conditions. To avoid further complexities, the effect of different covariates was assessed one at a time.

Monthly catch rate at age time series ($f_{t,a}(s)$) were estimated from integrated monthly catch statistics and integrated catch at age data per semester by assuming a constant age structure [ICES, 2012]. Catch at age data entered the model directly to include seasonal changes in fishing mortality for each age group [Mertz and Myers, 1996]. The model was completed with an estimate of spawning biomass in the first simulation year ($t = 0 \equiv 1987$), $x_{0,a}$, necessary for model initialization. Model parameters are presented in table 4.B.2 in the Appendix.

Table 4.2 (following page): Environmental variables and indexes employed to assess the potential importance of environmental forcing on inter annual changes in the strength of anchovy recruitment. Each covariate was associated to different hypotheses proposed to explain variations in recruitment (see table 4.1). Different integration domains and alternative processing schemes were selected *a priori* in order to reduce the number of candidate indexes to only one particular form for each environmental effect, as detailed in the third column. The selection of the set of candidate indexes was based on their ability to explain changes in an index of anchovy larval survival derived from stock assessment estimates of recruitment and spawning stock biomass [ICES, 2012]. Full details regarding data sources and preparation are available in the Appendix.

Environmental effect abbreviation [units]	Hypothesis* [Effect]	Proxy indexes, data availability and domain of integration# [References for data sources and processing methods]
Ekman transport ω_{coast} [$m\ s^{-1}$] ω_{curl} [$m\ s^{-1}$]	OPTENV [\sim] UPWRAT [\boxtimes] MMBVGR [\nwarrow]	Coastal and curl driven upwelling indexes. Derived from six-hourly wind speed maps available for the period 1988–2011. Data was integrated along the coast of the Bay of Biscay for coastal upwelling and for both coastal and open waters for curl-driven upwelling. Coastal upwelling during summer (Jul–Sep) in Armorican shelf (ICES area VIIa) was selected <i>a priori</i> . [Yelland and Taylor, 1996; Chelton et al., 1998; Yelland et al., 1998; Pickett and Paduan, 2003; Pickett and Schwing, 2006; Atlas et al., 2011]
Lasker events LE [#]	STBOCN [\searrow]	Number of Lasker events, defined as periods of a given duration below a given wind speed threshold. LE were detected on 0.25°six-hourly wind speed maps available for the period 1988–2011. Estimates for each pixel location were counted over the entire spawning season (Apr–Aug) and the average number was integrated over different domains. The number of LE with wind speed below $12\ m\ s^{-1}$ and during at least 7 days in Armorican shelf (ICES area VIIa) was selected <i>a priori</i> . [Peterman and Bradford, 1987; Atlas et al., 2011]
Natural enemies <i>Species name</i> [tonnes], [tonnes day fishing $^{-1}$]	STGDUR [\downarrow] SCHTRP [\nwarrow]	Abundance of potential predators and competitors, approximated by the biomass of recruits or spawners of; (i) Small pelagics like sardine (<i>Sardina pilchardus</i> , ICES areas VIIIC and IXa), North East Atlantic mackerel (<i>Scomber scombrus</i> , combined stock) and horse mackerel (<i>Trachurus trachurus</i> , western stock). Recruitment data available from fisheries stock assessments for the period 1987–2011; (ii) Demersal species like hake (<i>Merluccius merluccius</i> , ICES areas VIIIC and IXa) and blue whiting (<i>Micromesistius poutassou</i> , combined stock). Recruitment time series available from stock assessments for the period 1987–2011; (iii) Migrating schools of albacore tuna (<i>Thunnus alalunga</i>). Catch per unit effort data for the period 1987–2009 was derived for a $5 \times 5^\circ$ quadrangle centered on $5^\circ\text{W}, 40^\circ\text{N}$. The biomass of recruits was selected <i>a priori</i> in all cases except for blue whiting, where adult biomass was preferred. [ICES, 2013; ICCAT, 2013]
Phytoplankton abundance and phenology [<i>Phyto</i>] [$\text{mg chl } a\ m^{-3}$] δ_{spring} [day]	MATMIS [\sim] STBOCN [\nearrow]	Chlorophyll <i>a</i> concentration for different time periods, peak chlorophyll <i>a</i> and timing of the spring phytoplankton bloom. Data available for years 1998–2011; both indexes were estimated from daily, 0.25°remote sensing maps of chlorophyll <i>a</i> concentration. Indexes were estimated for each pixel location and averaged over different spatial domains. The timing of the spring phytoplankton bloom in the southeastern Bay of Biscay (ICES areas VIII b and c) was selected <i>a priori</i> . [Maritorena et al., 2002; Feldman and McClain, 2012]
River discharge Q [$m^3\ s^{-1}$]	STBOCN [\nearrow] MMBVGR [\nearrow] OCNTRD [\nearrow]	River discharge on anchovy spawning grounds in the Bay of Biscay. Integrated flow of rivers L'Adour, Garonne, and La Loire during the spawning season (Apr–Aug) for the period 1987–2011. L'Adour discharge was selected <i>a priori</i> . [HYDRO, 2013]
Sea Surface Temperature SST [K]	STGDUR [\nearrow]	Mean <i>SST</i> during the larval period (Apr–Oct) and total amount of habitat available for spawning during the spawning season (Apr–Aug; taken as the area where <i>SST</i> was within the optimum temperature range for spawning of $14\text{--}18^\circ\text{C}$, Motos et al. 1996). Indexes were estimated for each 0.25° pixel location based on daily <i>SST</i> data, and averaged over different domains and time periods within the Bay of Biscay for the period 1987–2011. Mean <i>SST</i> during summer (Jul–Sep) in Armorican shelf (ICES area VIIa) was selected <i>a priori</i> . [Reynolds et al., 2007]
Transport barriers LCS [km^2] λ [s^{-1}]	MMBVGR [\boxtimes] OCNTRD [\nearrow]	Presence, location and intensity of attracting and repelling Lagrangian Coherent Structures (<i>LCS</i>). Weekly high resolution (0.015°) <i>LCSs</i> maps for the period 1993–2011 were derived from maps of the finite time Lyapunov exponent (<i>FTLE</i> , λ), estimated from geostrophic ocean currents derived from altimetry data (0.25°). The distribution of λ , the area occupied by <i>LCSs</i> and their mean distance to the coast were estimated over the Bay of Biscay for different periods and areas during the spawning season (Apr–Aug). The 75 th percentile of the field of attracting <i>FTLE</i> over Aquitanian shelf (ICES division VIIIB) in spring and early summer (Mar–Jul) was selected <i>a priori</i> . [Le Traon et al., 1998; Shadden et al., 2005]
Turbulence ν [Wm^{-2}]	PLNCNT [\sim] STBOCN [\searrow]	Turbulence can be approximated by estimating wind work on the ocean surface. Kinetic energy flux was estimated based on six-hourly wind maps for the period 1988–2011. Data for each year were later averaged for the entire spawning season (Apr–Aug) over the coastal Bay of Biscay. Turbulence in early summer (Jul) in the Armorican-Aquitanian shelf (ICES areas VIIa and b) was selected <i>a priori</i> . [Yelland and Taylor, 1996; Yelland et al., 1998; Atlas et al., 2011; Simpson and Sharples, 2012]

*See table 4.1 for an explanation of the different hypotheses. The symbols within brackets indicate the relationship expected *a priori* between each variable and anchovy recruitment; positive [\nearrow], negative [\nwarrow], either positive or negative [\boxtimes], or dome shape [\sim].

See the description in the section Ancillary data and figure 4.A.1 in the Appendix for details about the different spatial domains considered.

4.2.4 Model fitting and inference

Model equations 4.1 to 4.4 correspond to the system equation of a Markovian nonlinear dynamic model [West and Harrison, 1997]. This kind of models has been widely used in fisheries research and it is ideally suited for Bayesian inference under a state-space representation [Schnute, 1994; Punt and Hilborn, 1997; Quinn and Deriso, 1999; Millar and Meyer, 2000]. State-space models try to reconstruct the latent or hidden Markov process $x_{t,a}$ (equation 4.1) based on sequential observations, $y_{t,a,k}$. Observations are considered independent between years given state estimates, while the states are unaffected by observational error and evolve between years through the system equation. In this way, state dynamics are added to the set of unknown model parameters and are estimated during model fit. Recognizing the separation between observation and process allows a better estimation of both unknown states and model parameters [Carlin et al., 1992; West and Harrison, 1997].

The model was fitted to available estimates of spawning stock biomass, $y_{t,a,k}$ (ICES 2012). Survey data are available for the period 1987–2011, with only one year missing observations. Depending on the year, only estimates based on the daily egg production method ($y_{t,a,depm}$) and/or based on acoustic surveys ($y_{t,a,acst}$) were available (see table 4.A.1 in the Appendix). The model can be formulated in state-space form by including an observation equation relating underlying state biomass and survey estimates:

$$\log(x_{t,a}) = \log(h(\mathbf{x}_{t-1})) + u_{t-1,a}, \quad u_{t-1,a} \sim N(0, \sigma_a^2), \quad (4.5)$$

$$\log(y_{t,a,k}) = \log(q_k x_{t,a}) + v_{t,k}, \quad v_{t,k} \sim N(0, \tau_k^2) \quad (4.6)$$

where in the state equation 4.5, h is a function updating states between years (*i.e.* the deterministic skeleton of equation 4.1). The observation equation 4.6 includes an unknown detectability (*i.e.* catchability) coefficient, q_k , included to account for the potential bias of each sampling method, $k = depm, acst$. The logarithmic transformation results in normally distributed process (u_t) and observation (v_t) errors. Process noise propagates between years, whereas observation errors were regarded as independent.

Bayesian inference relies on setting an appropriate likelihood function and on defining prior distributions for unknown parameters [Robert, 2001]. The likelihood function is a parametric statistical model returning the odds of available observations conditional on a given a parameter vector, while prior distributions allow the incorporation of any information about model parameters available before the analysis. Both distributions are combined using the Bayes-Laplace rule to update prior knowledge about the parameters given a set of observations, to produce the so called posterior parameter distribution:

$$p(\theta, \mathbf{x}_{0:T} | \mathbf{y}_{0:T}) \propto p(\theta) p(\mathbf{x}_0 | \theta) \underbrace{\prod_{t=0}^{T-1} p(\mathbf{x}_{t+1} | \mathbf{x}_t, \theta)}_{prior} \underbrace{\prod_{t=0}^T f(\mathbf{y}_t | \mathbf{x}_t, \theta)}_{likelihood} \quad (4.7)$$

where we omitted age class and survey method subscripts for clarity. The missing proportionality constant is the marginal distribution of the data. Prior distributions for model parameters in state and observation equations were considered independent (*i.e.* $p(\theta) = \prod_{t=0} T \theta_i$) and are presented in table 4.B.2 in the Appendix. Hyperparameters in these prior distributions were selected to locate the distributions around reasonable values although, following Ibaibarriaga et al. [2008, 2011], they left enough variation to be considered uninformative. The transition density between consecutive states completing the prior distribution in equation 4.7 corresponds to state equation (4.5), whereas the likelihood is defined by the observation equation (4.6). Despite the posterior density cannot be solved analytically, inference can be based on samples of the parameter and state vector obtained using Markov Chain Monte Carlo methods (MCMC, Robert and Casella 2004).

Parameter estimation in state-space models usually proceeds in two sequential steps by conditioning alternately on estimates of model parameters or on estimates of the state process [West and Harrison, 1997]. Here we used a sequential Monte Carlo algorithm (SMC, also called particle filters; see Doucet et al. 2001) to estimate the state process [Kantas et al., 2009; Andrieu et al., 2010; Parslow et al., 2013], adaptive Metropolis-Hastings steps to estimate physiological mortality [Haario et al., 2001, 2005; Roberts and Rosenthal, 2009; Peters et al., 2010], an adaptive Importance Sampling scheme to update the parameters of the Deriso-Schnute recruitment function [Cappé et al., 2008; Wraith et al., 2009], and conjugate Gibbs steps for the remainder parameters and missing covariate observations [Gelman et al., 2004; Hoff, 2009]. After a burn in period of 20000 iterations, 1000 samples were retrieved with an interval of ten iterations to characterize the distribution of parameters and to project estimation uncertainty to model based estimates. A detailed account of the fitting procedure, including sketched pseudocodes are presented in the section Model fitting algorithms in the Appendix.

Model selection and inference were based on the different ability of models varying in structure and in the environmental effect considered to predict observed changes in stock biomass. In this way, we set as a benchmark a simple model that considered a constant environment and no density dependent regulation of recruitment (*i.e.* constant productivity in model equation 4.3). This model was compared to models including different environmental effects and allowing or not for density dependent recruitment regulation. We focused on the prediction ability of different models, so we employed a series of model diagnostics based on the predictive distribution of one step ahead predictions ($\mathbf{x}_{0:T}^*$). We estimated

mean absolute deviations based on forecast errors ($e_{t,a,k} = \log y_{t,a,k} - \log q_k x_{t,a}^*$) and the predictive likelihood that, together with the number of parameters, was combined to yield Ando's [2010] Bayesian Predictive Information Criterion (*BPIC*):

$$BPIC = -2 \int \log f(\mathbf{y}_{0:T} | \mathbf{x}_{0:T}^*, \theta) p(\theta | \mathbf{y}_{0:T}) d\theta + 2 \dim \theta \quad (4.8)$$

where the criterion provides a balance between model fit and model complexity, with lower values pointing to models with the best predictive distribution. We also employed as a relative indicator of model performance the ratio between process variance estimates for different age classes with respect to benchmark estimates. Parameter estimates were also used to estimate the probability of collapse under scenarios differing in management practices and environmental variation. This *in silico* experiment consisted in simulating a large set of surrogate time series (4.2×10^6) keeping fishing mortality levels proportional to the actual pattern of fishing pressure experienced by the population, but reducing gradually fishing pressure (see Surrogate analysis of anchovy collapse in the Appendix for further details). The models considered both environmental effects on recruitment and random perturbations in both recruitment and adult survival associated to estimated process noise (*i.e.* σ_1 and σ_{2p}). This allowed us to assess the importance of different processes (environmental and internal regulation *vs.* fishing) on the recent collapse of the fishery.

Figure 4.1 (following page): Distribution and life cycle of European anchovy in the Bay of Biscay (Uriarte et al. [1996]; Irigoien et al. [2007]; ICES [2012]). Different patches in the map correspond to an idealized distribution of juveniles and adults at different times of the year. The main events in the annual cycle are summarized in the inset clock. European anchovy is a batch spawner with a long spawning season that begins in April and can last up to August [Motos, 1996]. The main spawning grounds are associated to the mouth of Garonne and Adour rivers, although a third spawning aggregation located in the shelf break and composed mainly by older individuals is detected in some years [Motos et al., 1996; Ibaibarriaga et al., 2013]. Fishers take advantage of these aggregations and, indeed, most catches are recorded in spring in coastal spawning grounds (Uriarte et al. 1996, see also figure 4.2). After spawning, eggs remain no more than three days floating near the surface before hatching a larva that expends 30–40 days in the plankton before metamorphosing into a juvenile. Currents in the Bay of Biscay during the spawning season (white arrows, Charria et al. [2013]) drift eggs and larvae away from spawning grounds, conditioning the distribution of juveniles [Koutsikopoulos and Le Cann, 1996]. The intensity of coastal upwelling and the presence of mesoscale features might contribute to drift and retain propagules away from the coast in a different degree, as well as to enhance plankton productivity. Following aggregation around the main spawning grounds in spring, adults remain together forming large feeding shoals that migrate northwards and westwards following the coast [Uriarte et al., 1996]. In late autumn, schools disaggregate and both adults and juveniles migrate to depth awaiting next spring, when anchovies about one year old will be mature to contribute spawning and recruit into the fishery massively. Bathymetric data from the GEBCO One Minute Grid, version 2.00, www.gebco.net.

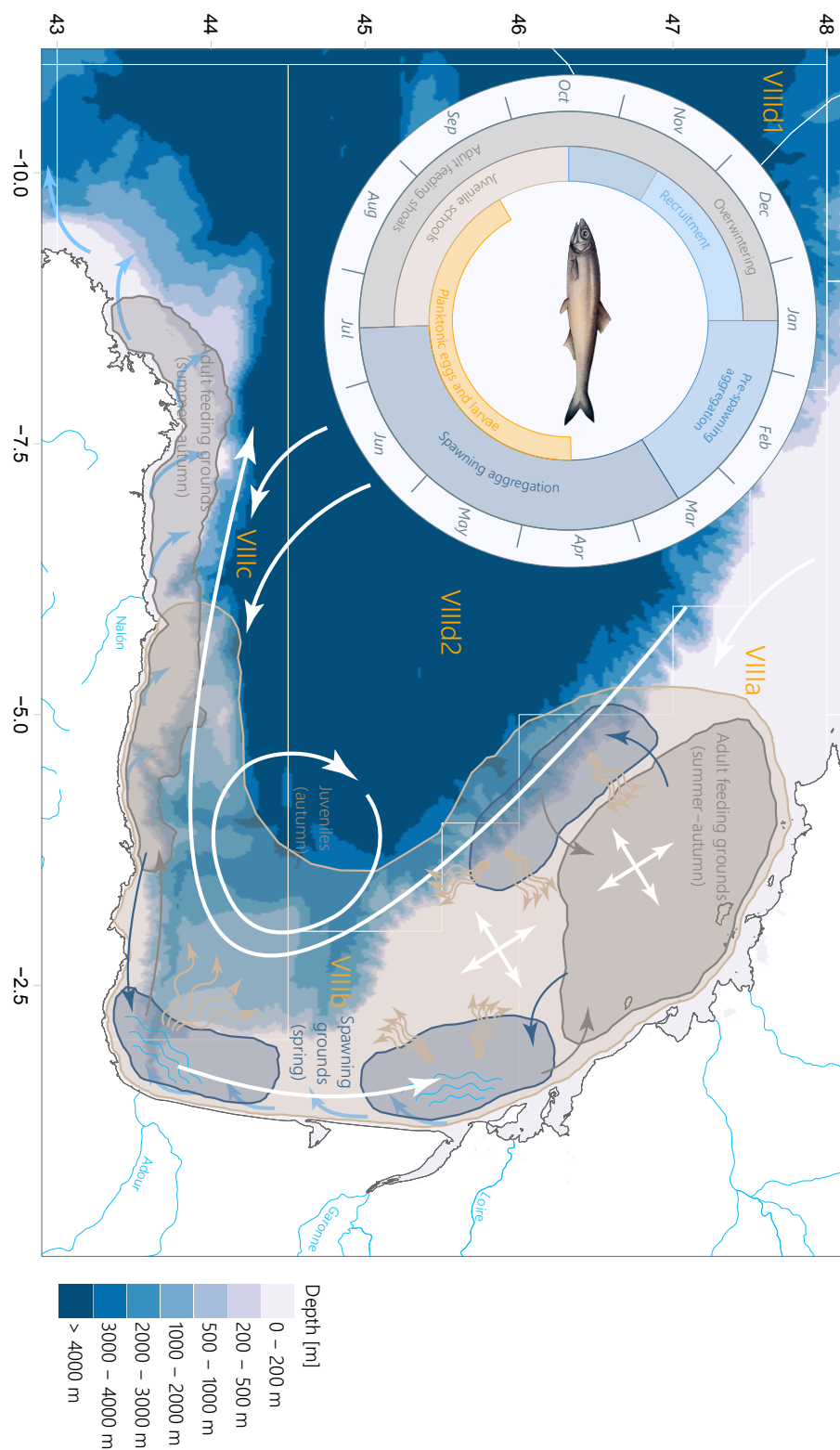


Table 4.3: Model diagnostics for the age structured models fitted to anchovy abundance data. As detailed in the section Model fitting and inference, we estimated for each model the posterior parameter distribution ($p(\theta, \mathbf{x}_{0:T}|\mathbf{y}_{0:T})$) by updating the prior ($p(\theta)$) with observed abundances using the predictive likelihood ($\log f(\mathbf{y}_{0:T}|\mathbf{x}_{0:T}^*, \theta)$). We also combined these measures to yield other model diagnostics like Ando's [2010] Bayesian Predictive Information Criterion (BPIC). Lower values of this criterion indicate a better predictive distribution in terms of a balance between model fit (higher likelihood) and parsimony (less parameters, n_θ). We also estimated the mean absolute deviation ($\sum |e_{t,a,k}|/n$) averaged over all years and only for the year when anchovy fishery collapsed ($t = 2005$). The upper table presents diagnostics for models with no density dependence, while the second corresponds to models including a Deriso-Schnute recruitment curve. Each row within each table corresponds to a different type of environmental effect on recruitment. Model diagnostics were summarized by their median and quantile based 90% credible intervals (square braces).

Constant productivity						
	$\log p(\theta)$	$\log f(\mathbf{y}_{0:T} \mathbf{x}_{0:T}^*, \theta)$	$\log p(\theta, \mathbf{x}_{0:T}^* \mathbf{y}_{0:T})$	n_θ	BPIC	$\sum e_{t,a,k} /n$
Constant environment	-49.8 [-51.9,-48.7]	-109.8 [-124.9,-99.5]	-159.9 [-174.8,-149.6]	8	239.6	0.70 [0.63, 0.79]
Ekman transport	-51.9 [-53.5,50.9]	-95.8 [-108.9,-84.9]	-147.7 [-161.0,-136.8]	10	212.7	0.54 [0.48, 0.60]
Lasker events	-51.8 [-53.8,50.5]	-104.4 [-118.0,-94.0]	-156.3 [-169.5,-145.5]	10	230.6	0.63 [0.57, 0.71]
Horse mackerel	-50.2 [-52.2,49.1]	-107.7 [-122.0,-97.9]	-158.0 [-172.4,-148.2]	9	236.6	0.65 [0.59, 0.74]
Mackerel	-50.1 [-52.2,49.0]	-109.5 [-124.0,-99.1]	-159.6 [-174.4,-149.4]	9	239.2	0.68 [0.62, 0.77]
Sardine	-50.1 [-52.5,49.0]	-109.9 [-122.8,-99.5]	-160.1 [-173.3,-149.5]	9	239.8	0.68 [0.62, 0.76]
Hake	-50.1 [-52.4,48.8]	-109.2 [-123.7,-99.3]	-159.5 [-173.8,-149.6]	9	240.5	0.68 [0.62, 0.78]
Blue whiting	-50.1 [-52.0,49.0]	-108.2 [-122.2,-98.1]	-158.4 [-172.3,-148.1]	9	237.2	0.67 [0.61, 0.75]
Albacore tuna	-53.0 [-55.6,51.4]	-109.8 [-124.2,-99.1]	-162.9 [-177.5,-152.3]	11	243.6	0.68 [0.61, 0.78]
Plankton phenology	-66.1 [-69.3,63.7]	-87.6 [-103.3,-75.5]	-153.7 [-170.5,-141.4]	20	220.1	0.48 [0.42, 0.55]
River discharge	-50.2 [-52.2,49.1]	-105.6 [-120.3,-95.5]	-156.0 [-170.5,-146.0]	9	232.0	0.66 [0.60, 0.74]
Temperature	-50.5 [-52.2,49.4]	-103.4 [-117.4,-93.4]	-154.2 [-168.1,-144.0]	9	226.8	0.60 [0.55, 0.67]
Transport barriers	-60.8 [-64.0,58.6]	-90.8 [-105.4,-79.0]	-151.8 [-166.8,-139.7]	15	213.9	0.51 [0.45, 0.59]
Turbulence	-51.8 [-53.8,50.7]	-100.6 [-115.4,-89.4]	-152.7 [-167.7,-141.3]	10	222.4	0.64 [0.57, 0.72]
Deriso-Schnute recruitment function						
	$\log p(\theta)$	$\log f(\mathbf{y}_{0:T} \mathbf{x}_{0:T}^*, \theta)$	$\log p(\theta, \mathbf{x}_{0:T}^* \mathbf{y}_{0:T})$	n_θ	BPIC	$\sum e_{t,a,k} /n$
Constant environment	-63.3 [-65.8,-62.2]	-105.9 [-117.2,-97.9]	-169.4 [-180.7,-161.0]	10	232.8	0.61 [0.57, 0.66]
Ekman transport	-66.1 [-68.6,64.5]	-93.9 [-105.8,-84.5]	-160.4 [-172.0,-150.3]	12	213.1	0.52 [0.47, 0.58]
Lasker events	-65.6 [-68.3,-64.0]	-102.4 [-113.3,-93.2]	-168.3 [-179.4,-158.6]	12	229.5	0.60 [0.55, 0.66]
Horse mackerel	-63.5 [-66.5,-62.2]	-105.8 [-116.3,-97.7]	-169.5 [-180.1,-161.3]	11	235.3	0.61 [0.57, 0.66]
Mackerel	-63.2 [-65.4,-62.2]	-103.7 [-115.6,-95.4]	-167.1 [-179.3,-159.1]	11	231.3	0.58 [0.54, 0.65]
Sardine	-63.4 [-65.9,-62.2]	-105.6 [-118.1,-97.4]	-169.2 [-181.9,-161.0]	11	234.6	0.59 [0.55, 0.66]
Hake	-63.4 [-65.5,-62.2]	-104.6 [-116.3,-96.2]	-168.1 [-179.9,-159.5]	11	232.4	0.61 [0.57, 0.66]
Blue whiting	-63.5 [-66.0,-62.3]	-105.4 [-116.9,-96.6]	-169.2 [-180.7,-160.5]	11	235.3	0.61 [0.57, 0.66]
Albacore tuna	-66.0 [-68.7,64.7]	-103.8 [-115.9,-95.1]	-169.9 [-182.4,-161.1]	13	235.4	0.59 [0.54, 0.65]
Plankton phenology	-82.3 [-87.1,79.2]	-88.4 [-101.8,-77.5]	-171.0 [-186.0,-159.6]	22	225.5	0.49 [0.43, 0.56]
River discharge	-63.8 [-67.3,-62.4]	-104.4 [-117.1,-95.1]	-168.4 [-182.2,-159.2]	11	231.9	0.62 [0.57, 0.69]
Temperature	-64.6 [-67.9,-63.0]	-102.6 [-114.7,-93.0]	-167.5 [-179.2,-158.0]	11	229.2	0.59 [0.54, 0.65]
Transport barriers	-75.0 [-78.9,72.5]	-89.4 [-101.9,-79.1]	-164.5 [-177.2,-153.9]	17	215.4	0.49 [0.43, 0.55]
Turbulence	-65.3 [-67.8,-64.0]	-98.1 [-110.6,-88.9]	-163.8 [-176.1,-154.2]	12	222.1	0.57 [0.53, 0.64]

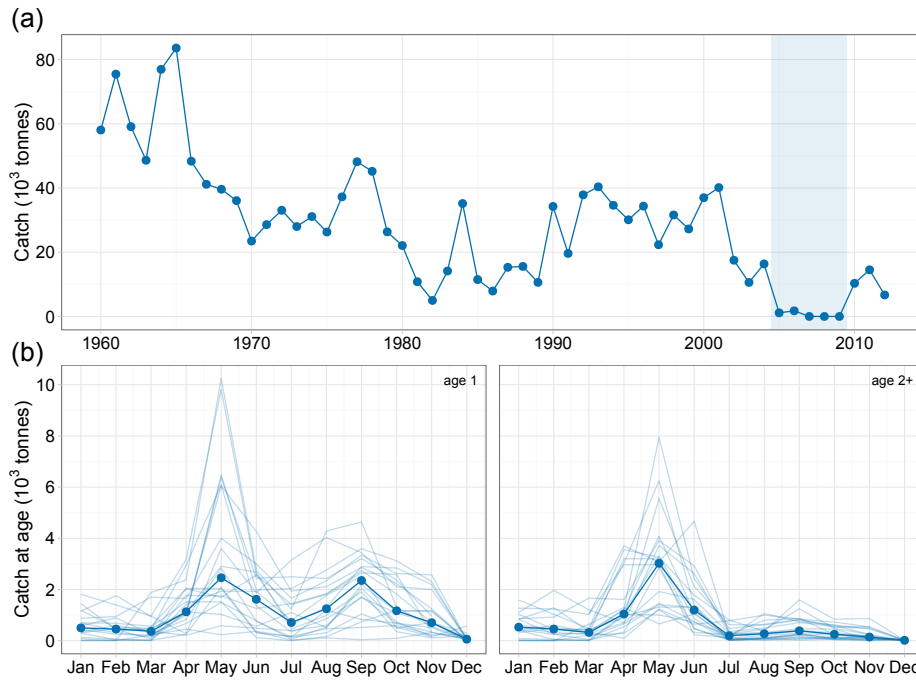


Figure 4.2: Anchovy catches in the Bay of Biscay between 1960 and 2011 (a), and seasonal catches at age between 1987 and 2011 (b). (a) Small scale purse seiners are responsible of most catches, which have declined steadily since the mid 60's. There was a period of extraordinarily low catches in the mid 80's and a collapse during the last decade which ended with fisheries closure in July 2005 (blue rectangle). The fishery was reopened in 2010 but a low fishing quota was established. (b) Fishing has a strong seasonal component, with catches concentrated on spawning grounds in the southeastern Bay of Biscay in spring and on feeding shoals in late summer and autumn (see figure 4.1). Recruits of the year predominate over older individuals in the catch throughout the year, especially during the second half Data from ICES [2012]; seasonal catches at age were derived from integrated monthly catch statistics by assuming a constant age structure during each half year.

4.3 Results

4.3.1 Model diagnostics and environmental effects on anchovy recruitment

All the models resulted in a relatively good fit, in the sense of their ability to assimilate biomass observations and met distributional assumptions (*i.e.* uncorrelated and normally distributed standard and forecast residuals). Posterior parameter estimates of initial population sizes ($x_{0,a}$), the physiological mortality rate (m) and process noise on adult survival (σ_{2p}) remained relatively constant among different model structures (coefficient of variation below 0.25; see also table 4.D.1 in the Appendix). According to these estimates, natural mortality alone might halve adult biomass during an average year ($m = 0.69 \text{ yr}^{-1}$ [0.45, 0.90]; median and 90% quantile based credible intervals), although the impact of process noise on adult survival was also relatively important ($\sigma_{2p} = 0.54$ [0.37, 0.79]). Nevertheless, changes in survival did not rival expected perturbations in recruitment of up to one order of magnitude for some of the models assessed (see below). Parameters of the observa-

tion equation remained also insensitive to model formulation ($cv < 0.30$). They highlighted however the complementarity of both survey methods; acoustic surveys presented a better accuracy ($q_{acst} = 0.97 [0.71, 1.27]$ and $q_{depm}/q_{acst} = 0.71 [0.61, 0.82]$) but estimates from the daily egg production method were more precise ($\tau_{acst}/\tau_{depm} = 1.32 [0.82, 2.24]$).

Models varying in structure differed nevertheless in key parameters determining huge changes in prediction ability like the magnitude of process noise in recruitment (σ_1) and the shape of the renewal function. In this way, model diagnostics resulted in a clear hierarchy among candidate mechanisms (table 4.3), indicating a greater importance of external environmental effects on recruitment with respect to density dependent regulation. Indeed, although the inclusion of a nonlinear recruitment function improved prediction ability in almost all cases, model skill depended mainly on the identity of the environmental covariate affecting recruitment (e.g. models with values of the predictive log likelihood above -100 in table 4.3). Models with the best performance included indexes related either to (i) enhanced larval survival when anchovy spawning match calm conditions over the Aquitanian shelf (*i.e.* timing of the bloom and transport barriers), or to (ii) a negative effect of strong winds during summer in the Armorican shelf (coastal upwelling, turbulence, mean temperature and Lasker events).

Within the two groups of best performing models, the model considering summer Ekman transport outperformed the others attending to the values of the Bayesian Prediction Information Criterion (*BPIC*). Constant or nonlinear recruitment received almost the same support, but prediction ability increased slightly in the second case. On the other hand, models considering transport barriers and, especially plankton phenology, presented the best prediction skill, although the estimation of missing values weighted down them in terms of parsimony. In these models, the inclusion of a nonlinear recruitment function resulted in a nil improvement or even in a deterioration of skill, that might be related to the large number of years with imputed covariate values. Diagnostics for models considering indexes related to natural enemies or river discharge were similar to models considering no environmental covariate (table 4.3). Including a Deriso-Schnute renewal function resulted in this case in highly nonlinear recruitment curves that improved skill considerably (table 4.3, figure 4.D.1 in the Appendix). Models including Ekman transport, plankton phenology and transport barriers were retained for further scrutiny (table 4.1, figure 4.1).

Table 4.1: Summary of the posterior distribution of process model parameters. Each cell presents the median and quantile based 90% credible intervals (square braces), estimated from 1000 posterior simulations. Parameters were summarized for benchmark models (constant productivity and/or no environmental effect on recruitment) and for models with the best prediction ability (see table 4.3 and the main text for details regarding the criteria used to select the models).

Parameter name [units]	Constant productivity				Deriso-Schnute recruitment function			
	Constant environment	Ekman transport	Plankton phenology	Transport barriers	Constant environment	Ekman transport	Plankton phenology	Transport barriers
<i>Initial biomass, $x_{0,1}$ and $x_{0,2p}$ [10^6 kg]</i>	36.4 [10.1, 120.1]	30.2 [12.1, 77.3]	32.6 [14.1, 70.6]	30.8 [13.0, 70.5]	30.4 [10.0, 109.5]	29.2 [12.4, 75.8]	32.8 [14.9, 72.1]	30.6 [14.2, 71.1]
	39.7 [20.1, 78.4]	33.8 [17.1, 68.5]	35.3 [18.5, 71.7]	34.0 [17.9, 70.6]	33.6 [17.2, 65.6]	34.1 [17.0, 68.9]	36.0 [18.1, 70.2]	33.5 [16.7, 65.7]
<i>Physiological mortality rate, m [yr^{-1}]</i>	0.742 [0.532, 0.953]	0.671 [0.455, 0.860]	0.688 [0.486, 0.881]	0.689 [0.491, 0.882]	0.632 [0.427, 0.841]	0.648 [0.452, 0.851]	0.679 [0.494, 0.879]	0.675 [0.472, 0.877]
<i>Environmental effect on recruitment, η [-]</i>	-	-0.717 [-0.913,-0.528]	-0.799 [-1.008,-0.592]	-0.776 [-0.996,-0.550]	-	-0.671 [-0.855,-0.482]	-0.774 [-0.980,-0.550]	-0.775 [-0.972,-0.578]
<i>Recruitment function</i>								
<i>Productivity, α' [$\text{kg recruit}_{\text{kg adult}}$]</i>	1.35 [1.05, 1.77]	0.84 [0.68, 1.03]	0.78 [0.63, 0.98]	0.77 [0.62, 0.95]	4.03 [2.67, 6.63]	1.38 [0.98, 2.13]	0.96 [0.76, 1.25]	1.12 [0.84, 1.50]
<i>Optimality, β^{-1} [10^6 kg adult]</i>	-	-	-	-	34.5 [16.5, 74.8]	38.6 [20.0, 136.0]	39.8 [23.7, 242.4]	50.9 [25.9, 160.3]
<i>Limitation, γ [-]</i>	-	-	-	-	-0.31 [-0.92, 0.33]	-3.29 [-13.86, 0.21]	-14.19 [-24.25,-0.85]	-4.22 [-15.44, 0.38]
<i>Process noise standard deviation, σ_1 and σ_{2p}</i>	1.169 [0.869, 1.632]	0.800 [0.603, 1.074]	0.620 [0.445, 0.873]	0.670 [0.497, 0.927]	1.050 [0.815, 1.369]	0.746 [0.568, 1.020]	0.629 [0.447, 0.893]	0.622 [0.445, 0.884]
	0.535 [0.365, 0.797]	0.525 [0.365, 0.751]	0.512 [0.345, 0.788]	0.530 [0.361, 0.775]	0.558 [0.388, 0.801]	0.528 [0.367, 0.758]	0.522 [0.357, 0.764]	0.527 [0.366, 0.779]

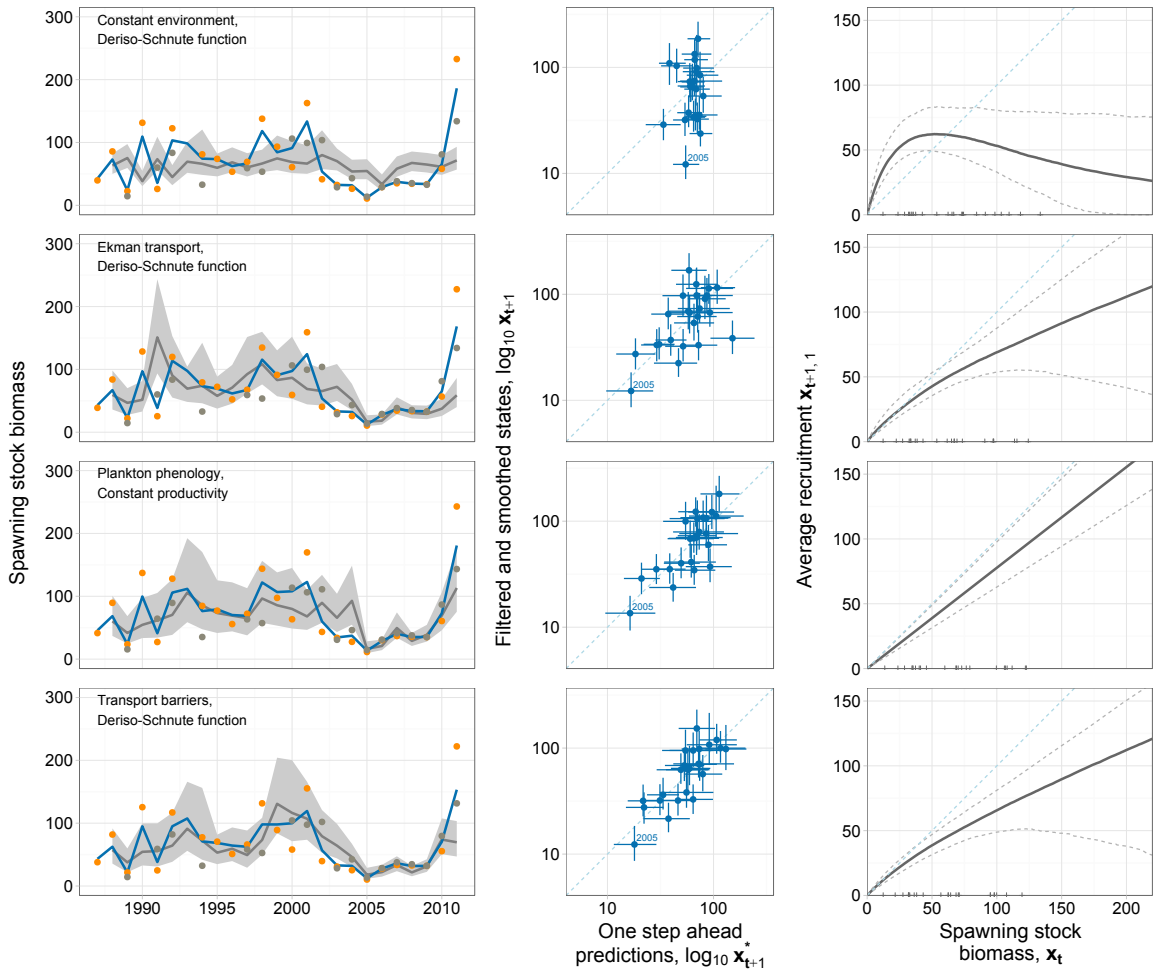


Figure 4.1: Summary of model fits on spawning stock biomass [10^6 kg]. Results are presented for models with no environmental effect on recruitment and for models including indexes representing Ekman transport, plankton phenology or transport barriers. We selected the model with a Deriso-Schnute renewal function in all cases except for plankton phenology, in which average recruitment was proportional to spawning biomass. Panels in the first column present observations for acoustic (grey dots) and daily egg production methods (orange dots) corrected by the median of estimated detectabilities (q_k); filtered and smoothed states (blue line), and one step ahead predictions (grey line; the shaded area correspond to quantile based 90% credible intervals). Panels in the central second column are scatter plots of one step ahead predictions vs filtered and smoothed states (i.e. the scatter in this plot represents process variance; the dashed blue line corresponds to a perfect fit [1:1]). Note that the plots present \log_{10} transformed estimates and that lines around the dots cover 90% credible intervals. The third column presents plots with posterior estimates of the renewal function (median and quantile based 90% credible intervals represented by the thick grey line and the dashed grey lines, respectively). The crosses in the abscissa correspond to the posterior median of filtered and smoothed states. The dashed blue line corresponds to a recruitment level equal to previous year spawning stock biomass [1:1].

4.3.2 Fishing, environmental variability and anchovy collapse

The experiment based upon the analysis of surrogate time series revealed a clear connection between fishing pressure and the recent collapse of the anchovy fishery in the Bay of Biscay (figure 4.1). According to our simulations, a 50% reduction in fishing pressure would have decreased the risk of collapse in a 40–80% with respect to the risk associated to the actual pattern of fishing pressure experienced by the population. Nevertheless, the most important

differences were related to how likely was the collapse under different model assumptions. Again, these differences depended to a great extent on assumptions related to recruitment regulation, specifically to the identity of the environmental covariate affecting recruitment rather than to the type of renewal function specified. Differences in model predictions regarding the causes of the collapse can be illustrated attending to the contrast between the benchmark reference model and models including an external covariate (figure 4.1).

Under the assumptions posed by the reference model –no structured effect of the environment on recruitment– the collapse might be interpreted as a very rare event due to the huge noise associated to recruitment (the estimated probability of a collapse with actual fishing rates was of 0.06 [0.03, 0.08], median and quantile based 50% credible intervals¹). On the other hand, models with a better ability to predict changes in recruitment presented a strong response to changes in fishing pressure, moving from a nill or very low likelihood of collapse to relatively high chances as fishing pressure increased. This pattern cannot be interpreted as a consequence of exceptionally high, random perturbations in recruitment (process noise in recruitment was indeed much lower for these models, e.g. $\sigma_{1,ref}/\sigma_{1,env} = 1.58$ [1.03, 2.49]; median and 90% quantile based interval). The model including plankton phenology, that presented the best skill for the year of the collapse (table 4.3), presented an almost linear sensitivity to reductions fishing pressure that contrasted with the nonlinear response of the other covariates. Also, this model predicted a higher baseline level for the probability of collapse that increased almost ten-fold as fishing pressure increased (from 0.06 [0.03, 0.12] with no fishing to 0.60 [0.52, 0.70] for actual fishing mortality rates).

4.4 Discussion

We assessed the importance of both density dependent and density independent mechanisms on the dynamics and recent collapse of Bay of Biscay anchovy. To this end, we embedded a detailed analysis of changes in the environment of anchovy early stages within a nonlinear, age structured population model fitted under a Bayesian framework. This approach allowed us to identify external environmental factors that present a great promise to improve our ability to anticipate future changes in the population, and to identify overfishing as a key destabilizing effect that seems to be behind the recent collapse of the anchovy fishery in the Bay of Biscay.

A first main result of our study was the identification of two groups of environmental effects that presented a great ability to predict changes in anchovy recruitment; (*i*) enhanced larval survival when anchovy spawning match calm conditions over the Aquitanian shelf (*i.e.* timing of the bloom and transport barriers) and, (*ii*) a negative effect of strong winds during summer in the Armorican shelf (especially Ekman transport). These effects point

¹Note that we used 50% intervals in this case to avoid the long tails associated to the distribution of these statistics.

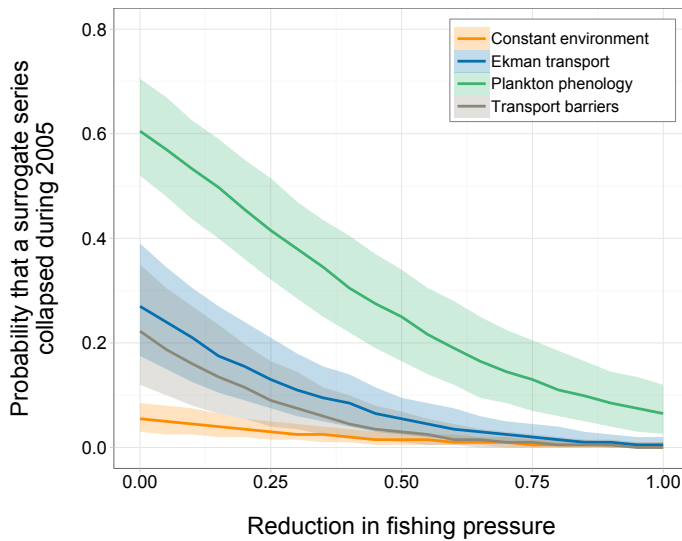


Figure 4.1: Summary of surrogate analysis of the collapse of anchovy fisheries in the Bay of Biscay. The graph presents changes in the probability that a surrogate time series collapsed in 2005 as a function of the reduction in fishing pressure (from realized fishing pressure [0.0] to no fishing [1.0]) for the same models presented in figure 4.1 (median [*line*] and 50% quantile based credible intervals [*shading*]). Results are presented for the best performing models, that considered the effect of the following covariates on recruitment: *Ekman transport*, *plankton phenology* and *transport barriers* (see the text for further details). The graph presents also the estimates derived from a reference model considering a *constant environment* with no structured environmental effect on recruitment and that presented a poor performance. All models included a Deriso-Schnute renewal function except in the case of plankton phenology, in which average recruitment was proportional to spawning biomass. See Surrogate analysis of anchovy collapse in the Appendix for further details about the experiment.

directly to Hjort [1914]–Cushing’s [1990] Match-mismatch and Iles and Sinclair’s [1982] Member/Vagrant hypotheses. Previous correlative studies have also invoked upwelling and calm conditions to explain changes in recruitment success [Borja et al., 1996, 1998, 2008; Allain et al., 2001, 2007a,b], although they were associated to other timings and locations. Our results also allowed us to discard other mechanisms, including river discharge and the detrimental effect of natural enemies and strong density dependent regulation of recruitment. Taken together, these results lead us to propose an alternative scheme for anchovy recruitment success in the Bay of Biscay.

According to our results, the strength of anchovy recruitment involves a sequence of several key events. First, although we detected weak density dependence on population renewal, average recruitment was a linear or weakly nonlinear function of previous year spawning biomass. This introduces certain degree of memory in anchovy dynamics by conditioning recruitment success. Early survival might be enhanced when spawning match calm spring conditions in the southeast. Then, spawning might be followed by either a northward drift of anchovy larvae or a secondary spawning peak in Armorican shelf. This secondary peak might be protagonized by larger adults with higher fecundity spawning in the shelf break [Motos et al., 1996; Ibaibarriaga et al., 2013]. The success of these anchovy recruits might be quite sensitive to a detrimental effect of seaward larval drift associated

to summer upwelling . Both scenarios contrast with the recent appeal to the advantageous effect of larval drift to open waters [Irigoién et al., 2007; Bachiller et al., 2013], an alternative that found no support in our analysis of changes in anchovy environment. We cannot clarify whether any of the two mechanisms proposed is actually working in the field or if any of the two just echoes the other. Although solving these questions is beyond this study, we think that our results point clear alternatives that can be tested in the field.

The second main result of our study deals with the potential role of overfishing in the collapse of Bay of Biscay anchovy fisheries in 2005. Surrogate analysis of models incorporating different assumptions about recruitment regulation revealed an increased risk of collapse associated to increases in fishing pressure. Although this response varied depending on the environmental factor affecting recruitment, overfishing was favored in all cases over alternative explanations involving random or structured environmental perturbations of recruitment and adult survival. This result has important implications for the management of the fisheries and lead us to paraphrase J. H. Connell [1980] and invoke a «ghost of over exploitation past» to explain reduced fishery yields in the late eighties and in the last decade. Historical catch records doubling recent levels provide a clue pointing in this direction. As an aside, reduced abundance associated to overfishing can be invoked to explain our inability to detect strong density dependent effects and especially, the lack of association with changes in the abundance of natural enemies that might have been already decimated.

In a more general context, our study highlighted the need to incorporate a careful assessment of environmental effects in population dynamics studies targeting the causes behind fluctuations in abundance (e.g. Anderson et al. [2008]; Shelton and Mangel [2011]). Assumptions about external forcing affected not only our conclusions about the prediction ability of different model structures; but also our inferences about the importance of density dependence and how interventions associated to fishing or other management actions altered population dynamics. An analysis like the one presented here was possible thanks to recent developments in Markov Chain Monte Carlo methods and Bayesian non-linear time series analysis [West and Harrison, 1997; Doucet et al., 2001; Robert and Casella, 2004]. This study provides just a glimpse of the advantages that these methods can bring to population ecology and resource management [Royle and Dozario, 2008; King et al., 2009]. Nevertheless, our approach rely on long term physical and biological databases. Continued monitoring is the key to solve the long standing puzzle of the causes of population fluctuations, as well as the only way to ensure a sustainable exploitation of small pelagic fisheries.

Appendix

4.A Primary data

Table 4.A.1: Spawning stock biomass at age ($x_{t,a}$, [10^3 kg]) of European anchovy in the Bay of Biscay in spring (1987–2011). Biomass estimates for age 1 recruits of the year ($x_{t,1}$) and for the total stock ($x_{t,\cdot}$) were derived based on the daily egg production method (*depm*) and on acoustic surveys (*acst*). Annual catches ($f_{t,\cdot}$) group captures at all ages and during the entire year (*i.e.* before and after the surveys; note that fishing mortality entered the model as the seasonal catches at age presented in figure 4.2). Data from ICES 2012; see Material and Methods in the main text for further details.

	<i>depm</i>		<i>acst</i>		
	$x_{t,1}$	$x_{t,\cdot}$	$x_{t,1}$	$x_{t,\cdot}$	$f_{t,\cdot}$
1987	14235	29365	—	—	14764
1988	53087	63500	—	—	15088
1989	7282	16720	6476	15500	10428
1990	90650	97239	—	—	33857
1991	11271	19276	28322	64000	19283
1992	85571	90720	84439	89000	37686
1993	—	—	—	—	40085
1994	34674	60062	—	35000	34487
1995	42906	54700	—	—	29844
1996	—	39545	—	—	34176
1997	38536	51176	38498	63000	21960
1998	80357	—	—	57000	31441
		101976			
1999	—	69074	—	—	26795
2000	—	44973	89363	—	36995
			113120		
2001	69110	—	67110	—	40149
		120403	—	105801	
2002	6352	30697	27642	—	17496
			110566		
2003	16575	23962	18687	30632	10595
2004	14649	19498	33995	45965	16361
2005	2063	8002	2467	14643	1127
2006	15064	21436	18282	30877	1753
2007	16030	25973	26230	40876	141
2008	7579	25377	10400	37574	0
2009	9295	24846	11429	34855	0
2010	33725	42979	64564	86355	10318
2011	—	—	—	—	14542
	140555	172223	115379	142601	

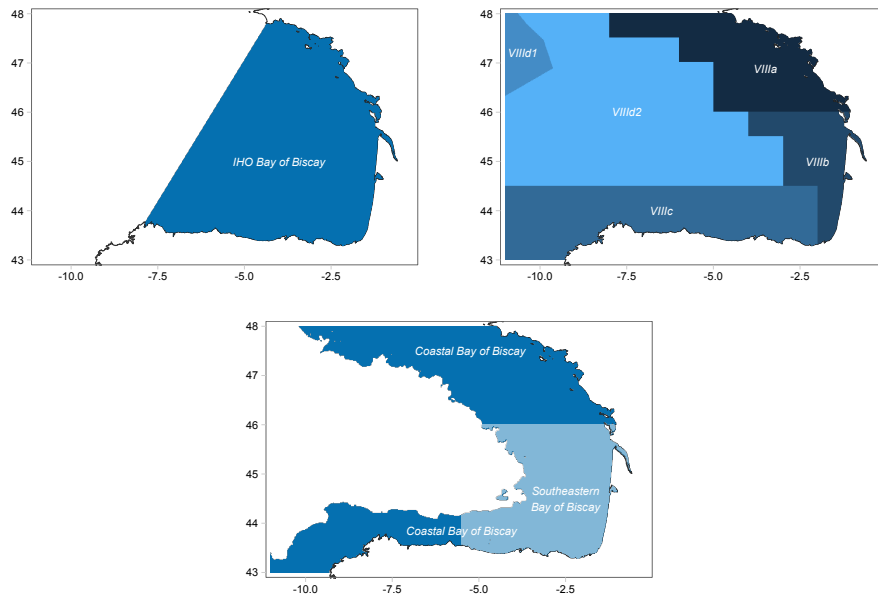


Figure 4.A.1: Maps of the Bay of Biscay with the different spatial domains used to integrate environmental indexes.

4.A.1 Ancillary data

Introduction

The following sections detail the methods and procedures used to derive the environmental indexes employed to assess different hypothesis about the success of anchovy recruitment in the Bay of Biscay (table 4.1). table 4.2 in the main text provides a summary of the different indexes and the expected relationship with anchovy recruitment. The subset of indexes presented in the text was selected *a priori* from a large set of candidate indexes differing in subtle details about their derivation, especially regarding the spatiotemporal domain of integration. Indeed, indexes were averaged over (figure 4.A.1);

- (i) IHO Bay of Biscay [$172 \times 10^3 \text{ km}^2$]; defined by the International Hydrographic Organization as the sea region located landwards of the line joining Cape Ortegal and Point Penmarc'h (IHO 1953, www.ihodata.int).
- (ii) ICES divisions within area VIII (figure 4.1, [$370 \times 10^3 \text{ km}^2$])); the Armorican shelf (North division, VIIIa [$60 \times 10^3 \text{ km}^2$]), the Aquitanian shelf (Central division, VIIIb [$34 \times 10^3 \text{ km}^2$]), the Cantabrian Sea (South division, VIIIc [$89 \times 10^3 \text{ km}^2$]) and open waters (Offshore division, VIIId [$262 \times 10^3 \text{ km}^2$]). We also considered combinations corresponding to the Armorican-Aquitian shelf (VIIIa and b) and the North Iberian shelf (VIIIb and c).
- (iii) Coastal Bay of Biscay [$186 \times 10^3 \text{ km}^2$]; that we customary defined as the portion of the Bay of Biscay (ICES area VIII) where mean depth was lower than 4000 m and the

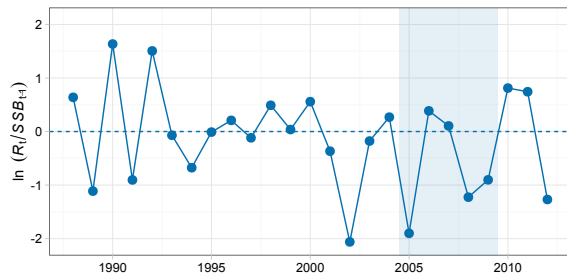


Figure 4.A.2: Larval survival index for anchovy recruitment in the Bay of Biscay for the period 1987–2011. The index was estimated as the natural logarithm of the ratio between recruitment (R_t , in this case, the biomass of age 1 individuals at the beginning of the year, $x_{t,1}^i$) and spawning stock biomass (SSB_{t-1} , that it is assumed to correspond to total biomass in the previous year at the time of the surveys, $x_{t-1,.}$). Values above or bellow zero ($R_t = SSB_{t-1}$, dashed line) correspond to reproductive success or failure to renew biomass (i.e. in the constant productivity model, the productivity parameter, α , is equal to unity). We used estimates of median R_t and SSB_{t-1} from the two-stage biomass dynamic model employed by ICES [2012] to assess the status of the fishery (see also Ibañarriaga et al. [2008]).

distance to the coast less than 300 km.

- (iv) Southeastern Bay of Biscay [$72 \times 10^3 \text{ km}^2$]; that we customary defined as the portion of the coastal Bay of Biscay located eastwards of the parallel 5.5°W and southwards of the meridian 46°N .

In all cases, the choice within each family of indexes was based on their ability (measured by the Pearson product-moment correlation coefficient, r) to explain changes in a larval survival index derived from stock assessment estimates (ICES 2012; figure 4.A.2). We later analyzed indexes that surpassed this first filter looking for incongruences and redundancies before deciding the final subset (see Summary).

Ekman transport

Positive Ekman transport is associated to the upwelling of deep waters and surface divergence. Upwelling during spring and early summer has been advocated as an important process for the success of anchovy recruitment in the Bay of Biscay, either through a direct effect on larval dispersal or by an indirect trophic effect mediated by the enhancement of primary production [Borja et al., 1996, 1998, 2008; Allain et al., 2001]. We followed these studies to derive an upwelling index, but we considered both coastal upwelling associated to alongshore wind stress and offshore Ekman pumping associated to wind stress curl [Pickett and Schwing, 2006; Rykaczewski and Checkley, 2008]. This allowed us to consider the potential effects of different types of upwelling on zooplankton size structure [Rykaczewski and Checkley, 2008], as well as in zooplankton abundance in offshore habitats [Chelton, 1982].

The vertical velocity for both coastal and curl driven upwelling mechanisms was estimated for the period 1988–2011 from six hourly, 0.25° wind speed maps ($w [\text{m s}^{-1}]$) ex-

tracted from the Level 3 Cross-Calibrated Multi-Platform Ocean Surface Wind Velocity product (CCMP, Atlas et al. 2011, available at PO.DAAC, podaac.jpl.nasa.gov). Wind stress, $\vec{\tau}$ [N m⁻²], was estimated from vector wind speed data using;

$$\vec{\tau} = \rho_{air} C_D \vec{w} |\vec{w}| \quad (4.9)$$

where ρ_{air} is air density (1.223 kg m⁻³, assuming a mean atmospheric temperature of 15.4°C), and C_D is the drag coefficient, that was estimated as a function of w based on Yelland and Taylor [1996] and Yelland et al. [1998].

Coastal upwelling (Q_{upw} , [m³ s⁻¹]) is defined as the seaward Ekman transport (T , [m² s⁻¹]) integrated along a segment of coast of a given length ($L = 1$ m), and can be estimated from wind data;

$$Q_{upw} = TL = \frac{\tau_a L}{\rho_{sw} f} \quad (4.10)$$

where τ_a is the alongshore component of wind stress acting along L , ρ_{sw} is seawater density (1025 kg m⁻³) and f is the Coriolis parameter. To derive τ_a , the mean coastal orientation within each 0.25° pixel location was estimated from a finer resolution, regularized coastline derived from a large scale landmask (0.017° cell side). Mean vertical upwelling velocity (ω_{coast} [m s⁻¹]) at the base of the Ekman layer can be derived directly from transport as:

$$\omega_{coast} = \frac{T}{R_d} \quad (4.11)$$

where R_d is the Rossby radius of deformation and represents the approximate offshore scale of transport (taken as 23.1 km from Chelton et al. [1998], see also their [Global Atlas of the First-Baroclinic Rossby Radius of Deformation and Gravity-Wave Phase Speed](#); see also Pickett and Paduan [2003]).

Curl driven upwelling (Ekman pumping) results from spatial gradients in wind stress. These gradients might cause surface divergence or convergence that results in open ocean upwelling or downwelling. We estimated the mean vertical velocity (ω_{curl} [m s⁻¹]) at the base of the Ekman layer due to wind stress curl following Risien and Chelton [2008];

$$\omega_{curl} = \frac{1}{\rho_{sw}} \nabla \times \left(\frac{\vec{\tau}}{f} \right) = \frac{1}{\rho_{sw} f} \left(\nabla \times \vec{\tau} + \frac{\beta}{f} \tau_x \right) \quad (4.12)$$

where β is the latitudinal gradient in f ([s m⁻¹]), and τ_x is the zonal component of wind

stress (positive eastwards). Wind stress curl, $\nabla \times \vec{\tau}$, was estimated using centered derivatives spanning two 0.25° cells [Pickett and Paduan, 2003].

We assessed indexes based on either coastal upwelling, curl driven upwelling or their sum, total Ekman transport. Upwelling estimates for each pixel location were integrated for the spawning season (Apr–Aug), and for spring (Mar–Jun) and summer (Jul–Aug) seasons, and later averaged over different spatial domains. Prior to data integration, six-hourly data was smoothed using a 5 day moving average filter in order to avoid the consideration of episodic upwelling events. Although there was some spatial variation, we detected in general trends towards an increase in coastal upwelling and a decrease in curl-driven upwelling during spring and summer in the Bay of Biscay between 1988 and 2011.

Larval survival presented a negative relationship with coastal upwelling and a slightly positive or nil relationship with curl driven upwelling. Indexes adding up the two upwelling components presented in general a poor performance when compared with their single components, except for a few exceptions. In all cases, the relationship improved when upwelling was integrated over ICES divisions VIIIa or VIIIa,b. Indeed, coastal upwelling in the Armorican shelf (VIIIa) during summer (Jul–Sep) presented the best relationship with the larval survival index ($r = -0.77$, slightly better than when combining data from VIIIa and b, $r = -0.74$, and much better than for VIIIb alone, $r = -0.10$). An index considering only positive values of coastal upwelling provided similar results, although we preferred the index integrating both upwelling and downwelling events (the correlation among them was nearly one; $r = 0.96$). Another spatial or time domains of integration did not outperform our best index (e.g. Mar–Jul in area VIIIa,b as in Borja et al.'s [1996] index, $r = -0.38$), including single summer months (July in ICES division VIIIa presented the best correlation, $r = -0.58$; that in this particular case improved when including Ekman pumping to $r = -0.62$). Only coastal summer upwelling in the Armorican shelf was retained for further exploration using the nonlinear population dynamics model.

Lasker events

Lasker events are periods of relatively calm wind allowing food and larvae to become vertically concentrated together in thin layers. Based on a combination of field observations and experiments, Lasker [1975, 1978] demonstrated that these events are critical for the survival of Northern anchovy (*Engraulis mordax*) larvae in the California Current. He also proposed that storms and wind induced mixing or upwelling might prevent the formation of aggregations and might produce a failure in recruitment. The potential application of these findings to European anchovy in the Bay of Biscay find support in the relationship found between water column stability and anchovy survival [Allain et al., 2001, 2007a,b].

Peterman and Bradford [1987] (see also Pauly 1989) proposed an index to characterize interannual changes in the importance of Lasker events. It is based on counting the

number of periods with a duration of at least i days with winds below a given wind speed threshold, j . Periods of calm with a longer duration are just considered as composed of several, partially overlapping events. We estimated the number of i/j Lasker events during anchovy spawning season (Apr–Aug) for the period 1988–2011 based on six hourly, 0.25° wind speed maps (w [$m s^{-1}$]) extracted from the Level 3 Cross-Calibrated Multi-Platform Ocean Surface Wind Velocity product (CCMP, Atlas et al. 2011, available at P.O.DAAC, podaac.jpl.nasa.gov).

The number of Lasker events detected during the spawning season (Apr–Aug) was counted for each pixel location and later averaged over the different spatial integration domains. We considered different combinations of the threshold wind speed and time span for Lasker events, with i ranging from 4 to 15 days and j from 4 to $15 m s^{-1}$. Irrespective of the i/j combination, the number of Lasker events detected during the spawning season presented a negative trend for the period 1988–2011. As expected, the larval survival index presented a positive correlation with the number of Lasker events, especially for indexes integrated over ICES divisions VIIIa,b that include anchovy spring spawning grounds. Among them, the number of 12/7 Lasker events integrated over area VIIIa resulted in the best relationship ($r = 0.49$), with a slightly better correlation than areas VIIIb or VIIIa,b ($r = 0.43$ and $r = 0.48$, respectively), and was retained for further analysis.

Natural enemies

Anchovy is a key link between lower and upper trophic levels in the Bay of Biscay [Sánchez and Olaso, 2004]. Anchovy is preyed upon a variety of predators including seabirds and mammals, although we focused on adults and juveniles of other fish species that prey upon anchovy larvae and juveniles. We might expect as well a potential role for competitive interactions, especially with sardine. Competition might arise from partial overlap in resource use and from the potential detrimental effect of participating in mixed schools when other species are more abundant (e.g. Bakun and Cury 1999). To assess the potential role of natural enemies on the success of anchovy recruitment, we used indexes of the abundance of:

- (i) Small pelagic fish species like sardine (*Sardina pilchardus*, ICES areas VIIc and IXa), North East Atlantic mackerel (*Scomber scombrus*, combined stock) and horse mackerel (*Trachurus trachurus*, western stock).
- (ii) Demersal species like hake (*Merluccius merluccius*, ICES areas VIIc and IXa) and blue whiting (*Micromesistius poutassou*, combined stock).
- (iii) Migrating schools of albacore tuna (*Thunnus alalunga*).

In the case of small pelagics and demersal species, we used time series of recruitment and spawning stock biomass estimates for the period 1987–2011 available from ICES's [2013]

Stock Assessment Summary Database. For albacore tuna, we retrieved bait boat catch per unit effort data ([tonnes day fishing⁻¹]) for the period 1987–2009 recorded in a 5 × 5° quadrangle centered on 5°W, 40°N from ICCAT's [2013] Task II Catch & Effort database.

Previous year abundance data were log transformed before checking the relationship with anchovy larval survival (*i.e.* mass action). In the case of small pelagic and demersal species, we screened both previous year recruit and adult abundance. In all cases except for blue whiting, the abundance of recruits resulted in a better correlation than the biomass of adults. For all species, the relationships were negative but very weak or nil (*e.g.* 0 > r > -0.20) except, again, for blue whiting spawning biomass ($r = -0.30$). We retained one index per species for further exploration using the nonlinear population model.

Phytoplankton abundance and phenology

Plankton phenology is a key indicator of the functioning of marine ecosystems that has been advocated as a major determinant of interannual fluctuations in fish recruitment in temperate and subpolar regions. Hjort [1914]–Cushing's [1990] Match-mismatch hypothesis states that larval survival depends on the degree of overlap in time between spawning and seasonal pulses of production (*e.g.* the spring and autumn phytoplankton bloom). As many other fish species, anchovy spawning peaks in spring in the Bay of Biscay, coinciding with the annual peak in production. On the other hand, previous studies conducted in the California Current ecosystem suggest an important effect of early feeding success on anchovy survival during the critical few days of live following hatching [Lasker, 1975]. It should be noted that direct effects of total resource availability or species composition on early survival are also possible [Lasker, 1975; Durant et al., 2007].

We estimated chlorophyll *a* (chl *a*) concentration for monthly and quarterly intervals ([*Phyto*] [mg chl *a* m⁻³]), as well as the timing (δ [day]) and magnitude ([*Phyto*]_{bloom} [mg chl *a* m⁻³]) of spring and fall phytoplankton blooms in the Bay of Biscay for the period 1998–2011 from ocean color remote sensing data. Daily chl *a* concentration [mg m⁻³] maps were retrieved from Level 3 SeaWiFS (Sept. 1997–Dec. 2007, reprocessing R2010) and Aqua MODIS (Jul. 2002–Apr. 2013, reprocessing R2013) standard mapped images available at the Ocean Color Web (SMI, O'Reilly et al. 2000; Feldman and McClain 2012; Goddard Space Flight Center, NASA; oceancolor.gsfc.nasa.gov). Original data at a nominal scale of 0.04° was averaged over a 0.25° grid (cell side ~25 km). We used chl *a* concentration maps estimated using the Garver-Siegel-Maritorena semi-analytical model (GSM, Garver and Siegel 1997; Maritorena et al. 2002, 2010). Bloom statistics were derived for each pixel location based on realizations of a model smoothing chl *a* observations [Taboada and Anadón, 2014]. The timing of each bloom was defined as the day of maximum net increase in chl *a*, and its magnitude as the peak chl *a* concentration attained.

The best correlation with the larval survival index was found for the timing of the spring

phytoplankton bloom averaged over the coastal Bay of Biscay within ICES division VIIIb,c ($r = -0.73$). Despite ICES division VIIIC covers areas located well away anchovy spring spawning grounds, it was included to compensate the lack of data in the Southeastern Bay of Biscay, especially in 2000 and 2002. The correlation between the timing of the spring bloom in the Southeastern Bay of Biscay and in division VIIIb,c was indeed very high when these years were dropped ($r = 0.94$). Bloom timing and magnitude presented a slight negative correlation among them (earlier blooms attained a larger peak chl *a* concentration, $r = -0.22$ for ICES division VIIIb,c), and thus they presented a relationship of opposite sign with anchovy survival (years with later blooms of less magnitude coincided with a lower survival). The timing of the spring bloom was by far a better predictor than bloom magnitude ($r = -0.73$ vs. $r = 0.24$). Instead, the relationship with bloom magnitude was also negative but more stronger when considering data integrated over the Armorican shelf (ICES division VIIIA, $r = -0.49$), where the relationship with bloom timing was weak ($r = -0.22$). Indeed, this negative relationship was confirmed by an even higher correlation with median chl *a* concentration during May over the same area ($r = -0.66$). Bloom timing in ICES division VIIIb,c and chl *a* concentration in May in ICES division VIIIA were retained for further analysis.

River discharge

Anchovy spawning is localized in two main spawning grounds in front of the mouth of rivers Adour and Garonne (Gironde estuary, Motos et al. 1996). Field studies on anchovy larval condition at these locations suggest that increased river discharge enhance larval survival by increasing water column stability and productivity [Bergeron, 2004; Bergeron et al., 2010]. On the other hand, correlative analyses have revealed a negative association between river discharge and recruitment, pointing towards alternative mechanisms [Planque and Buffaz, 2008; Borja et al., 2008].

River discharge ($Q [m^3 s^{-1}]$) has been recorded regularly by the Directions Régionales de l'Environnement, de l'Aménagement et du Logement (DREAL) and it is available at Banque HYDRO (www.hydro.eaufrance.fr), Ministère de L'Écologie, du Développement Durable et de L'Énergie, France. We explored the relationship between larval survival and integrated discharge for the three main rivers that lead into the anchovy spawning grounds: L'Adour (at Saint Vincent de Paul, produced by DREAL Aquitaine), Garonne (at Tonneins, produced by DREAL Midi-Pyrénées), and La Loire (at Montjean sur Loire, produced by DREAL Pays de Loire). Monthly river discharge was integrated over the spawning season (Apr-Aug) for the period 1986–2011. The time series presented a slight negative trend in river discharge for the three rivers. Rivers Garonne and L'Adour presented a high correlation between them ($r = 0.83$) but not with river La Loire ($r = 0.07$ and $r = 0.31$, respectively). Nevertheless, only the integrated discharge of river Garonne presented an appreciable relationship of negative

sign with anchovy recruitment ($r = -0.26$) and was retained for further consideration.

Sea surface temperature

In the Bay of Biscay, anchovy spawning is triggered by the onset of stratification during spring and is usually observed within values of sea surface temperature (SST) in the range of 14–18°C [Motos et al., 1996]. Temperature also affects the rate of any biological process, including anchovy larval growth rate and, consequently, the duration of the larval period. It can be also expected that adverse environmental conditions leave a signature in SST changes. To reflect all these potential effects, we derived a set of indexes for the period 1987–2011 based on NOAA Optimum interpolation 0.25° daily sea surface temperature analysis (OISST version 2, Reynolds et al. 2007). The database, which contains data since 1981 and is continuously updated with new images, is produced and maintained by C. Liu and R. W. Reynolds at NCDC (see www.ncdc.noaa.gov/sst).

To analyze the potential effect of SST on the amount of habitat available for spawning, we estimated the mean area within the appropriate temperature range for spawning during the spawning season (Apr–Aug). The index was estimated based on the classification of pixel locations within each daily SST map; then, the total amount of area available each day was averaged over different spatial domains. We also estimated mean SST for different periods during the larval period (Apr–Oct) in order to reflect potential changes in growing conditions. Both sets of indexes presented a good correlation with changes in anchovy survival when their values were integrated over the Armorican-Aquitanian shelf, although the best relationship was found when considering values over the Armorican shelf alone (ICES division VIIIa).

The amount of habitat available for spawning presented the best correlation with larval survival ($r = -0.60$), although its negative sign does not have an immediate explanation to us. In the case of mean temperature during the larval period, we found a positive correlation ($r = 0.50$ for mean SST in Jul–Sep) that might be interpreted either in terms of a presumed positive effect of temperature on the rate of growth or as an indirect correlation between SST and upwelling (see Ekman transport above). This second argument can be applied as well to explain the negative correlation found with the amount of habitat available for spawning (*i.e.* lack of upwelling results in warmer temperatures over the Armorican shelf and increased recruitment). We assessed other indexes looking for a detrimental effect of environmental hardness during overwintering, although the relationship with anchovy survival was nil (*e.g.* winter duration, taken as the number of days below 14°C between two consecutive SST maxima).

Mesoscale structures and transport barriers

The presence of filaments, fronts and mesoscale eddies is important for the retention and dispersal of planktonic propagules like anchovy eggs and larvae. At the same time, these mesoscale features represent patches of favorable habitat for the feeding larvae [Harrison et al., 2013]; they promote the concentration and retention of passive particles, and they are usually associated to increased biological production. The physical limits of these hydrographic structures can be revealed by way of *attracting* and *repelling* Lagrangian coherent structures (*LCSs*, Haller and Yuan 2000), that can be regarded as partial transport barriers that establish a divide between fluid parcels with different advection dynamics [Shadden, 2012]. Parcels of fluid located near a *LCS* will converge or diverge away from it. In this way, *LCSs* reveal the “hidden skeleton of fluid flows” [Peacock and Haller, 2013], and have been used in a variety of contexts to analyze geophysical flows and the impact of mesoscale features in marine life (e.g. d’Ovidio et al. 2004, 2010; Lehahn et al. 2007; Beron-Vera et al. 2008; Kai et al. 2009; Harrison and Glatzmaier 2012; Harrison et al. 2013).

In practice, *LCSs* can be defined as ridges in the spatial distribution of the exponential rate of divergence between two initially close trajectories for each parcel of a flowing fluid. The value of this Lyapunov exponent (λ [s^{-1}]) can be derived from space-time fields of ocean current data by measuring the rate at which the distance $|\delta|$ ([m]) between two parcels of fluid located nearby at time t_0 increases with time [Shadden et al., 2005];

$$|\delta_t| = |\delta_0| e^{\lambda(t-t_0)} \quad (4.13)$$

For a discrete grid of velocity measurements, the usual approach is to record the maximum divergence between the four nearest neighbors of each focal parcel. Two different approaches are possible to estimate λ numerically depending on whether the divergence between the fluid parcels is allowed to increase until it attains a given distance threshold or only during a given amount of time; resulting in the so called finite size and finite time Lyapunov exponents (*FSLE* and *FTLE*, respectively). Depending on whether divergence and Lyapunov exponents are estimated forward or backward in time, attracting or repelling *LCSs* can be identified.

In order to assess the potential effect of the presence of *LCSs* on the strength of anchovy recruitment, we derived a time series of maps of finite time Lyapunov exponents (*FTLEs*) for the period 1993–2011 based on satellite altimetry data available since October 1992 (figure 4.A.3). We used the reference series of weekly absolute geostrophic velocity components maps produced by *Ssalto/Duacs* and distributed by *Aviso* (www.aviso.altimetry.fr), with support from *CNES* (Centre National d’Etudes Spatiales). The reference series is obtained by merging data from various missions (Topex/Poseidon, Jason-1, European Remote

Sensing satellites [ERS 1 and 2], and Envisat) using the methods developed by Le Traon et al. [1998]. Weekly *LCSs* maps were calculated using methods similar to Shadden et al. [2005]. Weekly velocity 0.25° maps were interpolated to a six-hourly, 0.015° grid using space-time cubic interpolation (five weekly maps contributed to each time point). For each pixel location, the trajectory of its four nearest neighbors ($\delta_0 = 0.015^\circ \approx 1.4$ km) was integrated using six hourly, fourth-order Runge-Kutta steps for a total integration time of $t = 60$ days. The maximum relative increase in great-circle distances between the trajectories of the neighbors was then used to estimate the *FTLE*. The double gradient of the *FTLE* fields was then used to delimit *LCSs* using an arbitrary threshold ($\nabla^2 \lambda > 0.001 \times 10^{-6}$ day $^{-1}$ m $^{-2}$). Only *FTLE* values estimated for pixel locations 25 km away from the coastline were considered to avoid boundary effects. We also estimated the mean distance of *LCSs* to the coastline and the mean and quartiles of *FTLE* values over different spatial and time domains.

The presence, location and intensity of mesoscale features during spring and early summer in the Aquitanian shelf (ICES division VIIIb) presented the highest potential to explain changes in the strength of anchovy recruitment. In general, we found a prevalence of negative relationships with the larval survival index except for the distance of *LCSs* to the coastline, that presented a positive correlation with next year recruitment strength. Taken together, this suggest that the presence of mesoscale features and, in general, turbulent flow, either promotes larval drift to unfavorable habitats or instead, that it prevents the stabilization of the water column. The best relationships involved the 75th percentile of the field of attracting *FTLE* ($\lambda_{att}^{Q_3}$, s $^{-1}$) over ICES division VIIIb in spring and early summer (Mar–Jul, $r = -0.74$), and was retained for further analysis. A similar but weaker relationship was found for the field of repelling *FTLE*, but for a slightly different period (Mar–Jun, $r = -0.70$). Both indexes presented indeed an high correlation among them ($r = 0.81$), so only $\lambda_{att}^{Q_3}$ over ICES division VIIIb was retained for further analysis.

Turbulence

Wind stirring induces turbulent mixing in the surface ocean that might result at the same time in an increase in feeding opportunities for fish larvae or, in case of strong winds, an increased mortality by reduced encounter rates and physical damage [MacKenzie, 2000]. Theoretical studies predict a dome shaped relationship between feeding success and turbulence [Rothschild and Osborn, 1988; MacKenzie et al., 1994]. Thus, if the range of environmental conditions is wide enough and survival depends on feeding efficiency, we might expect this dome shaped relationship between turbulence and anchovy survival. In the case of a net detrimental effect of turbulence, we might instead expect a negative correlation.

To assess whether any of these two possibilities is applicable to anchovy larvae in the Bay of Biscay, we estimated an index of turbulent mixing (v [W m $^{-2}$]) based on the rate of wind work on the ocean surface [Simpson and Sharples, 2012];

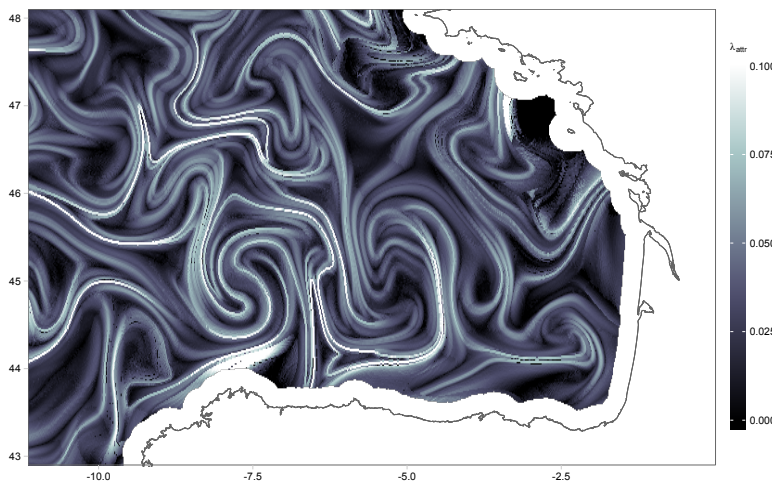


Figure 4.A.3: Example map of the field of attracting finite size Lyapunov exponents (λ_{attr}) in the Bay of Biscay in May 18th, 1998.

$$v = \vec{\tau} \cdot \vec{u}_s \approx \gamma_s (\vec{\tau} \cdot \vec{w}) \quad (4.14)$$

where $\vec{\tau}$ is wind stress (see equation 4.9 above) and \vec{u}_s ($[\text{m s}^{-1}]$) is the speed of the sea surface current induced by the wind (and aligned with it), that can be further approximated to be a constant fraction of wind speed, $\vec{u}_s = \gamma_s \vec{w}$, with $\gamma_s \approx 0.02$. This flux of turbulent kinetic energy was estimated based on six-hourly, Level 3 wind speed [m s^{-1}] maps of the Cross-Calibrated Multi-Platform Ocean Surface Wind Velocity product (CCMP, Atlas et al. 2011, available at [PO.DAAC, podaac.jpl.nasa.gov](http://podaac.jpl.nasa.gov)). Data for each year were later averaged for different time periods and spatial domains. As other wind derived indexes, time series of turbulence presented a positive trend in the Bay of Biscay.

Previous studies in the area have found a weak negative relationship between mean annual turbulence in the southeastern Bay of Biscay and the abundance of recruits in the next year (Borja et al. [2008] report a linear product moment correlation of $r = -0.21$). When compared with the larval survival index, mean turbulence in different time periods and areas within the Bay of Biscay presented in general a detrimental effect in recruitment. We found no evidence of a possible dome shape relationship (*i.e.* poor improvement in model fit when adding a second order term, beyond no visual indication of such a relationship). The correlation was stronger for summer when turbulence values were averaged over integration domains covering the eastern Bay of Biscay (*e.g.* for July, $r < -0.60$ for the Southeastern Bay, ICES divisions VIIIa, b or their combination, and even for the Bay of Biscay as defined by IHO). Turbulence during July in ICES division VIIIa,b presented the best correlation ($r = -0.64$) and was retained for further analysis.

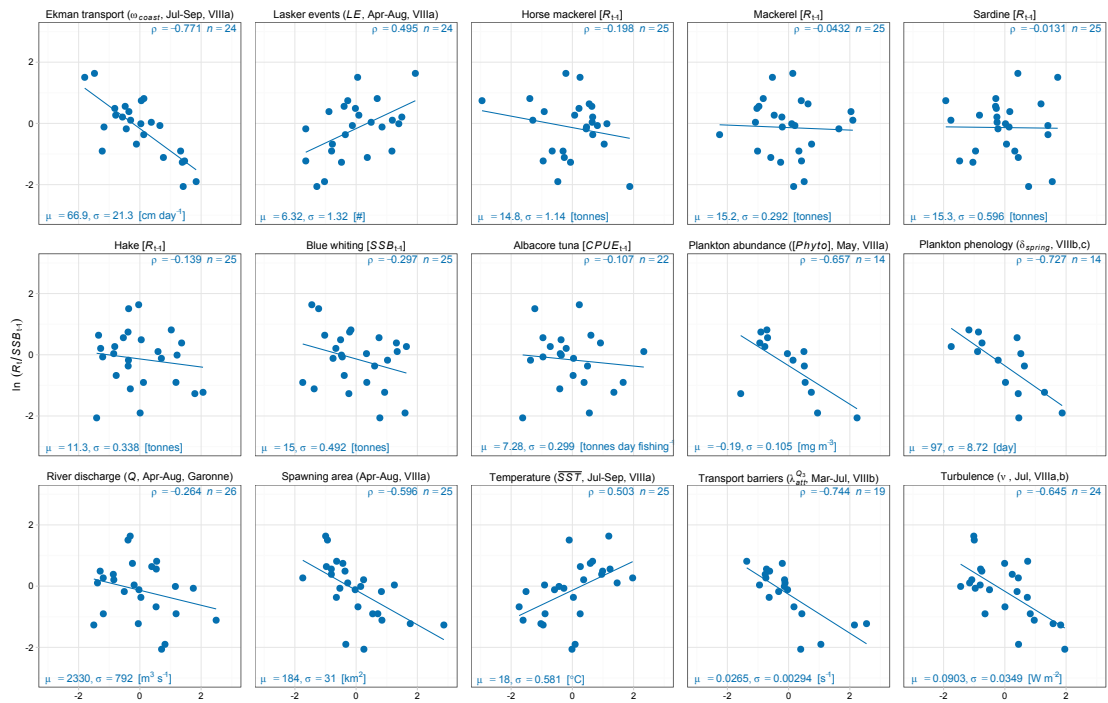


Figure 4.A.4: Relationship between selected environmental indexes and anchovy larval survival. The title of each panel details the corresponding covariate, as well as the temporal and spatial domains of integration that resulted in the best correlation with the larval survival index (p , upper right corner; n indicates sample size). A linear regression line is also included in each panel as a guide. Environmental covariates have been standardized to mean zero and unit standard deviation. The actual mean (μ) and standard deviation (σ) of each covariate is detailed in the lower left corner along with their units. Data for the abundance of natural enemies and plankton abundance was log transformed (\log_{10}). R_{t-1} and SSB_{t-1} are recruit and spawning biomass, respectively. All indexes were correlated with larval survival with a lag of one year (an environmental effect during year t results in recruitment success or failure in year $t + 1$).

Summary

A number of competing and complementary hypotheses involving external environmental forcing can explain fluctuations in fish recruitment (table 4.1). These fluctuations might result as well from density dependent regulatory mechanisms internal to the population. In the main text, we assess the potential ability of both types of mechanisms to explain the recent dynamics of European anchovy in the Bay of Biscay using a nonlinear, age structured population model. Before that, we selected *a priori* a subset of environmental indexes corresponding to different hypothesis about the success of anchovy recruitment (table 4.2; see previous sections for the detailed derivation of different indexes). The selection of the set of candidate indexes was based on their ability to explain changes in an index of anchovy larval survival derived from stock assessment estimates of recruitment and spawning stock biomass (figure 4.A.2, ICES [2012]).

The larval survival index assumes that potential recruitment can be described by a constant productivity model. In this way, any relationship found between the larval survival index and environmental indexes should be interpreted cautiously, given that the poten-

tially competing effect of density dependence is ignored. We nevertheless employed simple linear correlation coefficients and other exploratory tools to select the best index within each of the eight families of indexes considered (see table 4.2). The strength of the relationship with the recruitment index depended critically on the spatial and/or temporal domain selected to integrate the values of environmental indexes (*e.g.* for summer coastal upwelling in ICES divisions VIIIa and VIIIb correlation declines from $r = -0.77$ to -0.10). Differences in strength among integration domains as well as a discordance in the sign of a relationship were considered valuable cues in order to assess whether or not an environmental effect matched the arguments posed by a given hypothesis. We also considered the correlation between indexes in order to identify potential redundancies or indirect effects.

Environmental indexes related to coastal upwelling, transport barriers, turbulence, and plankton abundance and phenology, clearly outperformed indexes related to natural enemies and river discharge (figure 4.A.4, check also the last column in figure 4.A.5). Indexes like the area available for spawning, temperature conditions during the larval period or the number of Lasker events presented also a high correlation with larval survival. According to previous studies but in contrast to the recently proposed importance of offshore habitats for anchovy recruitment, indexes integrated over shelf areas clearly outperformed values integrated over open waters in all cases. Indeed, some of the relationships found suggests instead a detrimental effect of larval drift to open waters (*e.g.* summer coastal upwelling).

The sign of almost all the correlations matched the predictions of different hypotheses except for the negative correlation coefficients found for the area available for spawning and phytoplankton abundance and, to a less extent, the also negative correlation between survival and transport barriers. All these variables are expected to present a positive relationship with anchovy recruitment mediated by a direct enhancement of larval survival either by widening the opportunity of matching suitable conditions (*e.g.* spawning area) or by improving habitat suitability for anchovy larvae by a direct trophic effect (*e.g.* phytoplankton abundance) or by a combination of mechanisms (*e.g.* transport barriers). Examining the patterns of correlation between the different environmental indexes shed some light on these suspicious relationships.

The area available for spawning presented a strong positive correlation with summer coastal upwelling in the Armorican shelf ($r = 0.53$) and with the importance of transport barriers in spring in the Aquitanian shelf ($r = 0.71$). Both of these indexes were anticorrelated with larval survival (figure 4.A.4), suggesting that the negative relationship between potential spawning area and larval survival is spurious. Attending to the match in space and time, a tentative explanation consists in the direct decrease of temperatures over the shelf as a consequence of increased upwelling. The same reasoning can be applied to some extent to mean temperature (also anticorrelated with upwelling, $r = -0.42$), although in this case the positive relationship with survival is coherent with the expected effect of SST on the duration of the larval period. The case of phytoplankton biomass during May in the Ar-

morican shelf is more elusive. It is positively associated to a delayed timing of the bloom in the Aquitanian shelf and to increased summer coastal upwelling ($r = 0.48$ and 0.49 , respectively). There is no obvious link between these variables beyond the association among the timing of the bloom in Armorican and Aquitanian shelves ($r = 0.45$), given that the course of time overrides upwelling as a candidate mechanism. This might indicate again a spurious correlation; *i.e.* a delayed bloom in the south implies a delayed peak in the north. Both potential spawning area and phytoplankton abundance were regarded as spurious and were excluded from the second phase of our analysis.

Finally, in the case of the strength of attracting transport barriers in early spring over the Aquitanian shelf, we found again a great correlation with other indexes, especially coastal upwelling and spawning area ($r = 0.69$ and 0.71). Nevertheless, we found more plausible that this index reflects slower currents and calmer conditions over anchovy spawning grounds, an argument supported to some extent by the high association with bloom timing ($r = 0.60$). Considering this interpretation and the promising relationship with larval survival, we retained this index for further analysis. This lead us to the problem of our potential inability to distinguish between the effect of the variables presenting a high correlation with larval survival. Indeed, the top five indexes were highly correlated among them ($|r| > 0.55$), and thus it is difficult if not impossible to determine whether they reflect a direct effect on anchovy survival or an indirect relationship with a third variable. The location and timing of these effects help to identify at least two groups of indexes that reflect; (*i*) an enhancement of larval survival when anchovy spawning in spring match calm conditions over the Aquitanian shelf (transport barriers and the timing of the bloom), or (*ii*) a negative effect of strong winds during summer in the Armorican shelf (coastal upwelling, turbulence, mean temperature and Lasker events). Within these two groups, some indexes can explain more than half of the variance in the anchovy survival index, although we must assess whether these effects prevail when density dependent effects are taken into account.

	Lasker events	Horse mackerel	Mackerel	Sardine	Hake	Blue whiting	Albacore tuna	Plankton abundance	Plankton phenology	River discharge	Spawning area	Temperature	Transport barriers	Turbulence	Larval Survival Index
Ekman transport	-0.55	-0.04	0.11	-0.10	0.21	0.42	0.20	0.48	0.74	0.45	0.53	-0.42	0.69	0.67	-0.77
Lasker events	-0.02	-0.25	-0.00	-0.07	-0.57	0.10	-0.34	-0.52	-0.14	-0.24	0.36	-0.43	-0.67	0.49	
Horse mackerel	-0.25	0.55	-0.45	-0.11	-0.75	0.42	0.36	0.21	0.03	-0.26	-0.08	-0.06	-0.10	-0.20	
Mackerel	-0.26	0.19	0.34	0.33	0.08	-0.20	-0.08	0.01	-0.03	0.22	0.01	-0.04			
Sardine	-0.44	-0.28	-0.43	0.41	0.46	0.38	-0.35	-0.11	-0.19	-0.12	-0.01				
Hake	0.14	0.61	-0.31	0.07	-0.17	0.42	-0.11	0.46	0.26	-0.14					
Blue whiting	0.18	0.35	0.05	-0.15	-0.05	0.21	0.05	0.35	-0.30						
Albacore tuna	-0.02	0.02	-0.18	0.14	0.12	0.37	0.05	-0.11							
Plankton abundance	0.49	0.52	0.04	-0.24	0.21	0.24	-0.66								
Plankton phenology	0.44	0.49	-0.57	0.60	0.28	-0.73									
River discharge	-0.02	-0.45	0.01	0.13	-0.26										
Spawning area	-0.70	0.71	0.44	-0.60											
Temperature	-0.47	-0.33	0.50												
Transport barriers	0.53	-0.74													
Turbulence	-0.64														

Figure 4.A.5: Correlation matrix between selected environmental indexes and anchovy larval survival. Data for the abundance of natural enemies and plankton abundance was log transformed (\log_{10}). We used previous year recruitment biomass in all cases except for blue whiting, in which spawning biomass presented a better relationship with anchovy survival. Environmental indexes were correlated with larval survival with a lag of one year (last column). See the supporting text in the section Ancillary data or figure 4.A.4 for further details.

4.B Model fitting algorithms

As outlined in the main text, parameter estimation involved two sequential steps by conditioning alternately on estimates of model parameters and on estimates of the state process [West and Harrison, 1997]. Table 4.B.1 provides a general outline of the fitting procedure, while Table 4.B.2 details prior distributions and hyperparameters. The model was fitted under a Bayesian framework using Markov Chain Monte Carlo simulation methods (MCMC, Robert and Casella [2004]; Gelman et al. [2004]). Model fit began with randomly selected initial values and involved a total of 30000 iterations, with a burn-in of 20000 iterations that were discarded. The last 10000 samples were thinned to retrieve 1000 realizations of the estimated posterior distribution of states and parameters. This posterior sample was used to summarize the distribution of model unknowns and to project estimation uncertainty to model based estimates. Both in the estimation of model parameters and of the state process, the potential range of estimates was conditioned by observed catches to avoid nonsensical solutions. The model and fitting algorithms were coded in C# 4.5 taking advantage of par-

Table 4.B.1: Outline of model fitting process. See Material and Methods in the main text and, especially, the section Model fitting algorithms here in the Appendix for further details and references.

Single MCMC iteration of state and model parameters updating steps
<i>Particle MCMC sample of states</i>
Forward Sequential Importance Resampling (SIR)
Do: Generate $n = 5000$ particles from $x_{0,a}$ prior distribution.
Calculate normalized particle weights, $\omega_0 \propto p(\mathbf{x}_0)p(\mathbf{y}_0 \mathbf{x}_0)$, and effective sample size (<i>ESS</i>).
Resample if <i>ESS</i> < 0.8, reset weights.
For: $t = 1 \dots T$:
Propagate states from previous step, \mathbf{x}_{t-1} , using equation 4.5.
Update normalized particle weights, $\omega_t \propto \omega_{t-1}p(\mathbf{y}_t \mathbf{x}_t)$, and estimate effective sample size (<i>ESS</i>).
Resample if <i>ESS</i> < 0.8, reset weights.
Backward Simulation Smoother (BSS)
For: $t = T \dots 1$:
Sample last year states, \mathbf{x}_t , based on previous weights, ω_t .
Project states from the previous year, \mathbf{x}_{t-1} , to the current one using equation 4.5.
Update weights for the previous year, $\omega_{t-1} \propto \omega_t p(\mathbf{x}_t \mathbf{x}_{t-1})$.
<i>Model parameters</i>
Observation equation
For: $k = acst, depm$:
Update detectabilities, q_k , using normal-normal steps.
Update measurement variances, τ_k^2 , using a scaled inverse- χ^2 .
Process equation
Do: Update the parameters of the Deriso-Schnute curve (equation 4.3) using the adaptive importance sampling Population Monte Carlo (PMC) algorithm:
Do: Generate $n = 50000$ particles from $1/\beta \sim U(50 \times 10^3, 90 \times 10^3)$ and $\gamma \sim U(-5, 2)$.
Calculate importance weights, $\omega_0 \propto \prod_{t=0}^T p(\beta, \gamma)p(\mathbf{y}_t \mathbf{x}_t, \beta, \gamma)$, to sample an initial population of $n = 5000$ particles.
For: $t = 1 \dots 15$:
Update the importance function (a nine component mixture of two-dimensional Student t distributions) based on the previous sample and its weights.
Generate a new sample from the updated importance function and update importance weights.
Do: Update the physiological mortality rate, m , using an adaptive Hastings-Metropolis step.
Do: Update the recruitment productivity parameter, α' , and the strength of the effect of the environment on recruitment, η , using a normal linear model. If necessary, update missing values of the environmental covariate, z_t , using estimates of α' and η by inverting equation 4.4.
Do: Update independently the process variance for each age class, σ_a^2 , using a scaled inverse- χ^2 .

allel and numerical math libraries [Rüegg and Gael, 2014; Toub, 2010]. Model output was processed in R 3.02 [R Core Team, 2013] using several extra packages².

Estimates of the state process were updated using a sequential Monte Carlo algorithm (SMC, also called particle filters; see Doucet et al. [2001]; Kantas et al. [2009]; Andrieu et al. [2010]) involving a forward filtering step using sequential importance resampling

² Cairo [Urbanek and Horner, 2013], corrplot [Wei, 2013], data.table [Dowle et al., 2014], fields [Nychka et al., 2013], ggplot2 [Wickham, 2009], gtable [Wickham, 2012a], maps [Brownrigg, 2013], maptools [Bivand and Lewin-Koh, 2013], ncdf [Pierce, 2011], plyr [Wickham, 2011], RColorBrewer [Neuwirth, 2011], rgdal [Bivand et al., 2013], scales [Wickham, 2012b], sp [Pebesma and Bivand, 2005; Bivand et al., 2003] and spam [Furrer and Sain, 2010].

(SIR, Gordon et al. [1993]) and a backward simulation step using Godsill et al.'s [2004] backward simulation smoother (BSS). We used a population of 5000 particles that were regenerated using bootstrap sampling based on the weights of each particle trajectory. This regeneration step prevented sample degeneracy and was implemented when the estimated effective sample size dropped below an 80%. The initial particle distribution (*i.e.* spawning biomass at age in the first simulation year, $t = 0 \equiv 1987$) was sampled uniformly between 10 and 40×10^3 tonnes (range based on, but widely exceeding available observations).

Model parameters were estimated conditional on estimates of the state process within a Gibbs step (*i.e.* conditioning sequentially on the values of other parameters). The estimation of the recruitment limitation (β) and optimality (γ) parameters of the Deriso-Schnute curve was complicated by the inherent nonlinearity of this component of the model. This nonlinear character might delay or even prevent convergence when using standard iterative MCMC algorithms, that can become easily trapped in local modes. To surpass this limitation, we employed an adaptive importance sampling scheme called Population Monte Carlo (PMC, Cappé et al. [2008]; Wraith et al. [2009]). As part of each updating step, PMC was run up to complete 15 iterations, that began with a grid search using 50000 candidate parameter sets used to seed a population of 10000 particles (candidates were sampled uniformly for $1/\beta \in [50 \times 10^3, 90 \times 10^3]$ and $\gamma \in [-5, 2]$). In the following iterations, particles were weighted with respect to their likelihood to update the importance function, that was used in turn to generate new particles. The candidate importance function was a mixture distribution initially composed by nine multivariate Student t components with three degrees of freedom (see Cappé et al. [2008]; Wraith et al. [2009]). Redundant components of this initial mixture were pruned based on their relative contribution to the proposal distribution (weight less than 0.002). PMC updates were rejected when the perplexity dropped below 0.75.

The physiological mortality rate (m) was updated using an adaptive Metropolis-Hastings step [Haario et al., 2001, 2005; Peters et al., 2010]. Metropolis proposals were generated in this way using a truncated normal distribution (*i.e.* $m > 0$) centered on the previous value of the parameter. The standard deviation of the proposal was tuned after each step to match that of values accepted up to the current step but augmented by a factor of 2.38 (see Roberts and Rosenthal [2009]). A minimum scale of 0.01 was set to ensure scale positiveness. Ten simple Metropolis steps with a fixed proposal scale of 0.1 served as the burn in period. The rest of the parameters were estimated easily using conjugate Gibbs steps by conditioning on data, estimates of the state process and remainder model parameters [Gelman et al., 2004; Hoff, 2009].

The recruitment productivity parameter (α') and the strength of the environmental effect on recruitment (η) were estimated together by reordering equation 4.4 to yield a simple linear regression on spawning biomass after log transformation. In this regression, $\log \alpha'$ is the intercept and η is the slope. Both estimates were later used to impute values of

Table 4.B.2: Model parameters and prior distributions used to fit equation 4.1 to survey data. See Material and Methods for further details.

Parameter [units]	Prior distribution	Hyperparameters	Median [P_5, P_{95}]
<i>State equation</i>			
Initial spawning stock biomass [10^6 kg]	$x_{0,a} \sim U(a_{x_{0,a}}, b_{x_{0,a}})$	$a_{x_{0,a}} = 5.0, b_{x_{0,a}} = 80.0$	42.5 [8.8, 76.2]
Instantaneous physiological mortality rate [year^{-1}]	$m \sim LN(\mu_m, v_m^2)$	$\mu_m = -0.356, v_m^2 = 1$	0.70 [0.14, 3.62]
Recruitment productivity parameter (at average environmental conditions) [kg of recruit per kg of adult]	$\alpha' \sim LN(\mu_{\alpha'}, v_{\alpha'}^2)$	$\mu_{\alpha'} = 1.4, v_{\alpha'}^2 = 1.5$	4.0 [0.5, 30.0]
Recruitment optimality parameter [1/kg of adult]	$1/\beta \sim LN(\mu_\beta, v_\beta^2)$	$\mu_\beta = 11.0, v_\beta^2 = 0.25$	6.0×10^4 [$2.6 \times 10^4, 1.4 \times 10^5$]
Recruitment limitation parameter	$\gamma \sim N(\mu_\gamma, v_\gamma^2)$	$\mu_\gamma = 0, v_\gamma^2 = 100$	0.0 [-16.4, 16.4]
Strength of environmental effect on recruitment	$\eta \sim N(\mu_\eta, v_\eta^2)$	$\mu_\eta = 0, v_\eta^2 = 1$	0.0 [-1.6, 1.6]
Missing values of the environmental covariate	$zm_t \sim N(\mu_{zm_t}, v_{zm_t}^2)$	$\mu_{zm_t} = 0, v_{zm_t}^2 = 1.0$	0.0 [-1.6, 1.6]
Process noise variance	$\sigma_a^2 \sim U(a_{\sigma_a}, b_{\sigma_a})$	$a_{\sigma_a} = 0, b_{\sigma_a} = 100$	50 [5, 95]
<i>Observation equation</i>			
Detectability coefficient	$q_k \sim LN(\mu_{q_k}, v_{q_k}^2)$	$\mu_{q_k} = 0, v_{q_k}^2 = 0.5$	1.0 [0.3, 3.2]
Measurement noise variance	$\tau_k^2 \sim U(a_{\tau_k}, b_{\tau_k})$	$a_{\tau_k} = 0, b_{\tau_k} = 100$	50 [5, 95]

environmental covariates missing data for some years. Each missing year was treated independently assuming a normal prior with mean zero and variance one. This prior was updated by inverting again equation 4.4 to yield the expected value and the variance of the environmental covariate. In case of no environmental effect on recruitment (*i.e.* $\eta = 0$), α' can be updated in a simple Normal-Normal update after log transforming equation 4.4. Process and measurement error variances (σ_a^2 and τ_k^2) were updated directly by sampling from a scaled inverse- χ^2 distribution [Gelman, 2006]. Finally, simple Normal-Normal updates were used for the logarithm of detectability coefficients (q_k , see equation 4.6).

4.C Surrogate analysis of anchovy collapse

As outlined in the main text, posterior parameter estimates were used to conduct an *textitin silico* experiment to assess the probability of collapse of anchovy fishery in the Bay of Biscay under scenarios differing in management practices and environmental variation. The experiment was conducted for models differing in the renewal function implemented and in the consideration or not of structured environmental effects on recruitment. A sample of 1000 simulations of posterior process parameters was used to analyze the impact that would

have had a reduction in fishing pressure on the probability of observing a collapse in 2005. In these simulations, we kept fishing mortality proportional to estimates of fractional fishing mortality derived from observed catches and posterior estimates of the physiological mortality rate (m) and of filtered and smoothed states ($\mathbf{x}_{0:T}$). For each sample realization of posterior process parameters, we simulated a series of surrogate realizations reducing fishing rates by a factor between 0.0 (no change in fishing rates) and 1.0 (no fishing at all; we simulated 200 replicates per posterior sample and fractional reduction in fishing). With this approach, we tried to emulate the actual pattern of fishing pressure experienced by the population, but allowing at the same time for random perturbations in both recruitment and adult survival associated to estimated process noise (*i.e.* σ_1 and σ_{2p}). We further rejected unrealistic simulations that resulted in the nearly extinction of the population or in an exaggerated increase (*i.e.* if any of the two age classes considered dropped below 1.0×10^5 kg or if spawning biomass raised above 1.0×10^9 kg). For each surrogate, we recorded whether total spawning biomass in 2005 was below 20×10^6 kg, a threshold we selected to represent a collapse of the fishery. This approach allowed us to propagate uncertainty derived from the estimation of model parameters to these estimates, as well as to take into account the own stochastic nature of the models.

4.D Supplementary results

To complement the main results presented in the manuscript, we include here full summaries for all the models fitted. table 4.D.1 presents summaries of the posterior distribution of the parameters of the state (4.6) and the process (4.7) equations (see also table 4.B.2 for the definition, units and prior distribution of different parameters). Posterior parameter distributions are also presented in less compact form in figure 4.D.2 (note that the abscissa might change between graphs for parameters η and γ). We also present posterior estimates of the recruitment function for models considering constant productivity or a Deriso-Schnute recruitment function for each of the models fitted (figure 4.D.1). Finally, we include plots of one step ahead predictions for all the models that, in contrast to figure 4.1 in the main text, include projections for each age class.

Table 4.D.1: Summary of the posterior distribution of process and observation model parameters (median and 90% credible intervals; see table 4.B.2 for further details).

Constant productivity	$x_{0,1}$	$x_{0,2p}$	m	η	α'	σ_1	σ_{2p}	q_{depn}	τ_{depn}	q_{ast}	τ_{ast}
Constant environment	36.4	39.7	0.742	—	1.35	1.169	0.535	0.612	0.307	0.863	0.441
Ekman transport	[40.1, 102.1]	[20.1, 73.4]	[0.532, 0.953]	0.671	[1.05, 1.77]	[0.869, 1.632]	[0.365, 0.797]	[0.487, 0.757]	[0.208, 0.436]	[0.680, 1.100]	[0.335, 0.505]
Lasker events	[121, 77.3]	[17.1, 68.5]	[0.455, 0.860]	0.718	[-0.913, -0.282]	[0.68, 1.03]	[0.693, 0.704]	[0.365, 0.751]	[0.212, 0.426]	[0.835, 1.305]	[0.312, 0.554]
Horse mackerel	[121, 104.3]	[17.0, 80.6]	[0.477, 0.929]	0.492	[-0.717, 0.717]	[0.304, 0.709]	[0.77, 1.19]	[0.712, 1.286]	[0.387, 0.810]	[0.546, 0.818]	[0.259, 0.485]
Mackerel	[113, 125.3]	[20.5, 77.9]	[0.531, 0.938]	0.743	[-0.539, -0.032]	[0.92, 1.51]	[0.757, 1.482]	[0.370, 0.782]	[0.469, 0.706]	[0.220, 0.458]	[0.646, 1.020]
Sardine	[116, 126.3]	[20.1, 83.9]	[0.522, 0.928]	0.732	[-0.254, 0.246]	[0.93, 1.50]	[0.828, 1.508]	[0.362, 0.814]	[0.464, 0.716]	[0.224, 0.464]	[0.638, 1.027]
Albacore tuna	[117, 143.6]	[20.6, 83.7]	[0.516, 0.924]	0.731	[-0.158, 0.667]	[0.90, 1.51]	[0.847, 1.551]	[0.369, 0.923]	[0.470, 0.742]	[0.217, 0.465]	[0.642, 1.074]
Hake	[113, 39.0]	[40.6, 40.6]	0.689	0.699	[0.90, 1.51]	[0.847, 1.551]	[0.369, 0.923]	[0.470, 0.742]	[0.217, 0.465]	[0.642, 1.074]	[0.340, 0.559]
Blue whiting ³	[113, 134.9]	[19.5, 80.0]	[0.506, 0.922]	0.742	[-0.224, 0.366]	[0.94, 1.57]	[0.845, 1.529]	[0.364, 0.789]	[0.473, 0.720]	[0.216, 0.458]	[0.650, 1.052]
River discharge	[117, 105.4]	[19.4, 78.4]	[0.540, 0.929]	0.730	[-0.482, 0.058]	[0.90, 1.63]	[0.822, 1.520]	[0.365, 0.796]	[0.479, 0.775]	[0.213, 0.452]	[0.665, 1.117]
Plankton phenology	[10.8, 137.8]	[19.7, 78.5]	[0.534, 0.935]	0.728	[-0.771, 1.061]	[0.91, 1.78]	[0.830, 1.578]	[0.362, 0.800]	[0.482, 0.736]	[0.219, 0.448]	[0.658, 1.055]
River discharge	[14.1, 70.6]	[18.5, 71.7]	[0.486, 0.881]	0.725	[-1.008, 0.592]	[0.63, 0.98]	[0.445, 0.873]	[0.345, 0.788]	[0.582, 0.861]	[0.232, 0.455]	[0.805, 1.231]
Temperature	[119, 118.4]	[19.7, 80.1]	[0.527, 0.932]	0.725	[-0.673, 0.150]	[0.90, 1.59]	[0.790, 1.411]	[0.365, 0.784]	[0.481, 0.734]	[0.214, 0.452]	[0.664, 1.066]
Transport barriers	[124.4, 30.8]	[18.7, 70.5]	[0.528, 0.938]	0.689	[-0.334, 0.078]	[0.80, 1.26]	[0.697, 1.278]	[0.379, 0.803]	[0.515, 0.769]	[0.259, 0.488]	[0.706, 1.083]
Turbulence	[13.0, 35.6]	[17.9, 70.6]	[0.491, 0.882]	0.720	[-0.996, -0.559]	[0.62, 0.95]	[0.497, 0.927]	[0.361, 0.775]	[0.613, 0.921]	[0.232, 0.461]	[0.847, 1.329]
Deriso-Schmitte function	$x_{0,1}$	$x_{0,2p}$	m	η	α'	σ_1	σ_{2p}	q_{depn}	τ_{depn}	q_{ast}	τ_{ast}
Constant environment	30.4	33.6	0.632	—	4.03	34.5	-0.31	1.050	0.558	0.740	0.282
Ekman transport	[10.0, 109.5]	[17.2, 65.6]	[0.427, 0.841]	0.671	[2.67, 6.63]	[16.5, 74.8]	[0.92, 0.33]	[0.815, 1.369]	[0.592, 0.896]	[0.168, 0.411]	[0.833, 1.332]
Lasker events	[29.2, 124.5]	[34.1, 64.8]	0.648	0.671	1.38	38.6	-3.29	0.746	0.528	[0.757, 0.757]	[0.316, 0.411]
Horse mackerel	[33.3, 114.4]	[35.9, 60.5]	[0.452, 0.851]	0.678	[-0.885, -0.482]	[0.88, 2.13]	[0.20, 136.0]	[0.568, 1.020]	[0.367, 0.758]	[0.614, 0.932]	[0.309, 0.545]
Mackerel	[30.2, 114.4]	[18.0, 70.5]	[0.470, 0.874]	0.437	[0.241, 0.644]	[1.19, 2.86]	[20.8, 135.0]	[0.676, 1.127]	[0.392, 0.799]	[0.579, 0.851]	[0.226, 0.477]
Sardine	[33.0, 99.4]	[33.0, 66.6]	[0.427, 0.874]	0.605	2.89	5.615	-0.10	1.012	0.548	0.724	0.293
Hake	[29.9, 103.9]	[34.2, 63.5]	[0.377, 0.839]	0.655	[-0.269, 0.275]	[1.82, 4.76]	[22.7, 143.4]	[-1.35, 1.07]	[0.779, 1.361]	[0.353, 0.771]	[0.563, 0.915]
Blue whiting ³	[30.4, 96.0]	[16.6, 64.3]	[0.422, 0.836]	0.629	[-0.483, 0.012]	[2.33, 5.00]	[21.7, 95.5]	[-0.90, 0.47]	[0.749, 1.316]	[0.375, 0.797]	[0.578, 0.898]
Albacore tuna	[30.4, 99.4]	[17.6, 69.3]	[0.420, 0.838]	0.615	[-0.104, 0.339]	[1.89, 4.20]	[25.4, 123.9]	[-1.26, 0.80]	[0.772, 1.340]	[0.385, 0.802]	[0.567, 0.881]
Deriso-Schmitte function	$x_{0,1}$	$x_{0,2p}$	m	η	α'	σ_1	σ_{2p}	q_{depn}	τ_{depn}	q_{ast}	τ_{ast}
Constant environment	30.4	33.6	0.632	—	4.03	34.5	-0.31	1.050	0.558	0.740	0.282
Ekman transport	[10.0, 109.5]	[17.2, 65.6]	[0.427, 0.841]	0.671	[2.67, 6.63]	[16.5, 74.8]	[0.92, 0.33]	[0.815, 1.369]	[0.592, 0.896]	[0.168, 0.411]	[0.833, 1.332]
Lasker events	[29.2, 124.5]	[34.1, 64.8]	0.648	0.671	1.38	38.6	-3.29	0.746	0.528	[0.757, 0.757]	[0.316, 0.411]
Horse mackerel	[33.3, 114.4]	[35.9, 60.5]	[0.452, 0.851]	0.678	[-0.885, -0.482]	[0.88, 2.13]	[0.20, 136.0]	[0.568, 1.020]	[0.367, 0.758]	[0.614, 0.932]	[0.309, 0.545]
Mackerel	[30.2, 114.4]	[18.0, 70.5]	[0.470, 0.874]	0.437	[0.241, 0.644]	[1.19, 2.86]	[20.8, 135.0]	[0.676, 1.127]	[0.392, 0.799]	[0.579, 0.851]	[0.226, 0.477]
Sardine	[33.0, 99.4]	[33.0, 66.6]	[0.427, 0.874]	0.605	2.89	5.615	-0.10	1.012	0.548	0.724	0.293
Hake	[29.9, 103.9]	[34.2, 63.5]	[0.377, 0.839]	0.655	[-0.269, 0.275]	[1.82, 4.76]	[22.7, 143.4]	[-1.35, 1.07]	[0.779, 1.361]	[0.353, 0.771]	[0.563, 0.915]
Blue whiting ³	[30.4, 96.0]	[16.6, 64.3]	[0.411, 0.838]	0.621	[-0.314, 0.102]	[1.85, 4.11]	[23.2, 14.4]	[-1.75, 0.62]	[0.785, 1.386]	[0.387, 0.789]	[0.575, 0.910]
Albacore tuna	[30.4, 99.4]	[17.3, 66.8]	[0.389, 0.812]	0.617	[-1.669, 0.147]	[2.29, 7.49]	[19.2, 108.9]	[-0.73, 0.16]	[0.741, 1.325]	[0.385, 0.806]	[0.598, 0.900]
Deriso-Schmitte function	$x_{0,1}$	$x_{0,2p}$	m	η	α'	σ_1	σ_{2p}	q_{depn}	τ_{depn}	q_{ast}	τ_{ast}
Constant environment	30.4	33.6	0.632	—	4.03	34.5	-0.31	1.050	0.558	0.740	0.282
Ekman transport	[10.0, 109.5]	[17.2, 65.6]	[0.427, 0.841]	0.671	[2.67, 6.63]	[16.5, 74.8]	[0.92, 0.33]	[0.815, 1.369]	[0.592, 0.896]	[0.168, 0.411]	[0.833, 1.332]
Lasker events	[29.2, 124.5]	[34.1, 64.8]	0.648	0.671	1.38	38.6	-3.29	0.746	0.528	[0.757, 0.757]	[0.316, 0.411]
Horse mackerel	[33.3, 114.4]	[35.9, 60.5]	[0.452, 0.851]	0.678	[-0.885, -0.482]	[0.88, 2.13]	[0.20, 136.0]	[0.568, 1.020]	[0.367, 0.758]	[0.614, 0.932]	[0.309, 0.545]
Mackerel	[30.2, 114.4]	[18.0, 70.5]	[0.470, 0.874]	0.437	[0.241, 0.644]	[1.19, 2.86]	[20.8, 135.0]	[0.676, 1.127]	[0.392, 0.799]	[0.579, 0.851]	[0.226, 0.477]
Sardine	[33.0, 99.4]	[33.0, 66.6]	[0.427, 0.874]	0.605	2.89	5.615	-0.10	1.012	0.548	0.724	0.293
Hake	[29.9, 103.9]	[34.2, 63.5]	[0.377, 0.839]	0.655	[-0.269, 0.275]	[1.82, 4.76]	[22.7, 143.4]	[-1.35, 1.07]	[0.779, 1.361]	[0.353, 0.771]	[0.563, 0.915]
Blue whiting ³	[30.4, 96.0]	[16.6, 64.3]	[0.411, 0.838]	0.621	[-0.314, 0.102]	[1.85, 4.11]	[23.2, 14.4]	[-1.75, 0.62]	[0.785, 1.386]	[0.387, 0.789]	[0.575, 0.910]
Albacore tuna	[30.4, 99.4]	[17.3, 66.8]	[0.389, 0.812]	0.617	[-1.669, 0.147]	[2.29, 7.49]	[19.2, 108.9]	[-0.73, 0.16]	[0.741, 1.325]	[0.385, 0.806]	[0.598, 0.900]
Deriso-Schmitte function	$x_{0,1}$	$x_{0,2p}$	m	η	α'	σ_1	σ_{2p}	q_{depn}	τ_{depn}	q_{ast}	τ_{ast}
Constant environment	30.4	33.6	0.632	—	4.03	34.5	-0.31	1.050	0.558	0.740	0.282
Ekman transport	[10.0, 109.5]	[17.2, 65.6]	[0.427, 0.841]	0.671	[2.67, 6.63]	[16.5, 74.8]	[0.92, 0.33]	[0.815, 1.369]	[0.592, 0.896]	[0.168, 0.411]	[0.833, 1.332]
Lasker events	[29.2, 124.5]	[34.1, 64.8]	0.648	0.671	1.38	38.6	-3.29	0.746	0.528	[0.757, 0.757]	[0.316, 0.411]
Horse mackerel	[33.3, 114.4]	[35.9, 60.5]	[0.452, 0.851]	0.678	[-0.885, -0.482]	[0.88, 2.13]	[0.20, 136.0]	[0.568, 1.020]	[0.367, 0.758]	[0.614, 0.932]	[0.309, 0.545]
Mackerel	[30.2, 114.4]	[18.0, 70.5]	[0.470, 0.874]	0.437	[0.241, 0.644]	[1.19, 2.86]	[20.8, 135.0]	[0.676, 1.127]	[0.392, 0.799]	[0.579, 0.851]	[0.226, 0.477]
Sardine	[33.0, 99.4]	[33.0, 66.6]	[0.427, 0.874]	0.605	2.89	5.615	-0.10	1.012	0.548	0.724	0.293
Hake	[29.9, 103.9]	[34.2, 63.5]	[0.377, 0.839]	0.655	[-0.269, 0.275]	[1.82, 4.76]	[22.7, 143.4]	[-1.35, 1.07]	[0.779, 1.361]	[0.353, 0.771]	[0.563, 0.915]
Blue whiting ³	[30.4, 96.0]	[16.6, 64.3]	[0.411, 0.838]	0.621	[-0.314, 0.102]	[1.85, 4.11]	[23.2, 14.4]	[-1.75, 0.62]	[0.785, 1.386]	[0.387, 0.789]	[0.575, 0.910]
Albacore tuna	[30.4, 99.4]	[17.3, 66.8]	[0.389, 0.812]	0.617	[-1.669, 0.147]	[2.29, 7.49]	[19.2, 108.9]	[-0.73, 0.16]	[0.741, 1.325]	[0.385, 0.806]	[0.598, 0.900]
Deriso-Schmitte function	$x_{0,1}$	$x_{0,2p}$	m	η	α'	σ_1	σ_{2p}	q_{depn}	τ_{depn}	q_{ast}	τ_{ast}
Constant environment	30.4	33.6	0.632	—	4.03	34.5	-0.31	1.050	0.558	0.740	0.282
Ekman transport	[10.0, 109.5]	[17.2, 65.6]	[0.427, 0.841]	0.671	[2.67, 6.63]	[16.5, 74.8]	[0.92, 0.33]	[0.815, 1.369]	[0.592, 0.896]	[0.168, 0.411]	

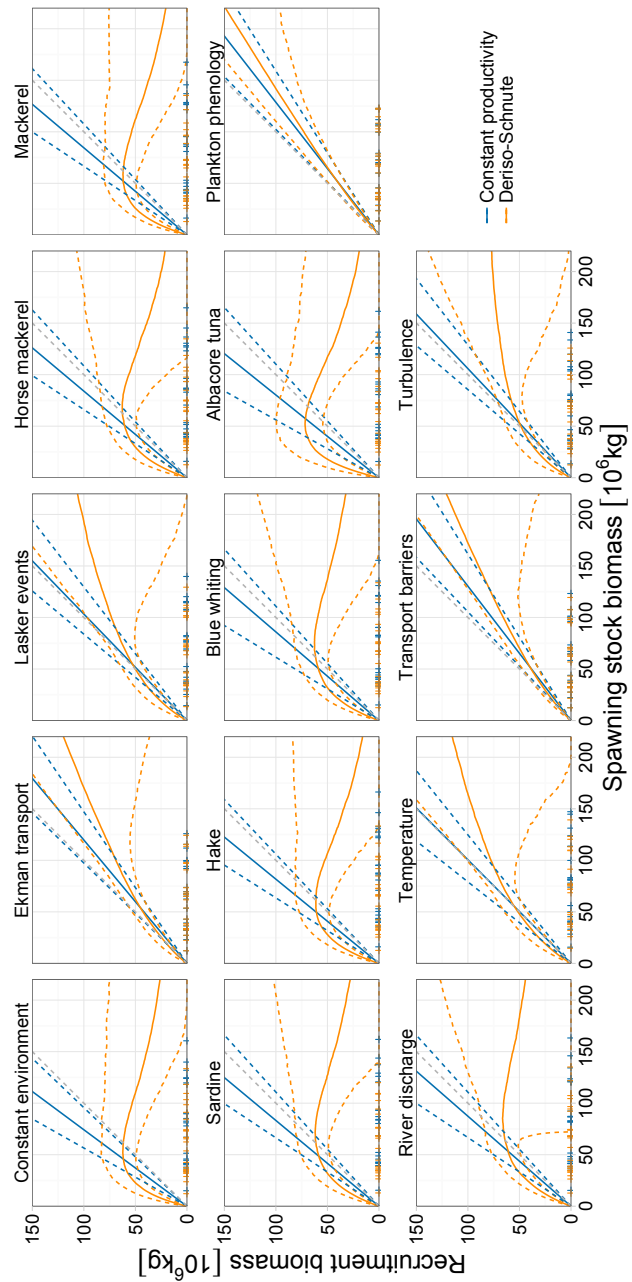


Figure 4.D.1: Posterior estimates of the recruitment function for different model structures (equation 4.3, median and 90% credible intervals). Each panel presents estimates for models with the same environmental forcing but differing in the recruitment function fitted (constant productivity or Deriso-Schnute). Posterior media estimates of spawning stock biomass for each year are included on the abscissa.

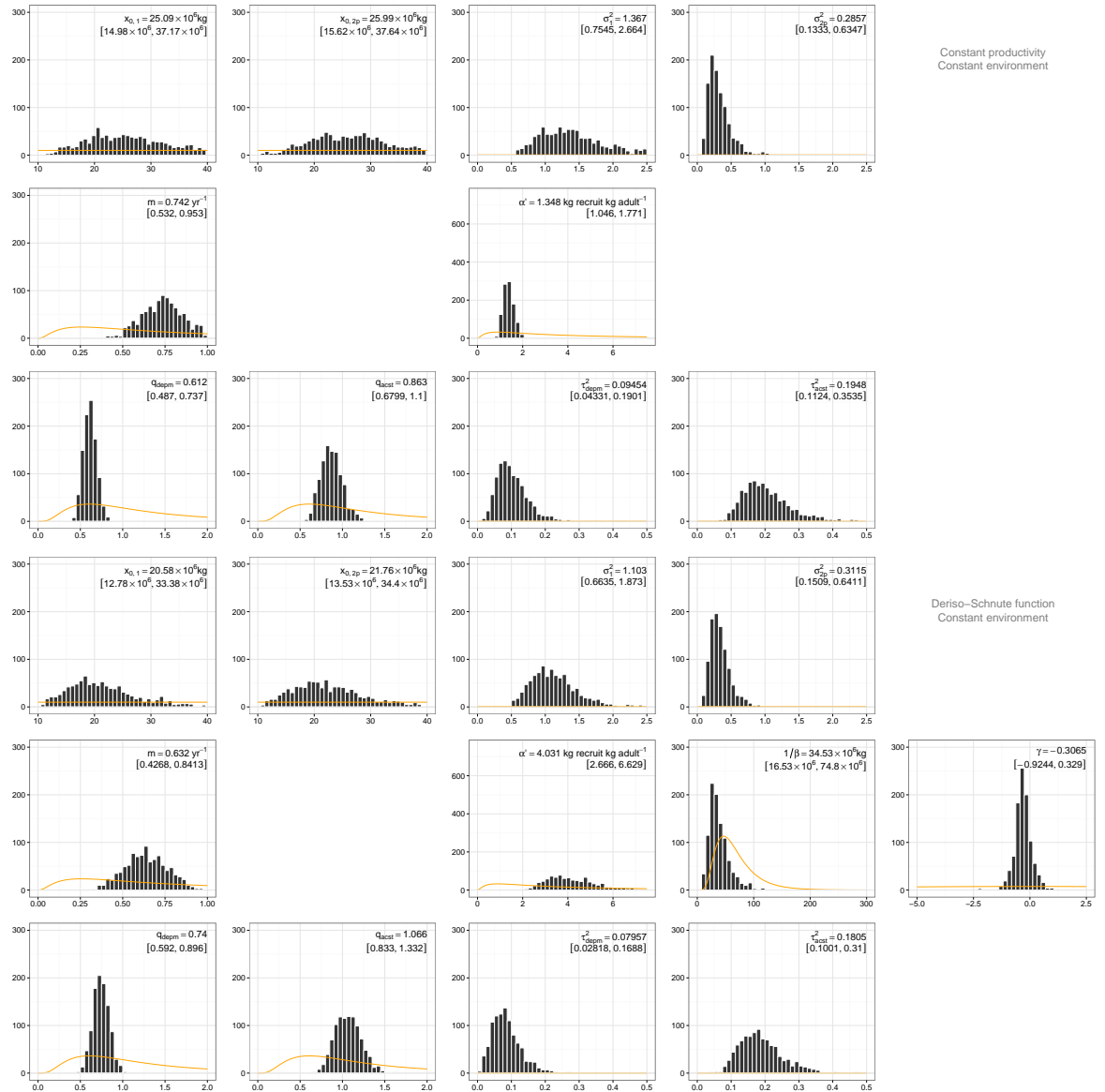


Figure 4.D.2: Posterior estimates for models with varying environmental forcing and renewal function (see also the following pages).

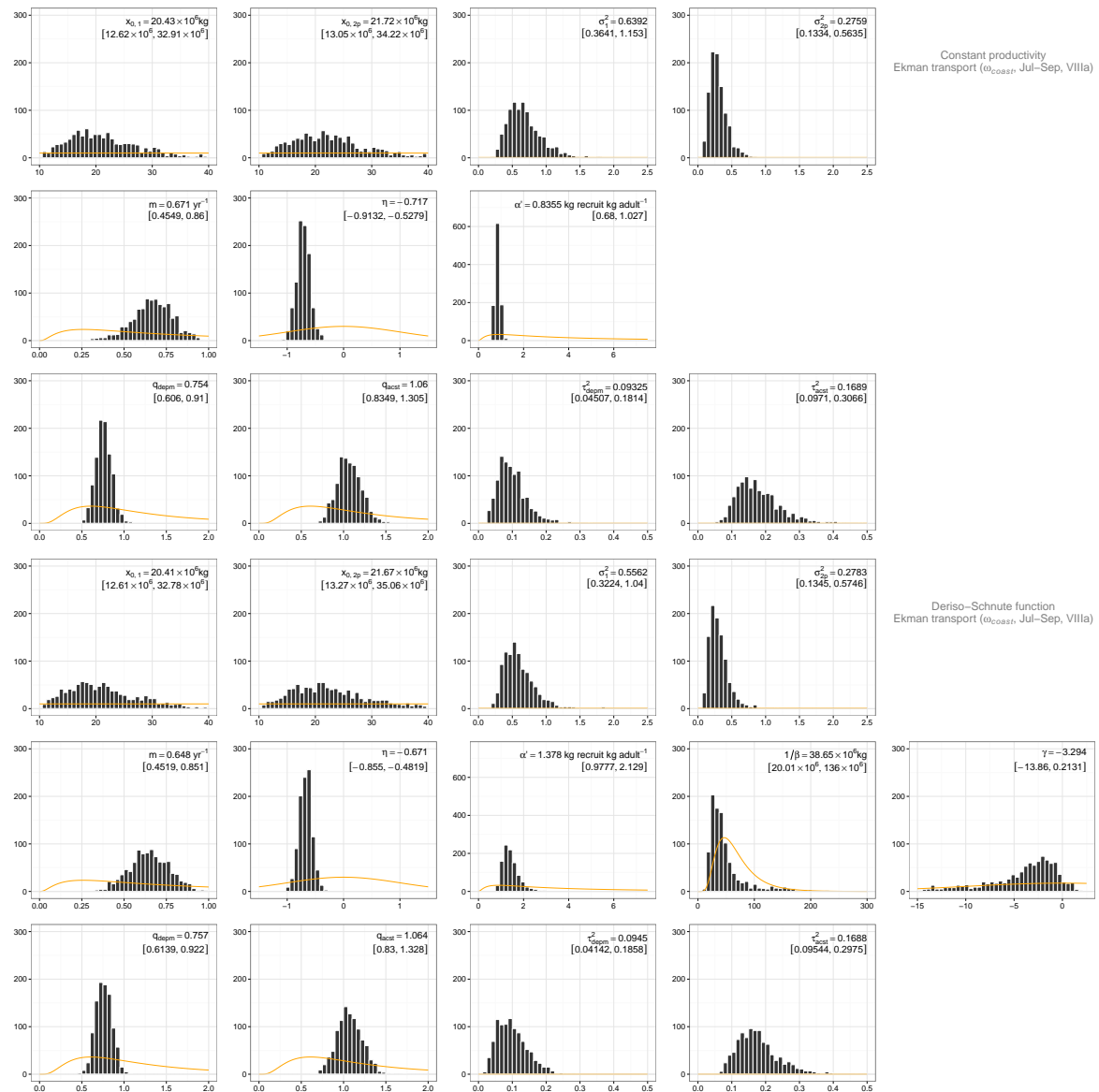


Figure 4.D.1: (Ekman transport).

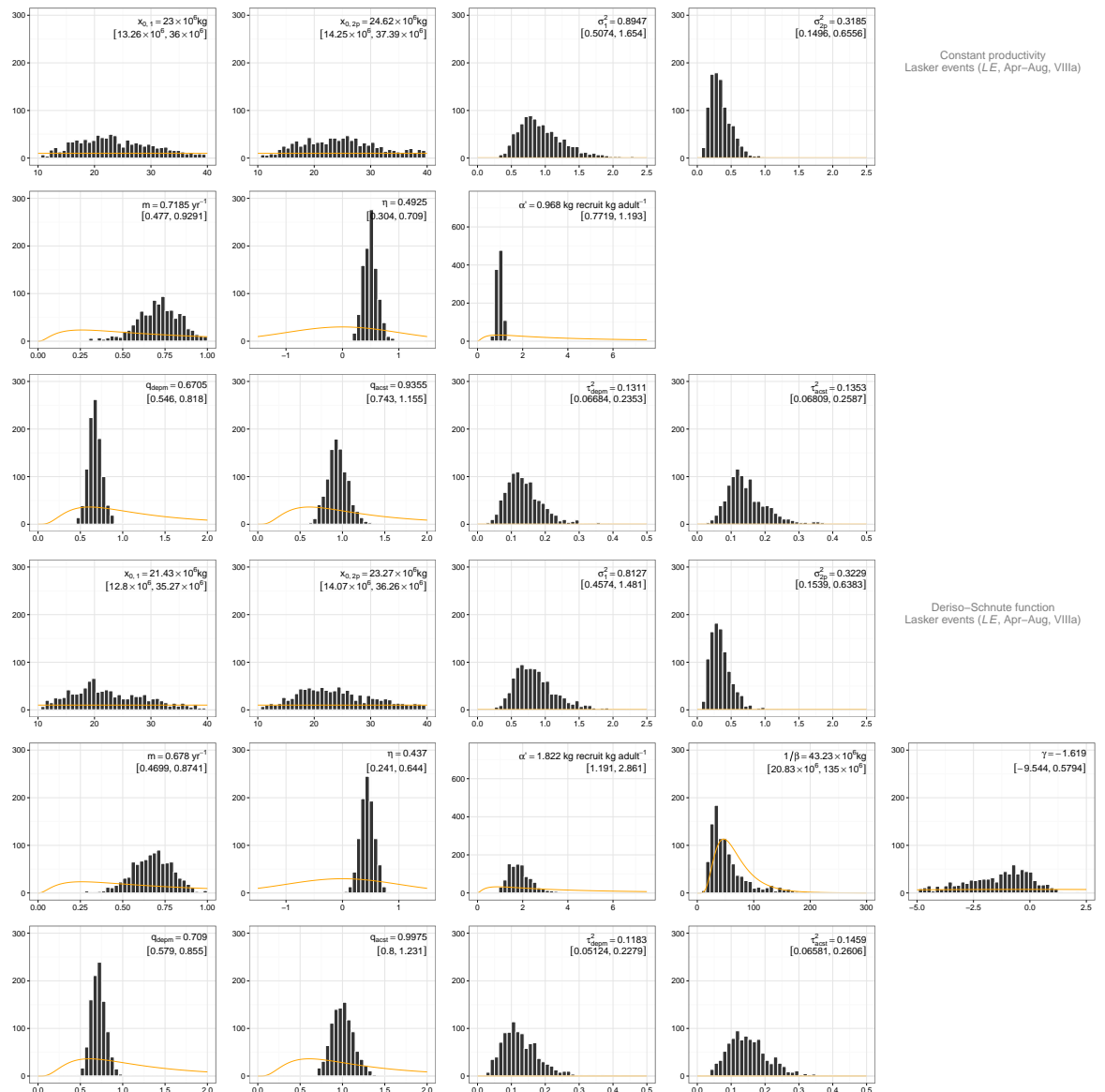


Figure 4.D.0: (Lasker events).

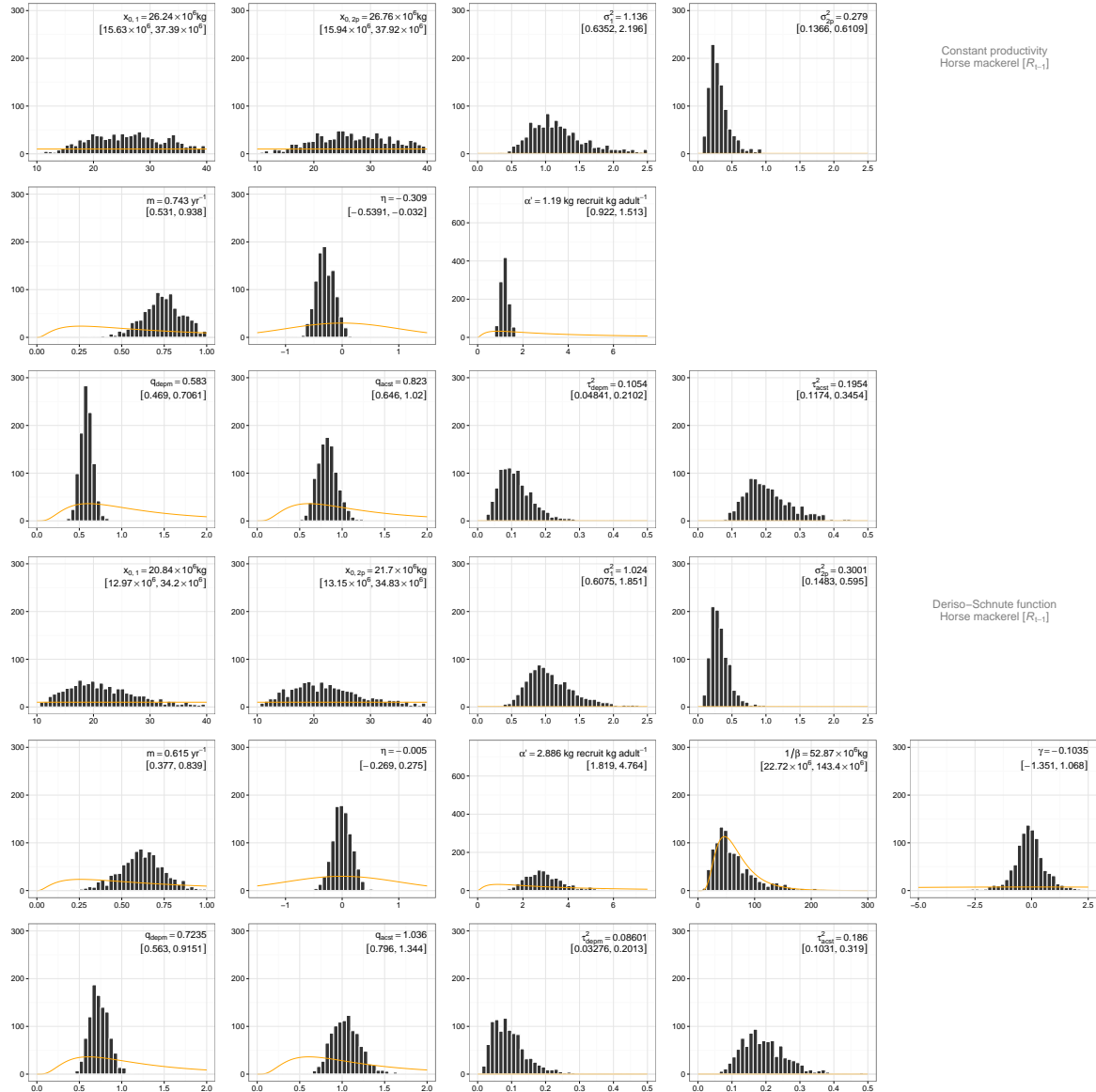


Figure 4.D.-1: (Horse mackerel).

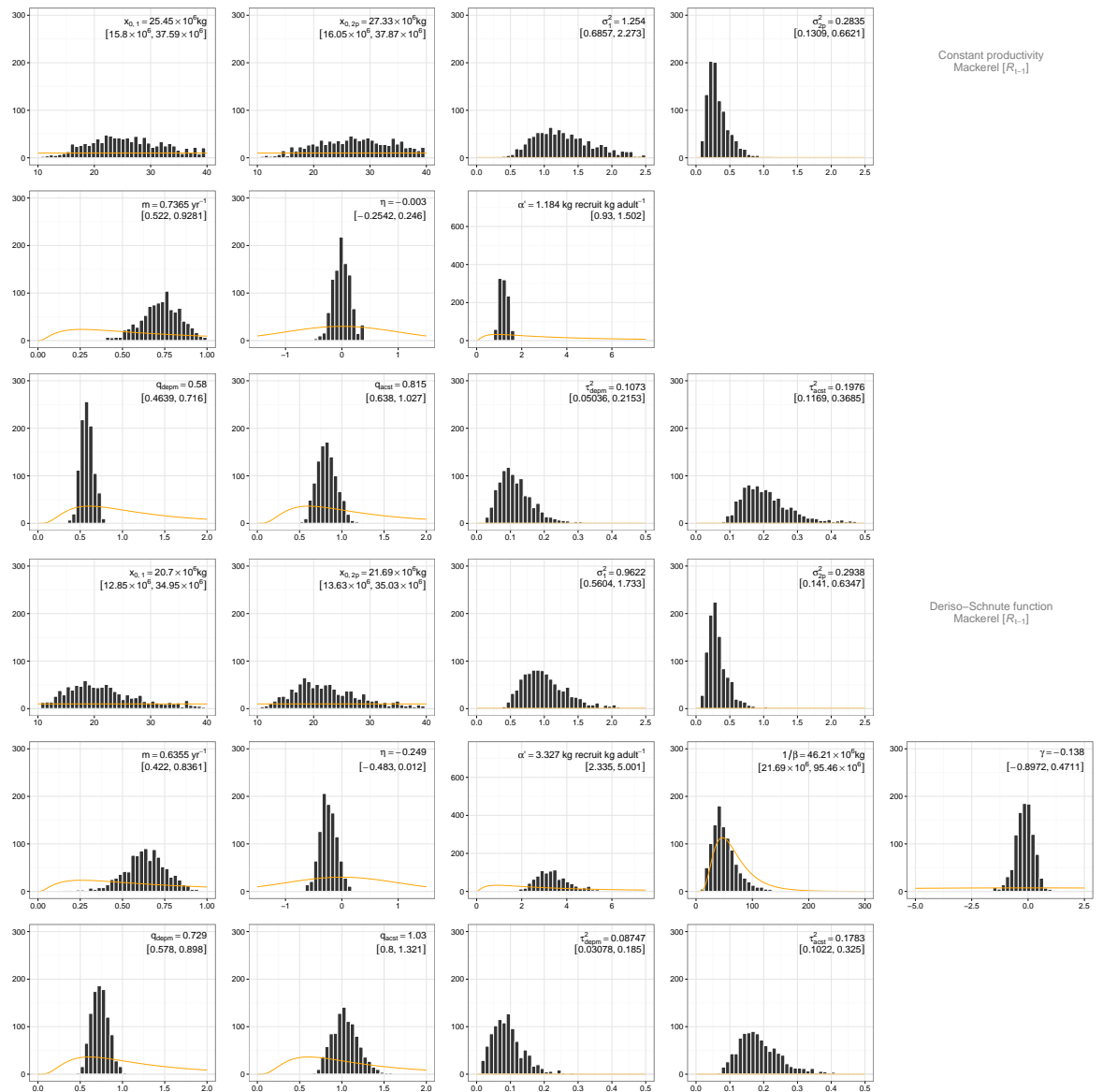


Figure 4.D.-2: (Mackerel).

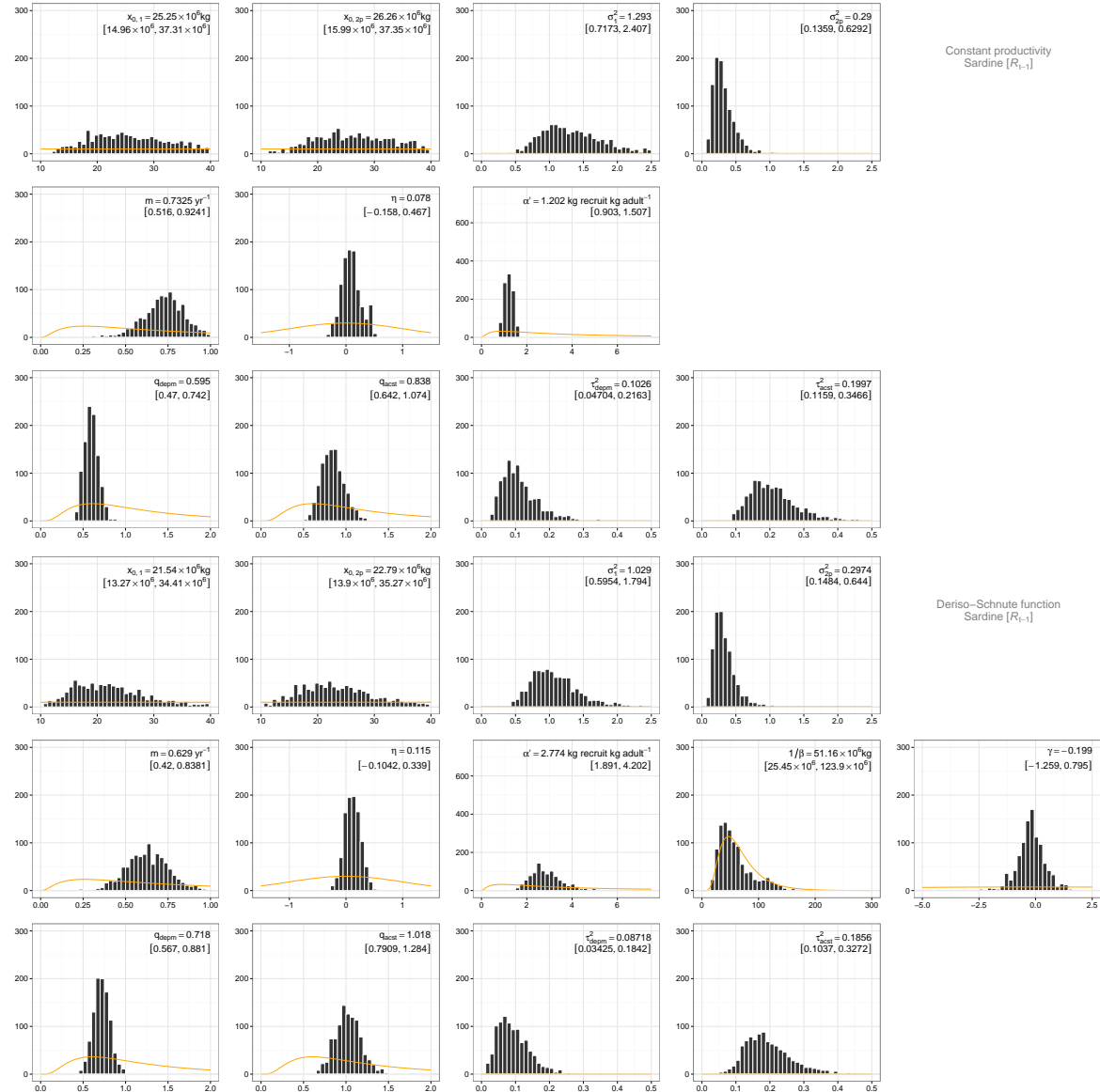


Figure 4.D.-3: (Sardine).

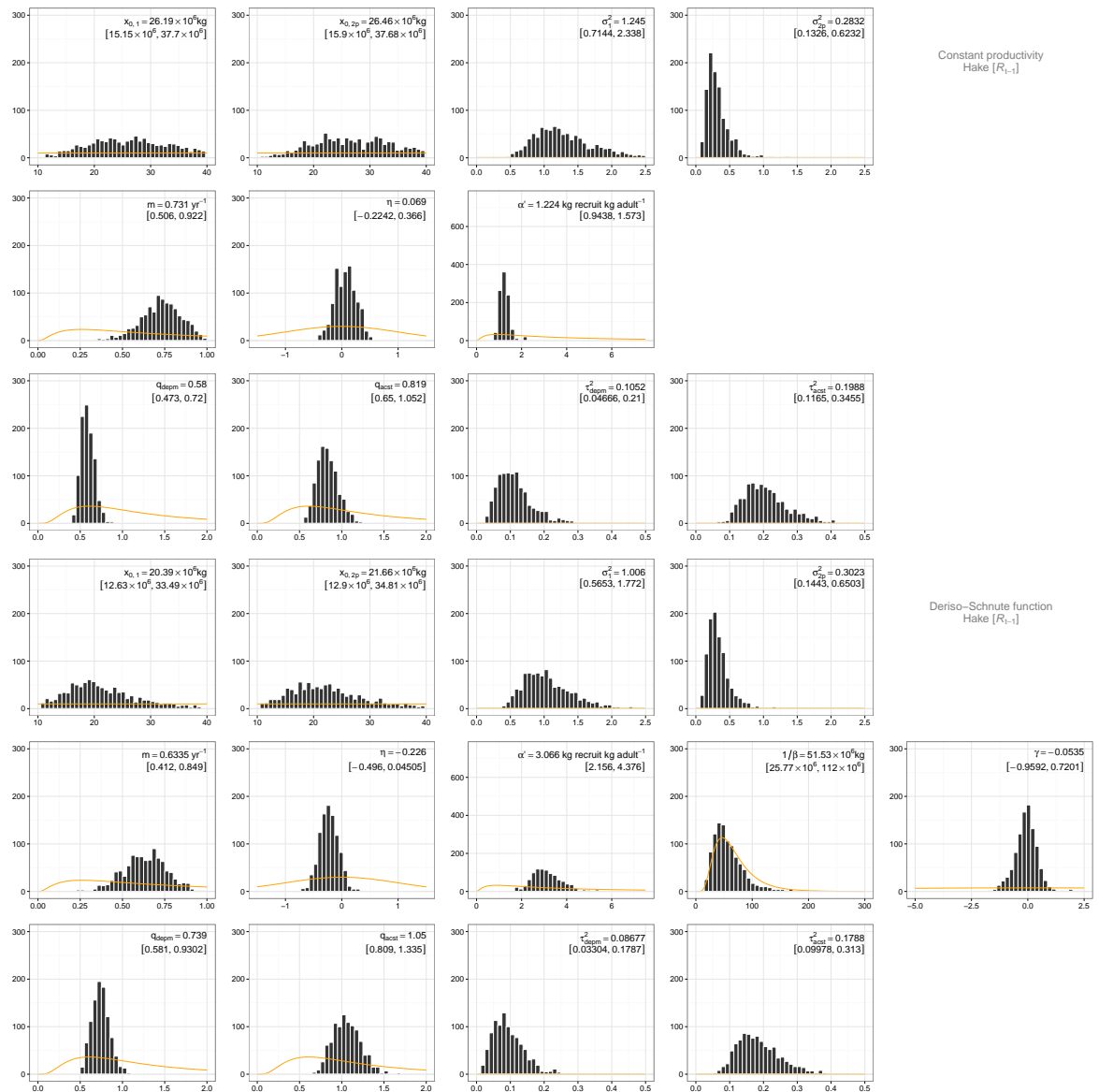


Figure 4.D.-4: (Hake).

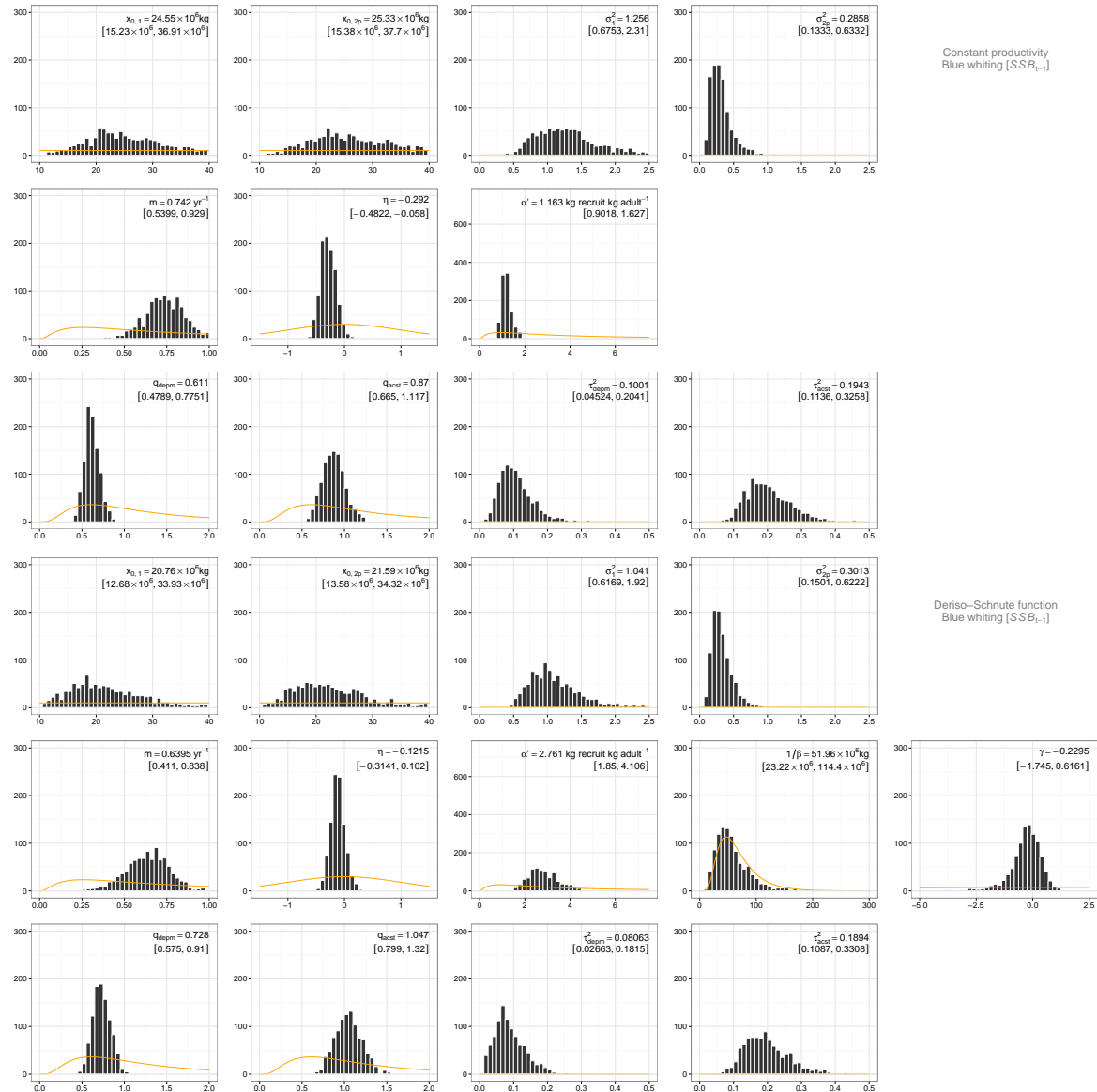


Figure 4.D.-5: (Blue whiting).

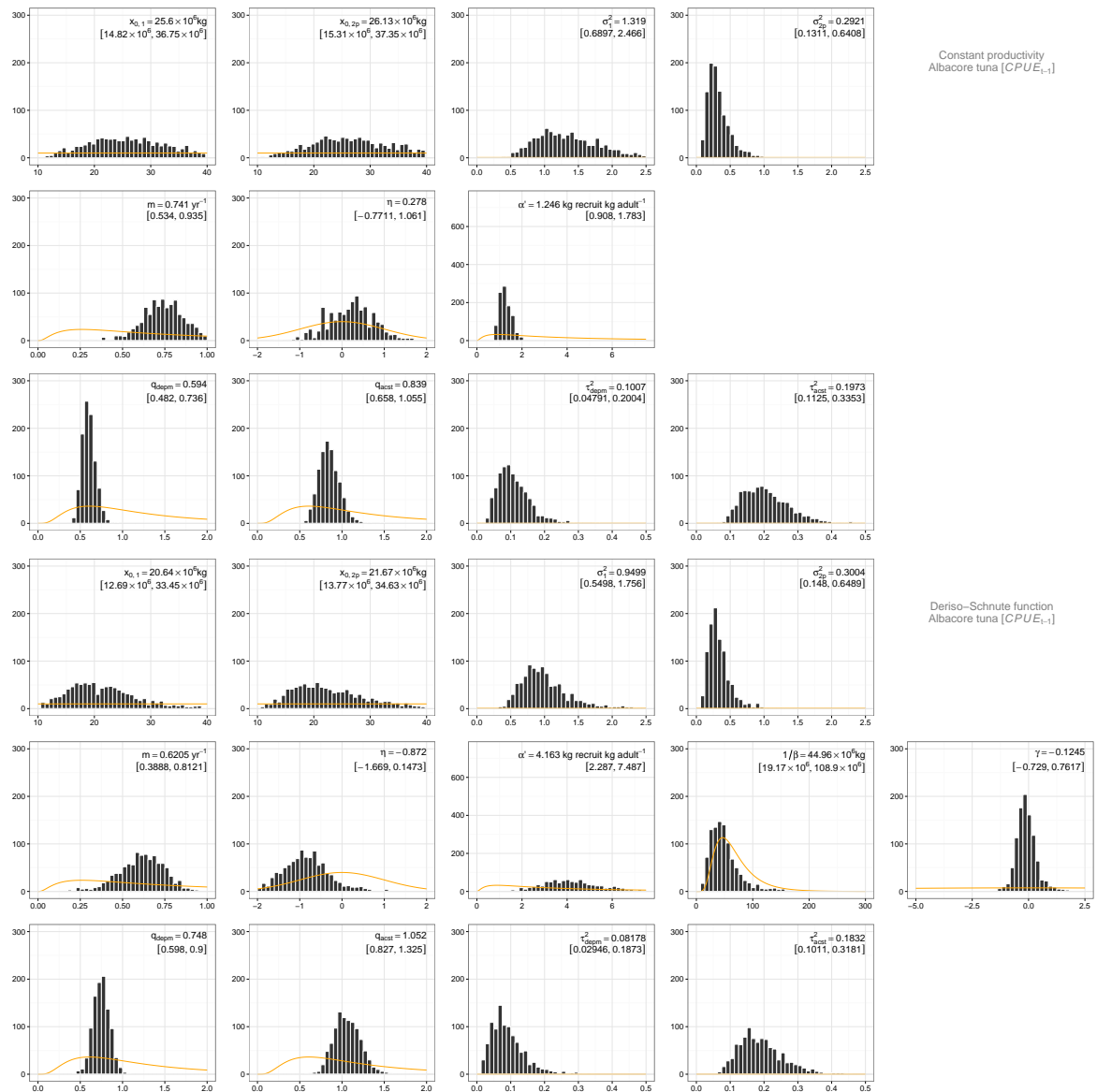


Figure 4.D.-6: (Albacore tuna).

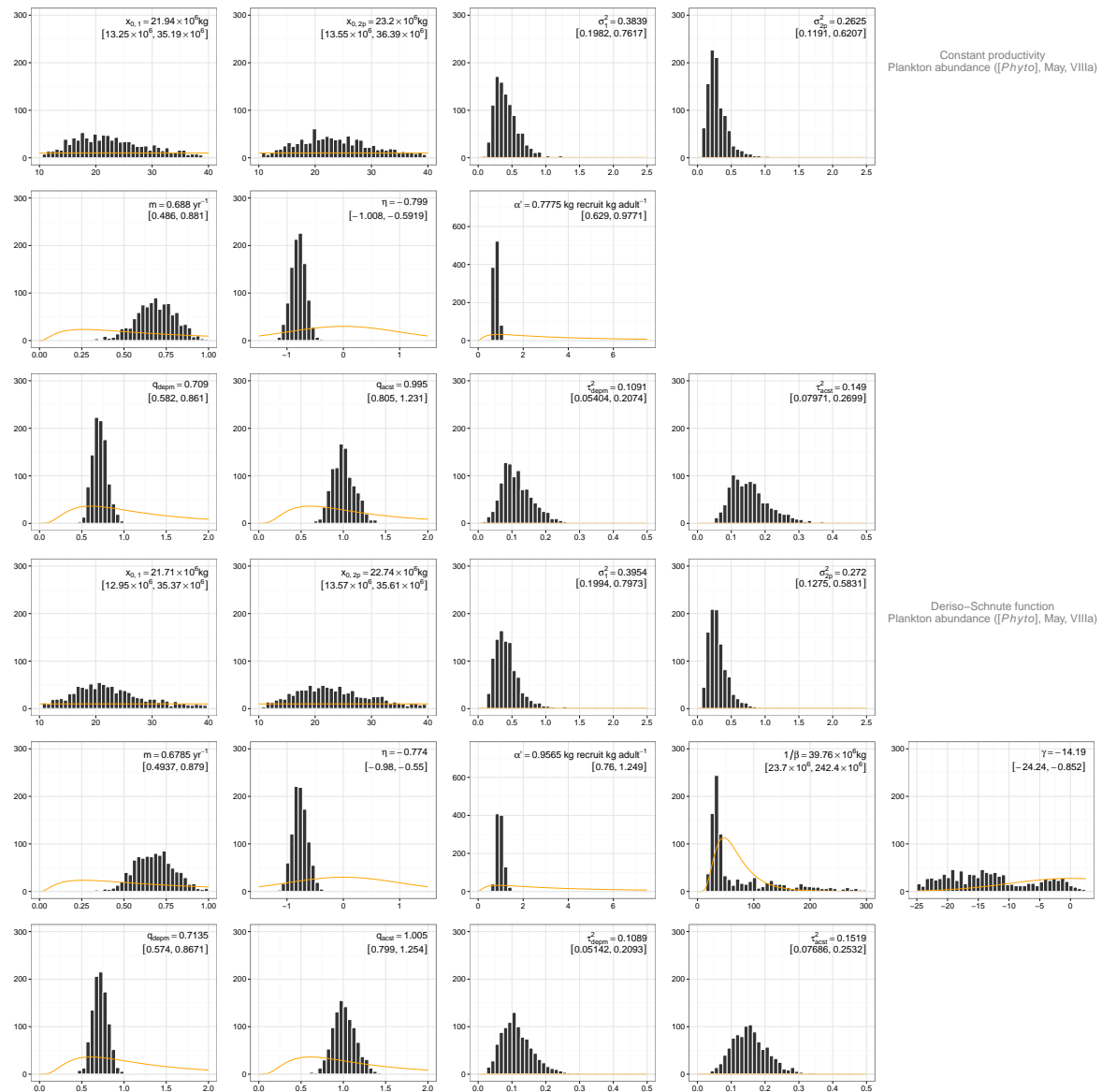


Figure 4.D.-7: (Plankton phenology).

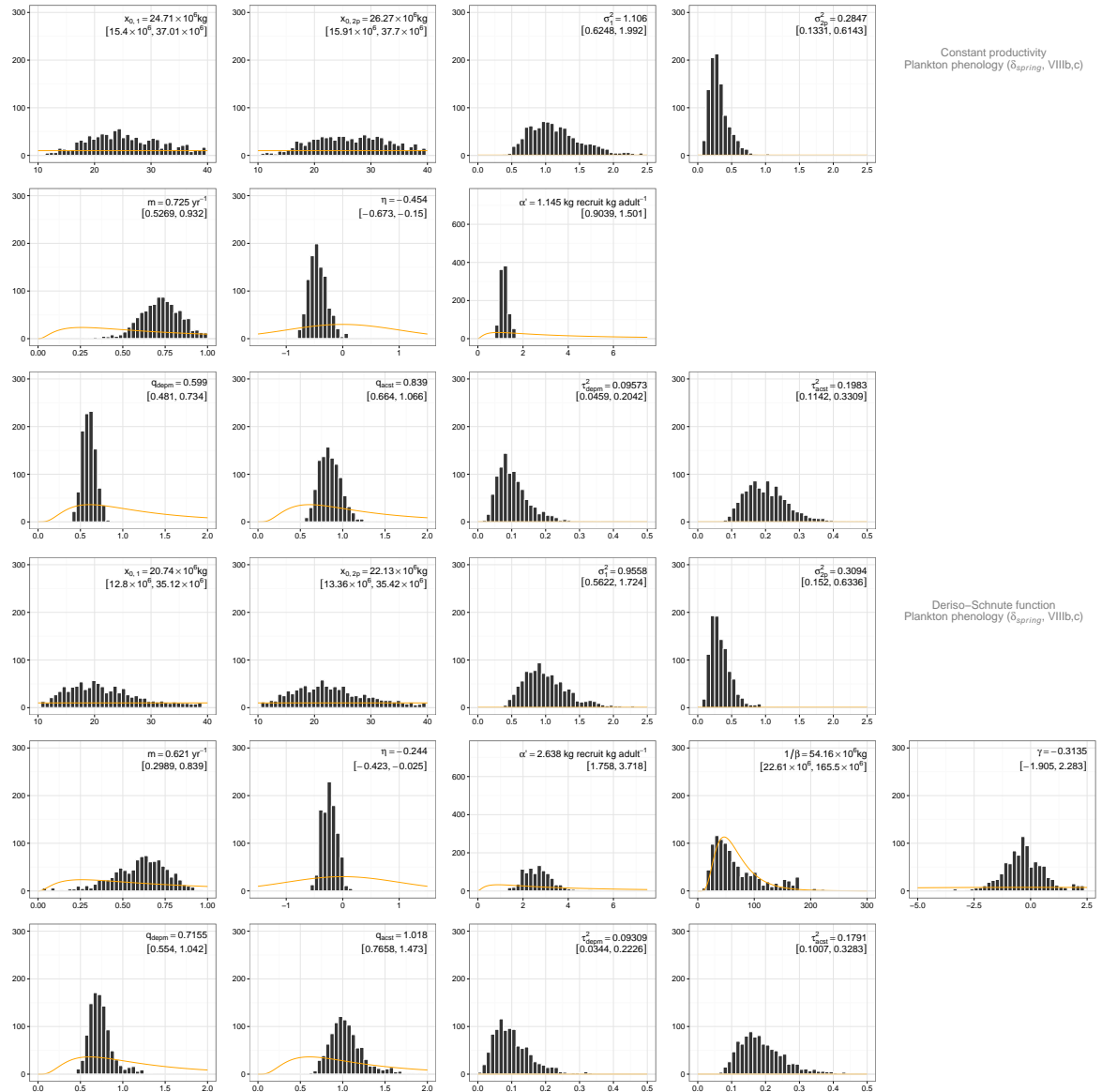


Figure 4.D.-8: (River discharge).

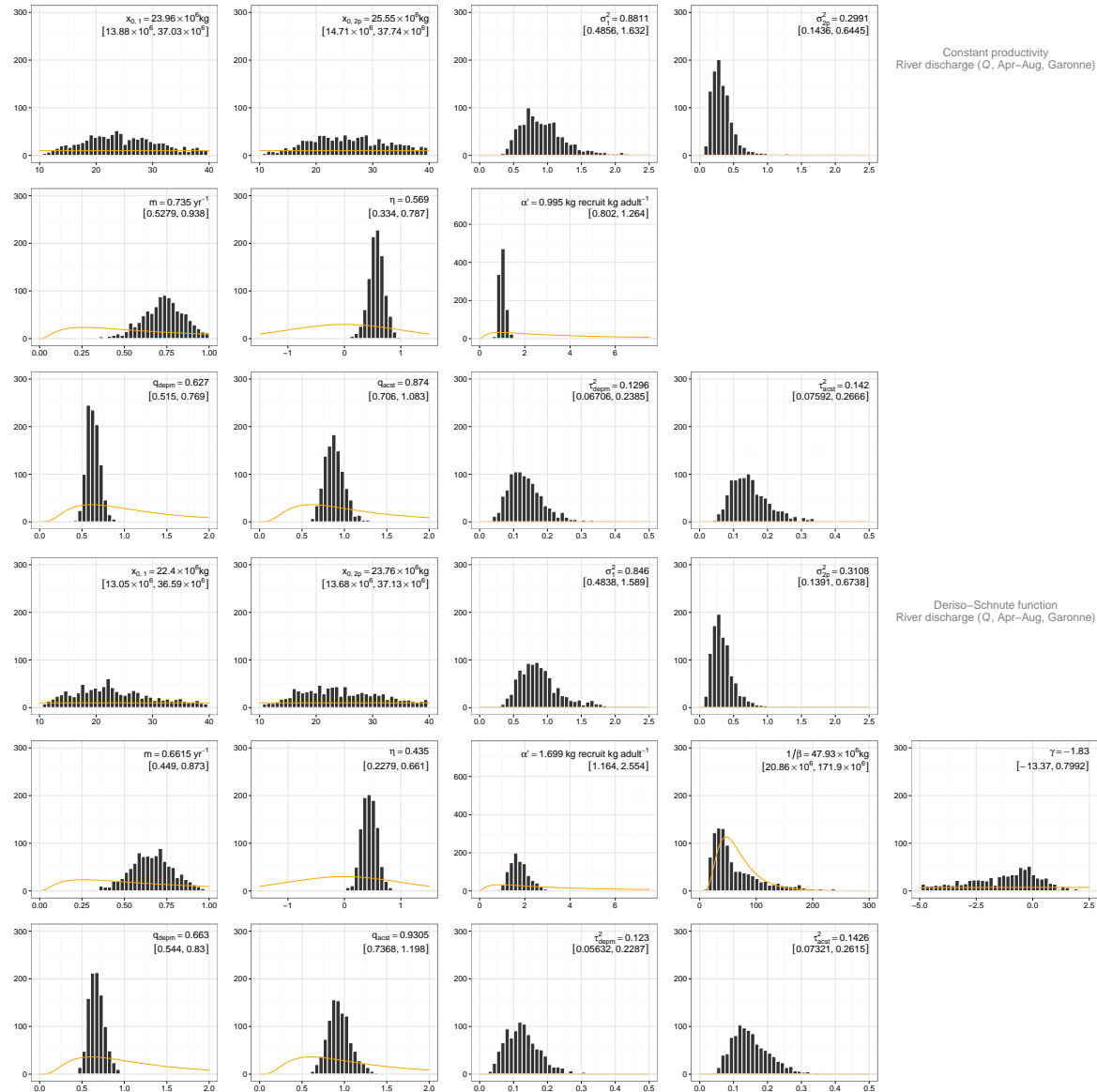


Figure 4.D.-9: (Temperature).

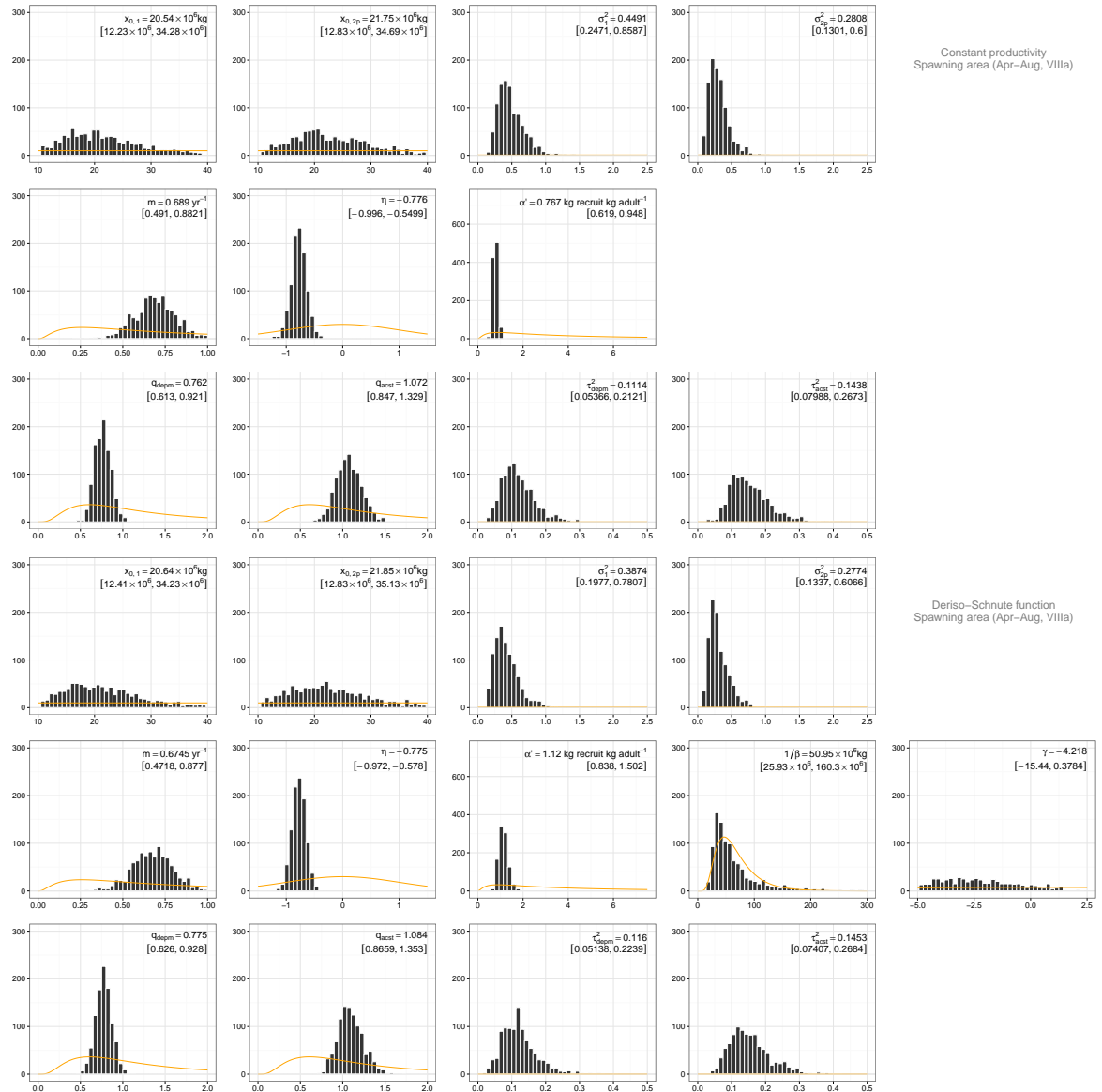


Figure 4.D.-10: (Transport barriers).

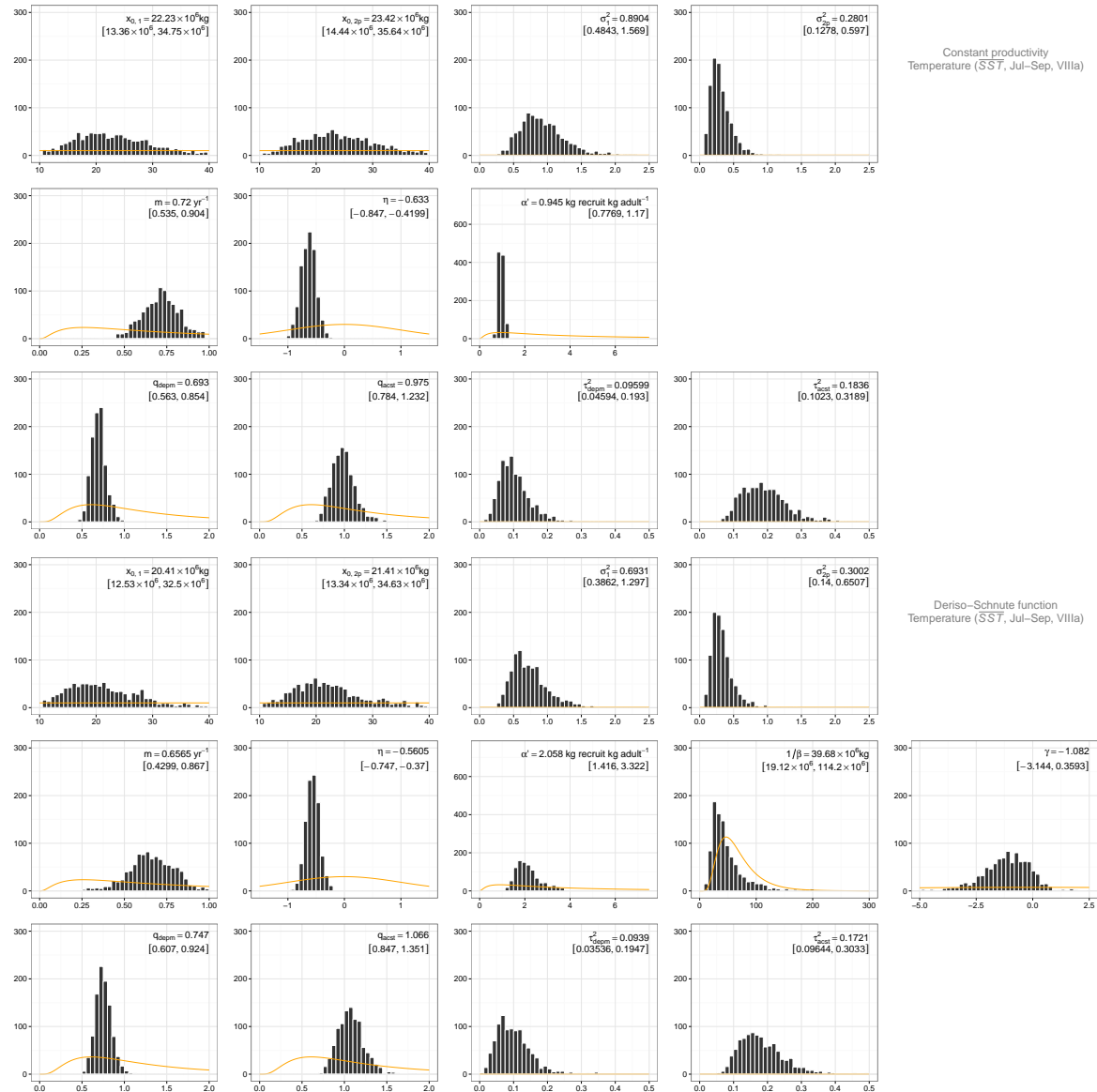


Figure 4.D.-11: (Turbulence).

Chapter 5

Discussion and conclusions

The previous chapters presented some applications of satellite oceanography that illustrate how environmental scientists and managers can take advantage of remote sensing data. Each chapter included the development and/or exploration of novel methodological approaches that were used to highlight different aspects of how remote sensing can advance the analysis of global change impacts on pelagic ecosystems. The approach focused on recent changes in the North Atlantic Ocean and revealed that beyond the generalized increase in sea surface temperatures, surface warming is affecting the seasonal cycle of temperature and promoting the arrangement of novel marine biological communities (chapter 2). Phytoplankton seasonal cycles presented a signature of the poleward expansion of the Sub-tropical Gyre, with changes in phenology in the whole basin that were mainly associated to changes in wind forcing and other physical agents (chapter 3). Finally, the analysis of physical forcing on recruitment and its interaction with fishing lead to the development of prognostic models for the anchovy fishery in the Bay of Biscay, and identified overfishing as the most probable cause of its recent collapse (chapter 4).

Considering that the work presented here have dealt to a great extent with the estimation of the rates of change of different environmental variables, it is worth asking whether it is expected that these trends will continue in a near future. Taking a more practical point of view, it is also interesting to try to anticipate how will the approaches proposed here evolve in the coming years (supposing they will not be just ignored and doomed to oblivion). Currently there is a wide consensus on our inability to stop global warming in the short term [Stocker et al., 2013], so we can adventure with almost full certainty that most of the changes highlighted in chapter 2 will continue in a near future. We can also anticipate that in our opinion patterns of increased stratification and spatial homogenization will probably become clearer in coming years, especially considering the increased effort to produce high resolution temperature products [*e.g.* Donlon et al. 2007], as well as expected advances in satellite oceanography [CESAS–NRC, 2007; Freeman et al., 2010; CANESP–NRC, 2012]. We

have also some confidence on the evolution of our approach to track isotherm migration that, in our opinion presents some advantages over other approaches to analyze the pace of climate change [e.g. Loarie et al. 2009; Burrows et al. 2011; Pinsky et al. 2013], particularly regarding the ability to track the migration of a given temperature level.

The poleward displacement of warmer climatic conditions was indeed highlighted as well when analyzing changes in phytoplankton seasonality (chapter 3). These changes in regional patterns of the type of prevalent phytoplankton seasonal cycles, together with the changes advanced in phenology will probably become even more apparent in the coming decades [Sarmiento et al., 2004; Henson et al., 2013]. Despite the difficulties to detect these type of changes [Beaulieu et al., 2013], we also highlighted environmental associations that seem to be behind changes in seasonality and deserve further scrutiny. On the other hand, at least those difficulties associated to data gaps seem to have their days numbered. Projected improvements in the resolution and revisit times of novel sensors [CESAS–NRC, 2007; Freeman et al., 2010; IOCCG, 2012a; CANESP–NRC, 2012], together with the incorporation of geostationary satellites [IOCCG, 2012b] and active sensors [Behrenfeld et al., 2013] to the ocean color constellation will improve data coverage to a great extent.

We expect nevertheless that the approach proposed to characterize changes in the seasonal cycle might indeed be useful in this respect, considering its ability to accommodate data from different satellite missions. However, we presume that rather than the simple models we employed to interpolate chlorophyll *a* retrievals in time, model assimilation experiments will be employed to generate continuous fields not only of phytoplankton pigments, but also of its biomass and other physiological properties. Perhaps the use and discussion of an alternative definition of the timing of the blooms might be more important. Taking the timing of maximum increase in phytoplankton accumulation contrasts with other definitions found in the recent literature [e.g. Siegel et al. 2002; Henson et al. 2009; Vargas et al. 2009; Cole et al. 2012; Sapiro et al. 2012; see also Rolinski et al. 2007 and Behrenfeld and Boss 2014]. Our choice primed practical considerations over tradition [e.g. Sverdrup 1953], but there are also ecological considerations to retain the point of maximum increase, as demonstrated by the success of this index to predict changes in anchovy recruitment in chapter 4.

Perhaps the most important and direct practical application of the work presented here deals with the prediction of anchovy recruitment in the Bay of Biscay (chapter 4). We proposed two mechanisms that in our opinion deserve further scrutiny and that might be easily tested directly in the field. From an environmental point of view, the future of anchovy seems to be tied to changes in spring conditions, including the timing of the bloom, and in summer wind forcing. To our knowledge, this was also the first application of Lagrangian coherent structures within a population model of a commercially exploited fish species; we anticipate that it will not be the last attempt. The evolution of these variables deserves in this way further attention. On the other hand, a direct implication of our simulation ex-

periments was the importance of reducing and regulating fishing quotas and effort. This might be the only way to attain a sustained exploitation of the fishery or, at least, to allow fishermen to distribute their effort to other species or economic activities. In chapter 4, as well as in chapter 3, the use of advanced Bayesian analysis techniques was key to attain the results discussed so far.

The use of Bayesian analysis techniques has a long tradition in environmental sciences, but in the context of life sciences, fishery scientists have played a pioneering and leading role in popularizing this approach [e.g. Schnute 1994; Hilborn and Mangel 1997; Punt and Hilborn 1997; McAllister and Kirkwood 1998; Millar and Meyer 2000]. Here we illustrated some of its advantages [Robert, 2001; Gelman et al., 2004], namely (i) the ability to propagate uncertainty from observations to posterior parameters summaries and functions of them, and (ii) to ease the fit of complex models by setting up a conditional hierarchical structure among model components, parameters and data that emerges naturally within this framework [Clark and Gelfand, 2006a; Cressie et al., 2009]. The first aspect has been particularly important to reveal complex trends in plankton phenology (chapter 3), considering the relatively lower precision of ocean color measurements and the unavoidable lack of observations associated to cloudy periods. Data augmentation via posterior simulation seems the best potential alternative to surpass the lack of data during cloudy periods, even considering the potential use of active sensors and that geostationary data will become a reality sooner than after [IOCCG, 2012b; Behrenfeld et al., 2013]. This advantage of Bayesian statistics over other approaches has profound philosophical considerations that are not exempt of certain controversy [see Ellison 2004 for an overview].

The second major advantage of Bayesian analysis is just a question of pure pragmatism. This aspect was illustrated in chapter 4 where we fitted a complex, nonlinear age structured model integrating the potential effect of environmental covariates and taking full advantage at the same time of differences between complementary sampling methods. To do that we adapted recently developed Markov Chain Monte Carlo methods to fit a Deriso-Schnute model [Cappé et al., 2008; Wraith et al., 2009; Andrieu et al., 2010; Peters et al., 2010]. We also illustrated there how these methods can be used to derive posterior quantities of interest. Specifically we conducted a surrogate analysis that allowed us to identify overexploitation as the most likely explanation of the recent collapse of the fishery. Although we stopped our analysis at this point, the Bayesian framework provides the opportunity to further pursue other potential implications for the management of the fishery.

In this way, there is no surprise in the growing interest in applying these methods in Oceanography [Wikle et al., 2013; Milliff et al., 2013], and even to include them early and as an integral part of undergraduate programs in environmental sciences [(Ellison and Dennis [2010]; see also Millspaugh and Gitzen [2010]; Dennis and Ellison [2010])]. This approach is not free of controversy and indeed, at the time of writing this memoir, a discussion about whether *p* values still deserve consideration in Ecology has been published

in a major ecological journal [see Ellison et al. [2014] and references therein]. We have obviated deliberately here the use of this statistical index in all major chapters and used instead a parameter-centric approach. If this approach comes at the price of recognizing the subjective nature of any inferential procedure and the unavoidable existence of uncertainty in parameter estimation, we consider it is clearly advantageous over the awkward and also subjective choice of more limited approaches assuming binary outcomes and fixed parameter values.

Together with remote sensing techniques, Bayesian analysis is expected to gain a growing importance in environmental science and management in the coming years [Clark and Gelfand, 2006b; IOCCG, 2008; Wilson et al., 2008; Morales et al., 2010]. As noted above, this framework eases the integration of different data sources and the propagation of uncertainty from model inference to a decision context [Robert, 2001]. The «emerging imperative» of anticipating and predicting the response of ecological systems to human intervention can take advantage of the approach employed here [Clark et al., 2001]. We have indeed highlighted the high potential of remote sensing to analyze ecological problems, especially considering the adequacy of a regional focus that emerged from the work presented here (from the heterogeneity found in changes in sea surface temperature to the particularities of the precise spatial and temporal signal of environmental forcing on anchovy recruitment success). Taking account of local effects might be especially important for the conservation and management of marine species, especially considering that marine life cycles usually involve free ranging stages [Barnes and Hughes, 1999]. Environmental forcing during these phases usually condition recruitment success, and in this respect we have exemplified how a careful analysis of the recruitment environment of a species might lead to improved management practices.

Last, but not least, the work presented here highlighted the importance of publicly available databases for oceanographic research and for the study of global change impacts. We combined a variety of data sources from different disciplines to study recent changes in the North Atlantic. These databases form part of long term monitoring programs originally developed and maintained thanks to the coordinated effort of several organizations around the world. Our analysis covered different aspects of the dynamics of marine pelagic ecosystems; ranging from changes in the physical environment to changes in the food web like the phenology of primary producers or the dynamics of a commercially exploited fish species. The analyses and accomplishments discussed above were possible only thanks to the availability of a large amount of well documented, high quality data.

Long term monitoring programs are an essential asset to cope with global change impacts on ecosystems [Lindenmayer and Likens, 2010], especially to deal with unexpected impacts [Lindenmayer et al., 2010]. They are also necessary to develop better forecasts of the consequences of human interventions, which is a growing societal demand to environmental scientists [Clark et al., 2001; CGCES–OCCGCES–NRC, 2001]. Earth Observing

Satellites and other automatic sampling methods are called to play a leading role in this respect in the coming decades [Johnson et al., 2007, 2009; Lindstrom and Maximenko, 2010; Freeman et al., 2010]. These data will favor the development of novel applications, especially if they are integrated with other sources of information derived from field sampling and experiments. At the same time, this approach should lead to increased concern about current environmental problems and about the importance of long term observation programs.

5.1 Conclusions

- Earth Observing Satellites retrieve data of great value that allowed us to characterize changes in North Atlantic sea surface temperature and phytoplankton phenology, as well as to assess the relative importance of environmental variation and overfishing on the recent collapse of Bay of Biscay anchovy fishery.
- The changes detected in sea surface temperature between 1982 and 2010 are coherent with expected impacts under human induced climate change, although statistics related to mean temperature, the seasonal cycle and the period of stratification, or the structuring of temperature spatial fields presented a different response.
- The spatial pattern of changes in sea surface temperature was very complex, highlighting the need of a more local and regional focus in future climate change studies.
- Changes in the seasonality of North Atlantic phytoplankton between 1998 and 2013 were coherent with the expansion of subtropical regions polewards. This change involved a redistribution of the different types of phytoplankton seasonal cycles, as well as changes in the timing and magnitude of seasonal blooms.
- Changes in the phenology of marine phytoplankton were associated mainly to changes in wind circulation patterns and, to a lesser extent, to changes in irradiance and temperature.
- We developed a probabilistic assessment method to propagate uncertainty in the detection and characterization of phytoplankton seasonal blooms to estimates of long term phenological change. The method highlighted also the advantage of semi-analytical chlorophyll algorithms over empirical ones to reduce biases among different sensors.
- Fluctuations in anchovy recruitment in the Bay of Biscay can be anticipated by considering either changes in the timing of the spring phytoplankton bloom or in summer upwelling over Armorican shelf.

- Despite the tight environmental regulation of anchovy recruitment in the Bay of Biscay, overfishing seems to be the main cause behind the collapse of the fishery in 2005.
- Bayesian analysis offers a great potential to develop better natural resources management and conservation practices, as well as to improve impact detection and monitoring systems.
- Ocean monitoring based on the combination of different sampling approaches is essential to cope with global change impacts; a challenge where Earth Observing Satellites are called to play a leading role. Ensuring the availability and access to ease the use of this information by the scientific community and the general public will contribute to increase public concern about current environmental problems and about the importance of long term observation programs.

Chapter 6

Summary and conclusions [*in Spanish*]

6.1 Resumen

Los satélites de observación terrestre recogen información de gran interés para el estudio del impacto global sobre los ecosistemas pelágicos marinos. Este tipo de sistemas de observación proporcionan medidas de distintas propiedades de la superficie del océano con una resolución espacial y temporal muy alta. Esta particularidad permite analizar la dinámica de los ecosistemas pelágicos desde el punto de vista de su componente biológico. En esta memoria se utiliza esta aproximación para analizar los cambios en la temperatura de la superficie del mar y en la fenología del fitoplancton en el Atlántico Norte durante las últimas décadas, así como para evaluar la importancia de la variación ambiental frente a la sobre-explotación en el colapso de la pesquería de anchoa del Cantábrico. En primer lugar, se propone una aproximación complementaria para el análisis de los cambios en la temperatura de la superficie del mar que da mayor énfasis a posibles cambios en la estacionalidad, así como a la distribución espacial de los cambios. Entre 1982 y 2010, los cambios en la temperatura de la superficie del mar registrados al analizar la serie producida a partir de las observaciones de los satélites NOAA-AVHRR fueron coherentes con el proceso de cambio climático global. La respuesta fue diferente en intensidad y en su distribución espacial entre estadísticos representando cambios en la temperatura media, el ciclo estacional y el período de estratificación, o la estructura espacial del campo de temperaturas. A continuación, se introduce un nuevo método para el análisis de los cambios en la estacionalidad del fitoplancton marino, tratando de incorporar la incertidumbre en las medidas satelitales de concentración de clorofila a la estimación de los cambios en la fenología. Este método permitió detectar un aumento de la prevalencia de ciclos estacionales propios de latitudes subtropicales en la zona templada entre 1998 y 2013, así como cambios en el momento del año en que producen las floraciones y en su intensidad congruentes con los impactos del

cambio climático. Estas tendencias parecen responder principalmente a cambios en los patrones de circulación atmosférica, y en menor medida a cambios en la radiación incidente o la temperatura. Este método ha demostrado también la mayor robustez de los algoritmos semi-analíticos de clorofila sobre los tradicionales al combinar datos procedentes de distintos sensores (SeaWiFS y MODIS). En último lugar, se analizó el colapso de la pesquería de anchoa del Cantábrico combinando técnicas de modelado de poblaciones con una cuidadosa caracterización de los cambios en ambientales en el golfo de Vizcaya basado principalmente en el análisis de datos satelitales. Se encontró que el éxito del reclutamiento de la anchoa se puede predecir con bastante precisión a partir de los cambios en la fenología y la estabilidad durante primavera en las áreas de desove o a partir del efecto del afloramiento estival sobre la deriva de larvas y huevos de anchoa fuera de la plataforma Armónica. Pese a que la regulación ambiental de la dinámica poblacional es muy importante, la sobrepesca parece haber jugado un papel fundamental en el colapso de la pesquería en 2005. En conjunto, el trabajo presentado en esta memoria indica la necesidad de una aproximación local y regional en los estudios de impacto del cambio global. Desde un punto de vista metodológico, también ilustra algunas de las ventajas que ofrecen las técnicas de análisis Bayesiano para mejorar la gestión y conservación de los recursos naturales, así como para mejorar los sistemas de detección y caracterización de impactos. Finalmente, este trabajo demuestra el valor de los datos satelitales en Oceanografía y la importancia de apoyar los programas públicos de observación a largo plazo del medio ambiente.

6.2 Conclusiones generales

- Los satélites de observación terrestre recogen datos de gran valor que han permitido caracterizar los cambios en la temperatura de la superficie del mar y en la fenología del fitoplancton en el Atlántico Norte, así como evaluar la importancia de la variación ambiental frente a la sobreexplotación en la pesquería de anchoa del Cantábrico.
- Los cambios en la temperatura de la superficie del mar entre 1982 y 2010 son coherentes con el proceso de cambio climático, aunque la respuesta difiere entre estadísticos que representan cambios en la temperatura media, el ciclo estacional y el período de estratificación, o la estructura espacial del campo de temperaturas.
- El patrón espacial de cambio en la temperatura de la superficie del mar es muy complejo, indicando la necesidad de una aproximación local y regional en los estudios de impacto de cambio climático.
- La estacionalidad del fitoplancton del Atlántico Norte muestra cambios consistentes con una expansión de las zonas subtropicales hacia los polos entre 1998 y 2013. Este

cambio afecta al patrón de distribución de los distintos tipos de ciclo estacional, así como al momento del año en que producen las floraciones y a su intensidad.

- Los cambios en la fenología del fitoplancton marino parecen responder principalmente a cambios en los patrones de circulación atmosférica, y en menor medida a cambios en la radiación incidente o la temperatura.
- Se propone un método de análisis probabilístico que permite propagar la incertidumbre en la detección y caracterización de las floraciones de fitoplancton a las estimas de cambios a largo plazo. Este método ha demostrado también la mayor robustez de los algoritmos semi-analíticos de clorofila sobre los tradicionales al combinar datos procedentes de distintos sensores.
- Las fluctuaciones en el reclutamiento de la anchoa del Cantábrico se pueden predecir con bastante precisión al considerar el efecto de los cambios en el momento de ocurrencia de la floración primaveral de fitoplancton o en los patrones de afloramiento sobre la plataforma Armónica en verano.
- A pesar de que la abundancia de anchoa varía principalmente en respuesta a cambios en las condiciones ambientales, la sobrepesca parece haber jugado un papel fundamental en el colapso de la pesquería en 2005.
- Las técnicas de análisis Bayesiano ofrecen un gran potencial para mejorar la gestión y conservación de los recursos naturales, así como para mejorar los sistemas de detección y caracterización de impactos.
- Garantizar la observación continuada de los océanos combinando distintos métodos de muestreo es esencial para combatir los impactos del cambio global; aspecto en el que los satélites de observación terrestres juegan un papel primordial. Facilitar la disponibilidad y el acceso a esta información por parte de la comunidad científica y de la sociedad en general contribuye a incrementar su uso, así como la concienciación sobre los problemas ambientales y la importancia de apoyar los programas de observación a largo plazo.

Bibliography

- G. Allain, P. Petitgas, and P. Lazure. The influence of mesoscale ocean processes on anchovy (*Engraulis encrasicolus*) recruitment in the Bay of Biscay estimated with a three-dimensional hydrodynamic model. *Fisheries Oceanography*, 10(2):151–163, 2001. doi: 10.1046/j.1365-2419.2001.00164.x.
- G. Allain, P. Petitgas, and P. Lazure. The influence of environment and spawning distribution on the survival of anchovy (*Engraulis encrasicolus*) larvae in the Bay of Biscay (NE Atlantic) investigated by biophysical simulations. *Fisheries Oceanography*, 16(6):506–514, 2007a. doi: 10.1111/j.1365-2419.2007.00442.x.
- G. Allain, P. Petitgas, P. Lazure, and P. Grellier. Biophysical modelling of larval drift, growth and survival for the prediction of anchovy (*Engraulis encrasicolus*) recruitment in the Bay of Biscay (NE Atlantic). *Fisheries Oceanography*, 16(6):489–505, 2007b. doi: 10.1111/j.1365-2419.2007.00443.x.
- C. N. K. Anderson, C.-H. Hsieh, S. A. Sandin, R. Hewitt, A. Hollowed, J. Beddington, R. M. May, and G. Sugihara. Why fishing magnifies fluctuations in fish abundance. *Nature*, 452:835–839, 2008. doi: 10.1038/nature06851.
- T. Ando. *Bayesian Model Selection and Statistical Modelling*. CRC Press, Boca Raton, USA, 1 edition, 2010.
- C. Andrieu, A. Doucet, and R. Holenstein. Particle Markov chain Monte Carlo methods. *Journal of the Royal Statistical Society: Series B (Statistical Methodology)*, 72(3):269–342, 2010. doi: 10.1111/j.1467-9868.2009.00736.x.
- D. Antoine, A. Morel, H. R. Gordon, V. F. Banzon, and R. H. Evans. Bridging ocean color observations of the 1980s and 2000s in search of long term trends. *Journal of Geophysical Research*, 110:C06009, 2005. doi: 10.1029/2004JC002620.
- R. Atlas, R. N. Hoffman, J. Ardizzone, S. M. Leidner, J. C. Jusem, D. K. Smith, and D. Gombos. A cross-calibrated, multiplatform ocean surface wind velocity product for meteorological and oceanographic applications. *Bulleting of the American Meteorological Society*, 92(2):157–174, 2011. doi: 10.1175/2010BAMS2946.1.
- E. Bachiller, U. Cotano, G. Boyra, and X. Irigoien. Spatial distribution of the stomach weights of juvenile anchovy (*Engraulis encrasicolus* L.) in the Bay of Biscay. *ICES Journal of Marine Science: Journal du Conseil*, 70(2):362–378, 2013. doi: 10.1093/icesjms/fss176.
- A. Bakun. *Patterns in the Ocean: Ocean Processes and Marine Population Dynamics*. Univ. California Sea Grant, San Diego, California, USA, in cooperation with Centro de Investigaciones Biológicas de Noroeste, La Paz, Baja California Sur, México, 1996.
- A. Bakun. Linking climate to population variability in marine ecosystems characterized by non-simple dynamics: conceptual templates and schematic constructs. *Journal of Marine Systems*, 79(3–4):361–373, 2010. doi: 10.1016/j.jmarsys.2008.12.008.
- A. Bakun and P. Cury. The "school trap": a mechanism promoting large-amplitude out-of-phase population oscillations of small pelagic fish species. *Ecology Letters*, 2(6):349–351, 1999. doi: 10.1046/j.1461-0248.1999.00099.x.
- S. Banerjee. On geodetic distance computations in spatial modeling. *Biometrics*, 61:617–625, 2005. doi: 10.1111/j.1541-0420.2005.00320.x.

- S. Banerjee, B. P. Carlin, and A. E. Gelfand. *Hierarchical Modeling and Analysis for Spatial Data*. Monographs on Statistics and Applied Probability 101. Chapman & Hall/CRC, Boca Raton, FL, USA, 2004. ISBN 1-58488-410-X.
- V. Barale, J. F. R. Gower, and L. Alberotanza, editors. *Oceanography from Space. Revisited*. Springer, Dordrecht, Netherlands, 2010. ISBN 978-90-481-8680-8.
- R. S. K. Barnes and R. Hughes. *An Introduction to Marine Ecology*. Blackwell Publishing, Oxford, UK, 3 edition, 1999.
- T. P. Barnett, D. W. Pierce, K. M. AchutaRao, P. J. Gleckler, B. D. Santer, J. M. Gregory, and W. M. Washington. Penetration of human-induced warming into the world's oceans. *Science*, 309:284–287, 2005. doi: 10.1126/science.1112418.
- G. Beaugrand, P. C. Reid, F. Ibañez, J. A. Lindley, and M. Edwards. Reorganization of North Atlantic marine copepod biodiversity and climate. *Science*, 296:1692–1694, 2002. doi: 10.1126/science.1071329.
- G. Beaugrand, K. M. Brander, J. A. Lindlay, S. Souissi, and P. C. Reid. Plankton effect on cod recruitment in the North Sea. *Nature*, 426:661–664, 2003. doi: 10.1038/nature02164.
- G. Beaugrand, M. Edwards, K. Brander, C. Luczak, and F. Ibañez. Causes and projections of abrupt climate-driven ecosystem shifts in the north atlantic. *Ecol Lett*, 11:1157–1158, 2008. doi: 10.1111/j.1461-0248.2008.01218.x.
- C. Beaulieu, S. A. Henson, J. L. Sarmiento, J. P. Dunne, S. C. Doney, R. R. Rykaczewski, and L. Bopp. Factors challenging our ability to detect long-term trends in ocean chlorophyll. *Biogeosciences*, 10(4):2711–2724, 2013. doi: 10.5194/bg-10-2711-2013.
- M. J. Behrenfeld. Abandoning Sverdrup's Critical Depth Hypothesis on phytoplankton blooms. *Ecology*, 91(4):977–989, 2010. doi: 10.1890/09-1207.1.
- M. J. Behrenfeld and E. S. Boss. Resurrecting the ecological underpinnings of ocean plankton blooms. *Annual Review of Marine Science*, 6(1):167–194, 2014. doi: 10.1146/annurev-marine-052913-021325.
- M. J. Behrenfeld, E. Boss, D. A. Siegel, and D. M. Shea. Carbon-based ocean productivity and phytoplankton physiology from space. *Global Biogeochemical Cycles*, 19:GB1006, 2005. doi: 10.1029/2004GB002299.
- M. J. Behrenfeld, R. T. O'Malley, D. A. Siegel, C. R. McClain, J. L. Sarmiento, G. C. Feldman, A. J. Milligan, P. G. Falkowski, R. M. Letelier, and E. S. Boss. Climate-driven trends in ocean contemporary ocean productivity. *Nature*, 444:752–754, 2006. doi: 10.1038/nature05317.
- M. J. Behrenfeld, Y. Hu, C. A. Hostetler, G. Dall'Olmo, S. D. Rodier, J. W. Hair, and C. R. Trepte. Space-based lidar measurements of global ocean carbon stocks. *Geophysical Research Letters*, 40(16):4355–4360, 2013. doi: 10.1002/grl.50816.
- J.-P. Bergeron. Contrasting years in the Gironde estuary (Bay of Biscay, NE Atlantic) springtime outflow and consequences for zooplankton pyruvate kinase activity and the nutritional condition of anchovy larvae: an early view. *ICES Journal of Marine Science: Journal du Conseil*, 61(6):928–932, 2004. doi: 10.1016/j.icesjms.2004.06.019.
- J.-P. Bergeron, D. Delmas, and N. Koueta. Do river discharge rates drive the overall functioning of the pelagic ecosystem over the continental shelf of the Bay of Biscay (NE Atlantic)? A comparison of two contrasting years with special reference to anchovy (*Engraulis encrasicolus* L.) nutritional state. *Journal of Oceanography*, 66(5):621–631, 2010. doi: 10.1007/s10872-010-0051-7.
- F. J. Beron-Vera, M. J. Olascoaga, and G. J. Goni. Oceanic mesoscale eddies as revealed by Lagrangian coherent structures. *Geophysical Research Letters*, 35:L12603, 2008. doi: 10.1029/2008GL033957.
- R. J. H. Beverton and S. J. Holt. *On the Dynamics of Exploited Fish Populations*. Fishery Investigations Series II. Ministry of Agriculture, Fisheries and Food, London, UK, 1 edition, 1957.
- D. S. M. Billett, R. S. Lampitt, A. L. Rice, and R. F. C. Mantoura. Seasonal sedimentation of phytoplankton to

- the deep-sea benthos. *Nature*, 302:520–522, 1983. doi: 10.1038/302520a0.
- R. Bivand and N. Lewin-Koh. *maptools: Tools for reading and handling spatial objects*, 2013. URL <http://CRAN.R-project.org/package=maptools>. R package version 0.8-27.
- R. Bivand, T. Keitt, and B. Rowlingson. *rgdal: Bindings for the Geospatial Data Abstraction Library*, 2013. URL <http://CRAN.R-project.org/package=rgdal>. R package version 0.8-14.
- R. S. Bivand, E. Pebesma, and V. Gómez-Rubio. *Applied spatial data analysis with R*. Springer, New York, USA, 2 edition, 2003. URL <http://www.asdar-book.org#>.
- Á. Borja, A. Uriarte, V. Valencia, L. Motos, and A. Uriarte. Relationships between anchovy (*Engraulis encrasicolus* L.) recruitment and the environment in the Bay of Biscay. *Scientia Marina*, 60(Suppl. 2):179–292, 1996.
- Á. Borja, A. Uriarte, J. Egaña, L. Motos, and V. Valencia. Relationships between anchovy (*Engraulis encrasicolus*) recruitment and environment in the Bay of Biscay (1967–1996). *Fisheries Oceanography*, 7(3-4): 375–380, 1998. doi: 10.1046/j.1365-2419.1998.00064.x.
- A. Borja, A. Fontán, J. Saénz, and V. Valencia. Climate, oceanography, and recruitment: the case of the Bay of Biscay anchovy (*Engraulis encrasicolus*). *Fisheries Oceanography*, 17(6):477–493, 2008. doi: 10.1111/j.1365-2419.2008.00494.x.
- E. Bosc, A. Bricaud, and D. Anderson. Seasonal and interannual variability in algal biomass and primary production in the Mediterranean Sea, as derived from 4 years of seawifs observations. *Global Biogeochem Cycles*, 18:GB1005, 2004. doi: 10.1029/2003GB002034.
- P. W. Boyd and S. C. Doney. Modelling regional responses by marine pelagic ecosystems to global climate change. *Geophys Res Lett*, 29:1806, 2002. doi: 10.1029/2001GL014130.
- K. M. Brander. Global fish production and climate change. *Proc Natl Acad Sci USA*, 104:19709–19714, 2007. doi: 10.1073/pnas.0702059104.
- R. Brownrigg. *maps: Draw Geographical Maps*, 2013. URL <http://CRAN.R-project.org/package=maps>. Original S code by Richard A. Becker and Allan R. Wilks. Enhancements by Thomas P Minka. R package version 2.3-6.
- K. P. Burnham and D. Anderson. *Model Selection and Multi-Model Inference: a Practical Information-Theoretic Approach*. Springer, New York, USA, 2 edition, 2003.
- M. T. Burrows, D. S. Schoeman, L. B. Buckley, P. Moore, E. S. Poloczanska, K. M. Brander, C. Brown, J. F. Bruno, C. M. Duarte, B. S. Halpern, J. Holding, C. V. Kappel, W. Kiessling, M. I. O'Connor, J. M. Pandolfi, C. Parmesan, F. B. Schwing, W. J. Sydeman, and A. J. Richardson. The pace of shifting climate in marine and terrestrial ecosystems. *Science*, 334(6056):652–655, 2011. doi: 10.1126/science.1210288.
- C. Cabanes, A. Cazenave, and C. L. Provost. Sea level rise during past 40 years determined from satellite and in situ observations. *Science*, 294:840–842, 2001. doi: 10.1126/science.1063556.
- G. Campbell and J. E. Mosimann. Multivariate analysis of size and shape: modelling with the dirichlet distribution. In R. M. Heiberger, editor, *Computer Science and Statistics: Proceedings of the 19th Symposium on the Interface*, pages 93–101. American Statistical Association, aug 1987.
- CANESP–NRC. *Earth Science and Applications from Space: A Midterm Assessment of NASA's Implementation of the Decadal Survey*. Committee on the Assessment of NASA's Earth Science Program, Space Studies Board, Division on Engineering and Physical Sciences, National Research Council, The National Academies Press, 2012. ISBN 9780309257022. URL http://www.nap.edu/openbook.php?record_id=13405.
- O. Cappé, R. Douc, A. Guillin, J.-M. Marin, and C. P. Robert. Adaptive importance sampling in general mixture classes. *Statistics and Computing*, 18(4):447–459, 2008. doi: 10.1007/s11222-008-9059-x.
- B. P. Carlin, N. G. Polson, and D. S. Stoffer. A Monte Carlo approach to nonnormal and nonlinear state-space modeling. *Journal of the American Statistical Association*, 87(418):493–500, 1992. doi:

- 10.1080/01621459.1992.10475231.
- K. S. Casey and P. Cornillon. Global and regional sea surface temperature trends. *J Clim*, 14:3801–3818, 2001. doi: 10.1175/1520-0442(2001)014<3801:GARSST>2.0.CO;2.
- K. S. Casey, T. B. Brandon, P. Cornillon, and R. Evans. *The Past, Present, and Future of the AVHRR Pathfinder SST Program*. In Barale et al. [2010], pages 273–287. ISBN 978-90-481-8680-8.
- CESAS–NRC. *Earth Science and Applications from Space: National Imperatives for the Next Decade and Beyond*. Committee on Earth Science and Applications from Space: A Community Assessment and Strategy for the Future, National Research Council, The National Academies Press, 2007. ISBN 9780309667142. URL http://www.nap.edu/openbook.php?record_id=11820.
- CGCES–OCCGCES–NRC. *Grand Challenges in Environmental Sciences*. Committee on Grand Challenges in Environmental Sciences, Oversight Commission for the Committee on Grand Challenges in Environmental Sciences, National Research Council, The National Academies Press, Washington, D.C., USA, 2001. ISBN 9780309072540. URL http://www.nap.edu/openbook.php?record_id=9975.
- G. Charria, P. Lazure, B. L. Cann, A. Serpette, G. Reverdin, S. Louazel, F. Batifoulier, F. Dumas, A. Pichon, and Y. Morel. Surface layer circulation derived from Lagrangian drifters in the Bay of Biscay. *Journal of Marine Systems*, 109–110, Supplement:S60–S76, 2013. doi: 10.1016/j.jmarsys.2011.09.015.
- D. Checkley, J. Alheit, Y. Oozeki, and C. Roy, editors. *Climate Change and Small Pelagic Fish*. Cambridge University Press, Cambridge, UK, 1 edition, 2009.
- D. B. Chelton. Large-scale response of the California Current to forcing by the wind stress curl. *California Cooperative Oceanic Fisheries Investigation Report*, XXIII:130–148, 1982.
- D. B. Chelton and M. G. Schlax. Global observations of oceanic rossby waves. *Science*, 272(5259):234–238, 1996. doi: 10.1126/science.272.5259.234.
- D. B. Chelton, R. A. deSzoeke, M. G. Schlax, K. E. Naggar, and N. Siwertz. Geographical variability of the first baroclinic Rossby radius of deformation. *Journal of Physical Oceanography*, 28:433–460, 1998. doi: 10.1175/1520-0485(1998)028<0433:GVOTFB>2.0.CO;2.
- D. B. Chelton, M. G. Schlax, M. H. Freilich, and R. F. Milliff. Satellite measurements reveal persistent small-scale features in ocean winds. *Science*, 303(5660):978–983, 2004. doi: 10.1126/science.1091901.
- J. H. Christensen, B. Hewitson, A. Busuioc, A. Chen, X. Gao, I. Held, R. Jones, R. K. Kolli, W.-T. Kwon, R. Laprise, V. M. Rueda, L. Mearns, C. G. Menéndez, J. Räisänen, A. Rinke, A. Sarr, and P. Whetton. *Regional Climate Projections*, chapter In: IPPC, *Climate Change 2007: The Physical Science Basis. Contribution of Working Group I to the Fourth Assessment Report of the Intergovernmental Panel on Climate Change* [Solomon, S, D Qin, M Manning, Z Chen, M Marquis, KB Averyt, M Tignor and HL Miller (eds.)], pages 847–940. Cambridge University Press, Cambridge, UK and New York, NY, USA, 2007.
- V. Christensen and J. Maclean, editors. *Ecosystem Approaches to Fisheries. A Global Perspective*. Cambridge University Press, Cambridge, UK, 1 edition, 2011.
- P. C. Chu, C. Fan, and W. T. Liu. Determination of vertical thermal structure from sea surface temperature. *J Atmos Ocean Technol*, 17:971–979, 2000. doi: 10.1175/1520-0426(2000)017<0971:DOVTSF>2.0.CO;2.
- J. S. Clark and A. Gelfand, editors. *Hierarchical Modelling for the Environmental Sciences. Statistical Methods and Applications*. Oxford University Press, Oxford, UK, 2006a. ISBN 9780198569671.
- J. S. Clark and A. E. Gelfand. A future for models and data in environmental science. *Trends in Ecology & Evolution*, 21(7):375–380, 2006b. doi: 10.1016/j.tree.2006.03.016.
- J. S. Clark, S. R. Carpenter, M. Barber, S. Collins, A. Dobson, J. A. Foley, D. M. Lodge, M. Pascual, R. P. Jr., W. Pizer, C. Pringle, W. V. Reid, K. A. Rose, O. Sala, W. H. Schlesinger, D. H. Wall, and D. Wear. Ecological forecasts: An emerging imperative. *Science*, 293(5530):657–660, 2001. doi: 10.1126/science.293.5530.657.
- H. Cole, S. Henson, A. Martin, and A. Yool. Mind the gap: the impact of missing data on the calcu-

- lation of phytoplankton phenology metrics. *Journal of Geophysical Research*, 117:C08030, 2012. doi: 10.1029/2012JC008249.
- V. J. Coles, C. Wilson, and R. R. Hood. Remote sensing of new production fuelled by nitrogen fixation. *Geophysical Research Letters*, 31:L06301, 2004. doi: 10.1029/2003GL019018.
- J. H. Cowan and R. F. Shaw. *Recruitment*. In Fuiman and Werner [2002], pages 88–111.
- N. Cressie and D. M. Hawkins. Robust estimation of the variogram. *Math Geol*, 12:115–125, 1980. doi: 10.1007/BF01035243.
- N. Cressie, C. A. Calder, J. S. Clark, J. M. V. Hoef, and C. K. Wikle. Accounting for uncertainty in ecological analysis: the strengths and limitations of hierarchical statistical modeling. *Ecological Applications*, 19(3): 553–570, 2009. doi: 10.1890/07-0744.1.
- CSAEOS–NRC. *Earth Observations from Space: The First 50 Years of Scientific Achievements*. Committee on Scientific Accomplishments of Earth Observations from Space, The National Academies Press, Washington, D.C., USA, 2008. ISBN 9780309110952. URL http://www.nap.edu/openbook.php?record_id=11991.
- P. Cury and C. Roy. Optimal environmental window and pelagic fish recruitment success in upwelling areas. *Canadian Journal of Fisheries and Aquatic Sciences*, 46(4):670–680, 1989. doi: 10.1139/f89-086.
- D. Cushing. Plankton production and year-class strength in fish populations: an update of the Match/Mismatch Hypothesis. *Advances in Marine Biology*, 26:249–293, 1990. doi: 10.1016/S0065-2881(08)60202-3.
- C. de Boyer Montégut, G. Madec, A. S. Fischer, A. Lazar, and D. Iudicone. Mixed layer depth over the global ocean: An examination of profile data and a profile-based climatology. *J Geophys Res*, 109:C12003, 2004. doi: 10.1029/2004JC002378.
- B. Dennis and A. M. Ellison. A reply to millspaugh and gitzen. *Frontiers in Ecology and the Environment*, 8 (10):515–516, 2010. doi: 10.1890/10.WB.27.
- R. B. Deriso. Harvesting strategies and parameter estimation for an age-structured model. *Canadian Journal of Fisheries and Aquatic Sciences*, 37(2):268–282, 1980. doi: 10.1139/f80-034.
- W. G. Deuser and E. H. Ross. Seasonal change in the flux of organic carbon to the deep Sargasso Sea. *Nature*, 283:364–365, 1980. doi: 10.1038/283364a0.
- C. Deutsch, J. L. Sarmiento, D. M. Sigman, N. Gruber, and J. P. Dunne. Spatial coupling of nitrogen inputs and losses in the ocean. *Nature*, 445:163–167, 2007. doi: 10.1038/nature05392.
- R. J. Diaz and R. Rosenberg. Spreading dead zones and consequences for marine ecosystems. *Science*, 321 (5891):926–929, 2008. doi: 10.1126/science.1156401.
- S. C. Doney, V. J. Fabry, R. A. Feely, and J. A. Kleypas. Ocean acidification: the other CO₂ problem. *Ann Rev Mar Sci*, 1:169–192, 2009. doi: 10.1146/annurev.marine.010908.163834.
- C. Donlon, N. Rayner, I. Robinson, D. J. S. Poulter, K. S. Casey, J. Vazquez-Cuervo, E. Armstrong, A. Bingham, O. Arino, C. Gentemann, D. May, P. LeBorgne, J. Piollé, I. Barton, H. Beggs, C. J. Merchant, S. Heinz, A. Harris, G. Wick, B. Emery, P. Minnett, R. Evans, D. Llewellyn-Jones, C. Mutlow, R. H. Reynolds, and H. Kawamura. The global ocean data assimilation experiment high-resolution sea surface temperature pilot project. *Bulletin of the American Meteorological Society*, 88(8):1197–1213, 2007. doi: 10.1175/BAMS-88-8-1197.
- A. Doucet, N. de Freitas, and N. Gordon, editors. *Sequential Monte Carlo Methods in Practice*. Springer-Verlag, New York, USA, 2001.
- F. d’Ovidio, V. Fernández, E. Hernández-García, and C. López. Mixing structures in the Mediterranean Sea from finite-size Lyapunov exponents. *Geophysical Research Letters*, 31:L17203, 2004. doi: 10.1029/2004GL020328.
- F. d’Ovidio, S. De Monte, S. Alvain, Y. Dandonneau, and M. Lévy. Fluid dynamical niches of phytoplankton types. *Proceedings of the National Academy of Sciences*, 107(43):18366–18370, 2010. doi:

- 10.1073/pnas.1004620107.
- M. Dowle, T. Short, S. Lianoglou, A. S. with contributions from R Saporta, and E. Antoneyan. *data.table: Extension of data.frame*, 2014. URL <http://CRAN.R-project.org/package=data.table>. R package version 1.9.2.
- B. G. Drake, L. Hughes, E. A. Johnson, B. A. Seibel, M. A. Cochrane, V. J. Fabry, D. Rasse, and L. Hannah. *Synergistic Effects*, chapter In: Lovejoy TE and Hannah L (eds) *Climate Change and Biodiversity*, pages 296–316. Yale University Press, New Haven, CT, USA, 2005.
- J. E. Duffy and J. J. Stachowicz. Why biodiversity is important to oceanography: potential roles of genetic, species, and trophic diversity in pelagic ecosystem processes. *Mar Ecol Prog Ser*, 311:179–189, 2006. doi: 10.3354/meps311179.
- M. D. DuRand, R. J. Olson, and S. W. Chrisholm. Phytoplankton population dynamics at the Bermuda Atlantic Time-series station in the Sargasso Sea. *Deep-Sea Res Part II Top Stud Oceanogr*, 48:1983–2003, 2001. doi: 10.1016/S0967-0645(00)00166-1.
- J. M. Durant, D. Ø. Hjermann, G. Ottersen, and N. C. Stenseth. Climate and the match or mismatch between predator requirements and resource availability. *Climate Research*, 33:271–283, 2007. doi: 10.3354/cr033271.
- S. Dutkiewicz, M. Follows, J. Marshall, and W. W. Gregg. Interannual variability of phytoplankton abundances in the North Atlantic. *Deep-Sea Res Part II Top Stud Oceanogr*, 48:2323–2344, 2001. doi: 10.1016/S0967-0645(00)00178-8.
- D. R. Easterling, G. A. Meehl, C. Parmesan, S. A. Changnon, T. R. Karl, and L. O. Mearns. Climate extremes: Observations, modeling, and impacts. *Science*, 289:2068–2074, 2000. doi: 10.1126/science.289.5487.2068.
- M. Edwards and A. J. Richardson. Impact of climate change on marine pelagic phenology and trophic mismatch. *Nature*, 430:881–884, 2004. doi: 10.1038/nature02808.
- M. Edwards, P. Reid, and B. Planque. Long-term and regional variability of phytoplankton biomass in the Northeast Atlantic (1960–1995). *ICES Journal of Marine Science*, 58:39–49, 2001. doi: 10.1006/jmsc.2000.0987.
- A. M. Ellison. Bayesian inference in ecology. *Ecology Letters*, 7(6):509–520, 2004. doi: 10.1111/j.1461-0248.2004.00603.x.
- A. M. Ellison and B. Dennis. Paths to statistical fluency for ecologists. *Frontiers in Ecology and the Environment*, 8(7):362–370, 2010. doi: 10.1890/080209.
- A. M. Ellison, N. J. Gotelli, B. D. Inouye, and D. R. Strong. P values, hypothesis testing, and model selection: it's déjà vu all over again. *Ecology*, 95(3):609–610, 2014. doi: 10.1890/13-1911.1.
- P. G. Falkowski, R. T. Barber, and V. Smetacek. Biogeochemical controls and feedbacks on ocean primary production. *Science*, 281:200–206, 1998. doi: 10.1126/science.281.5374.200.
- FAO. *The State of World Fisheries and Aquaculture 2012*. Fisheries and Aquaculture Department, Food and Agriculture Organization of the United Nations, Rome, Italy, 2013.
- R. A. Feely, C. L. Sabine, K. Lee, W. Berelson, J. Kleypas, V. J. Fabry, and F. J. Millero. Impact of anthropogenic CO₂ on the CaCO₃ system in the oceans. *Science*, 305:362–366, 2004. doi: 10.1126/science.1097329.
- G. C. Feldman and C. R. McClain. Ocean Color Web, SeaWiFS and Aqua MODIS Reprocessing 2010.0, NASA Goddard Space Flight Center. Ed. by N. Kuring, and S. W. Bailey. Accessed 20 January 2012. <http://oceancolor.gsfc.nasa.gov/>, 2012.
- K. T. Frank, B. Petrie, and N. L. Shackell. The ups and downs of trophic control in continental shelf ecosystems. *Trends Ecol Evol*, 22:236–242, 2007. doi: 10.1016/j.tree.2007.03.002.
- A. Freeman, V. Zlotnicki, T. Liu, B. Holt, R. Kwok, S. Yueh, J. Vazquez, D. Siegel, and G. Lagerloef. Ocean measurements from space in 2025. *Oceanography*, 23(4):144–161, 2010. doi: 10.5670/oceanog.2010.12.
- P. Fréon, P. Cury, L. Shannon, and C. Roy. Sustainable exploitation of small pelagic fish stocks challenged by environmental and ecosystems changes: a review. *Bulletin of Marine Science*, 76(2):385–462, 2005.

- L.-L. Fu. *Determining Ocean Circulation and Sea Level from Satellite Altimetry: Progress and Challenges*. In Barale et al. [2010], pages 147–163. ISBN 978-90-481-8680-8.
- L. A. Fuiman and R. G. Werner, editors. *Fishery Science*. Blackwell Publishing, Osney Mead, Oxford, UK, 1 edition, 2002.
- R. Furrer and S. R. Sain. *spam*: A sparse matrix *R* package with emphasis on MCMC methods for Gaussian Markov Random Fields. *Journal of Statistical Software*, 36(10):1–25, 2010. URL <http://www.jstatsoft.org/v36/i10/>.
- S. A. Garver and D. A. Siegel. Inherent optical property inversion of ocean color spectra and its biogeochemical interpretation: I. time series from the Sargasso Sea. *Journal of Geophysical Research*, 102:18607–18625, 1997. doi: 10.1029/96JC03243.
- A. Gelman. Prior distributions for variance parameters in hierarchical models (comment on article by Browne and Draper). *Bayesian Analysis*, 1(3):515–534, 09 2006. doi: 10.1214/06-BA117A.
- A. Gelman and J. Hill. *Data Analysis Using Regression and Multilevel/Hierarchical Models*. Cambridge University Press, New York, USA, 1 edition, 2007.
- A. Gelman, J. B. Carlin, H. S. Stern, and D. B. Rubin. *Bayesian Data Analysis*. Chapman & Hall/CRC, Boca Raton, USA, 2 edition, 2004.
- A. Gelman, A. Jakulin, M. G. Pittau, and Y. S. Su. A weakly informative default prior distribution for logistic and other regression models. *The Annals of Applied Statistics*, 2:1360–1383, 2008. doi: 10.1214/08-AOAS191.
- A. Gelman, Y. S. Su, M. Yajima, J. Hill, M. G. Pittau, J. Kerman, and T. Zheng. *arm: Data Analysis Using Regression and Multilevel/Hierarchical Models. R package version 1.2-9*, 2009.
- C. L. Gentemann, F. J. Wentz, M. Brewer, K. Hilburn, and D. Smith. *Passive Microwave Remote Sensing of the Oceans: An Overview*. In Barale et al. [2010], pages 13–33. ISBN 978-90-481-8680-8.
- S. J. Godsill, A. Doucet, and M. West. Monte Carlo smoothing for nonlinear time series. *Journal of the American Statistical Association*, 99(465):156–168, 2004. doi: 10.1198/016214504000000151.
- S. A. Good, G. K. Corlett, J. J. Remedios, E. J. Noyes, and D. T. Llewellyn-Jones. The global trend in sea surface temperature from 20 years of Advanced Very-High Resolution Radiometer data. *J Clim*, 20:1255–1264, 2007. doi: 10.1175/JCLI4049.1.
- H. R. Gordon. Oceanography from space. revisited. In Barale et al. [2010], chapter *Some reflections on Thirty-Five Years of Ocean Color Remote Sensing*, pages 289–306. ISBN 978-90-481-8680-8.
- N. J. Gordon, D. J. Salmond, and A. F. M. Smith. Novel approach to nonlinear/non-Gaussian Bayesian state estimation. *Radar and Signal Processing, IEE Proceedings F*, 140(2):107–113, Apr 1993. doi: 10.1049/ip-f-2.1993.0015.
- V. Gouretsky and K. P. Koltermann. How much is the ocean really warming? *Geophys Res Lett*, 34:L01610, 2007. doi: 10.1029/2006GL027834.
- W. W. Gregg and N. W. Casey. Sampling biases in MODIS and SeaWiFS ocean chlorophyll data. *Remote Sensing of the Environment*, 111:25–35, 2007. doi: 10.1016/j.rse.2007.03.008.
- W. W. Gregg and M. E. Conkright. Decadal changes in global ocean chlorophyll. *Geophysical Research Letters*, 29:1730, 2002. doi: 10.1029/2002GL014689.
- W. W. Gregg, N. W. Casey, and C. R. McClain. Recent trends in global ocean chlorophyll. *Geophysical Research Letters*, 32:L03606, 2005. doi: 10.1029/2004GL021808.
- R. Grigoriev, editor. *Transport and Mixing in Laminar Flows: From Microfluidics to Oceanic Currents*. Wiley-VCH Verlag GmbH & Co. KGaA, Weinheim, Germany, 1 edition, 2012.
- H. Haario, E. Saksman, and J. Tamminen. An adaptive Metropolis algorithm. *Bernoulli*, 7(2):223–242, 2001.
- H. Haario, E. Saksman, and J. Tamminen. Componentwise adaptation for high dimensional MCMC. *Computational Statistics*, 20(2):265–273, 2005. doi: 10.1007/BF02789703.

- S. Hakkinen and P. B. Rhines. Decline of subpolar North Atlantic gyre circulation during the 1990s. *Science*, 304:555–559, 2004. doi: 10.1126/science.1094917.
- S. Hakkinen and P. B. Rhines. Shifting surface currents in the northern North Atlantic Ocean. *J Geophys Res*, 114:C04005, 2009. doi: 10.1029/2008JC004883.
- G. Haller and G. Yuan. Lagrangian coherent structures and mixing in two-dimensional turbulence. *Physica D: Nonlinear Phenomena*, 147(3–4):352–370, 2000. doi: 10.1016/S0167-2789(00)00142-1.
- B. S. Halpern, S. Walbridge, K. A. Selkoe, C. V. Kappel, F. Micheli, C. D’Agrosa, J. F. Bruno, K. S. Casey, C. Ebert, H. E. Fox, R. Fujita, D. Heinemann, H. S. Lenihan, E. M. P. Madin, M. T. Perry, E. R. Selig, M. Spalding, R. Steneck, and R. Watson. A global map of human impact on marine ecosystems. *Science*, 319:948–952, 2008. doi: 10.1126/science.1149345.
- J. Hansen, M. Sato, R. Ruedy, K. Lo, D. W. Lea, and M. Medina-Elizade. Global temperature change. *Proc Natl Acad Sci USA*, 103:14288–14293, 2006. doi: 10.1073/pnas.0606291103.
- J. Hansen, R. Ruedy, M. Sato, and K. Lo. Global surface temperature change. *Reviews of Geophysics*, 48:RG4004, 2010. doi: 10.1029/2010RG000345.
- C. S. Harrison and G. A. Glatzmaier. Lagrangian coherent structures in the California Current System – sensitivities and limitations. *Geophysical & Astrophysical Fluid Dynamics*, 106(1):22–44, 2012. doi: 10.1080/03091929.2010.532793.
- C. S. Harrison, D. A. Siegel, and S. Mitarai. Filamentation and eddy-eddy interactions in marine larval accumulation and transport. *Marine Ecology Progress Series*, 472:27–44, 2013. doi: 10.3354/meps10061.
- S. Henson, H. Cole, C. Beaulieu, and A. Yool. The impact of global warming on seasonality of ocean primary production. *Biogeosciences*, 10(6):4357–4369, 2013. doi: 10.5194/bg-10-4357-2013.
- S. A. Henson, J. P. Dunne, and J. L. Sarmiento. Decadal variability in North Atlantic blooms. *Journal of Geophysical Research*, 114:C04013, 2009. doi: 10.1029/2008JC005139.
- S. A. Henson, J. L. Sarmiento, J. P. Dunne, L. Bopp, I. Lima, S. C. Doney, J. John, and C. Beaulieu. Detection of anthropogenic climate change in satellite records of ocean chlorophyll and productivity. *Biogeosciences*, 7(2):621–641, 2010. doi: 10.5194/bg-7-621-2010.
- J. G. Hiddink and R. Ter Hofstede. Climate induced increases in species richness of marine fishes. *Global Change Biology*, 14:453–460, 2008. doi: 10.1111/j.1365-2486.2007.01518.x.
- R. H. Hijazi and R. W. Jernigan. Modelling compositional data using Dirichlet regression models. *Journal of Applied Probability and Statistics*, 4:10–17, 2009.
- R. Hilborn and M. Mangel. *The Ecological Detective. Confronting Models with Data*, volume 28 of *Monographs in Population Biology*. Princeton University Press, Princeton, USA, 1 edition, 1997.
- J. Hjort. Fluctuations in the great fisheries of northern Europe viewed in the light of biological research. *Rapports et Procs-Verbaux des Reunions, Conseil International pour l’Exploration de la Mer*, 20:1–228, 1914.
- P. D. Hoff. *A First Course in Bayesian Statistical Methods*. Springer Texts in Statistics, Breinigsville, PA USA, 1 edition, 2009.
- R. Holman and M. C. Haller. Remote sensing of the nearshore. *Annual Review of Marine Science*, 5(1):95–113, 2013. doi: 10.1146/annurev-marine-121211-172408.
- S. Honjo. Seasonality and interaction of biogenic and lithogenic particulate flux at the Panama Basin. *Science*, 218:883–884, 1982. doi: 10.1126/science.218.4575.883.
- R. R. Hood, V. J. Coles, and D. G. Capone. Modeling the distribution of *trichodesmium* and nitrogen fixation in the atlantic ocean. *Journal of Geophysical Research*, 109:C06006, 2004. doi: doi:10.1029/2002JC001753.
- E. D. Houde. Mortality. In Fuiman and Werner [2002], pages 64–87.
- E. D. Houde. Emerging from Hjort’s shadow. *Journal of the Northwest Atlantic Fishery Science*, 41:53–70, 2008. doi: 10.2960/J.v41.m634.

- C. Hu, Z. Lee, and B. Franz. Chlorophyll *a* algorithms for oligotrophic oceans: A novel approach based on three-band reflectance difference. *Journal of Geophysical Research*, 117:C01011, 2012. doi: 10.1029/2011JC007395.
- J. W. Hurrell and C. Deser. North Atlantic climate variability: The role of the North Atlantic Oscillation. *Journal of Marine Systems*, 78:28–41, 2009a. doi: 10.1016/j.jmarsys.2008.11.026.
- J. W. Hurrell and C. Deser. North atlantic climate variability: The role of the north atlantic oscillation. *J. Marine Syst.*, 78:28–41, 2009b. doi: 10.1016/j.jmarsys.2008.11.026.
- J. W. Hurrell and R. R. Dickson. *Climatic Variability over the North Atlantic*. In N. C. Stenseth, G. Ottersen, J. W. Hurrell, and A. Belgrano, editors, *Marine Ecosystems and Climate Variation*, pages 15–31. Oxford University Press, Oxford, UK, 2005.
- HYDRO. *Discharge of river Garonne at Tonneins, produced by DREAL Midi-Pyrénées*. Banque HYDRO, Ministère de L’Écologie, du Développement Durable et de L’Énergie. Accessed Nov 2013, 2013. URL <http://www.hydro.eaufrance.fr>.
- L. Ibaibarriaga, C. Fernández, A. Uriarte, and B. A. Roel. A two-stage biomass dynamic model for Bay of Biscay anchovy: a Bayesian approach. *ICES Journal of Marine Science: Journal du Conseil*, 65(2):191–205, 2008. doi: 10.1093/icesjms/fsn002.
- L. Ibaibarriaga, C. Fernández, and A. Uriarte. Gaining information from commercial catch for a Bayesian two-stage biomass dynamic model: application to Bay of Biscay anchovy. *ICES Journal of Marine Science: Journal du Conseil*, 68(7):1435–1446, 2011. doi: 10.1093/icesjms/fsr094.
- L. Ibaibarriaga, A. Uriarte, U. Laconcha, M. Bernal, M. Santos, M. Chifflet, and X. Irigoién. Modelling the spatio-temporal distribution of age-1 Bay of Biscay anchovy (*Engraulis encrasicolus*) at spawning time. *Scientia Marina*, 77(3):461–472, 2013. doi: 10.3989/scimar.03851.05C.
- ICCAT. *Sample fishing statistics and fish sizes: Task II Catch & Effort Data Base*. Version Nov 2013, 2013. URL <http://www.iccat.int>.
- ICES. *Report of the Working Group on Acoustic and Egg Surveys for Sardine and Anchovy in ICES Areas VIII and IX (WGACEGG)*. ICES CM 2009/LRC:20, 16-29 November 2009, Lisbon, Portugal, 2009.
- ICES. *Report of the Working Group on Southern Horse Mackerel, Anchovy and Sardine (WGHANSA)*. ICES CM 2012/ACOM:16, 23-28 June 2012, Azores (Horta), Portugal, 2012.
- ICES. *Stock Assessment Summary Database*. Version Apr 2013, 2013. URL <http://www.ices.dk>.
- IHO. *Limits of Oceans and Seas*, volume 23 of *Special Publication*. International Hydrographic Organization, Monte Carlo, Monaco, 3 edition, 1953.
- T. D. Iles and M. Sinclair. Atlantic herring: Stock discreteness and abundance. *Science*, 215(4533):627–633, 1982. doi: 10.1126/science.215.4533.627.
- IOCCG. Why ocean colour? the societal benefits of ocean-colour technology. Reports of the International Ocean-Colour Coordinating Group 7, IOCCG, Dartmouth, Canada, 2008.
- IOCCG. Mission requirements for future ocean-colour sensors. Reports of the International Ocean-Colour Coordinating Group 13, IOCCG, Dartmouth, Canada, 2012a.
- IOCCG. Ocean-colour observations from a geostationary orbit. Reports of the International Ocean-Colour Coordinating Group 12, IOCCG, Dartmouth, Canada, 2012b.
- IPCC. *Climate Change 2007: The Physical Science Basis. Contribution of Working Group I to the Fourth Assessment Report of the Intergovernmental Panel on Climate Change [Solomon, S, D Qin, M Manning, Z Chen, M Marquis, KB Averyt, M Tignor and HL Miller (eds.)]*. Cambridge University Press, Cambridge, UK and New York, NY, USA, 2007.
- X. Irigoién, K. J. Flynn, and R. P. Harris. Phytoplankton blooms: a 'loophole' in microzooplankton grazing impact? *Journal of Plankton Research*, 27(4):313–321, 2005. doi: 10.1093/plankt/fbi011.

- X. Irigoien, Ø. Fiksen, U. Cotano, A. Uriarte, P. Alvarez, H. Arribalaga, G. Boyra, M. Santos, Y. Sagarminaga, P. Otheguy, E. Etxebeste, L. Zarauz, I. Artetxe, and L. Motos. Could Biscay Bay anchovy recruit through a spatial loophole? *Progress in Oceanography*, 74:132–148, 2007.
- A. J. Irwin and M. J. Oliver. Are ocean deserts getting larger? *Geophysical Research Letters*, 36:L18609, 2009. doi: 10.1029/2009GL039883.
- J. H. Connell. Diversity and the coevolution of competitors, or the Ghost of Competition Past. *Oikos*, 35(2): 131–138, 1980. doi: 10.2307/3544421.
- J. Jackson and J. Jacquet. *The shifting baselines syndrome: perception, deception, and the future of our oceans*. In Christensen and Maclean [2011], chapter 9, pages 128–141.
- J. B. C. Jackson. Ecological extinction and evolution in the brave new ocean. *Proceedings of the National Academy of Sciences*, 105(Suppl. 1):11458–11465, 2008. doi: 10.1073/pnas.0802812105.
- J. B. C. Jackson, M. X. Kirby, W. H. Berger, K. A. Bjoerndal, L. W. Botsford, B. J. Bourque, R. H. Bradbury, R. Cooke, J. Erlandson, J. A. Estes, T. P. Hughes, S. Kidwell, C. B. Lange, H. S. Lenihan, J. M. Pandolfi, C. H. Peterson, R. S. Steneck, M. J. Tegner, and R. R. Warner. Historical overfishing and the recent collapse of coastal ecosystems. *Science*, 293(5530):629–637, 2001. doi: 10.1126/science.1059199.
- P. Jönsson and L. Eklundh. Seasonality extraction by function fitting to time-series of satellite sensor data. *IEEE Transactions on Geoscience and Remote Sensing*, 10:1824–1832, 2002. doi: 10.1109/TGRS.2002.802519.
- K. S. Johnson, J. A. Needoba, S. C. Riser, and W. J. Showers. Chemical sensor networks for the aquatic environment. *Chemical Reviews*, 107(2):623–640, 2007. doi: 10.1021/cr050354e.
- K. S. Johnson, W. M. Berelson, E. S. Boss, Z. Chase, H. Claustre, S. R. Emerson, N. Gruber, A. Körtzinger, M. J. Perry, and S. C. Riser. Observing biogeochemical cycles at global scales with profiling floats and gliders: Prospects for a global array. *Oceanography*, 22(3):216–225, 2009. doi: 10.5670/oceanog.2009.81.
- M. Kahru, V. Brotas, M. Manzano-Sarabia, and B. G. Mitchell. Are phytoplankton blooms occurring earlier in the Arctic? *Global Change Biology*, 17:1733–1739, 2011. doi: 10.1111/j.1365-2486.2010.02312.x.
- E. T. Kai, V. Rossi, J. Sudre, H. Weimerskirch, C. Lopez, E. Hernandez-Garcia, F. Marsac, and V. Garçon. Top marine predators track Lagrangian coherent structures. *Proceedings of the National Academy of Sciences*, 106(20):8245–8250, 2009. doi: 10.1073/pnas.0811034106.
- N. Kantas, A. Doucet, S. S. Singh, and J. Maciejowski. An overview of sequential Monte Carlo methods for parameter estimation on general state space models. In E. Walter, editor, *15th IFAC Symp. Syst. Identification 15 (Saint Malo, France)*. International Federation of Automatic Control, 2009.
- A. B. Kara, P. A. Rochford, and H. E. Hurlbert. An optimal definition for ocean mixed layer depth. *J Geophys Res*, 105(C7):16803–16821, 2000.
- B. Karrasch, H. G. Hoppe, S. Ullrich, and S. Podewski. The role of mesoscale hydrography on microbial dynamics in the northeast atlantic: results of a spring bloom experiment. *J Mar Res*, 54:99–122, 1996. doi: 10.1357/0022240963213420.
- K. A. Kilpatrick, G. P. Podesta, and R. Evans. Overview of the NOAA/NASA Advanced Very High Resolution Radiometer Pathfinder algorithm for sea surface temperature and associated matchup database. *J Geophys Res*, 106(C5):9179–9197, 2001. doi: 10.1029/1999JC000065.
- R. King, B. J. T. Morgan, O. Gimenez, and S. P. Brooks. *Bayesian Analysis for Population Ecology*. Chapman & Hall/CRC Interdisciplinary Statistics, Boca Raton, USA, 1 edition, 2009.
- P. Koeller, C. Fuentes-Yaco, T. Platt, S. Sathyendranath, A. Richards, P. Ouellet, D. Orr, U. Skúladóttir, K. Wieland, L. Savard, and M. Aschan. Basin-scale coherence in phenology of shrimps and phytoplankton in the North Atlantic Ocean. *Science*, 324:791–793, 2009. doi: 10.1126/science.1170987.
- C. Koutsikopoulos and B. Le Cann. Physical processes and hydrological structures related to the Bay of Biscay anchovy. *Scientia Marina*, 60(Suppl. 2):9–19, 1996.

- T. Kristiansen, K. F. Drinkwater, R. G. Lough, and S. Sundby. Recruitment variability in North Atlantic cod and match-mismatch hypothesis. *PLoS ONE*, 6(3):e17456, 2011. doi: 10.1371/journal.pone.0017456.
- G. Lagerloef and J. Font. SMOS adn aquarius/SAC-D missions: The era of spaceborne salinity measurements is about to begin. In Barale et al. [2010], pages 35–58. ISBN 978-90-481-8680-8.
- R. Lasker. Field criteria for survival of anchovy larvae: the relation between inshore chlorophyll maximum layers and successful first feeding. *Fishery Bulletin*, 73(3):453–462, 1975.
- R. Lasker. The relationship between oceanographic conditions and larval anchovy food in the California Current: identification of factors contributing to recruitment failure. *Rapports et Procès-verbaux des Réunions, Conseil International pour l'Exploration de la Mer*, 173:212–230, 1978.
- S. P. Lawrence, D. T. Llewellyn-Jones, and S. J. Smith. The measurement of climate change using data from the Advanced Very High Resolution and Along Track Scanning Radiometers. *J Geophys Res*, 109:C08017, 2004. doi: 10.1029/2003JC002104.
- E. A. Laws and T. T. Bannister. Nutrient- and light-limited growth of *thalassiosira fluviatilis* in continuous culture, with implications for phytoplankton growth in the ocean. *Limnol Oceanogr*, 25:457–473, 1980.
- C. Le Quéré, R. J. Andres, T. Boden, T. Conway, R. A. Houghton, J. I. House, G. Marland, G. P. Peters, G. van der Werf, A. Ahlström, R. M. Andrew, L. Bopp, J. G. Canadell, P. Ciais, S. C. Doney, C. Enright, P. Friedlingstein, C. Huntingford, A. K. Jain, C. Jourdain, E. Kato, R. F. Keeling, K. Klein Goldewijk, S. Levis, P. Levy, M. Lomas, B. Poulter, M. R. Raupach, J. Schwinger, S. Sitch, B. D. Stocker, N. Viovy, S. Zaehle, and N. Zeng. The global carbon budget 1959–2011. *Earth System Science Data Discussions*, 5(2):1107–1157, 2012. doi: 10.5194/essdd-5-1107-2012. URL <http://www.earth-syst-sci-data-discuss.net/5/1107/2012/>.
- P. Y. Le Traon. From satellite altimetry to Argo and operational oceanography: three revolutions in oceanography. *Ocean Science*, 9(5):901–915, 2013. doi: 10.5194/os-9-901-2013. URL <http://www.ocean-sci.net/9/901/2013/>.
- P. Y. Le Traon, F. Nadal, and N. Ducet. An improved mapping method of multisatellite altimeter data. *J. Atmos. Oceanic Tech.*, 15:522–534, 1998. doi: 10.1126/science.1170987.
- Y. Lehahn, F. d’Ovidio, M. Lévy, and E. Heifetz. Stirring of the northeast Atlantic spring bloom: A Lagrangian analysis based on multisatellite data. *J. Geophys. Res.*, 112:C08005, 2007. doi: 10.1029/2006JC003927.
- R. Letelier, L. L. Bidigare, D. V. Hebel, M. Ondrusek, C. D. Winn, and D. M. Karl. Temporal variability of phytoplankton community structure based on pigment analysis. *Limnol Oceanogr*, 38:1420–1437, 1993.
- S. Levitus. *Climatological Atlas of the World Ocean*. Geophysical Fluid Dynamics Laboratory, Princeton, NJ, USA, 1982. ISBN 9780318187334.
- S. Levitus, J. Antonov, and T. Boyer. Warming of the world ocean, 1955–2003. *Geophys Res Lett*, 32:L02604, 2005. doi: 10.1029/2004GL021592.
- S. Levitus, J. I. Antonov, T. P. Boyer, R. A. Locarnini, H. E. García, and A. V. Mishonov. Global ocean heat content 1955–2008 in light of recently revealed instrumentation problems. *Geophys Res Lett*, 36:L07608, 2009. doi: 10.1029/2008GL037155.
- D. B. Lindenmayer and G. E. Likens. *Effective Ecological Monitoring*. CSIRO Publishing, Collingwood, VIC, Australia, 2010.
- D. B. Lindenmayer, G. E. Likens, C. J. Krebs, and R. J. Hobbs. Improved probability of detection of ecological “surprises”. *Proceedings of the National Academy of Sciences*, 107(51):21957–21962, 2010. doi: 10.1073/pnas.1015696107.
- E. J. Lindstrom and N. Maximenko. The future of oceanography from space: Introduction to the special issue. *Oceanography*, 23(4):12–13, 2010. doi: 10.5670/oceanog.2010.01.
- E. Litchman, C. A. Klausmeier, J. R. Miller, O. M. Schofield, and P. G. Falkowski. Multi-nutrient, multi-group model of present and future oceanic phytoplankton communities. *Biogeosci*, 3:585–606, 2006.

- W. T. Liu and K. B. Katsaros. *Air-Sea Fluxes from Satellite Data*. In Siedler et al. [2001], pages 173–179.
- S. R. Loarie, P. B. Duffy, H. Hamilton, G. P. Asner, C. B. Field, and D. D. Ackerly. The velocity of climate change. *Nature*, 462:1052–1055, 2009. doi: 10.1038/nature08649.
- A. R. Longhurst. *Ecological Geography of the Sea*. Academic Press, London, UK, 2 edition, 2007.
- K. Lorenzen. Fish population regulation beyond "stock and recruitment": the role of density-dependent growth in the recruited stock. *Bulletin of Marine Science*, 83(1):181–196, 2008.
- B. R. MacKenzie. Turbulence, larval fish ecology and fisheries recruitment: a review of field studies. *Oceanologica Acta*, 23(4):357–375, 2000. doi: 10.1016/S0399-1784(00)00142-0.
- B. R. MacKenzie, T. Miller, S. Cyr, and W. C. Leggett. Evidence for a dome-shaped relationship between turbulence and larval fish ingestion rate. *Limnology and Oceanography*, 39(8):1790–1799, 1994.
- A. Mahadevan, E. D'Asaro, C. Lee, and M. J. Perry. Eddy-driven stratification initiates North Atlantic spring phytoplankton blooms. *Science*, 337(6090):54–58, 2012. doi: 10.1126/science.1218740.
- S. Maritorena, D. A. Siegel, and A. R. Peterson. Optimization of a semianalytical ocean color model for global-scale applications. *Applied Optics*, 41:2705–2714, 2002. doi: 10.1364/AO.41.002705.
- S. Maritorena, O. H. F. d'Andon, A. Magin, and D. A. Siegel. Merged satellite ocean color data products using a bio-optical model: Characteristics, benefits and issues. *Remote Sensing of the Environment*, 114:1791–1804, 2010. doi: 10.1016/j.rse.2010.04.002.
- E. Martinez, D. Antoine, F. D'Ortenzio, and B. Gentili. Climate-driven basin-scale decadal oscillations of oceanic phytoplankton. *Science*, 326(5957):1243–1256, 2009. doi: 10.1126/science.1177012.
- E. Martinez, D. Antoine, F. D'Ortenzio, and C. de Boyer Montegut. Phytoplankton spring and fall blooms in the North Atlantic in the 1980s and 2000s. *J. Geophys. Res.*, 116:C11029, 2011. doi: 10.1029/2010JC006836.
- J. Massé. Acoustic observations in the Bay of Biscay: schooling, vertical distribution, species assemblages and behaviour. *Scientia Marina*, 60(Suppl. 2):227–234, 1996.
- M. K. McAllister and G. P. Kirkwood. Bayesian stock assessment: a review and example application using the logistic model. *ICES Journal of Marine Science: Journal du Conseil*, 55(6):1031–1060, 1998. doi: 10.1006/jmsc.1998.0425.
- C. R. McClain. A decade of satellite ocean color observations. *Annu Rev Mar Sci*, 1:19–42, 2009. doi: 10.1146/annurev.marine.010908.163650.
- C. R. McClain, W. E. Esaias, G. C. Feldman, J. Elrod, D. Endres, J. Firestone, M. Darzi, R. Evans, and J. Brown. Physical and biological processes in the north atlantic during the first garp global experiment. *Journal of Geophysical Research: Oceans*, 95(C10):18027–18048, 1990. doi: 10.1029/JC095iC10p18027.
- C. R. McClain, G. C. Feldman, and S. B. Hooker. An overview of the SeaWiFS project and strategies for producing a climate research quality global ocean bio-optical time series. *Deep Sea Res Part II Top Stud Oceanogr*, 51:5–42, 2004a. doi: doi:10.1016/j.dsr2.2003.11.001.
- C. R. McClain, S. R. Signorini, and J. R. Christian. Subtropical gyre variability observed by ocean-color satellites. *Deep-Sea Res Part II Top Stud Oceanogr*, 51:281–301, 2004b. doi: 10.1016/j.dsr2.2003.08.002.
- G. Meister, B. A. Franz, E. J. Kwiatkowska, and C. R. McClain. Corrections of the calibration of MODIS Aqua ocean color bands derived from SeaWiFS data. *IEEE Transactions on Geoscience and Remote Sensing*, 50: 310–319, 2012. doi: 10.1109/TGRS.2011.2160552.
- G. Mertz and R. A. Myers. An extended cohort analysis: incorporating the effect of seasonal catches. *Canadian Journal of Fisheries and Aquatic Sciences*, 53(1):159–163, 1996. doi: 10.1139/f95-156.
- P. J. Michaels, R. C. B. Jr, R. S. Vose, and P. C. Knappenberger. Analysis of trends in the variability of daily and monthly historical temperature measurements. *Clim Res*, 10:27–33, 1998. doi: 10.3354/cr010027.
- R. B. Millar and R. Meyer. Non-linear state space modelling of fisheries biomass dynamics by using Metropolis-Hastings within-Gibbs sampling. *Journal of the Royal Statistical Society: Series C (Applied Statistics)*, 49(3):

- 327–342, 2000. doi: 10.1111/1467-9876.00195.
- R. F. Milliff, J. Fiechter, W. B. Leeds, R. Herbe, C. K. Wikle, M. B. Hooten, A. M. Moore, T. M. Powell, and J. Brown. Uncertainty management in coupled physical-biological lower trophic level ocean ecosystem models. *Oceanography*, 26(4):98–115, 2013. doi: 10.5670/oceanog.2013.78.
- J. J. Millspaugh and R. A. Gitzen. Statistical danger zone. *Frontiers in Ecology and the Environment*, 8(10):515, 2010. doi: 10.1890/10.WB.26.
- P. C. D. Milly, A. Cazenave, and C. Genero. Contribution of climate-driven change in continental water storage to recent sea-level rise. *Proc Natl Acad Sci USA*, 100:13158–13161, 2003. doi: 10.1073/pnas.2134014100.
- G. A. Milne, W. R. Gehrels, C. W. Hughes, and M. E. Tamisiea. Identifying the causes of sea-level change. *Nat Geosci*, 2:471–478, 2009. doi: 10.1038/ngeo544.
- J. Morales, V. Stuart, T. Platt, and S. Sathyendranath. *Handbook of Satellite Remote Sensing Image Interpretation: Applications for Marine Living Resources Conservation and Management*. EU PRESPO Project and the International Ocean-Colour Coordinating Group (IOCCG), 2010. URL <http://www.ioccg.org/handbook.html>.
- L. Motos. *Estimación de la biomasa desovante de la población de anchoa del Golfo de Vizcaya (*Engraulis encrasicolus*) a partir de su producción de huevos. Bases metodológicas y su aplicación*. PhD thesis, University of the Basque Country, 1994.
- L. Motos. Reproductive biology and fecundity of the Bay of Biscay anchovy population (*Engraulis encrasicolus* L.). *Scientia Marina*, 60(Suppl. 2):195–207, 1996.
- L. Motos, A. Uriarte, and V. Valencia. The spawning environment of the Bay of Biscay anchovy (*Engraulis encrasicolus* L.). *Scientia Marina*, 60(Suppl. 2):117–140, 1996.
- E. Neuwirth. *RCColorBrewer: ColorBrewer palettes*, 2011. URL <http://CRAN.R-project.org/package=RCColorBrewer>. R package version 1.0-5.
- R. J. Nicholls and A. Cazenave. Sea-level rise and its impact on coastal zones. *Science*, 328:1517–1520, 2010. doi: 10.1126/science.1185782.
- D. Nychka, R. Furrer, and S. Sain. *fields: Tools for spatial data*, 2013. URL <http://CRAN.R-project.org/package=fields>. R package version 6.9.1.
- A. W. Omta, S. Dutkiewicz, and M. J. Follows. Dependence of the ocean-atmosphere partitioning of carbon on temperature and alkalinity. *Global Biogeochem Cycles*, 25:GB1003, 2011. doi: 10.1029/2010GB003839.
- J. E. O'Reilly, S. Maritorena, D. A. Siegel, M. C. O'Brien, D. Toole, B. G. Mitchell, M. Kahru, F. P. Chavez, P. Strutton, G. F. Cota, S. B. Hooker, C. R. McClain, K. L. Carder, F. Müller-Karger, L. Harding, A. Magnuson, D. Phinney, G. F. Moore, J. Aiken, K. R. Arrigo, R. Letelier, and M. Culver. *Ocean color chlorophyll a algorithms for SeaWiFS, OC2, and OC4: Version 4*. In J. E. O'Reilly, S. Maritorena, M. C. O'Brien, D. A. Siegel, D. Toole, D. Menzies, R. C. Smith, J. L. Muller, B. G. Mitchell, M. Kahru, F. P. Chavez, P. Strutton, G. F. Cota, S. B. Hooker, C. R. McClain, K. L. Carder, F. Müller-Karger, L. Harding, A. Magnuson, D. Phinney, G. F. Moore, J. Aiken, K. R. Arrigo, R. Letelier, and M. Culver, editors, *SeaWiFS Postlaunch Calibration and Validation Analyses, Part 3. NASA Tech. Memo. 2000-206892, Vol. 11, S.B. Hooker and E.R. Firestone, (eds.)*, NASA Goddard Space Flight Center, 49 pp., pages 9–23. NASA, Goddard Space Flight Center, 2000.
- OSB-NRC. *50 Years of Ocean Discovery: National Science Foundation 1950-2000*. Ocean Studies Board, National Research Council, The National Academies Press, Washington, D.C., USA, 2000. ISBN 9780309063982. URL http://www.nap.edu/openbook.php?record_id=9702.
- K. Parker. A direct method for estimating northern anchovy, *Engraulis mordax*, spawning biomass. *Fishery Bulletin*, 78(2):541–544, 1980.
- C. Parmesan. Ecological and evolutionary responses to recent climate change. *Ann Rev Ecol Evol Syst*, 37: 637–669, 2006. doi: 10.1146/annurev.ecolsys.37.091305.110100.
- C. Parmesan. Influences of species, latitudes and methodologies on estimates of phenological response to

- global warming. *Global Change Biology*, 13:1860–1872, 2007. doi: 10.1111/j.1365-2486.2007.01404.x.
- J. Parslow, N. Cressie, E. P. Campbell, E. Jones, and L. Murray. Bayesian learning and predictability in a stochastic nonlinear dynamical model. *Ecological Applications*, 23(4):679–698, 2013. doi: 10.1890/12-0312.1.
- D. Pauly. An eponym for Reuben Lasker. *Fishery Bulletin*, 87(3):383–384, 1989.
- T. Peacock and G. Haller. Lagrangian coherent structures: The hidden skeleton of fluid flows. *Physics Today*, 66(2):41–47, 2013. doi: 10.1063/PT.3.1886.
- E. J. Pebesma and R. S. Bivand. Classes and methods for spatial data in *R*. *R News*, 5(2):NA, 2005. URL <http://cran.r-project.org/doc/Rnews>.
- M. J. Perry. Assessing marine primary production from space. *BioScience*, 36(7):461–467, 1986. doi: 10.1126/science.235.4786.354.
- R. M. Peterman and M. J. Bradford. Wind speed and mortality rate of a marine fish, the northern anchovy (*Engraulis mordax*). *Science*, 235(4786):354–356, 1987. doi: 10.1126/science.235.4786.354.
- G. W. Peters, G. R. Hosack, and K. R. Hayes. Ecological non-linear state space model selection via adaptive particle Markov chain Monte Carlo (AdPMCMC). page 1005.2238, 2010. URL <http://arxiv.org/abs/1005.2238>.
- J. Peñuelas and I. Filella. Responses to a warming world. *Science*, 294:793–795, 2001. doi: 10.1126/science.1066860.
- C. J. Philippart, R. Anadón, R. Danovaro, J. W. Dippner, K. F. Drinkwater, S. J. Hawkins, T. Oguz, G. O’Sullivan, and P. C. Reid. Impacts of climate change on the european marine and coastal environment. Marine Board Position Paper 9, European Science Foundation, 2007.
- C. J. Philippart, R. Anadón, R. Danovaro, J. W. Dippner, K. F. Drinkwater, S. J. Hawkins, G. O’Sullivan, T. Oguz, and P. C. Reid. Impacts of climate change on european marine ecosystems: observations, expectations and indicators. *J Exp Mar Biol Ecol*, 400:52–69, 2011. doi: 10.1016/j.jembe.2011.02.023.
- M. H. Pickett and J. D. Paduan. Ekman transport and pumping in the California Current based on the U.S. Navy’s high-resolution atmospheric model (COAMPS). *Journal of Geophysical Research: Oceans*, 108(C10):3327, 2003. doi: 10.1029/2003JC001902.
- M. H. Pickett and F. B. Schwing. Evaluating upwelling estimates off the west coasts of North and South America. *Fisheries Oceanography*, 15(3):256–269, 2006. doi: 10.1111/j.1365-2419.2005.00400.x.
- D. Pierce. *ncdf: Interface to Unidata netCDF data files*, 2011. URL <http://CRAN.R-project.org/package=ncdf>. R package version 1.6.6.
- M. L. Pinsky, B. Worm, M. J. Fogarty, J. L. Sarmiento, and S. A. Levin. Marine taxa track local climate velocities. *Science*, 341(6151):1239–1242, 2013. doi: 10.1126/science.1239352.
- B. Planque and L. Buffaz. Quantile regression models for fish recruitment-environment relationships: four case studies. *Marine Ecology Progress Series*, 357:213–223, 2008. doi: 10.3354/meps07274.
- T. Platt and S. Sathyendranath. Oceanic primary production: Estimation by remote sensing at local and regional scales. *Science*, 241(4873):1613–1620, 1988. doi: 10.1126/science.241.4873.1613.
- T. Platt and S. Sathyendranath. Ecological indicators for the pelagic zone of the ocean from remote sensing. *Remote Sensing of Environment*, 112:3426–3436, 2008. doi: 10.1016/j.rse.2007.10.1016.
- T. Platt, D. F. Bird, and S. Sathyendranath. Critical depth and marine primary productivity. *Proc R Soc B*, 246: 205–217, 1991. doi: 10.1098/rspb.1991.0146.
- T. Platt, C. Fuentes-Yaco, and K. T. Frank. Spring algal bloom and larval fish survival. *Nature*, 423:398–399, 2003. doi: 10.1038/423398b.
- J. J. Polovina and P. A. Woodworth. Declines in phytoplankton cell size in the subtropical oceans estimated from satellite remotely-sensed temperature and chlorophyll, 1998–2007. *Deep Sea Research II – Topical Studies in Oceanography*, 2012. doi: 10.1016/j.dsr2.2012.04.006.
- J. J. Polovina, E. A. Howell, and M. Abecassis. Ocean’s least productive waters are expanding. *Geophys Res*

- Lett*, 35:L03618, 2008. doi: 10.1029/2007GL031745.
- A. Punt and R. Hilborn. Fisheries stock assessment and decision analysis: the Bayesian approach. *Reviews in Fish Biology and Fisheries*, 7(1):35–63, 1997. doi: 10.1023/A:1018419207494.
- T. J. Quinn and R. B. Deriso. *Quantitative Fish Dynamics*. Oxford University Press, New York, USA, 1999.
- R Core Team. *R: A Language and Environment for Statistical Computing*. R Foundation for Statistical Computing, Vienna, Austria, 2013. URL <http://www.R-project.org/>.
- M.-F. Racault, C. Le Quéré, E. Buitenhuis, S. Sathyendranath, and T. Platt. Phytoplankton phenology in the global ocean. *Ecological Indicators*, 14:152–163, 2012. doi: 10.1016/j.ecolind.2011.07.010.
- N. A. Rayner, D. E. Parker, E. B. Horton, C. K. Folland, L. V. Alexander, D. P. Rowell, E. C. Kent, and A. Kaplan. Global analyses of sea surface temperature, sea ice, and night marine air temperature since the late nineteenth century. *J Geophys Res*, 108:4407, 2003. doi: 10.1029/2002JD002670.
- C. Rüegg and J. V. Gael. Math.NET Numerics, Feb. 2014. URL <http://numerics.mathdotnet.com/>.
- P. C. Reid, M. Edwards, H. G. Hunt, and A. J. Warner. Phytoplankton change in the North Atlantic. *Nature*, 391:546, 1998. doi: 10.1038/35290.
- C. S. Reynolds. *Successional Development, Energetics and Diversity in Planktonic Communities*. In T. Abe, S. A. Levin, and M. Higashi, editors, *Biodiversity: An Ecological Perspective*, pages 167–202. Springer, New York, NY, USA, 1997.
- R. W. Reynolds and D. B. Chelton. Comparisons of daily sea surface temperature analyses for 2007–08. *J Clim*, 23:3545–3562, 2010. doi: 10.1175/2010JCLI3294.1.
- R. W. Reynolds, T. M. Smith, C. Liu, D. B. Chelton, K. S. Casey, and M. G. Schlax. Daily high-resolution-blended analyses for sea surface temperature. *Journal of Climate*, 20:5473–5496, 2007. doi: 10.1175/2007JCLI1824.1.
- W. E. Ricker. Stock and recruitment. *Journal of the Fisheries Research Board of Canada*, 11(5):559–623, 1954. doi: 10.1139/f54-039.
- C. M. Risien and D. B. Chelton. A global climatology of surface wind and wind stress fields from eight years of QuikSCAT scatterometer data. *Journal of Physical Oceanography*, 38:2379–2413, 2008. doi: 10.1175/2008JPO3881.1.
- C. P. Robert. *The Bayesian Choice*. Springer Texts in Statistics, New York, USA, 2 edition, 2001.
- C. P. Robert and G. Casella. *Monte Carlo Statistical Methods*. Springer Texts in Statistics, New York, USA, 2 edition, 2004.
- G. O. Roberts and J. S. Rosenthal. Examples of adaptive MCMC. *Journal of Computational and Graphical Statistics*, 18(2):349–367, 2009. doi: 10.1198/jcgs.2009.06134.
- I. S. Robinson. *Measuring the Oceans from Space*. Springer-Praxis Publishers Ltd, Chichester, UK, 2004.
- I. S. Robinson. *Discovering the Ocean from Space: The Unique Applications of Satellite Oceanography*. Springer-Praxis Publishers Ltd, Chichester, UK, 2010.
- S. Rolinski, H. Horn, T. Petzoldt, and L. Paul. Identifying cardinal dates in phytoplankton time series to enable the analysis of long-term trends. *Oecologia*, 153:997–1008, 2007. doi: 10.1007/s00442-007-0783-2.
- B. Rothschild and T. Osborn. Small-scale turbulence and plankton contact rates. *Journal of Plankton Research*, 10(3):465–474, 1988. doi: 10.1093/plankt/10.3.465.
- J. A. Royle and R. M. Dozario. *Hierarchical Modeling and Inference in Ecology. The Analysis of Data from Populations, Metapopulations and Communities*. Academic Press, Elsevier, China, 1 edition, 2008.
- R. R. Rykaczewski and D. M. Checkley. Influence of ocean winds on the pelagic ecosystem in upwelling regions. *Proceedings of the National Academy of Sciences*, 105(6):1965–1970, 2008. doi: 10.1073/pnas.0711777105.
- M. R. P. Sapiano, C. W. Brown, S. Schollaert Uz, and M. Vargas. Establishing a global climatology of marine phytoplankton phenological characteristics. *Journal of Geophysical Research*, 117:C08026, 2012. doi:

- 10.1029/2012JC007958.
- J. L. Sarmiento, T. M. C. Hughes, R. J. Stouffer, and S. Manabe. Simulated response of the ocean carbon cycle to anthropogenic climate warming. *Nature*, 393:245–249, 1998. doi: 10.1038/30455.
- J. L. Sarmiento, R. Slater, R. Barber, L. Bopp, S. C. Doney, A. C. Hirst, J. Kleypas, R. Matear, U. Mikolajewicz, P. Monfray, V. Soldatov, S. A. Spall, and R. Stouffer. Response of ocean ecosystems to climate warming. *Global Biogeochem Cycles*, 18:GB3003, 2004. doi: 10.1029/2003GB002134.
- M. B. Schaefer. Some aspects of the dynamics of populations important to the management of the commercial marine fisheries. *Bulletin of the Inter-American Tropical Tuna Commission*, 1(2):27–56, 1954.
- A. Schmittner. Decline of the marine ecosystem caused by a reduction in the atlantic overturning circulation. *Nature*, 434:628–632, 2005. doi: 10.1038/nature03476.
- W. J. Schmitz Jr. and M. S. McCartney. On the North Atlantic circulation. *Rev Geophys*, 31:29–49, 1993. doi: 10.1029/92RG02583.
- J. Schnute. A general theory for analysis of catch and effort data. *Canadian Journal of Fisheries and Aquatic Sciences*, 42(3):414–429, 1985. doi: 10.1139/f85-057.
- J. T. Schnute. A general framework for developing sequential fisheries models. *Canadian Journal of Fisheries and Aquatic Sciences*, 51(8):1676–1688, 1994. doi: 10.1139/f94-168.
- D. J. Seidel, Q. Fu, W. J. Randel, and T. J. Reichler. Widening of the tropical belt in a changing climate. *Nature Geoscience*, 1:21–24, 2007. doi: 10.1038/ngeo.2007.38.
- E. R. Selig, K. S. Casey, and J. F. Bruno. New insights into global patterns of ocean temperature anomalies: implications for coral reef health and management. *Glob Ecol Biogeogr*, 19:397–411, 2010. doi: 10.1111/j.1466-8238.2009.00522.x.
- M. C. Serreze, M. M. Holland, and J. Stroeve. Perspectives on the arctic's shrinking sea-ice cover. *Science*, 315 (5818):1533–1536, 2007. doi: 10.1126/science.1139426.
- S. C. Shadden. *Lagrangian Coherent Structures*. In Grigoriev [2012], pages 59–89.
- S. C. Shadden, F. Lekien, and J. E. Marsden. Definition and properties of Lagrangian coherent structures from finite-time Lyapunov exponents in two-dimensional aperiodic flows. *Physica D: Nonlinear Phenomena*, 212 (3–4):271–304, 2005. doi: 10.1016/j.physd.2005.10.007.
- A. O. Shelton and M. Mangel. Fluctuations of fish populations and the magnifying effects of fishing. *Proceedings of the National Academy of Sciences*, 108(17):7075–7080, 2011. doi: 10.1073/pnas.1100334108.
- G. Siedler, J. Church, and J. Gould, editors. *Ocean Circulation and Climate. Observing and Modelling the Global Ocean*, volume 77 of *International Geophysics Series*. Academic Press, London, UK, 1 edition, 2001.
- D. A. Siegel, S. C. Doney, and J. A. Yoder. The North Atlantic spring phytoplankton bloom and Sverdrup's Critical Depth Hypothesis. *Science*, 296(5568):730–733, 2002. doi: 10.1126/science.1069174.
- D. A. Siegel, S. Maritorena, N. B. Nelson, and M. J. Behrenfeld. Independence and interdependencies among global ocean color properties: Reassessing the bio-optical assumption. *Journal of Geophysical Research*, 110:C07011, 2005. doi: 10.1029/2004GB002299.
- J. J. Simpson and J. Sharples. *Introduction to the Physical and Biological Oceanography of Shelf Seas*. Cambridge University Press, Cambridge, UK, 2012.
- H. Sletzer and E. Post. Seasons and life cycles. *Science*, 324:886–887, 2009. doi: 10.1126/science.1171542.
- J. B. Smith, S. H. Schneider, M. Oppenheimer, G. W. Yohe, W. Hare, M. D. Mastrandrea, A. Patwardhang, I. Burton, J. Corfee-Morlot, C. H. D. Magadza, H.-M. Füssel, A. B. Pittock, A. Rahman, A. Suarez, and J.-P. van Ypersele. Assessing dangerous climate change through an update of the intergovernmental panel on climate change (ipcc) "reasons for concern". *Proc Natl Acad Sci USA*, 106:4133–4137, 2009. doi: 10.1073/pnas.0812355106.
- F. Sánchez and I. Olaso. Effects of fisheries on the Cantabrian Sea shelf ecosystem. *Ecological Modelling*, 172

- (2–4):151–174, 2004. doi: 10.1016/j.ecolmodel.2003.09.005.
- S. Somarakis, I. Palomera, A. Garcia, L. Quintanilla, C. Koutsikopoulos, A. Uriarte, and L. Motos. Daily egg production of anchovy in european waters. *ICES Journal of Marine Science: Journal du Conseil*, 61(6): 944–958, 2004. doi: 10.1016/j.icesjms.2004.07.018.
- W. Steffen, R. A. Sanderson, P. D. Tyson, J. Jäger, P. A. Matson, B. Moore III, F. Oldfield, K. Richardson, H. J. Schellnhuber, B. L. Turner II, and R. J. Wasson. *Global Change and the Earth System. A Planet Under Pressure*. IGBP series. Springer, Berlin Heidelberg, Germany, 2004. ISBN 978-3-540-26594-8.
- A. R. Stine, P. Huybers, and I. Y. Fung. Changes in the phase of the annual cycle of surface temperature. *Nature*, 457:435–440, 2009. doi: 10.1038/nature07675.
- T. F. Stocker, D. Qin, G. Plattner, M. Tignor, S. K. Allen, J. Boschung, A. Nauels, Y. Xia, V. Bex, and P. M. Midgley, editors. *Climate Change 2013: The Physical Science Basis. Contribution of Working Group I to the Fifth Assessment Report of the Intergovernmental Panel on Climate Change*. Cambridge University Press, Cambridge, UK and New York, NY, USA, 2013.
- L. Stramma, G. C. Johnson, J. Sprintall, and V. Mohrholz. Expanding oxygen-minimum zones in the tropical oceans. *Science*, 320(5876):655–658, 2008. doi: 10.1126/science.1153847.
- J. O. Street, R. J. Carroll, and D. Ruppert. A note on computing robust regression estimates via iteratively reweighted least squares. *Amer Statistician*, 42:152–154, 1988. doi: 10.2307/2684491.
- A. Subramaniam, P. L. Yager, E. J. Carpenter, C. Mahaffey, K. Björkman, S. Cooley, A. B. Kustka, J. P. Montoya, S. A. Sañudo-Wilhelmy, R. Shipe, and D. G. Capone. Amazon river enhances diazotrophy and carbon sequestration in the tropical north atlantic ocean. *Proc Natl Acad Sci USA*, 105(30):10460–10465, 2008. doi: 10.1073/pnas.0710279105.
- H. U. Sverdrup. On conditions for the vernal blooming of phytoplankton. *J Cons Expl Mer*, 18:287–295, 1953. doi: 10.1093/icesjms/18.3.287.
- F. G. Taboada and R. Anadón. Seasonality of North Atlantic phytoplankton from space: impact of environmental forcing on a changing phenology (1998–2012). *Global Change Biology*, 20(3):698–712, 2014. doi: 10.1111/gcb.12352.
- S. J. Thackeray, T. H. Sparks, M. Frederiksen, S. Burthe, P. J. Bacon, J. R. Bell, M. S. Botham, T. M. Brereton, P. W. Bright, L. Carvalho, T. Clutton-Brock, A. Dawson, M. Edwards, J. M. Elliott, R. Harrington, D. Johns, I. D. Jones, J. J. Jones, D. I. Leech, D. B. Roy, W. A. Scott, M. Smith, R. J. Smithers, I. J. Winfield, and S. Wanless. Trophic level asynchrony in rates of phenological change for marine, freshwater and terrestrial environments. *Global Change Biology*, 16:3304–3313, 2010. doi: 10.1111/j.1365-2486.2010.02165.x.
- S. J. Thomalla, N. Fauchereau, S. Swart, and P. M. S. Monteiro. Regional scale characteristics of the seasonal cycle of chlorophyll in the southern ocean. *Biogeosciences*, 8(10):2849–2866, 2011. doi: 10.5194/bg-8-2849-2011. URL <http://www.biogeosciences.net/8/2849/2011/>.
- R. E. Thomson and I. V. Fine. Estimating mixed layer depth from oceanic profile data. *J Atmos and Ocean Technol*, 20:319–329, 2003. doi: 10.1175/1520-0426(2003)020<0319:EMLDO>2.0.CO;2.
- J. R. Toggweiler and J. Russell. Ocean circulation in a warming climate. *Nature*, 451:286–288, 2008. doi: 10.1038/nature06590.
- M. Tomczak and J. S. Godfrey. *Regional Oceanography: An Introduction*. Daya Publishing House, New Delhi, India, 2 edition, 2003. ISBN 8170353076.
- S. Toub. *Patterns of Parallel Programming. Understanding and Applying Parallel Patterns with the .NET Framework 4 and Visual C#*. Microsoft Corporation, 2010. URL <http://www.microsoft.com/en-us/download/details.aspx?id=19222>.
- D. W. Townsend, L. M. Cammen, P. M. Holligan, D. E. Campbell, and N. R. Pettigrew. Causes and consequences of variability in the timing of spring phytoplankton blooms. *Deep-Sea Res Part I Oceanogr Res Papers*, 41:

- 747–765, 1994. doi: 10.1016/0967-0637(94)90075-2.
- S. Tuljapurkar, C. Boe, and K. W. Wachter. Nonlinear feedback dynamics in fisheries: analysis of the Deriso-Schnute model. *Canadian Journal of Fisheries and Aquatic Sciences*, 51(7):1462–1473, 1994. doi: 10.1139/f94-146.
- P. Turchin. *Complex Population Dynamics: A Theoretical/Empirical Synthesis*, volume 35 of *Monographs in Population Biology*. Princeton University Press, Princeton, USA, 1 edition, 2003.
- R. Ueyama and B. C. Monger. Wind-induced modulation of seasonal phytoplankton blooms in the North Atlantic derived from satellite observations. *Limnol Oceanogr*, 50(6):1820–1829, 2005.
- UNEP. Marine and coastal ecosystems and human well-being: A synthesis report based on the findings of the Millennium Ecosystem Assessment. Technical report, United Nations Environmental Programme (UNEP), 2006.
- UNEP-GPA. The state of the marine environment: Trends and processes. Technical report, United Nations Environmental Programme (UNEP)–Global Programme of Action for the Protection of the Marine Environment from Land-based Activities (GPA), The Hague, Netherlands, 2006.
- S. Urbanek and J. Horner. *Cairo: R graphics device using cairo graphics library for creating high-quality bitmap (PNG, JPEG, TIFF), vector (PDF, SVG, PostScript) and display (X11 and Win32) output.*, 2013. URL <http://CRAN.R-project.org/package=Cairo>. R package version 1.5-5.
- A. Uriarte, P. Prouzet, and B. Villamor. Bay of Biscay and Ibero Atlantic anchovy populations and their fisheries. *Scientia Marina*, 60(Suppl. 2):237–255, 1996.
- V. Vantrepotte and F. Mélin. Temporal variability of 10-year global seawifs time-series of phytoplankton chlorophyll a concentration. *ICES Journal of Marine Science*, 66:1547–1556, 2009. doi: 10.1093/icesjms/fsp107.
- V. Vantrepotte, H. Loisel, F. Mélin, D. Desailly, and L. Duforet-Gaurier. Global particulate matter pool temporal variability over the SeaWiFS period (1997–2007). *Geophysical Research Letters*, 38:L01608, 2011. doi: 10.1029/2010GL046167.
- M. Vargas, C. W. Brown, and M. R. P. Sapiro. Phenology of marine phytoplankton from satellite ocean color measurements. *Geophysical Research Letters*, 36:L01608, 2009. doi: 10.1029/2008GL036006.
- P. G. Verity and V. Smetacek. Organism life cycles, predation, and the structure of marine food webs. *Mar Ecol Prog Ser*, 130:277–293, 1996. doi: 10.3354/meps130277.
- M. H. Visbeck, J. W. Hurrell, L. Polvani, and H. M. Cullen. The North Atlantic Oscillation: past, present and future. *Proc Natl Acad Sci USA*, 98:12876–12877, 2006. doi: 10.1073/pnas.231391598.
- T. Wei. *corrplot: Visualization of a correlation matrix*, 2013. URL <http://CRAN.R-project.org/package=corrplot>. R package version 0.73.
- F. J. Wentz, C. Gentemann, D. Smith, and D. Chelton. Satellite measurements of sea surface temperature through clouds. *Science*, 288(5467):847–850, 2000. doi: 10.1126/science.288.5467.847.
- F. J. Wentz, L. Ricciardulli, K. Hilburn, and C. Mears. How much more rain will global warming bring? *Science*, 317(5835):233–235, 2007. doi: 10.1126/science.1140746.
- M. West and J. Harrison. *Bayesian Forecasting and Dynamic Models*. Springer Series in Statistics, New York, USA, 2 edition, 1997.
- T. Westberry, M. J. Behrenfeld, D. A. Siegel, and E. Boss. Carbon-based primary productivity modeling with vertically resolved photoacclimation. *Global Biogeochemical Cycles*, 22:GB2024, 2008. doi: 10.1029/2007GB003078.
- P. J. P. Whitehead, G. J. Nelson, and T. Wongratana. *Clupeoid fishes of the world (Suborder Clupoidei; Part II, Engraulidae)*, volume 7 of *FAO species catalogue*. FAO, Rome, Italy, 1988. URL <http://www.fao.org/docrep/009/t0835e/t0835e00.htm>.

- H. Wickham. *ggplot2: Elegant Graphics for Data Analysis*. Springer New York, 2009. ISBN 978-0-387-98140-6. URL <http://had.co.nz/ggplot2/book>.
- H. Wickham. The split-apply-combine strategy for data analysis. *Journal of Statistical Software*, 40(1):1–29, 2011. URL <http://www.jstatsoft.org/v40/i01/>.
- H. Wickham. *gridExtra: Arrange grobs in tables.*, 2012a. URL <http://CRAN.R-project.org/package=gridExtra>. R package version 0.1.2.
- H. Wickham. *scales: Scale functions for graphics.*, 2012b. URL <http://CRAN.R-project.org/package=scales>. R package version 0.2.3.
- C. K. Wikle, R. F. Milliff, R. Herbei, and W. B. Leeds. Modern statistical methods in oceanography: A hierarchical perspective. *Statistical Science*, 28(4):466–486, 11 2013. doi: 10.1214/13-STS436. URL <http://dx.doi.org/10.1214/13-STS436>.
- J. W. Williams and S. T. Jackson. Novel climates, no-analog communities, and ecological surprises. *Front Ecol Environ*, 5:475–482, 2007. doi: 10.1890/070037.
- J. W. Williams, S. T. Jackson, and J. E. Kutzbach. Projected distributions of novel and disappearing climates by 2100 ad. *Proc Natl Acad Sci USA*, 104:5738–5742, 2007. doi: 10.1073/pnas.0606292104.
- C. Wilson, J. Morales, S. Nayak, I. Asanuma, and G. Feldman. *Ocean-Colour Radiometry and Fisheries*. In IOCCG [2008], reports of the international ocean-colour coordinating group 6, pages 47–58.
- R. J. Wootten. *Ecology of Teleost Fishes*, volume 24 of *Fish and Fisheries Series*. Kluwer Academic, Dordrecht, Netherlands, 2 edition, 1999.
- B. Worm, E. B. Barbier, N. Beaumont, J. E. Duffy, C. Folke, B. S. Halpern, J. B. C. Jackson, H. K. Lotze, F. Micheli, S. R. Palumbi, E. Sala, K. A. Selkoe, J. J. Stachowicz, and R. Watson. Impacts of biodiversity loss on ocean ecosystem services. *Science*, 314(5800):787–790, 2006. doi: 10.1126/science.1132294.
- D. Wraith, M. Kilbinger, K. Benabed, O. Cappé, J.-F. Cardoso, G. Fort, S. Prunet, and C. P. Robert. Estimation of cosmological parameters using adaptive importance sampling. *Physical Review D*, 80:023507, Jul 2009. doi: 10.1103/PhysRevD.80.023507.
- C. Wunsch. *Global Problems and Global Observations*. In Siedler et al. [2001], pages 47–58.
- M. Yelland and P. K. Taylor. Wind stress measurements from the open ocean. *Journal of Physical Oceanography*, 26(4):541–558, 1996. doi: 10.1175/1520-0485(1996)026<0541:WSMFTO>2.0.CO;2.
- M. J. Yelland, B. I. Moat, P. K. Taylor, R. W. Pascal, J. Hutchings, and V. C. Cornell. Wind stress measurements from the open ocean corrected for airflow distortion by the ship. *Journal of Physical Oceanography*, 28(7): 1511–1526, 1998. doi: 10.1175/1520-0485(1998)028<1511:WSMFTO>2.0.CO;2.
- J. A. Yoder, C. R. McClain, G. C. Feldman, and W. E. Esaias. Annual cycles of phytoplankton chlorophyll concentrations in the global ocean: A satellite view. *Global Biogeochemical Cycles*, 7(1):181–193, 1993. doi: 10.1029/93GB02358.
- J. A. Yoder, C. R. McClain, J. O. Blanton, and L.-Y. Oey. Spatial scales in CZCS-chlorophyll imagery of the southeastern U.S. continental shelf. *Limnology and Oceanography*, 32(4):929–941, 1998.
- J. A. Yoder, S. C. Doney, D. A. Siegel, and C. Wilson. Study of marine ecosystems and biogeochemistry now and in the future: Examples of the unique contributions from space. *Oceanography*, 34(4):104–117, 2010. doi: 10.5670/oceanog.2010.09.
- I. R. Young, S. Zieger, and A. V. Babanin. Global trends in wind speed and wave height. *Science*, 332(6028): 451–455, 2011. doi: 10.1126/science.1197219.
- L. Zhai, T. Platt, C. Tang, S. Sathyendranath, and R. Hernández Walls. Phytoplankton phenology on the Scotian Shelf. *ICES Journal of Marine Science: Journal du Conseil*, 68(4):781–791, 2011. doi: 10.1093/icesjms/fsq175.